

University of Southampton Research Repository ePrints Soton

Copyright © and Moral Rights for this thesis are retained by the author and/or other copyright owners. A copy can be downloaded for personal non-commercial research or study, without prior permission or charge. This thesis cannot be reproduced or quoted extensively from without first obtaining permission in writing from the copyright holder/s. The content must not be changed in any way or sold commercially in any format or medium without the formal permission of the copyright holders.

When referring to this work, full bibliographic details including the author, title, awarding institution and date of the thesis must be given e.g.

AUTHOR (year of submission) "Full thesis title", University of Southampton, name of the University School or Department, PhD Thesis, pagination

UNIVERSITY OF SOUTHAMPTON

**FACULTY OF MEDICINE, HEALTH AND LIFE
SCIENCES**

School of Medicine

**The synergistic interaction between CD20 monoclonal antibodies and
Histone Deacetylase inhibitors in B cell Non Hodgkin's Lymphoma**

By

David Francis Luke Nolan

Thesis for degree of Doctor of Philosophy

January 2010

UNIVERSITY OF SOUTHAMPTON
ABSTRACT

**FACULTY OF MEDICINE, HEALTH AND LIFE
SCIENCES**
School of Medicine

Doctor of Philosophy

**The synergistic interaction between CD20 monoclonal antibodies and
Histone Deacetylase inhibitors in B Cell Non Hodgkin's Lymphoma**
By David Francis Luke Nolan

Recent improvements in molecular sub typing of Non Hodgkin's lymphomas have resulted in targeted therapies becoming incorporated into treatment paradigms. The anti-CD20 monoclonal antibody, Rituximab, has resulted in dramatic improvements in survival for patients with B cell Non Hodgkin's lymphoma. Histone deacetylase inhibitors are a novel class of anti cancer agents targeting epigenetic regulation.

This thesis addresses the interaction between histone deacetylase inhibitors and anti-CD20 monoclonal antibodies, including Rituximab, both *in vitro* and *in vivo*. The initial approach identified synergistic induction of apoptosis in a number of B cell lines. In a Ramos xenograft model, combination treatment with suberoylanilide hydroxamic acid (SAHA) and Rituximab reduced tumour growth compared to either agent alone, without discernable toxicity. This effect appears specific to CD20 since monoclonal antibodies directed to other surface molecules (CD32b, CD22, CD37) did not exhibit cooperative effect. Analysis of apoptotic pathways demonstrated that PARP cleavage and caspase processing is significantly higher in cells receiving both treatments. Co-treatment of Ramos cells with the pan caspase inhibitor QVD-OPH abolished the synergy observed with CD20 monoclonal antibodies, suggesting that caspase processing is necessary for synergy. Treatment of Ramos cells stably transfected to overexpress Bcl-2 resulted in loss of synergy with Rituximab, but not with the type II CD20 mAb B1 (Tositumomab).

Gene expression array analysis of Ramos cells was performed. Geneset enrichment analysis identified significant regulation of NF κ B target genes in some genesets (Rituximab Vs control, $p < 0.001$) with a number associated with apoptosis and B cell activation (Bcl2A1, LTA, CD69) which were confirmed using RT-Q-PCR.

This novel combination elicits the induction of apoptosis *in vitro*, potentially through regulation of Bcl-2 family proteins and should be tested in a phase I/II clinical trial.

List of Contents

1	INTRODUCTION	- 9 -
1.1	NON HODGKIN'S LYMPHOMA	- 9 -
1.2	B CELL DEVELOPMENT AND LYMPHOMAGENESIS	- 11 -
1.3	APOPTOTIC PATHWAY AND LYMPHOMAGENESIS	- 15 -
1.4	NFκB PATHWAY AND LYMPHOMAGENESIS	- 19 -
1.5	ESTABLISHED TARGETED THERAPY FOR B CELL NHL.....	- 24 -
1.6	NOVEL TARGETED THERAPIES FOR B CELL NHL.....	- 32 -
2	MATERIALS AND METHODS	- 58 -
2.1	MATERIALS.....	- 58 -
2.2	METHODS	- 63 -
2.3	STATISTICAL ANALYSIS	- 73 -
3	PROJECT AIMS AND OUTLINE OF INVESTIGATION	- 74 -
4	SYNERGISTIC CELL KILLING IN B CELL NHL CELL LINES	- 75 -
4.1	INTRODUCTION	- 75 -
4.2	EFFECT OF HDAC INHIBITORS	- 75 -
4.3	EFFECT OF CD20 MONOCLONAL ANTIBODIES	- 80 -
4.4	EFFECT OF COMBINATION TREATMENT	- 83 -
4.5	SYNERGY CALCULATIONS	- 88 -
4.6	COMBINATION THERAPY IN A XENOGRAFT MODEL.....	- 97 -
4.7	DISCUSSION	- 102 -
5	MECHANISMS UNDERLYING CYTOTOXICITY.....	- 105 -
5.1	INTRODUCTION	- 105 -
5.2	INDUCTION OF HISTONE ACETYLATION	- 105 -
5.3	MODULATION OF CD20 EXPRESSION	- 111 -
5.4	MEASUREMENT OF Ca ²⁺ FLUX AND ERK PHOSPHORYLATION.....	- 114 -
5.5	MECHANISMS OF CELL DEATH	- 117 -
5.6	DISCUSSION	- 130 -
6	TRANSCRIPTIONAL MECHANISMS FOR COOPERATIVE ACTIVITY.....	- 135 -
6.1	INTRODUCTION	- 135 -
6.2	MICROARRAY DESIGN AND SAMPLE PREPARATION	- 136 -
6.3	VALIDATION	- 146 -
6.4	FUNCTIONAL ANNOTATION CLUSTERING ANALYSIS	- 152 -
6.5	RT-Q-PCR ANALYSIS OF NFκB TARGET GENES	- 157 -
6.6	CD69 AS A BIOMARKER OF HDI TRANSCRIPTIONAL REGULATION.....	- 162 -
6.7	UP REGULATION OF SURFACE CD69 EXPRESSION	- 164 -
6.8	DISCUSSION	- 172 -
7	DISCUSSION AND FUTURE WORK.....	- 176 -
	REFERENCES.....	- 180 -

List of Figures

Figure 1-1 Normal B cell development and lymphoma counterparts:	12 -
Figure 1-2 Apoptotic pathways:	17 -
Figure 1-3 NFκB activation pathways:.....	22 -
Figure 1-4 structure of CD20 receptor:.....	26 -
Figure 1-5 Potential mechanisms of action of CD20 mAb:	28 -
Figure 1-6: Histone structure and sites of modification:	36 -
Figure 1-7 Non histone targets of HDAC enzymes:.....	38 -
Figure 1-8 Action of HDAC and HAT enzymes:	40 -
Figure 1-9 Histone Deacetylase family:	42 -
Figure 1-10 The role of HDACs in tumourigenesis:	44 -
Figure 1-11 Structure of HDI molecule:.....	47 -
Figure 4-1 The effect of SAHA on Ramos cell survival:	76 -
Figure 4-2 the effect of FK228 on Ramos cell survival:	78 -
Figure 4-3 Effect of CD20 monoclonal antibodies in Ramos cell line:.....	81 -
Figure 4-4 Effect of rituximab and B1 in a panel of B cell NHL cell lines:	82 -
Figure 4-5 effect of SAHA in combination with rituximab in Ramos cell line:	84 -
Figure 4-6 effect of FK228 and Rituximab in Ramos cell line:	85 -
Figure 4-7 Effect of combination treatment in other cell lines:.....	87 -
Figure 4-8 Induction of apoptosis in Ramos cell line:	89 -
Figure 4-9 The specificity of CD20 mAb at inducing apoptosis:	91 -
Figure 4-10 Synergistic induction of apoptosis in Ramos cell line:.....	93 -
Figure 4-11 Synergistic interactions in Ramos cells.	95 -
Figure 4-12 Ramos xenograft:.....	98 -
Figure 4-13 Western blot of tumours from Ramos xenografts:	99 -
Figure 4-14 Rate of tumour growth in SCID mice with established tumours:	99 -
Figure 4-15 cumulative survival in xenograft model.....	101 -
Figure 5-1 Histone acetylation in Ramos cells:.....	106 -
Figure 5-2 Histone acetylation in RL cells:	106 -
Figure 5-3 Histone acetylation in Ramos cells:	108 -
Figure 5-4 Histone acetylation in SU-DHL-4 cell line:.....	109 -
Figure 5-5 HDAC enzyme assay in SU-DHL-4 cell line:.....	110 -
Figure 5-6 CD20 expression in panel of B cell NHL cell lines:.....	112 -
Figure 5-7 Effect of SAHA on CD20 expression in Ramos cells:	113 -
Figure 5-8 Ca ²⁺ flux following Rituximab treatment in Ramos cells	115 -
Figure 5-9 ERK phosphorylation in SU-DHL-4 cell line	116 -
Figure 5-10 Apoptosis following SAHA treatment:.....	118 -
Figure 5-11 Mechanism of induction of cell death with CD20 mAb in Ramos cells:	119 -
Figure 5-12 Combination treatment in B cell NHL cell lines:	121 -
Figure 5-13 Induction of PARP cleavage following combination treatment:	122 -

Figure 5-14 Effect of caspase inhibitor on induction of apoptosis in Ramos cell line:	124 -
Figure 5-15 Effect of QVD-oph on caspase processing in Ramos cell line:	125 -
Figure 5-16 Expression of Bcl-2 in B cell NHL cell lines:	127 -
Figure 5-17 Induction of apoptosis in Bcl-2 overexpressing Ramos:	128 -
Figure 5-18 Caspase processing in Bcl-2 Ramos:.....	129 -
Figure 5-19 Model of interaction between HDI and type I and II CD20 mAb:	134 -
Figure 6-1 Microarray sample preparation:.....	137 -
Figure 6-2 Cluster dendrogram of Ramos cells gene expression analysis:.....	141 -
Figure 6-3 expression of all significant genes compared to control:	143 -
Figure 6-4 Differentially expressed genes following combination treatment:.....	144 -
Figure 6-5: Scatter plot of Rituximab regulated genes.	147 -
Figure 6-6 RT-Q-PCR validation of microarray:.....	151 -
Figure 6-7 Regulation of NF κ B target genes:	156 -
Figure 6-8 RT-Q-PCR timecourse of BclX _L regulation:	158 -
Figure 6-9 RT-Q-PCR of NF κ B target genes in Ramos cells:	160 -
Figure 6-10 CD69 upregulation in SU-DHL-4 cell line	163 -
Figure 6-11 cell surface upregulation of CD69 in CD19 positive PBMC	165 -
Figure 6-12 CD69 upregulation in primary cells:.....	166 -
Figure 6-13 Induction of CD69 in a dose dependent manner by HDI	168 -
Figure 6-14 Effect of NF κ B inhibition on CD69 upregulation:.....	170 -
Figure 6-15 specific upregulation of CD69:	171 -

List of Tables

Table 1-1 WHO classification of Non Hodgkin's Lymphoma:.....	10 -
Table 1-2 HDAC inhibitors in clinical development.	49 -
Table 2-1 Cell lines used for this work:	59 -
Table 2-2 Antibodies used in this study:	66 -
Table 2-3 Gene Expression assays used for real time PCR:	69 -
Table 2-4 Antidodies used for flow cytometric analysis:	72 -
Table 4-1 Sensitivity of B cell NHL cell lines to HDI:	79 -
Table 4-2 Summary of combination index across panel of B cell NHL cell lines.....	96 -
Table 6-1 Differentially expressed transcripts:	140 -
Table 6-2: Differentially expressed genes following 6 hours combination treatment.....	145 -
Table 6-3 Connectivity score for SAHA dataset compared to Cmap database:	149 -
Table 6-4 Functional annotation clustering analysis:	153 -
Table 6-5: top ranked functionally associated genes.	153 -
Table 6-6 Geneset enrichment analysis:	155 -

DECLARATION OF AUTHORSHIP

I David Francis Luke Nolan declare that the thesis entitled 'The synergistic interaction between CD20 monoclonal antibodies and Histone Deacetylase inhibitors in B Cell Non Hodgkin's Lymphoma' and the work presented in the thesis are both my own, and have been generated by me as the result of my own original research. I confirm that:

- this work was done wholly or mainly while in candidature for a research degree at this University;
- where any part of this thesis has previously been submitted for a degree or any other qualification at this University or any other institution, this has been clearly stated;
- where I have consulted the published work of others, this is always clearly attributed;
- where I have quoted from the work of others, the source is always given. With the exception of such quotations, this thesis is entirely my own work;
- I have acknowledged all main sources of help;
- where the thesis is based on work done by myself jointly with others, I have made clear exactly what was done by others and what I have contributed myself;
- none of this work has been published before submission.

Signed:

Date:.....

Acknowledgements

I would like to acknowledge and thank Professor Graham Packham and Professor Peter Johnson who acted as supervisors for the project presented in this work.

From Professor Packham's laboratory Dr Simon Crabb, Mr Matthew Brimmell, Dr Melanie Howell and Dr Abigail Lapham each provided help and instruction in the various techniques used within this thesis. Dr Steve Beers and Professor Martin Glennie provided help and advice regarding anti CD20 antibodies. In addition I thank all current and past members of Professor Packham's laboratory who have been of assistance throughout this work.

Finally I am grateful to Cancer Research UK, who funded my position as a Clinical Research Fellow, and work within Professor Packham's laboratory, to allow me to undertake the project presented in this thesis.

1 Introduction

1.1 Non Hodgkin's lymphoma

Non Hodgkin's lymphoma (NHL) is a major cause of morbidity and mortality with an estimated 66,000 new cases in the US in 2008 [1] and 10,310 cases in the UK in 2005. The incidence is still rising, partly due to its association with human immunodeficiency virus infection (HIV), but mainly due to an ageing population. Classification of this disease is evolving as expression profiling facilitates a greater understanding of the molecular events responsible. In the 1990's the Revised European American Lymphoma (REAL) classification system superseded prior methods and was based on morphological, immunological and clinical characteristics. Evolution of this system has resulted in the most recent WHO classification system which was published in 2008 and this incorporates molecular profiling of diffuse large B cell NHL for the first time [**Table 1-1**]. B cell NHL makes up approximately 80% of all cases with diffuse large B cell NHL responsible for between 34% and 44% of all cases, closely followed by follicular NHL in published series [2, 3]. It is within these two commonest subsets that recent therapeutic advances, especially the widespread use of the CD20 monoclonal antibody Rituximab, have resulted in improvements in survival [4, 5]. In parallel with these improvements, gene expression profiling has demonstrated that within currently classified subtypes there is further heterogeneity which has significant predictive value for both prognosis and response to targeted therapies.

B-cell neoplasms***Precursor B-cell neoplasm***

Precursor B-lymphoblastic leukemia/lymphoma (precursor B-cell acute lymphoblastic leukemia)

Mature (peripheral) B-cell neoplasms

B-cell chronic lymphocytic leukemia/small lymphocytic lymphoma

B-cell prolymphocytic leukemia

Lymphoplasmacytic lymphoma

Splenic marginal zone B-cell lymphoma (with or without villous lymphocytes)

Hairy cell leukaemia

Plasma cell myeloma/plasmacytoma

Extranodal marginal zone B-cell lymphoma (with or without monocytoid B cells)

Nodal marginal zone B-cell lymphoma (with or without monocytoid B cells)

Follicular lymphoma

Mantle cell lymphoma

Diffuse large B-cell lymphoma

Burkitt lymphoma/Burkitt cell leukaemia

T-cell and NK-cell neoplasms***Precursor T-cell neoplasm***

Precursor T-lymphoblastic lymphoma/leukemia (precursor T-cell acute lymphoblastic leukemia)

Mature (peripheral) T/NK-cell neoplasms

T-cell prolymphocytic leukaemia

T-cell granular lymphocytic leukaemia

Aggressive NK-cell leukaemia

Adult T-cell lymphoma/leukemia (HTLV1+)

Extranodal NK/T-cell lymphoma, nasal type

Enteropathy-type T-cell lymphoma

Hepatosplenic gamma delta T-cell lymphoma

Subcutaneous panniculitis-like T-cell lymphoma

Mycosis fungoides/Sezary syndrome

Anaplastic large cell lymphoma, T/null cell, primary cutaneous type

Peripheral T-cell lymphoma, not otherwise characterized

Angioimmunoblastic T-cell lymphoma

Anaplastic large cell lymphoma, T/null cell, primary systemic type

Table 1-1 WHO classification of Non Hodgkin's Lymphoma:

1.2 B cell development and lymphomagenesis

It is widely acknowledged that normal lymphocyte differentiation exposes developing cells to a multitude of potentially oncogenic events [Figure 1-1]. Immunophenotyping, gene expression profiling and genomic analysis are now starting to demonstrate how these events link lymphoid malignancies to their underlying cell of origin. B cell development occurs in two stages, the earliest committed B cell progenitors are pro B cells, these express CD10, CD34 and CD19. Cells at this stage have commenced Ig heavy chain recombination. This is the first potentially oncogenic hurdle in normal B cell development and is critical to developing the necessary B cell repertoire for effective antibody specificity. To achieve this diversity pro B cells undergo double strand DNA breaks and rearrangement of the V(D)J genes. This event is initiated and controlled by recombination activating genes (RAG1, RAG2) [6]. Successful recombination results in μ heavy chain synthesis and association with two surrogate light chain proteins Vpre-B and $\lambda 5$ [7], surface expression of this 'pre B cell receptor (BCR)' is a defining feature of the pre B cell stage. The next critical transition is from pre B cell to mature B cell and is the result of Ig light chain rearrangement by similar mechanisms. It is worth noting that at both these transitional stages approximately two thirds of cells develop non productive rearrangements and are eliminated by apoptosis. Secondary B cell development occurs in the spleen and results in negative selection of B cells with self antigen again by apoptosis and positive selection of a small subset (1-2%) by antigen. This process results in naïve B cells which are able to circulate and occupy lymphoid tissue. In response to antigen, naïve cells can respond in a number of different ways, regulated by the micro environment in which the encounter occurs. T independent responses have a low threshold for activation and occur as a result of polymeric antigens and usually occur in the splenic white pulp (marginal zone). This results in the rapid production of low affinity IgM and IgG3 antibodies.

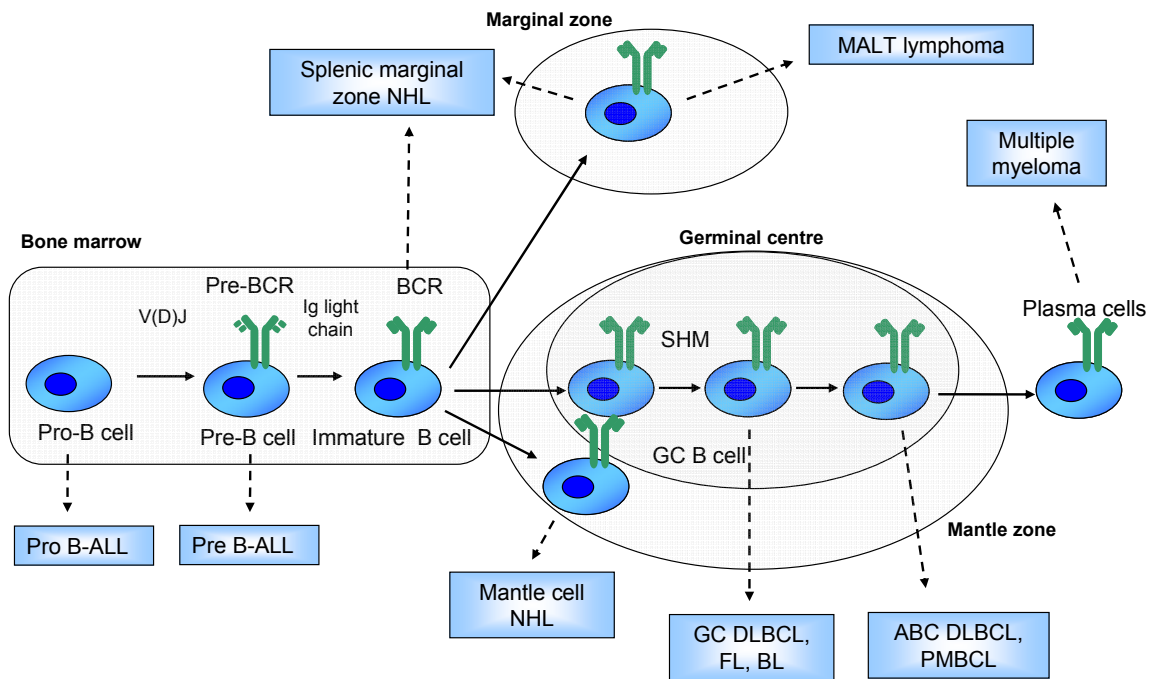


Figure 1-1 Normal B cell development and lymphoma counterparts:

Stages of normal B cell development are shown with counterpart B cell malignancies depicted. Adapted from figure by *Kuppers et al* [8].

A more specific response occurs when antigen is presented to B cells by T cells in the germinal centre (GC). This results in B cell activation with differentiation of some cells into plasma cells secreting low affinity antibody, with other cells undergoing affinity maturation due to repeated antigen exposure resulting in high specificity plasma cells and memory B cells. At all stages of B cell development there is selection pressure with only the cells that express a functional BCR selected for survival. This mechanism depends on functional signalling through the BCR and in particular activation of NF κ B to induce the expression of anti apoptotic Bcl-2 family proteins. It is becoming increasingly apparent that events occurring at these key stages in B cell development result in inappropriate survival of cells through evasion of this apoptotic elimination.

V(D)J recombination requires double strand DNA breaks and can result in chromosomal translocations. The t(14:18) seen in Follicular lymphoma (FL), is a defining example of this. This translocation results in fusion of the Bcl-2 gene to the immunoglobulin heavy chain locus. This results in constitutive expression of Bcl-2 and this discovery was a key event in describing the function of this anti apoptotic protein [9]. A similar event is also seen in mantle cell lymphoma (MCL) where t(11:14) results in overexpression of cyclin D1 [10]. Interestingly these early oncogenic events do not arrest B cell differentiation. It has been well described that FL frequently displays GC features suggesting that the cell of origin has been exposed to antigen in the GC [8].

Potentially as important are oncogenic events occurring in the germinal centre during affinity maturation. As discussed earlier this process is involved in developing and potentiating antibody specificity following antigen presentation by T cells in the GC and is facilitated by two mechanisms; Class switch recombination (CSR) and somatic hypermutation (SHM). CSR is implicated in the t(8:14) seen in sporadic Burkitt's lymphoma (BL) which results in overexpression of the c-MYC oncoprotein [11] and may also account for Bcl6 overexpression seen in GC NHL [12, 13]. These events again act to render cells independent of microenvironment growth signals and demonstrate how avoidance of apoptosis is fundamental to lymphomagenesis.

The advent of molecular profiling has offered a new approach for understanding the sequelae of these oncogenic events and specifically how they act to overcome the normal homeostatic mechanisms and drive lymphomagenesis. In 2000 Alizadeh et al published results from DNA microarray analysis of 96 normal and malignant lymphocytes [14]. They observed clustering of samples from common lineages. Chronic lymphocytic leukaemia (CLL) and FL samples clustered closely with normal B cells, where as diffuse large B cell lymphoma (DLBCL) clustered separately and were characterised by expression of genes associated with a high proliferative index. When DLBCL cases were reclustered using only genes that defined the germinal centre B cells, two distinct groups appeared; these groups were defined as germinal centre B-like DLBCL (GC) and activated B-like DLBCL (ABC). Using the expression profiling data from these cases they were able to demonstrate differences in prognosis following multimodality treatment. These data were reinforced by another study using a 100 gene signature to divide a larger case series between ABC and GC subtypes [15]. Gene expression subtyping was again able to predict outcome following anthracycline based chemotherapy.

More recent analysis has demonstrated that these subtypes harbour novel oncogenic events, for example an amplicon on chromosome 19 was seen in 26% of ABC but in only 3% of GC subtypes. Knockdown of a highly up-regulated gene in this amplicon (SPIB) was toxic to ABC but not GC subtypes [16]. One of the other most consistent ABC characteristics is constitutive NF κ B activation, resulting in activation of known NF κ B target genes [17]. Use of a library of short hairpin RNA (shRNA) constructs representing 2,500 genes, demonstrated synthetic lethality of NF κ B target genes and identified CARD11 as a key upstream target [18]. Professor Staudt's group has gone on to demonstrate activating mutations in the coiled coil domain of CARD11 of ABC subtype cell lines, which when inhibited result in lethality to these cells [19].

Despite a wide range of upstream events all the mutations and translocations discussed act to enhance cell growth; inhibit apoptosis; or block differentiation. For example in the germinal centre the NF κ B transcription factor family are repressed leading to low expression of their target genes

potentially resulting in the negative selection observed [14]. Physiological activation of this pathway leads to upregulation of Bcl X_L, Bcl2A1 and Bcl-2 [20-22] resulting in positive selection of appropriate cells. Many NHL subtypes have been shown to activate the NFκB pathway at some point during lymphomagenesis and as described above ABC DLBCLs are critically dependent on this pathway [17]. As our knowledge of the critical oncogenic events increases, it is becoming possible to devise strategies for specifically targeting the pathways concerned.

1.3 Apoptotic pathway and lymphomagenesis

Evasion of apoptosis is one of the key features required for maintaining the malignant phenotype and one of the hallmarks of cancer [23]. Broadly speaking apoptosis is mediated by two distinct pathways with a common terminal signalling cascade involving proteolytic cleavage of a family of cysteine proteases (caspases) resulting in death [Figure 1-2]. This family is divided into two types: initiator (apical) caspases (2,8,9) and effector (executioner) caspases ([3](#), [6](#), [7](#))

The intrinsic pathway is initiated by hypoxia, radiation, cytotoxics and a whole range of genotoxic stimuli. These stimuli act to alter the balance of Bcl-2 family proteins. Pro apoptotic members induce mitochondrial membrane depolarization resulting in release of cytochrome c (Cc) [24]. Cc binds to apoptotic protease-activating factor-1 (APAF-1) initiating formation of the apoptosome. The apoptosome recruits procaspase 9, resulting in cleavage into the active caspase 9 (35, 10 kDa subunits) [25]. Once activated, caspase 9 recruits the effector caspase, 'caspase 3', which is cleaved at Asp-28/Ser-29 and Asp-175/Ser-176, generating 17 and 12 kDa subunits [26]. Activated caspase 3 can translocate to the nucleus and initiates proteolytic cleavage of many key molecules, including poly(ADP-ribose) polymerase (PARP) [27].

The extrinsic pathway in contrast can act independently of the mitochondria. Activation occurs through cell membrane death receptors (e.g. CD95/Fas, DR4, DR5) which bind specific pro apoptotic ligands (eg. FasL, Apo2/TRAIL) [28]. The intracellular domains of these receptors are known as the 'death domains' and bind to the adaptor protein Fas-associated death domain

(FADD). This leads to the assembly of the death-inducing signalling complex (DISC) [29]. Recruitment and assembly of initiator caspases 8 and 10, allows processing of these molecules with release of active enzyme molecules and activation of caspase 3. It has been shown that in some cells (type I cells) active caspase 8 can activate the effector caspases directly [30], however in other cells (type II cells) the proapoptotic signal requires a mitochondrial amplification loop via cleavage of Bid, Bax/Bak to achieve full activation of casapse 3 [31].

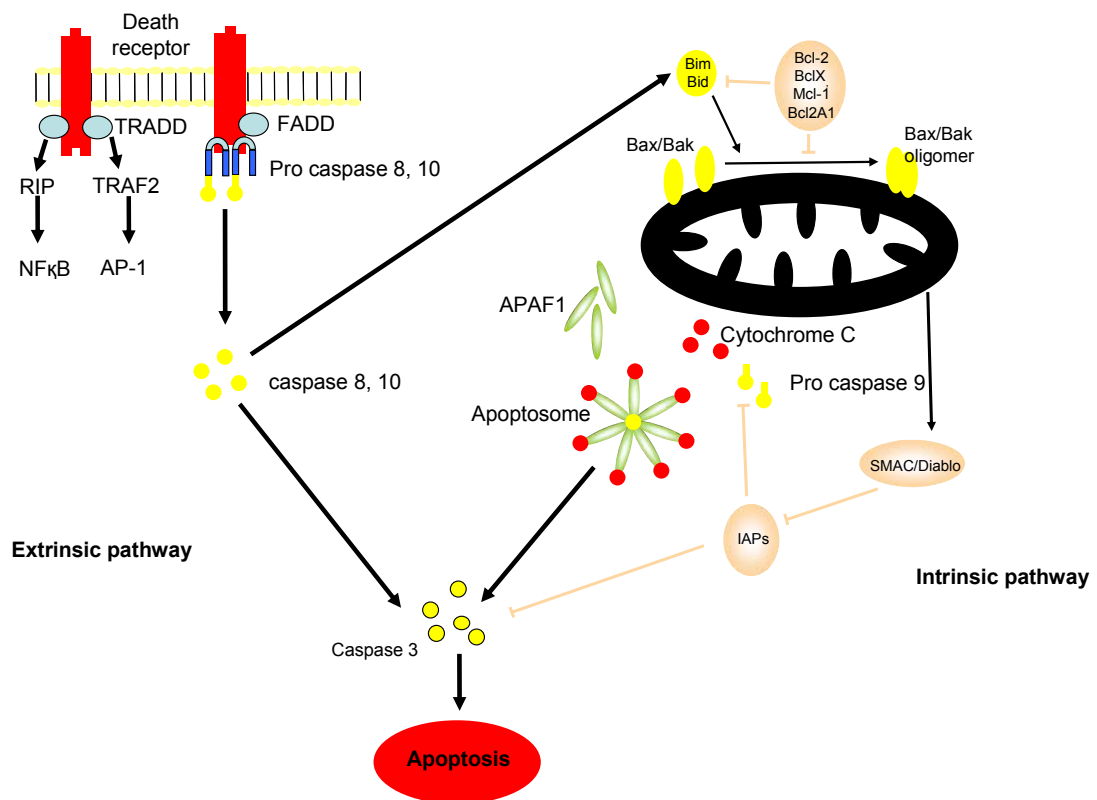


Figure 1-2 Apoptotic pathways:

Schematic representation of caspase dependent apoptotic pathways. Pro apoptotic Bcl-2 family members induce Cytochrome C release from the mitochondria. This together with (APAF-1) apoptotic protease-activating factor-1 and pro caspase 9 initiates Apoptosome formation. Caspase 9 cleavage and activation occurs resulting in activation of the effector caspase (caspase 3). The extrinsic pathway is activated by ligation of death receptors. This induces formation of a death inducing signalling complex (DISC) with the adaptor protein Fas-associated death domain (FADD) and pro caspase 8 and 10. Proteolysis releases the active caspase components once more initiating effector caspase activation. Adapted in part [32].

Both these pathways are subject to regulation by transcriptional and post transcriptional mechanisms.

One of the key regulatory steps of the intrinsic pathway occurs at the mitochondrial membrane where a balance between pro and anti- apoptotic Bcl-2 family proteins decide the fate of a cell. The Bcl-2 family of proteins share at least one of four conserved Bcl-2 homology domains (BH1-4). Anti apoptotic family members (Bcl-2, Mcl-1, Bcl2A1, Bcl-X_L, Bcl-W) contain BH1-4. Pro apoptotic members contain only the BH3 domain and are subdivided into: effector proteins (Bak, Bax); direct activator proteins (Bid, Bim) and derepressor/sensitizer proteins (BAD, BIK, BMF, bNIP3, HRK, Noxa and PUMA). BH1 and BH2 appear to be necessary for anti apoptotic members to dimerise with Bax and inhibit apoptosis [33], where as BH3 is required for Bax and Bak to dimerise with Bcl-2 and Bcl-X_L and initiate apoptosis [34]. Their basic structure consists of a hydrophobic helical region surrounded by amphipathic helices; most contain a membrane binding region and are predominantly bound to the mitochondrial outer membrane. A number of investigators have shown that the membrane binding region is crucial to the function of these peptides [35, 36], which is logical considering that they act by inhibiting or initiating mitochondrial membrane depolarisation and cytochrome C release. Two models for activation have been proposed. The direct activation model proposes that only the activators (Bid, Bim) can activate the effectors (Bax, Bak), a second level of regulation involves the sensitisers (BAD, BIK, BMF, bNIP3, HRK, Noxa and PUMA) which can displace the effectors from anti apoptotic (Bcl-2, Mcl-1, Bcl2A1, Bcl-X_L, Bcl-W) proteins [37, 38]. The indirect model suggests that all BH3 only members can bind anti apoptotic molecules, resulting in release of effectors [38-40]. A further level of control is exerted down stream of the mitochondria. The inhibitors of apoptosis (IAPs) are a family of antiapoptotic proteins which act by binding the effector caspases and inhibiting their activation. In response to proapoptotic signals, release of second mitochondria-derived activator of caspases (SMAC/DIABLO) results in inhibition of IAPs, promoting apoptosis. As well as the dynamic balance between pro and antiapoptotic family members, these proteins are also subject to post translational modifications. *Chang et al* performed mutational analysis of the loop domains of Bcl-2 and

Bcl-X_L, they observed that loss of serine/threonine phosphorylation sites enhanced the antiapoptotic function of these proteins without affecting their dimerisation [41]. It appears that pro apoptotic Bad is also subject to phosphorylation on serine residues, interestingly this sequesters it in the cytoplasm inhibiting its pro apoptotic function [42].

As already discussed, evasion of apoptosis is an important mechanism in lymphomagenesis. The t(14:18) translocation occurs in 85% of follicular lymphomas and approximately 20% of DLBCL, and is the most common oncogenic event observed in lymphoid malignancies [43, 44]. This translocation results in over expression of Bcl-2-Ig chimeric RNA. In transgenic mice a polyclonal follicular lymphoproliferation occurs, which progresses to DLBCL, mimicking the effect observed in humans [45]. It appears that this event occurs during V(D)J recombination, early in B cell development and infers an inappropriate survival advantage following exposure to antigen in the germinal centre. Mutations of pro apoptotic family members have also been documented, a Japanese group performed array CGH in 29 Mantle lymphoma cases and observed homozygous deletions within the Bim gene in 17% of cases [46]. More recent data in E μ -myc mice has shown that loss of noxa and puma together promotes lymphomagenesis [47].

These wealth of data demonstrate how our understanding of the structure and function of these key survival molecules is rapidly advancing and how it has heralded the advent of molecularly targeted therapies

1.4 NF κ B pathway and lymphomagenesis

One of the key pathways for regulation of apoptosis in developing B cells is the NF κ B pathway. This transcription factor (TF) family is made up of 5 mammalian proteins p65 (RelA), RelB, c-Rel, p50/p105 (NF κ B1), p52/p100 (NF κ B2) [48]. These proteins appear to be expressed in a wide range of cell types but were first described in B cells by nature of their ability to induce immunoglobulin kappa light chain transcription [49]. The importance of these transcription factors is reinforced by the fact that they are evolutionarily

conserved [50]. They act to orchestrate transcriptional response to a wide range of inflammatory signals.

All members of this TF family are characterised by a 300 amino acid Rel-homology domain which mediates nuclear localisation, dimerisation and DNA binding. NF κ B proteins are activated by a wide range of signals via the 'canonical' and 'alternative' pathways, and different dimerisation partnering partially accounts for the diversity of gene expression observed [Figure 1-3]. Inactive NF κ B complexes are maintained in the cytoplasm through interaction with the inhibitor of κ B (I κ B) proteins. This family consists of I κ B α , I κ B β , I κ B ϵ , Bcl-3, p100 and p105 and all contain ankyrin-like repeats, their role is prevention of NF κ B nuclear localisation and hence interaction with DNA. Activation of the canonical pathway occurs through the I κ B kinase (IKK) complex, which leads to phosphorylation and degradation of I κ B proteins via ubiquitination by the SCF- β TrCP complex and subsequent proteasomal degradation. The alternative pathway has a more restricted set of stimuli with activation of IKK α leading to phosphorylation and degradation of p100 to p52, which in turn dimerises with RelB. As well as these post translational modifications there is also a transcriptional element to this regulation with Bcl-3 capable of acting as a transcriptional co-activator for p50 and p52 [51]. Once released, complexes are free to translocate to the nucleus where they can bind to NF κ B binding sites within the promoter and enhancer regions of specific genes. The N terminal domain is primarily responsible for sequence specificity, and hydrophobic residues within the c terminal interact to mediate dimerisation. RelA, RelB and c-Rel contain C terminal transactivation domains (TAD) and are required in dimers to activate gene transcription. p50 and p52 are able to bind DNA but without TADs cannot activate gene expression, and in fact may inhibit it [52]. Further inhibitory feedback mechanisms include the synthesis of I κ B α by activated NF κ B resulting in transport of NF κ B back to the cytoplasm terminating the activation [53]. More recent data have demonstrated that NF κ B activation and specifically DNA binding is subject to a whole range of other regulatory mechanisms including post translational modifications and association with co factors [54, 55]. Kim et al demonstrated that p50 was capable of positively and negatively

regulating the metastasis suppressor gene *Kal1* and the nature of the response was controlled by recruitment of co repressors to the p50 transcriptional activating complex [56]. Chen et al have observed that p300 acetylates p65/RelA at multiple lysine residues, each with its own specific effect on NF κ B activity [55].

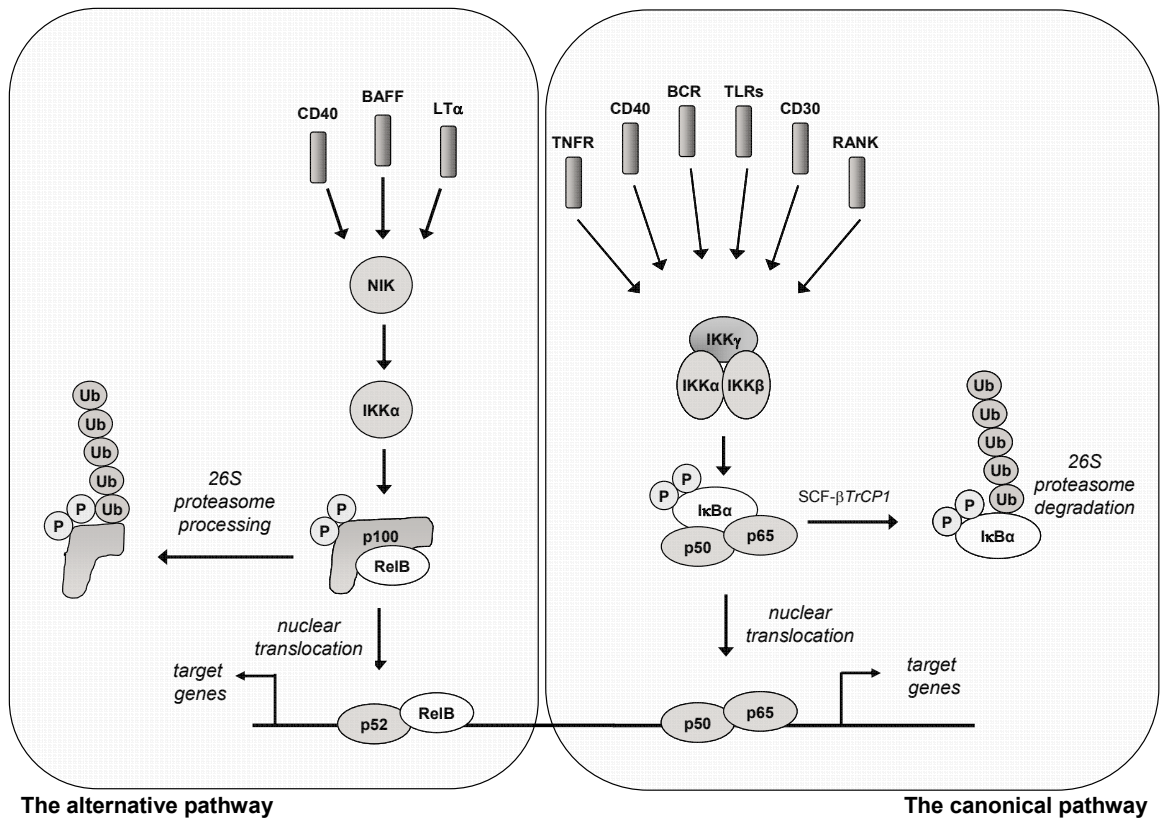


Figure 1-3 NFκB activation pathways:
Adapted from G Packham [57].

The target genes of the NF κ B family are wide ranging and at least 400 have been described [58].

As discussed earlier the NF κ B pathway has been heavily implicated in initiating and maintaining the malignant phenotype in lymphomas, and this is almost certainly due to its importance in controlling apoptosis during B cell development. In mouse knockdown experiments, p65^{-/-} mice demonstrate lethality from liver degeneration secondary to apoptosis [59], knockdown of TNF α (TNF α ^{-/-}, TNFR^{-/-}) rescues mice from this event. Double knockdown mice exhibit impaired innate immunity, class switching in B cells and lymphocyte proliferation [60, 61]. In contrast to this p50 knockdown results in impaired humoral immunity, p52 null mice fail to develop normal germinal centres and secondary lymphoid organs.

The role of constitutive NF κ B activation in ABC DLBCL has already been discussed (section 1.4), activation of NF κ B is not exclusive to this lymphoma subtype. Compared to TNF stimulated fibroblasts GC DLBCL expresses higher levels of NF κ B [62] and deletions of the 3' end of the p52/p100 gene leading to oncogenic p100 lacking C-terminal ankyrin-repeats have been observed [63, 64]. Another well documented event is Rel amplifications which occur in a subset of GC DLBCL, FL, primary mediastinal B-cell lymphoma (PMBL) and mucosa-associated lymphoid tissue (MALT) lymphoma [63]. The exact consequences of these mutations remain to be elucidated, work by Davis et al has shown that GC DLBCL are not dependent on NF κ B activity [17], however this work has only been performed in a small set of cell lines. It may be that activation of NF κ B is an early event that occurs in the germinal centre but is not crucial to survival of the malignant clone.

1.5 Established targeted therapy for B cell NHL

1.5.1 Introduction

Until the mid 1990's the treatment outcome of B cell NHL had changed very little over the preceding two decades. For DLBCL standard treatment remained CHOP chemotherapy (cyclophosphamide, vincristine, doxorubicin and prednisolone), with no benefit observed with more intensive regimens [65]. The median survival of follicular lymphoma had improved to almost 10 years [66], compared to only 5 years prior to the widespread use of chemotherapy [67]. However attempts to intensify chemotherapy have not resulted in improvements in this.

The CD20 receptor is expressed on more than 95% of normal and neoplastic B-cells, but not on plasma cells or early pro B-cells, it has not been detected in other tissues [68]. This makes it an excellent molecular target and prompted the development of anti CD20 therapy.

1.5.2 CD20 Receptor and monoclonal antibodies

The human CD20 gene is located on chromosome 11, close to the breakpoint site of t(11:14) translocation seen in some lymphomas. Two groups cloned CD20 simultaneously [69, 70]. It is a non-glycosylated 33 to 37-kDa phosphoprotein, with four transmembrane domains, a single extracellular loop between the 3rd and 4th transmembrane domain and the N- and C-termini inside the cell [Figure 1-4]. CD20 is highly phosphorylated in malignant B-cells and nonphosphorylated in nonproliferating B-cells, suggesting that phosphorylation is associated with proliferation [71]. Once expressed CD20 resides as multimers, usually dimers/tetramers and has been reported to localise with CD40, MHC II and B cell receptor for antigen (BCR) [72]. The exact role of the CD20 receptor remains unclear and knockout mice have been shown to have no phenotype [73]. A number of theories concerning its function have been proposed.

It has been suggested that CD20 acts as a membrane ion channel controlling the flux of calcium [71]. This is supported by an increasing body of evidence. Bubein *et al* [74] demonstrated that CD20 transfection into a number of cell

lines resulted in an increase in the basal level of cytosolic Ca^{2+} , in Daudi B cells calcium flux was dependent on the type of CD20 antibody used. As CD20 has no known ligand, this effect on calcium flux is transduced by other mechanisms. Li *et al* [75] have hypothesised that CD20 acts as a store operated ion channel by allowing entry of extracellular calcium to replace diminishing stores in the endoplasmic reticulum resulting from B cell activation. The exact mechanism of this is not fully understood, however CD20 receptor expression correlates with cytosolic Ca^{2+} levels. Its structure resembles other store operated ion channels [70, 76, 77]. It can exist in oligomeric state on cell surface, and in hairy cell leukaemia CD20 expression correlates with elevated cytosolic Ca^{2+} [78, 79]. A new role for CD20 has been proposed by Kuijpers *et al* [80]. This group demonstrated that CD20 deficiency resulted in impaired T cell independent antibody responses. It has been shown that monoclonal antibody binding results in the translocation of the CD20 receptor to lipid insoluble rafts [81, 82]. These rafts are highly ordered domains rich in glycosphingolipids, cholesterol and signalling proteins like Src kinases. It is not clear what facilitates this reorganisation; it does not seem to be linked to kinase activity, cytoskeletal function or mAb binding and may be an epitope dependent phenomenon. With no known ligand our understanding of signalling events resulting from CD20 activation is derived from studying the effect of anti-CD20 mAbs.

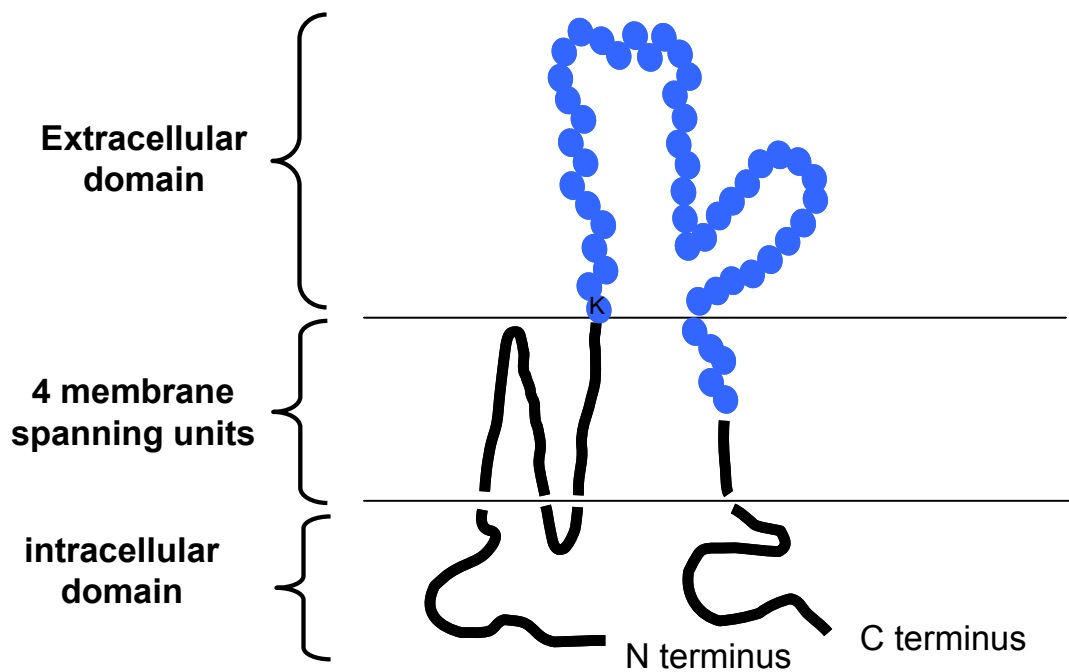


Figure 1-4 structure of CD20 receptor:

Cartoon depicting the structure of the human CD20 receptor, there are 4 membrane spanning domains with the N and C terminals situated in the cytoplasm.

1.5.3 Anti CD20 monoclonal antibodies (mAbs)

CD20 monoclonal antibodies were the first monoclonal antibodies to be used for the treatment of cancer. Rituximab (Roche) was licensed for the treatment of B-cell malignancies in 1997, and is a crucial element of multimodality therapy primarily in combination with conventional cytotoxic agents. A new wave of CD20 mAbs are in clinical development with the promise of improving outcomes even further [83]. *In vitro* anti-CD20 mAbs have been shown to act via three distinct mechanisms: Complement-dependent cytotoxicity (CDC): Antibody dependent cell mediated cytotoxicity (ADCC): growth arrest and apoptosis in certain cell lines [Figure 1-5] [84, 85]. Despite its widespread usage and success in the treatment of B-cell malignancies [4, 86], the exact mechanism of action of the human/mouse chimeric CD20 mAb Rituximab *in vivo* is not known.

CD20 mAbs can be divided into two types, based on their ability to translocate CD20 into insoluble 'lipid rafts' [82, 87]. Type I mAbs (Rituximab, LT20, AT80, IF5, 2H7, 7D8, 2F2) are so classified because of their ability to translocate the CD20 receptor into "lipid rafts", they are potent at inducing CDC and are less effective inducers of apoptosis. Type II mAb (B1 and 11B8, GA101) are ineffective in CDC but potent at inducing homotypic adhesion and apoptosis. Both types are equally effective at inducing ADCC. What is not clear is what characteristic of CD20 mAb binding is important for these differential effects, for example both Rituximab and B1 appear to bind to the same region of the CD20 receptor.

Lipid rafts are widely acknowledged to be the main signalling platforms for B-lymphocytes, yet Chan et al have demonstrated that induction of apoptosis by a panel of type I and II mAbs is independent of movement of CD20 into TX-100 insoluble membrane rafts [87]. Despite this work some investigators maintain that smaller rafts, not detected by TX-100, may develop following CD20 ligation and that these remain an integral part of the signalling cascade [88, 89]. Another effect of formation of these microdomains is the provision of an optimal environment for activation of the classical complement cascade and this may account for the effectiveness of type I over type II mAb in inducing CDC.

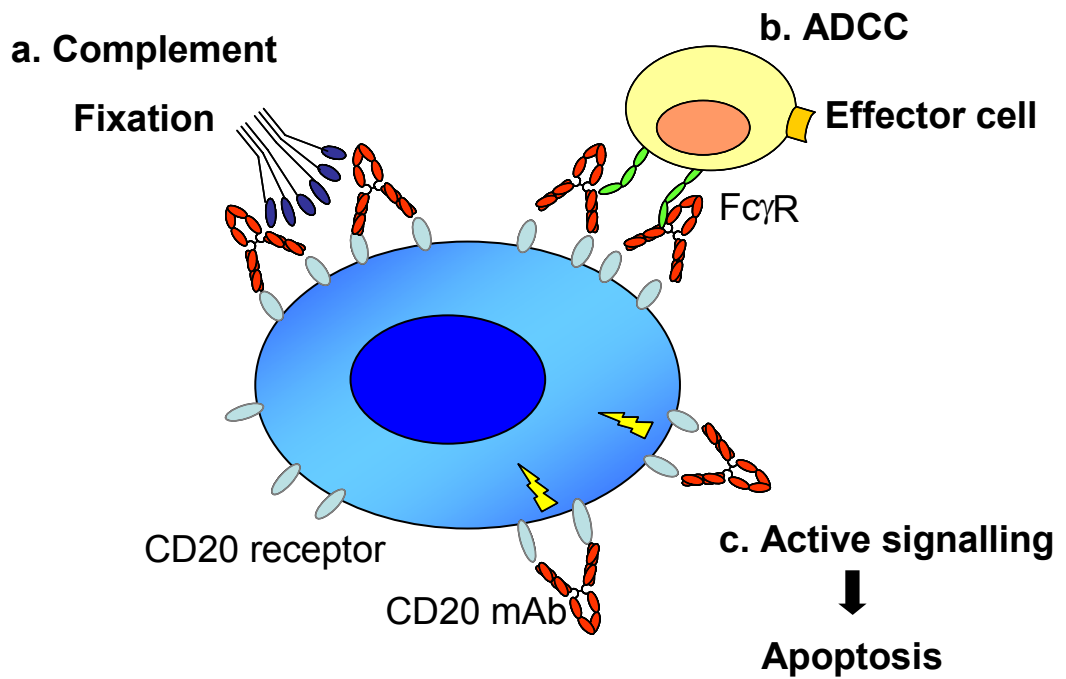


Figure 1-5 Potential mechanisms of action of CD20 mAb:

The three potential mechanisms of action of CD20 mAb are shown. **(a.)** CD20 mAb binding results in clustering of Fc domains, this allows binding of C1q and activation of the classical complement pathway. **(b.)** CD20 mAb bound to B cells can directly recruit effector cells via the FcγR receptor family. This results in phagocytosis of CD20 mAb bound cells. **(c.)** CD20 mAb *in vitro*, in the presence of crosslinking, induce cytosolic Ca²⁺ flux and can induce apoptosis. Adapted from figure by Professor MJ Glennie.

As discussed earlier CD20 mAb cytotoxic activity is mediated by three main mechanisms.

Complement dependent cytotoxicity (CDC)

CD20 mAb binding results in clustering of Fc domains, this allows binding of C1q and activation of the classical complement pathway, resulting in phagocytosis and activation of effector cells and potentially lysis via c3b and the membrane attack complex (MAC). There is conflicting literature on the importance of complement in CD20 mAb activity. Various groups have demonstrated the importance of complement pathways in tumour cell depletion in xenograft models [90, 91]. The evidence supporting the importance of complement activity *in vivo* is compelling, but not clear cut [92]. Following treatment with Rituximab, complement depletion rapidly occurs, and is implicated in infusion related toxicity. Whilst cells surviving treatment have been shown to have increased expression of CD59, a complement defence molecule.[93]

Antibody dependent cellular cytotoxicity (ADCC)

As discussed above both type I and II mAb are equally effective at inducing ADCC. FcγR are expressed on macrophages, NK cells and neutrophils, they can be both inhibitory and stimulatory and their activation results in release of cytokines, chemokines, proteases and reactive oxygen species [94]. FcγR can be activated by complement, but CD20 mAb bound to B cells can directly recruit effector cells via this receptor family, resulting in phagocytosis [95]. In mouse models FcγR activity appears to be important for CD20 activity, such that removal of FcγR activity results in loss of therapeutic activity of Rituximab [96]. This mechanism explains the rapid depletion of circulating CD20 positive cells, where FcγR effector levels are high, and slower depletion in tissues where levels are lower following mAb treatment. The importance of this mechanism is apparent in humans as well, where polymorphisms in FcγR result in differential response rates to Rituximab therapy [97].

Intracellular signalling and induction of apoptosis

This mechanism has been difficult to demonstrate *in vivo*. *In vitro* the treatment of Burkitt's lymphoma cell lines with CD20 monoclonal antibodies resulted in induction of apoptosis [85]. This effect is usually dependent on

the addition of an Fc region cross-linking agent or Fc-receptor-bearing accessory cells, and is employed in most studies of signalling events following CD20 mAb treatment [85, 98]. It is argued that cross linking *in vitro* with anti IgG antibodies or using homodimers of Rituximab mimics the action of effector cells recapitulating *in vivo* mechanisms, but this hypothesis remains unproven.

The mechanisms of cell death resulting from mAb binding appear to differ depending on the class of mAb used (review [83]). Rituximab treatment in the presence of crosslinking results in Ca^{2+} flux but this is not seen with type II mAb [99]. This appears in part to be due to 'hijacking' of the BCR signalling cascade and culminates in classical apoptosis with caspase activation and PARP cleavage [84, 85]. Recent data from *Ivanov, Beers et al* have shown that type II mAb act in an entirely different fashion [100]. They induce cell death through non apoptotic, non autophagic mechanisms, ultimately through a lysosome-dependent pathway.

The intermediate signalling events following type I mAb ligation are becoming increasingly clear. *Jazirehi et al* have demonstrated that Rituximab down regulates Bcl- X_L through modulation of the NF κ B pathway. Upregulation of Raf-1 kinase inhibitor protein (RKIP) results in inhibition of NF κ B activity and downregulation Bcl- X_L [68]. They also demonstrated that over expression of Bcl- X_L blocked the sensitizing effect of Rituximab on paclitaxel induced apoptosis, whilst pharmacological Bcl- X_L inhibitors augmented this effect [101, 102]. In support of this *Stolz et al* observed that over expression of Bcl- X_L blocked the therapeutic effect of Rituximab *in vitro* and in a xenograft model [103]. They were also able to resensitise cells by using pharmacological inhibition of Bcl-2 and Bcl- X_L .

1.5.4 Clinical trials of CD20 monoclonal antibodies

Rituximab is now well established in the treatment of all CD20 positive lymphomas, and has had a dramatic effect on outcomes. Anti idiotypic antibodies were first used in the early 1990's with some encouraging results. However these studies were hampered by the immunogenicity of these murine antibodies [104]. As technology evolved chimeric antibodies were developed with the emergence of Rituximab in animal studies and early phase clinical trials [105, 106]. Phase II studies of Rituximab 375mg/m² weekly x4 as a single agent demonstrated a response rate 46%-50% with median time to progression of 10.2 months in follicular NHL and helped to achieve FDA approval [107, 108]. Following these studies phase II trials of Rituximab in combination with chemotherapy were performed [5, 109, 110]. The subsequent randomised studies commenced to investigate the overall survival benefit of this approach, have resulted in the incorporation of Rituximab with combination chemotherapy as the first line treatment of follicular and other indolent B cell NHL [111-113]. The most recent adaptation to standard practice is the addition of maintenance Rituximab for up to two years. This has again resulted in improvements in progression free survival with an improved 5 year survival in some studies [114-117]. With the well recognised standard therapy of CHOP chemotherapy for diffuse large B cell NHL for the last 20 years, the logical approach was the addition of Rituximab to this. The pivotal study by *Coiffier et al* in 2002 [4] demonstrated an 18% benefit in 5-year event free survival for R-CHOP compared to CHOP. This impressive benefit has been recapitulated in a number of other studies, with longer term follow up confirming an overall survival benefit [118-121].

Although clinical trials of CD20 monoclonal antibodies have been dominated by the archetypal type I antibody Rituximab, other CD20 mAb have been utilised. The fully human antibody ofatumumab offers potential benefit over Rituximab in view of its in vitro efficacy especially at inducing complement activity. A phase I/II dose escalation trial resulted in excellent tolerability, B cell depletion and promising activity in pre treated follicular lymphoma [122]. Despite encouraging pre clinical data the type II antibody Tositumomab has

only been utilised in radioimmunotherapy with conjugation to Iodine¹³¹. This approach resulted in encouraging results [123], and is now being assessed in randomised clinical trials.

What is clear is that CD20 mAb have shown their most potent clinical activity when given in combination with other agents, which have classically been standard chemotherapeutic drug combinations. This effect is presumed to occur due to synergistic induction of apoptotic pathways, based on pre clinical studies [102]. There remains untapped potential in maximising the effects of these agents through potentiating apoptosis and effector cell mechanisms with novel combinations.

1.6 Novel targeted therapies for B cell NHL

1.6.1 Introduction

Understanding what molecular events drive the malignant phenotype is not only key to understanding the aetiology and mechanisms of lymphomagenesis, but has resulted in a targeted approach to treating these conditions.

Monoclonal antibodies

The CD20 monoclonal antibody Rituximab is now well established in the treatment of B cell NHL. It is widely regarded as one of the first successful targeted treatments for cancer. Other monoclonal antibodies have also shown activity in lymphoma. The clinical activity of anti CD19 antibodies have been investigated [124] with mixed responses, current studies are attempting to exploit this attractive target utilising mAb with improved ADCC function [125]. Other B cell targeting antibodies include Galiximab (anti CD80) [126], and Epratuzumab (anti CD22) [127, 128] Based on its activity in other tumour sites [129] and evidence of high levels of VEGF in 'poor responders' [130] clinical trials of the VEGF monoclonal antibody bevacizumab are also underway. Its activity as a single agent has proved disappointing [131]. Its benefit in combination with CHOP-R is currently being assessed [132]. It remains to be seen whether any of these approaches will match the outcomes from targeting CD20.

Agents targeting intracellular signalling

A novel approach is the use of inhibitors of Bcl-2 family members with a number of promising agents already in early phase clinical trial for lymphoma. The principal agents in development are ABT-737/ABT-263, the first agents with nM potency against Bcl-2 and Bcl-X_L [133]. Pre clinical studies have also demonstrated μ M EC50's against NHL cell lines harbouring t(14:18) and primary FL cells. Efficacy was also seen in xenograft studies with evidence of caspase 3 processing, consistent with the mechanism of action of this agent. ABT-737 has been superseded by ABT-263 which has oral bioavailability [134] and is in phase I/II clinical trials [www.cancer.gov]. These agents bind the hydrophobic BH3 domain binding site. This inhibits dimerisation with pro apoptotic family members leading to induction of apoptosis. One of the concerns with ABT-263 is its inability to inhibit Mcl-1 activity. A strategy to overcome this issue is combination with Obatoclax (GX015-070) which inhibits Mcl-1 dimerisation [135, 136]. However it remains to be seen what the clinical efficacy and toxicity of these agents will be alone and in combination.

Targeting the proteasome is another novel strategy that has already shown promising clinical activity in some NHL subtypes. The 26S proteasome is a major part of the ubiquitin-proteasome pathway. It is responsible for the degradation of a wide range of cellular proteins including cyclins, cyclin-dependent kinase inhibitors such as p21 and p27 and the tumour suppressor p53. Perhaps the most important target for its efficacy in NHL is I κ B [137]. As discussed earlier I κ B binds to NF κ B subunits and is degraded by poly ubiquitination via the 26S proteasome. Proteasome inhibitors have shown good pre clinical activity in MCL, with inhibition of constitutive NF κ B activation, down-regulation of bcl-2 family members Bcl-X_L and Bcl2A1 and induction of apoptosis [138]. Bortezomib (velcade) has shown promising efficacy as a single agent in clinical trials in heavily pretreated FL and MCL [139]. Interestingly in the study by *Strauss et al* response to bortezomib correlated with reduction in plasma TNF α levels, consistent with the hypothesis that inhibiting NF κ B may be important. Recent studies have

assessed the benefit of bortezomib in combination with a range of other agents including chemotherapeutics [140] and Rituximab [141].

One such combination approach is dual targeting of the NF κ B pathway with histone deacetylase inhibitors and bortezomib. Treating myeloma cell lines with bortezomib followed by vorinostat produced synergistic induction of mitochondrial injury, caspase activation, and apoptosis associated with NF κ B inactivation [142]. Similar findings were also observed in BCR/ABL positive and negative leukaemia cell lines [143]. This approach also produced synergistic cell killing in solid tumour cell lines (hepatoma and head and neck squamous cell carcinoma), again with induction of caspase mediated apoptosis [144-147]

1.6.2 Chromatin and histone modifications

Histone deacetylase inhibitors (HDI) are a novel class of anticancer agents which have moved rapidly into clinical trials. Their therapeutic activity arises from targeting chromatin regulation and the post translational modification of a rapidly expanding number of non histone proteins.

In Eukaryotic organisms DNA is coated with an equal mass of protein and stored in the nucleus[148], this protein-DNA complex is called chromatin, The protein components are called histones, which are evolutionarily conserved and equivalents have been identified in single-cell prokaryotic organisms [149]. In dividing cells this complex is seen as chromosomes, in non-dividing cells it is distributed throughout the nucleus as euchromatin (open) and heterochromatin (condensed).

Core histones are made up of an octamer of two each of H2A, H2B, H3 and H4. Core histone assembly relies on two pairs of H3 and H4 dimerising to form a stable tetramer. This in turn binds 2 dimers of H2A and H2B to form a stable octamer that binds 2 superhelical turns of DNA (165 base pairs), this structure was discovered by X-ray diffraction, to a resolution of 2.8Å [150]. Nucleosomes are joined to each other by a short segment of linker DNA, this is stabilised by histone H1, which assists in higher order structural organisation.

In the 1960s it was first described how histones control gene expression and the importance of post translational modification in the control of gene expression and hence RNA synthesis [151]. Core histones contain multiple potential sites for modification, predominantly on the tail domains [152]. It is somewhat contentiously postulated that these modifications work to create an epigenetic 'histone code', where the isolated changes in histone tails combine to create their effects on gene transcription[153]. Modifications can be methylation (on lysine and arginine residues), acetylation (upon lysine residues), phosphorylation (upon serine and threonine residues) ubiquitination or ADP-ribosylation [**Figure 1-6**].

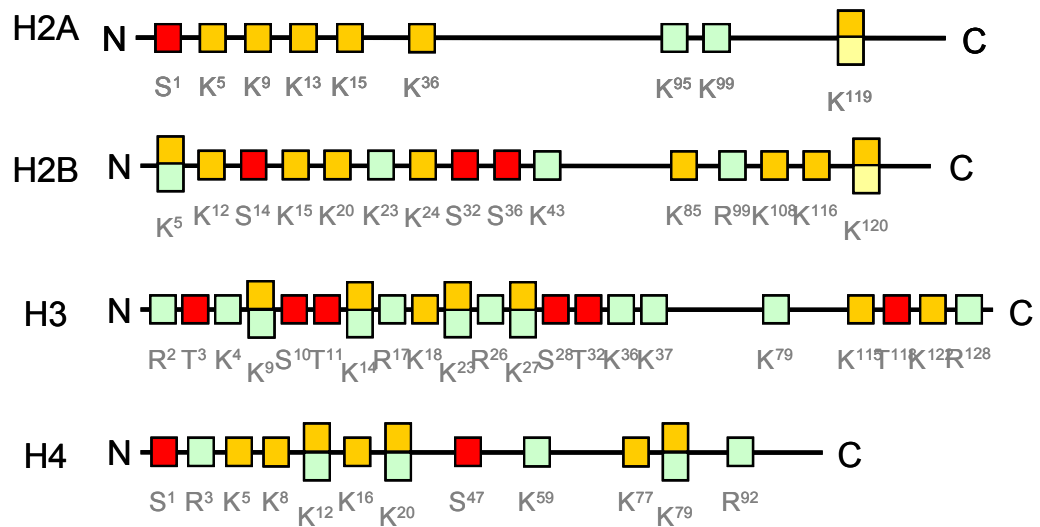
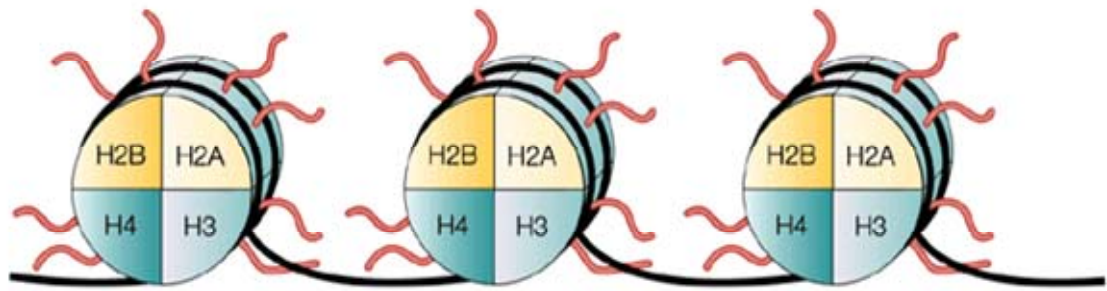


Figure 1-6: Histone structure and sites of modification:

Cartoon depicting octamer of core histones binding 2.5 turns of DNA. Sites of histone tail modification are shown. ■ Phosphorylation, ■ methylation, ■ acetylation and ■ ubiquitination. Adapted from Marks *et al* [154].

Histone modifications result in two structural effects on chromatin. Firstly modification of histone tails result in changes in electrostatic charge resulting in structural and DNA binding changes, For example studies have shown that phosphorylation of H1 reduces the DNA:H1 binding affinity, and that this is a function of changes in charge [155]. Secondly, changes in the binding surface can allow recruitment of protein complexes to sites that were previously hidden. One of the best examples of this was shown by Lachner *et al*, who demonstrated that H3K9 methylation, catalysed by the histone methyltransferase (Suv39h) facilitated a specific binding site for HP1 leading to its specific chromatin regulatory effects [156]. Through these mechanisms post translational modifications are implicated in DNA transcription, replication and repair as well as instigating chromatin conformational changes.

Of these 'marks' lysine acetylation has been one of the most studied [157] partly due to the early identification of the regulatory enzymes responsible. Histone acetyltransferases (HATs)[158] and histone deacetylases (HDACs)[159]. Dynamic acetylation and deacetylation of the lysine residues is catalysed by these complementary enzymes. It is the discovery of pharmacological inhibitors of these enzymes that has facilitated our understanding of the enzymatic effects.

The dynamic acetylation and deacetylation of lysine residues is not confined to histones[160]. An ever increasing number of proteins have been identified which undergo lysine acetylation as part of their post translational regulation [Figure 1-7]. One of the best described groups is DNA binding proteins [161-163]. For example the transcriptional repressor Bcl6, which is expressed in the germinal centre has been shown to be acetylated on lysine residues by p300 and use of the Histone Deacetylase inhibitor (HDI), Trichostatin A (TSA), demonstrated the it also binds HDAC enzymes [163]. Moreover acetylation inhibited its transcriptional repressor function. Other examples include the molecular chaperone hsp 90 [164], the structural protein tubulin[165], and nuclear import factors (importin- α family)[166].

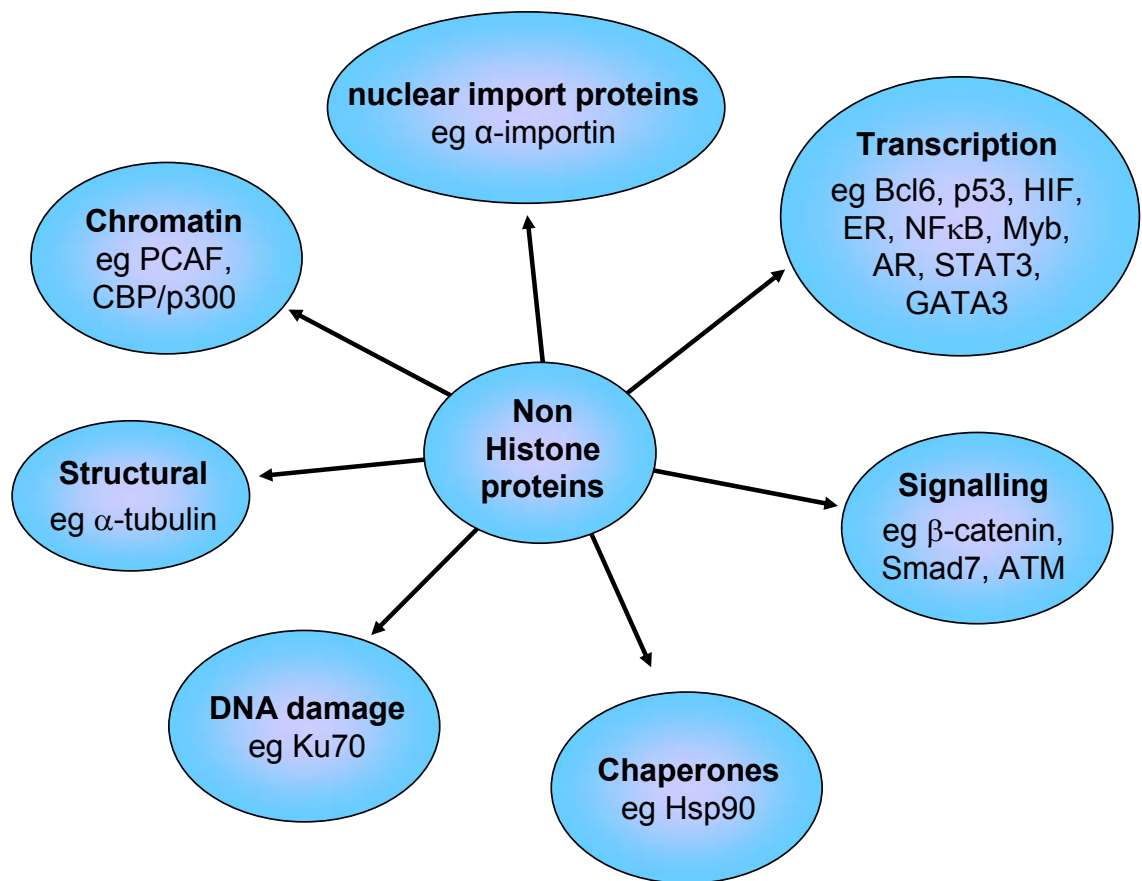


Figure 1-7 Non histone targets of HDAC enzymes:
Cartoon depicting known non Histone targets of HDAC enzymes.

1.6.3 Acetyltransferases and deacetylases

These 2 classes of enzymes regulate the lysine acetylation state of histones and other proteins [Figure 1-8]. Acetylation, catalysed by HATs, in association with transcriptional activators, neutralises the positive charge associated with the ϵ -amino group of conserved lysine residues within the NH₂ terminal domains of core histones. This decreases their DNA affinity, allowing the nucleosomes to unfold and increasing access to transcription factors, resulting in up regulation of gene expression [167-170]. HATs can be divided into three major families based on a number of structural motifs (GNAT, MYST, p300/CBP)[154].

At least 18 proteins with Zn dependent Deacetylase catalytic activity have been reported. They are divided into two families; the histone deacetylases and Sir2-like deacetylases (sirtuins). Sirtuins contains seven members, they all contain a highly conserved catalytic domain different to the conventional HDACs, consist of homologues of yeast and mouse Sir2 and require nicotinamide adenine dinucleotide (NAD⁺) as a 1:1 co-factor. The therapeutic potential of their inhibition is currently being investigated (review [171]).

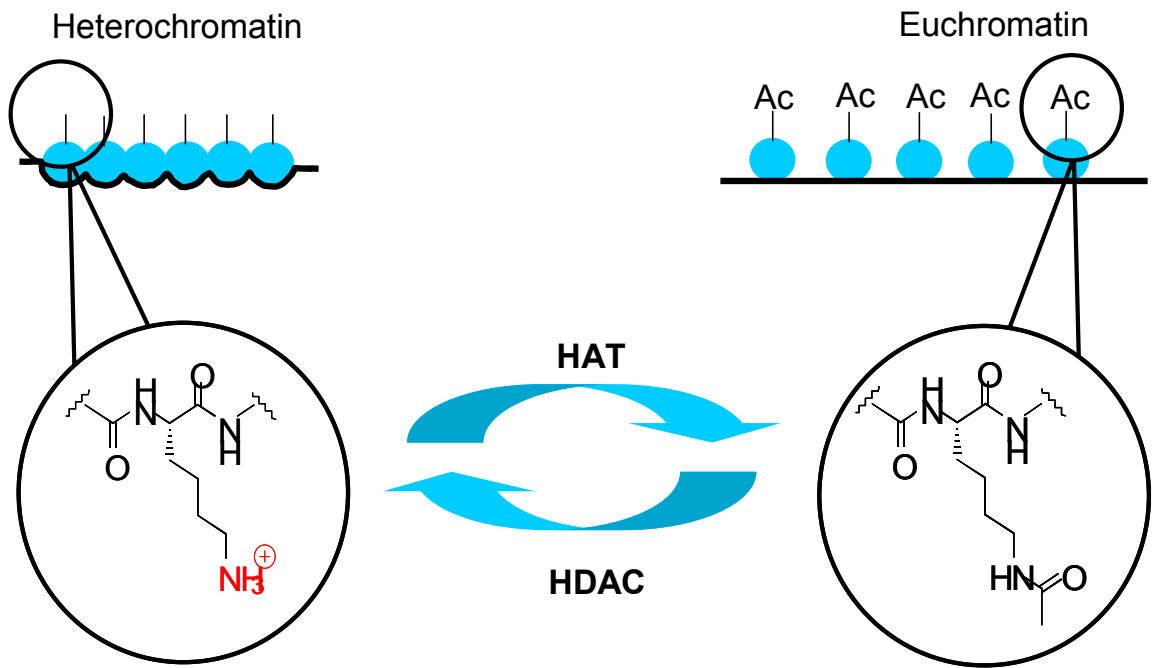


Figure 1-8 Action of HDAC and HAT enzymes:

HDACs counter the effects of HATs by hydrolysing the ϵ -amino acetyl group within core histones and restoring their positive charge at physiological pH. This results in tighter DNA binding and transcriptional repression.

1.6.4 HDAC family members

The first human HDAC (HDAC1) was isolated using its high affinity for the naturally occurring histone deacetylase inhibitor trapoxin A [159]. This tied together earlier work that had identified a cDNA homologue to yeast Rpc3, with unknown protein function [172]; demonstrated trapoxin binding to an unknown protein [173, 174]; and the histone deacetylase function of an unknown protein (Allfrey 1971).

These proteins are evolutionarily conserved from insects to humans suggesting they perform a critical function [175]. Phylogenetic analysis of bacterial HDAC suggests their development precedes that of histone proteins indicating that the primary activity of some family members may be against non histone proteins [176].

To date 11 human HDACs have been identified, this classical HDAC family is divided into three classes; HDAC1, -2, -3 and -8 (Class I, 377-488 amino acids) [177]; HDAC4, -5, -6, -7, -9 and -10 (class II, 700-1215 amino acids) and HDAC11 (class IV, 347 amino acids) [Figure 1-9]. They have a highly conserved catalytic domain containing a zinc cation and restore the positive charge to lysine residues upon hydrolysis of ϵ -amino acetyl moieties.

HDAC1 and -2 share high levels of homology, and require co-factors for their activity. They are found together in three complexes Sin3, NuRD and Co-REST, but can also directly bind DNA binding proteins [178-180]. HDAC1 knockout in mice is embryologically lethal, even with compensatory upregulation of other class I HDACs [181]. HDAC3 shares less homology but also contains the nuclear localisation sequence (NLS) seen in all class I HDACs and a nuclear export sequence (NES). It is mainly found in multiple protein complexes with N-CoR (nuclear receptor co-repressor) and SMRT (silencing mediator for retinoic acid and thyroid hormone receptors) cofactors. It appears to regulate gene expression mediated via nuclear hormone receptors [180]. It also inhibits acetylation of non histone targets, for example NF κ B [182]. In contrast to other class I HDACs, HDAC8 has not been found in these complexes, and appears to be expressed at low levels except in smooth muscle. It has also been shown that HDAC3 oligomerises with other HDACs.

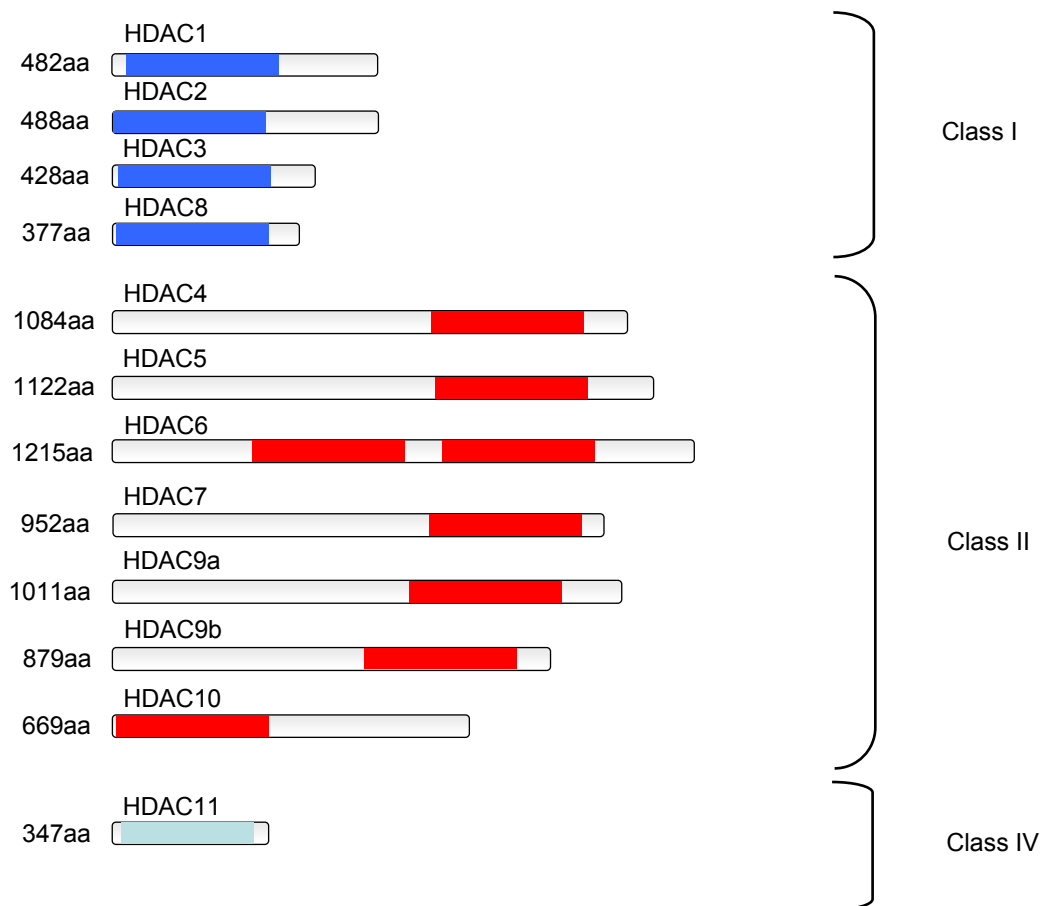


Figure 1-9 Histone Deacetylase family:

Schematic diagram of HDAC family. Class I (HDAC 1, 2, 3, 8) contain a common homology domain ■ [177]; class II (HDAC4, -5, -6, -7, -9 and -10) also share a different common domain ■. Class IV (HDAC11) has similar properties to class I and II but has a different structure.

Class II are larger proteins that shuttle between cytoplasm and nucleus, they all share a distinct homology domain. HDAC4, -5 and -7 are closely related [183]. They all contain binding domains for myocyte enhancer factor 2 (MEF2) and C-terminal binding protein (CtBP) and can interact with the SMRT and N-CoR complexes. It appears they control differentiation in muscle and cartilaginous tissue, with knock out mice dying of chondrocyte hypertrophy [184]. HDAC6 is preferentially cytoplasmic and regulates microtubule dependent cell motility [185], it also regulates HSP90 deacetylation [164]. HDAC9 exists as a number of different splice variants, allowing for different function in different cell types. HDAC10 is usually found to interact with other HDACs, and although it has some deacetylase activity it may function as a recruiter.

HDAC11 appears to share features of both class I and II but is structurally different [186]. It has been shown to have deacetylase activity, but is not found in the characteristic multicomponent complexes.

1.6.5 HDACs in tumourgenesis

It has become increasingly clear that repression of genes via HDAC over activity in these multicomponent HDAC complexes is a hallmark of many cancers [187] **[Figure 1-10]**. Trimethylation of lysine 20 (K20-H4) and loss of acetylation of lysine 16 (K16-H4), of histone 4 is commonly seen in human cancers and cancer cell lines [188]. Hypoacetylation can occur through a number of mechanisms. Firstly it may result from reduced HAT activity or aberrant HDAC activity. Aberrant HDAC activity can affect lysine acetylation on core histones as well as non histone proteins. There is evidence of overexpression of individual HDAC family members in a number of cancers. *Zhu et al* demonstrated how in some colorectal cancers overexpression of HDAC2 results from increased signalling of the APC/ β -catenin/c-Myc pathway, and that this inhibits apoptosis [189]. HDAC2 overexpression has been documented in gastric cancer [190] and cervical cancer [191]. *Huang et al* also demonstrated the functional significance of HDAC2, with knockdown resulting in increased apoptosis through upregulation of p21^{cip1/waf1} [191].

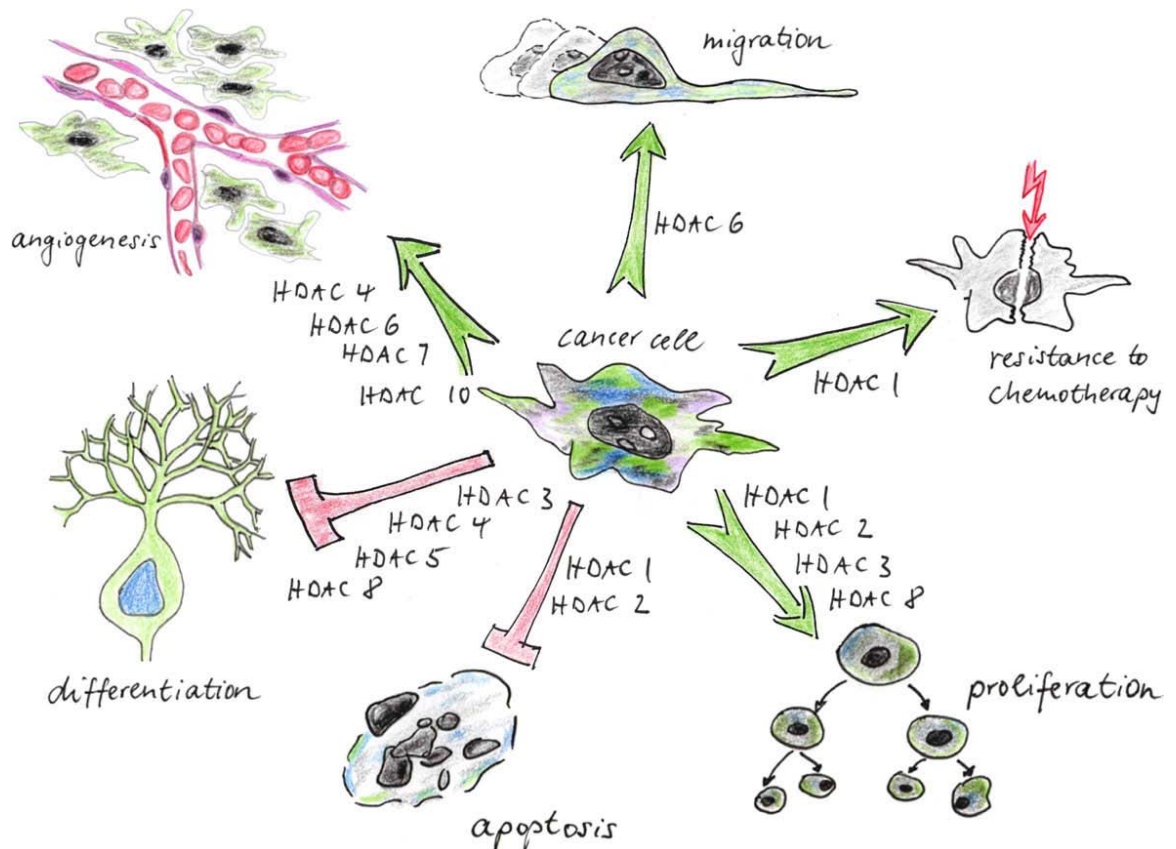


Figure 1-10 The role of HDACs in tumourgenesis:

Diagram summarising the role of HDAC family members in tumourigenesis taken from review by Witt *et al.*[192]

Overexpression of other class I HDACs is also seen. The only class II HDAC that has been shown to be overexpressed is HDAC6, although it appeared to correlate with a favourable response to endocrine therapy in breast cancer [193]. HDAC over expression is also involved in tumour progression and metastasis. Hypoxia results in over expression of HDAC1, this results in repression of the p53 and VHL tumour suppressors and over expression of HIF-1 α and VEGF [194].

A second mechanism by which HDACs are implicated in tumourgenesis is through their interaction with protooncogene fusion proteins. One of the clearest examples of this is in acute promyelocytic leukaemia (APL). APL is characterised by translocations of the retinoic acid receptor A (RARA) gene most commonly with the PML gene. The resulting fusion protein transcription factor has enhanced co-repressor binding properties, increasing HDAC and DNA methyltransferase recruitment. This aberrant retinoid signalling results in potent transcriptional silencing of target genes maintaining the malignant phenotype [195]. Another example of this is in AML where the AML-1/ETO fusion protein resulting from the t(8:21) translocation, represses transcription through recruitment of HDACs [196].

A third mechanism by which HDACs are implicated in tumourgenesis is through their interactions with non histone proteins. As discussed earlier transcription factors (e.g. p53, NF κ B, Bcl-6, Bcl-2, HIF, and VEGF), nuclear binding proteins, molecular chaperones, and cytoskeletal proteins are all known to require acetylation for their activation and regulation. Many of these molecules are under or over expressed in malignant phenotypes. p53 was one of the first of these non histone proteins shown to be regulated by acetylation. It has been shown that mutation of K120 to arginine, which occurs in some cancers, results in loss of acetylation at that site rendering p53 unable to activate proapoptotic genes, suggesting other mechanisms of deacetylation may also have a similar effect [197]. Acetylation is also important for P53 stability in that lysine residues are also prone to ubiquitination; deacetylation of these residues allows ubiquitin binding and degradation reducing p53 stability.

This evidence linking aberrant HDAC activity with cancer has provided a clear rationale for exploring the effects of HDIs as anti cancer agents.

1.6.6 HDAC inhibitors (HDIs)

HDIs were first identified in the literature in the 1970's [198, 199], n-Butyrate was shown to reversibly inhibit partially purified HDAC and cause accumulation of acetylated histones in the nucleus [200]. It was the discovery of these inhibitory compounds that enhanced our understanding of HDAC function and led to the development of more specific synthetic inhibitors. HDIs are structurally diverse, but all chelate the Zn atom in the active site of Class I and/or II HDACs, thereby blocking enzyme activity. These inhibitors conform to a common pharmacophore, comprising a "linker" mimicking the side chain of lysine, and a "cap" structure of variable size that makes additional covalent interactions around the rim of the enzyme active site **[Figure 1-11A]**. Their potency and selectivity varies greatly mainly due to the strength of these covalent interactions, the more potent molecules have an aliphatic chain, which very closely mimics the lysine side chain and interacts tightly with the Zn atom, and a hydrophobic "cap" which interacts with the catalytic pocket. Less potent compounds have an acyl group which interacts less tightly with the Zn atom and cannot interact with the catalytic pocket. As well as these structural differences affecting their enzymatic potency, there is also evidence that a reduction step is necessary for the activity of FK228 [201] **[Figure 1-11B]**.

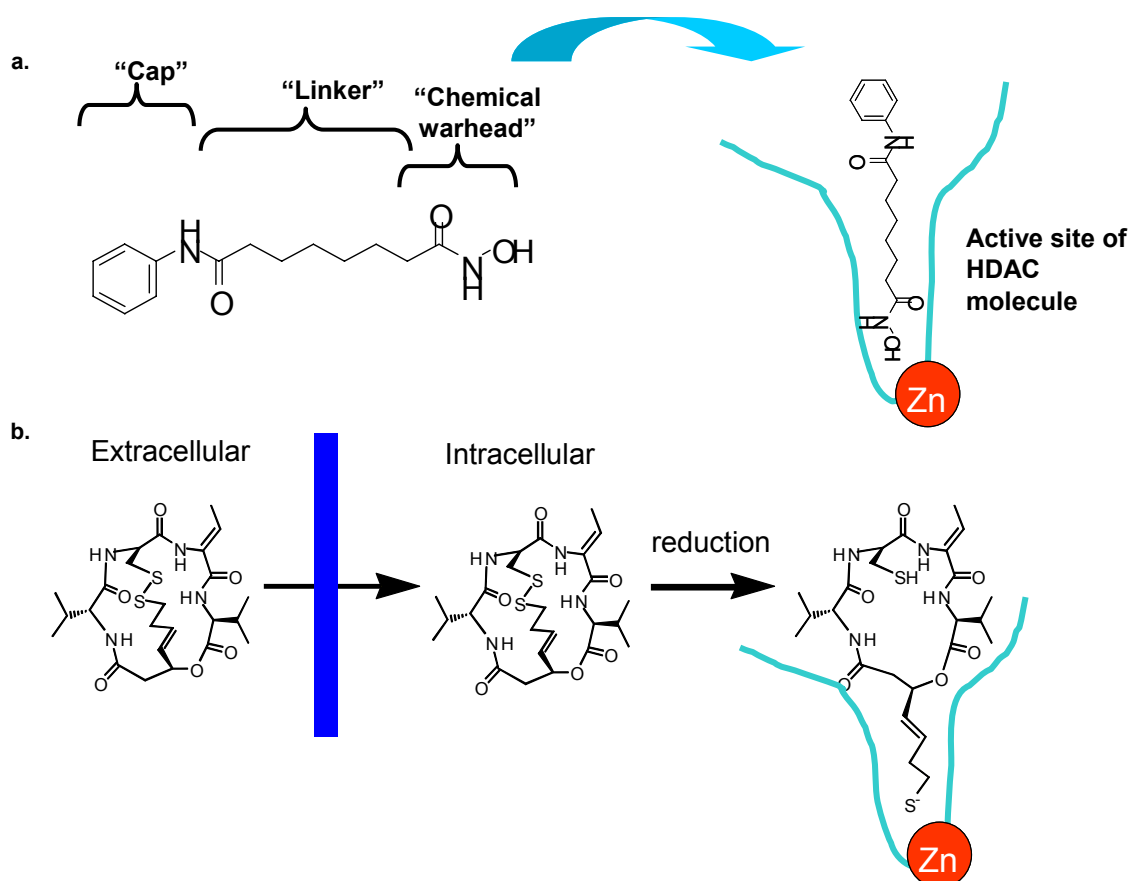


Figure 1-11 Structure of HDI molecule:

Basic structure of HDI molecule, with cartoon depiction of Zn binding at HDAC enzyme active site. Molecules shown are **(A.)** SAHA (vorinostat). **(B.)** FK228 (depsipeptide) requires intracellular reduction to facilitate effective binding within enzymatic groove, adapted from *Furumai et al* [201].

HDI are divided into a number of classes based on their structure (**Table 1-2**)

Trichostatin A (TSA), a naturally occurring hydroxamate, was originally identified as a fungistatic antibiotic in 1976 [202]. It was subsequently shown to induce histone acetylation resulting in Friend leukaemia cell differentiation as well as causing G1 and G2 arrest [203]. This class includes suberoylanilide hydroxamic acid (SAHA), Cinnamic acid bishydroxamic acid (CBHA), LAQ-824, sulphonamide hydroxamic acids and oxamflatin.

SAHA is a less complex molecule than TSA, and has a 30-fold weaker inhibitory activity. It contains the crucial hydroxamic acid group which inserts into the hydrophobic pocket and binds to the zinc atom. This aliphatic chain fits less snugly into the pocket and this together with the phenyl-amino ketone group cap accounts for the weaker inhibition than TSA [204]. Studies have shown SAHA to have antitumour activity *in vitro*, *in vivo* and in phase I/II clinical trials [154, 205]. SAHA gained FDA approval for the treatment of cutaneous T cell lymphoma (CTCL) in 2007.

Cyclic peptides are the next most developed class in terms of clinical trials.

These are the most structurally complex class, with potency at nanomolar concentrations. depsipeptide (FK228) has also shown good activity in CTCL [206], and solid tumours. Aliphatic Acids are the weakest of HDIs, only active at millimolar concentrations. This class includes the anticonvulsant valproic acid and phenyl-butyrate. The compounds in this group have an acyl group which interacts with the zinc atom but cannot interact with the catalytic pocket, resulting in reduced potency. The Benzamide class includes the agents MS275 and MGCD0103. They are both less potent than the corresponding hydroxamic acids and cyclic tetrapeptides, but are class I HDAC selective. These agents are also currently in a multitude of phase I and II studies.

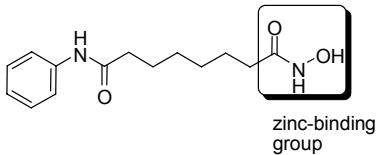
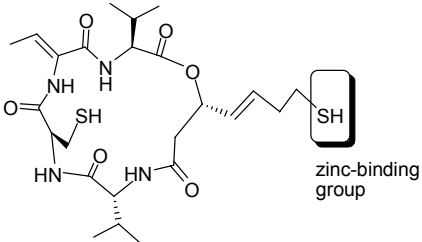
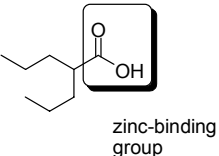
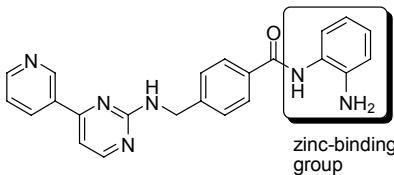
compound	Class	HDAC class selectivity	potency	Structure
SAHA (Vorinostat) Merck	Hydroxamate	I, II, IV	~μM	
FK228 (Romidepsin) Gloucester	Cyclic peptide	I	~nM	
Valproic acid	Aliphatic acid	I, II	~mM	
MGCD0103 MethylGene	Benzamide	I	~μM	

Table 1-2 HDAC inhibitors in clinical development.

Mechanisms of action

As can be predicted from the function of HDAC enzymes, HDIs cause accumulation of acetylated histone and non histone proteins by blocking the deacetylation catalysed by the HDAC family of enzymes. The reasons behind their differential toxicity between normal and malignant cells are not fully understood.

Expression profiling has shown that in the presence of HDAC inhibitors only a small number of genes show altered expression (2-10 %) [207-210], with both up regulation and down regulation of genes, which is surprising considering their transformation of chromatin into an open state. Interestingly it seems that there are a core set of genes which are persistently regulated across different cell lines and with different HDI (for example p21^{waf1}), there are also reproducible changes which are cell line and HDI specific [210, 211]. The overall effect on cells is to induce terminal differentiation, cell cycle arrest and apoptosis, through regulation of gene expression [212]. For example in MCF-7 cells incubated with SAHA, differentiation was confirmed by the presence of milk fat proteins [213]. Cell cycle arrest (G2M) was observed by microscopy. Interestingly these changes were reversed within 24 hours of removal of the drug.

The ability to induce apoptosis appears to be cell line and HDI specific. Gene expression studies in CEM and Jurkat cells have demonstrated regulation of genes from the intrinsic apoptotic pathway, as well as genes associated with regulation of this pathway [211]. The role of the intrinsic pathway is supported by other investigators [214, 215]. In contrast to this there is evidence that the extrinsic pathway can also be modulated albeit in combination [216]. The role of caspases in B cell NHL has also been questioned [217]

Induction of apoptosis can also occur as a result of acetylation of non histone proteins. In Bcr-Abl positive CML K562 cells, inhibition of HDAC6 by LAQ824 resulted in depletion of HSP90 client proteins [164].

HDIs have been utilised as single agents in a large number of early phase clinical trials. The first clinical reports of HDI activity were published in 2001 with a case report of a complete response to FK228 (depsipeptide) in a patient with CTCL [218]. Until recently SAHA and FK228 were the two most advanced agents in clinical development. Phase I studies have shown SAHA to be well tolerated in intravenous and oral preparations. Dose limiting toxicities were diarrhoea, nausea and vomiting, fatigue, dehydration, anorexia and myelosuppression [205, 219-221]. Based on these studies the maximum tolerated dose (MTD) was 400mg daily or 200mg twice daily for continuous dosing or 300mg twice daily for three days per week. Phase II studies in CTCL [222, 223] have shown response rates of 24.2% and 29% in heavily pretreated patients and have formed the basis for the FDA approval. FK228 has also shown its most promising activity in CTCL. As a result of the studies discussed SAHA was licensed in 2006 for the treatment of CTCL. More recently early phase studies of 'second generation' HDI have been published. The isoform specific HDI MGCD0103, which targets class I HDACs, was well tolerated in solid tumours but showed limited anti tumour activity [224]. This agent has shown more promising activity in haematological malignancies, but its benefit over SAHA remains to be seen [225]. One of the overriding issues from these studies was the poor correlation between the pharmacokinetic (PK) and pharmacodynamic (PD) endpoints. Universally histone acetylation has been used as a PD endpoint. It has been measured by a number of techniques including western blotting, ELISA and confocal microscopy. More recently an *in vitro* HDAC enzyme assay has also been used [224]. In the study by Kelly *et al* there was 2 fold increase in histone acetylation at the MTD, but this had fallen at the 8 hour timepoint [205]. In the recent study of MGCD0103 1.3 to 1.5 fold histone acetylation was detected using an ELISA [225]. There is a clear need for a more robust biomarker of HDI target effect. Current clinical and preclinical studies are concentrating on their activity in combination with other agents.

1.6.7 HDAC inhibitors in combination

HDIs have been tested in combination with a variety of conventional cytotoxic chemotherapeutic agents, monoclonal antibodies, anti hormonal therapies and other epigenetic modifiers [226]

Conventional cytotoxics

The most robust combinations with chemotherapeutics have been seen with topoisomerase I inhibitors (camptothecin, irinotecan, topotecan) topoisomerase II inhibitors (epirubicin, doxorubicin, etoposide, mitoxantrone). This approach has been used *In vitro* [227, 228] and in breast cancer xenograft models [228, 229]. A phase I clinical trial of VPA combined with epirubicin showed a 22% partial response rate in multiply pre-treated solid malignancies with acceptable toxicity [230]. A phase II trial combining VPA with chemotherapy (5FU, epirubicin and cyclophosphamide) is currently recruiting in metastatic breast cancer [231]. These effects are underpinned by compelling mechanistic data. For example, with reference to topoisomerase II inhibitors, HDAC1 and 2 have been shown to bind and interact with topoisomerase II, and form an integral part of the NuRD complex [232, 233]. It appears that Pre-exposure of breast cancer cells to vorinostat for 48 hours is needed to induce synergistic apoptosis, increase nuclear epirubicin levels and increase DNA damage. Shorter pre-exposure periods abrogated synergy and exposure after chemotherapy resulted in antagonistic effects, implying that HDI relaxation of chromatin allows greater access for topoisomerase II inhibition. Expression of the chemotherapeutic target may also be crucial as potentiation was lost in topoisomerase II null cells if the HDI was combined with epirubicin but not topotecan [234]. Conversely sequencing was also important for combination with topoisomerase I inhibition but with apparent benefit for HDI exposure after the chemotherapeutic to exploit cell cycle effects of each agent. Potentiation has been shown for an HDI added 24 to 48 hours after camptothecin in breast and lung cancer cells [235]. Cells arrested in G2-M by camptothecin appeared most sensitive to subsequent HDI addition possibly through HDI induced decreases in cyclin B levels, and of the anti-apoptotic proteins XIAP and survivin. These findings suggested reduced expression of these anti-

apoptotic factors could increase efficacy of topoisomerase I inhibitors if given in a sequence that does not prevent tumour cell progression through S phase [235]. Enhancement of cisplatin induced apoptosis by HDIs in oral squamous cell carcinoma [236, 237] and Taxanes in endometrial cancer and breast cancer [238, 239].

Agents targeting the epidermal growth factor receptors

Another encouraging approach is combination with agents targeting the HER family of receptors. Trastuzumab, a humanized monoclonal antibody to the HER2 extra cellular domain, is effective for those with receptor over expression, however optimization of HER2 targeted therapy and avoidance of resistance mechanisms is required [240]. *In vitro* studies indicate that HDI have single agent activity in HER2 over expressing breast cancer cell lines including attenuation of HER2 expression, its tyrosine kinase activity, its cell membrane localisation and dimerization with HER3. [238, 241, 242].

Combination with trastuzumab produced synergistic induction of apoptosis [238, 242]. Synergy may result from counteracting HER2 over expression as HDAC inhibition reduced HER2 mRNA transcript expression and induced HER2 protein degradation [241-243]. The latter mechanism occurred via acetylation of heat shock protein (HSP) 90 causing its inactivation and loss of multiple HSP90 client proteins. HSP90 acetylation decreased ATP binding inducing a shift from HER2 binding with HSP90 to HSP70, resulting in HER2 targeting for ubiquitination and proteasomal degradation [242]. On the basis of these *in vitro* data, clinical trials of trastuzumab and HDI combinations are in progress for locally advanced and metastatic breast cancer .

It remains unproven to what degree synergism between HDIs and trastuzumab in HER2 positive breast cancer models might also apply to other HER2 directed therapeutics which are in various stages of clinical testing [240]. However, inhibition of proliferation, apoptosis and signalling inhibition were potentiated when vorinostat was co-administered with the pan-HER tyrosine kinase inhibitor CI-1033 in breast as well as prostate and head and neck squamous carcinoma cells [241].

Regarding other members of the HER family, in non small cell lung cancer (NSCLC), synergy has been shown between HDIs and the HER1 (EGFR) tyrosine kinase inhibitors erlotinib and gefitinib [244, 245]. HDACs are recruited by transcriptional repressors such as Slug/Snail and ZEB1 which are implicated in resistance mechanisms to these agents and gefitinib sensitivity appeared to be restored in NSCLC cell line models of gefitinib resistance when combined with an HDI [245]. In a separate study, HSP90 acetylation and reduced association with HER1, Akt, and STAT3 was seen in cell lines harbouring HER1 kinase mutations following exposure to HDIs leading to apoptosis. Conversely, little effect on apoptosis was seen in cells not dependent on HER1 through kinase mutations. Therefore, HER1 mutation status might be a predictive factor for HDI combination with HER1 inhibitors in this setting [244]. This highlights the value in dissecting the mechanisms underlying beneficial combinations to allow for rational targeting of appropriate cancer phenotypes early in clinical development.

Proteasome inhibitors

Proteasome inhibitors act by binding within the catalytic 26S core of the proteasome, resulting in the build up of proteins targeted for degradation. Cancer cells appear more likely to accumulate misfolded proteins than normal cells producing a therapeutic window with promising activity in haematological malignancies [246]. Evidence exists regarding synergistic interactions with HDIs. Treating myeloma cell lines with bortezomib followed by vorinostat produced synergistic induction of mitochondrial injury, caspase activation, and apoptosis associated with NFκB inactivation [142]. Similar findings were also observed in BCR/ABL positive and negative leukaemia cell lines [143]. Interestingly this approach also produced synergistic cell killing in solid tumour cell lines (hepatoma and head and neck squamous cell carcinoma), again with induction of caspase mediated apoptosis [144, 145]. Combined HDAC-proteasomal inhibition may be effective because both interact with NFκB pathways. Proteasome inhibitors cause accumulation of IκBα increasing its NFκB binding, thereby preventing nuclear localisation and activation of NFκB target genes. NFκB subunits are acetylated at multiple lysine residues by p300/CBP acetyltransferases. Acetylation of different residues regulates different NF-κB functions (including transcriptional

activation, DNA binding affinity, I κ B α assembly and sub-cellular localization) and HDIs manipulate gene expression patterns resulting from NF- κ B activation both via direct NF- κ B subunit acetylation and indirectly through chromatin remodelling [146, 147].

Retinoic acid

Another combination approach for targeting aberrant gene silencing directly is with retinoic acid in acute promyelocytic leukaemia (APL). APL is characterised by translocations of the retinoic acid receptor A (RARA) gene most commonly with the PML gene. The resulting fusion protein transcription factor has enhanced co-repressor binding properties increasing HDAC and DNA methyltransferase recruitment. This aberrant retinoid signalling results in potent transcriptional silencing of target genes. All trans-retinoic acid (ATRA), alone or combined with chemotherapy, is effective in reversing this silencing but resistance may occur. Addition of an HDI to this combination is logical in view of the enhanced co-repressor binding and HDAC recruitment by RARA-fusion proteins. HDI therapy alone does not induce differentiation in APL but can induce this in retinoic acid resistant cell lines when the two agents are combined [247]. In APL, this approach requires clinical testing to prove its effectiveness over retinoic acid treatment alone. In acute myeloid leukaemia (AML) or myelodysplastic syndrome (MDS) unsuitable for, or relapsed following, conventional therapy, combined VPA and ATRA has produced modest efficacy in phase I/II clinical trials [248, 249].

HDIs may be of value in combination with hormonal therapy for breast cancer. They potentiate the anti-proliferative effects of the selective oestrogen receptor (ER) modulators tamoxifen and raloxifene, the pure anti-oestrogen fulvestrant and the aromatase inhibitor letrozole in breast cancer cell lines. Interestingly the partial agonist effect of endometrial adenocarcinoma cell proliferation induced by tamoxifen was blocked by HDI co-administration [250]. In further work, treatment with an HDI rendered formerly unresponsive ER α negative breast cancer cells responsive to tamoxifen. The HDI enhanced overall ER transcriptional activity in these cells. Interestingly this appeared to be by inducing expression and nuclear translocation of ER β but not ER α . Reduction of ER β expression by short

interfering RNA abrogated this HDI-induced sensitization effect [251]. Other evidence exists that DNA methylation and histone deacetylation interact to maintain a repressive chromatin complex at the ER promoter. Inhibition of either may be sufficient to activate the silenced ER gene [252]. Clinical investigation following from these observations is in progress.

HDI combination with targeted agents for BCR/ABL positive leukaemia

The role of HDIs in combination with agents targeting the BCR/ABL oncoprotein has been investigated in chronic myeloid leukaemia (CML) where the BCR/ABL tyrosine kinase inhibitor imatinib is now standard therapy but resistance can develop. In vitro, vorinostat has been shown to synergistically enhance the activity of imatinib and the second generation agent dasatinib possibly via inhibition of HSP90 chaperone function. In addition to down regulation of BCR/ABL expression, multiple perturbations in signalling and cell cycle-regulatory proteins are induced by this combination including the Ras/Raf/MEK/ERK, Akt, STAT and JNK pathways and cyclin D1 [253, 254]. Subsequently, combination of HDI with sorafenib, an inhibitor of multiple kinases including Raf-1, platelet-derived growth factor, vascular endothelial growth factor receptors 1 and 2, and FLT3, was found to induce synergistic cell death in BCR/ABL positive cells, imatinib resistant cells and primary CD34+ bone marrow cells from CML patients [255].

Interestingly, both imatinib and sorafenib blocked HDI mediated induction of p21WAF1/CIP1, perhaps the most consistently observed HDI downstream molecular effect. Forced expression of p21WAF1/CIP1 depleted the combined HDI/sorafenib effect, implying that this may be required for synergism. Potential mechanisms include disruption of p21WAF1/CIP1 mediated G1 arrest, interference with its direct anti-apoptotic actions such as inhibition of caspase-3 or c-Jun NH2-terminal kinase activation or disruption of the upstream Raf/MEK/ERK axis. [254, 255].

Other epigenetic modifiers

One reason for the relatively modest number of genes affected by HDIs is the dominant effect of methylation status over acetylation. Dual administration of HDIs with DNA hypomethylating agents is therefore of interest. Aberrant DNA methylation is characteristic of a number of myeloid leukaemias [256]

and dual epigenetic modulation might allow suppression of the malignant clone. In vitro, combination of VPA and 5-aza-2'-deoxycytidine (decitabine) produced synergistic growth inhibition and induction of apoptosis in leukaemia cell lines [257]. In a subsequent phase I/II clinical trial of this combination, 54 patients with AML or high risk MDS, either relapsed or unsuitable for first line chemotherapy, received a fixed dose of decitabine and escalating doses of VPA. Twelve (22%) had objective responses with 10 complete remissions. Major cytogenetic response was documented in 6 of 8 responders. Of five target genes investigated, hypomethylation of the key cell cycle regulating gene p15INK4B was found to be the best indicator of response. Pre-treatment p15 methylation was significantly lower in responders versus non-responders, however neither the absolute or percentage change in p15INK4B methylation was statistically significant and responses were not correlated with induction of H3 or H4 acetylation [258]. In another study, utilising phenylbutyrate and 5-azacytidine in a similar patient population, 11 of 29 patients responded. Furthermore, 6 of 6 with pre-treatment methylation of p15INK4B or CDH-1 (E-cadherin) promoters reversed methylation during the first cycle of therapy whereas none of 6 non-responders showed any demethylation [259]. Further identification and validation of predictive biomarkers would be of immense value in the ongoing clinical assessment of HDIs in this and other settings but may need to be tumour and combination specific.

2 Materials and methods

2.1 Materials

2.1.1 Cancer cell lines

Ramos, Akata 6, SU-DHL-4 and RL cell lines were a gift from Professor Packham, DoHH2 cell line was a gift from Professor Stevenson. Ramos cells stably transfected to overexpress Bcl-2 were a kind gift from Dr M Cragg. All cell lines were maintained in logarithmic growth in a humidified cell incubator (HERA Cell, Heraeus) at 37°C and 5% CO₂ with cell density between 2.0×10^5 and 1.0×10^6 . Complete growth medium of RPMI (Roswell Park Memorial Institute 1640 medium, Invitrogen, UK) supplemented with 10% (v/v) heat inactivated fetal calf serum (FCS, Invitrogen, UK), 2.0 mM L-glutamine (Invitrogen, UK) and 1.0 mM sodium pyruvate was used. Cell viability was assessed using Trypan blue exclusion prior to their usage.

This panel of B cell NHL cell lines was selected as they have been routinely used to investigate the *in vitro* activity of Rituximab. They were all initially used to investigate for synergistic cell killing, but subsequent studies utilised predominantly the SU-DHL-4 and Ramos cell lines.

2.1.2 Peripheral Blood Mononuclear Cells (PBMCs)

10ml whole blood was collected from volunteers into EDTA collection tubes (BD, UK) in accordance with local ethics procedures. 5mls of lymphoprepTM (AXIS-SHIELD Poc AS, Norway) was placed in a Falcon tube (BD, UK) and 5 mls of whole blood was layered on top. Samples were centrifuged at 2500 RPM (1349Xg) for 15 minutes and the interphase was removed to a fresh Falcon tube. This was washed twice in complete medium and cells were resuspended in complete medium at 1.0×10^6 cells/ml prior to utilisation.

2.1.3 Laboratory animals

Severe combined immunodeficient (SCID) mice (CB17 strain), bred locally, were kept under standard conditions in accordance with local ethics policy.

Cell line	Source	Notes
Ramos	Professor G. Packham	Burkitt's lymphoma
Bcl-2 Ramos	Dr M Cragg	Burkitt's lymphoma
RL	Professor G. Packham	Diffuse large B cell Non Hodgkin's lymphoma
SU-DHL-4	Professor G. Packham	Diffuse large B cell Non Hodgkin's lymphoma
Dohh2	Professor F Stevenson	Transformed follicular lymphoma
Akata 6	Professor G. Packham	Burkitt's lymphoma

Table 2-1 Cell lines used for this work:

Cell lines were sourced as indicated. All cell lines were originally sourced from the European Collection of Cell Cultures (ECACC) or the American Type Culture collection (ATCC).

2.1.4 Solutions

RIPA Lysis Buffer (5X Concentrate)

NaCl	0.75 M
IGEPAL (Sigma, U.K)	5 % (v/v)
Sodium Deoxycholate	2.5 % (w/v)
Sodium Dodecyl Sulphate	0.5 % (w/v)
Tris Hcl pH 8.0	0.25 M

Protein Running Buffer

Tris HCl	25 mM
Glycine	200 mM
Sodium Dodecyl Sulphate	0.1 % (w/v)

Protein Transfer Buffer

Tris HCl	25 mM
Glycine	200 mM
Sodium Dodecyl Sulphate	0.1 % (w/v)
Ethanol	25 % (v/v)

Tris-Buffered Saline (TS)

Tris-HCl pH 8	10 mM
NaCl	150 mM

Tris-Buffered Saline – Tween (TS-T)

Tris-HCL pH 8	10 mM
NaCl	150 mM
Tween 20	0.1 % (v/v)

Phosphate Buffered Saline (PBS)

NaCl	125 mM
Sodium Phosphate	16 mM
Sodium Hydrogen Phosphate	10 mM
pH 7.3	

Phosphate Buffered Saline – Tween (PBS-T)

NaCl	125 mM
Sodium Phosphate	16 mM
Sodium Hydrogen Phosphate	10 mM
pH 7.3	
Tween 20	0.1 % (v/v)

2.1.5 Investigational compounds and reagents

HDAC inhibitors

1. SAHA (Alexis Biochemicals, UK)
2. FK228 was a kind gift from Dr Minoru Yoshida, RIKEN, Japan

These were diluted in DMSO and aliquots were stored at -20⁰c

CD20 monoclonal antibodies

1. Rituximab was a kind gift from Southampton University Hospital Trust pharmacy
2. B1 was a kind gift from Professor MJ Glennie [90]

These were diluted in PBS and stored at 4⁰c.

Cross linking agent

1. Rabbit anti Human IgG1 cross linking agent was a kind gift from Professor MJ Glennie

This was diluted in PBS and stored at 4⁰c

2.2 Methods

2.2.1 Propidium iodide exclusion assay

This assay is routinely used for assessing levels of cell death. Cells are stained with propidium iodide (PI), apoptotic or dead cells allow PI to enter where it binds DNA resulting in a 20-30 fold increase in fluorescence, live cells have impermeable membranes so display no change in fluorescence.

This assay was performed in 96 well plates (Greiner, UK). Cells suspended in 100µl complete medium were plated in each well (4.5×10^4 /well). These were incubated for 48 hours with investigational agents in a humidified cell incubator. Following this cells were resuspended and transferred to Falcon tubes (BD, UK) prior to centrifugation at 1500 rpm (486Xg) for 5 minutes. Medium was removed and cells were resuspended in 400µl of 10µg/ml propidium iodide (PI) solution (Sigma, UK) and incubated in the dark at room temperature for 15 minutes. Levels of cell death were measured by flow cytometry, with the proportion of dead cells calculated relative to the live cell peaks. Control samples were treated with complete medium or the corresponding dilution of DMSO or PBS.

2.2.2 Apoptosis Assays

A flow cytometry based assay was used for measuring levels of apoptosis. Phospholipid phosphatidylserine (PS) translocation from the inner to the outer leaflet of the plasma membrane is one of the earliest events identified in cells undergoing apoptosis. Annexin V, a 35-36 kDa, Ca^{2+} -dependent, phospholipid binding protein with a high affinity for PS is used to identify cells in the early stages of apoptosis. Cells are co stained with FITC conjugated Annexin V and PI this allows measurement of early and late apoptosis.

These assays were performed in 96 well plates (Greiner, UK). Cells suspended in 100µl complete medium were plated in each well (4.5×10^4 /well). They were incubated for different times with investigational agents in an humidified cell incubator. Following this cells were resuspended and transferred to Falcon tubes (BD, UK) prior to centrifugation at 1500 rpm

(486Xg) for 5 minutes. Following this cells were resuspended and transferred to Falcon tubes (BD, UK) prior to centrifugation at 1500 rpm (486Xg) for a further 5 minutes. Medium was removed and cells were resuspended in 300 μ l annexin V binding buffer (BD, UK) with 2.5 μ l (50 μ g/ml) PI and 2.5 μ l FITC labelled annexin V (Annexin V:FITC Apoptosis Detection Kit I, BD, UK). Cells were subjected to flow cytometry with levels of early and late apoptosis measured as a percentage of all cells, and normalized to levels in untreated cells.

2.2.3 Western Blotting

Western blotting is a method to detect the levels of a specific protein in a given sample. Samples are subjected to gel electrophoresis to separate native or denatured proteins by the length of the polypeptide. The proteins are then transferred to a nitrocellulose membrane, where they are detected by a specific antibody and a labeled conjugated secondary antibody.

Sample preparation

Whole cell lysates

2x10⁶ cells were treated in 24 well plates for different time periods, and then harvested and transferred to Falcon tubes. Samples were then centrifuged at 1500 RPM (486Xg) for 3mins at 4°C. Samples were washed once with ice cold PBS, recentrifuged and the supernatant removed leaving the cell pellet. Cell pellets were snap frozen in liquid nitrogen and stored at -80°C. Cell lysis was performed with addition of 50 μ l 3X reducing SDS loading buffer per 1x10⁶ cells (1/10 volume 30X Reducing Agent to 1 volume of 3X SDS, Cell signalling, USA) used prior to sonication (Sonicator 3000, Misonix, Inc., USA), samples were stored at -80°C until required.

RIPA cell lysis

2x10⁶ cells were treated in 24 well plates for variable time periods, and then harvested and transferred to Falcon tubes. Samples were then centrifuged (Heraeus Biofuge Fresco, Rotor F-8134) at 1500 rpm (486xg) for 3mins at

4°C. Supernatant was removed and cell pellet was washed once with ice cold PBS, recentrifuged and the supernatant removed leaving the cell pellet. Pellets were re-suspended in 100 µl of 1X RIPA buffer and incubated on ice for 30 minutes. Samples were then subject to centrifugation at 4 °C for 20 minutes at 12000 rpm (13700xg) (Heraeus Biofuge Fresco, Rotor F-8134). The supernatant was transferred to new 1.5 ml eppendorf (Griener, U.K) and the cell debris discarded. Samples were subject to protein quantification using Bio-Rad protein assay reagent (Bio-Rad, U.K) and a BSA standard curve. Protein concentrations were equalised by addition of 1X RIPA.

Immunoblotting

Samples were heated at 95°C for 3 minutes and 15µl was loaded onto a pre cast 4-15 % gradient tris HCl SDS- polyacrylamide gel (Bio-Rad, UK). Electrophoresis was carried out at 200Volts for 30-45 minutes, using MiniProtean III apparatus (Bio-Rad, UK) in protein running buffer. Protein was transferred from polyacrylamide gel onto nitrocellulose membrane (Protran, Schleicher and Schuell, Germany) using MiniProtean II apparatus at 100 Volts for 1 hour.

Nitrocellulose was blocked in non fat marvel milk for one hour, incubation with primary antibodies were overnight at 4⁰C, incubation with the appropriate secondary antibodies was for one to two hours at room temperature. Nitrocellulose was treated with HRP substrate (Super Signal West Pico Substrate Chemoluminescence working solution, Pierce, UK) for 5 minutes at room temperature. Chemoluminescence was performed using Quantity One software package (V4.3.0).

Antibody to	Name/Clone	Source	Type	Antigen
Bcl-2	C-2	Santa Cruz	Mouse monoclonal	amino acids 1-205 of human Bcl-2
H4K8Ac	#2594	Upstate	Rabbit polyclonal	KLH-H4 amino acids 7-17(Ac-K8)
Caspase 3	#9662	Cell signalling	Rabbit polyclonal	full length (35kDa) and large cleaved fragment (17kDa)
Caspase 9	#9502	Cell signalling	Rabbit polyclonal	full length (47kDa) and large cleaved fragments
Caspase 8	1-3-9	BD	Mouse monoclonal	full length (55/50kDa) and cleaved fragment (40/36kDa) and 23kDa
PARP	C2-10	R&D	Mouse monoclonal	full length (116kDa) and large cleaved fragment (85kDa)
PCNA	PC10	Cancer Research UK	Mouse monoclonal	Rat PCNA

Table 2-2 Antibodies used in this study:

Antibodies were either kind gifts from Professor G Packham or sourced as indicated.

2.2.4 Xenograft studies

Severe combined immunodeficient mice (SCID) were inoculated subcutaneously in the left flank with 5×10^7 Ramos cells diluted in 200 μ l of complete medium. After 7 days mice were divided into 4 groups and received intraperitoneal injection of a DMSO control solution, SAHA, Rituximab or the combination of SAHA and Rituximab. Tumour volume was measured in millimetres (mm) in two dimensions three times weekly and mice were weighed three times weekly. Mice were culled according to home office guidelines when a single tumour measurement exceeded 15mm. Following culling tumours were removed and cell suspensions were created as described earlier.

2.2.5 Nucleic acid isolation

RNA isolation for microarray analysis

Ramos cells in logarithmic growth phase were treated with SAHA and crosslinked Rituximab alone or in combination and cells were harvested together with untreated cells at 6 and 16 hours. Samples were washed twice with ice cold PBS and maintained in RNase free conditions at all times. Cell pellets were treated with Trizol reagent (Invitrogen, UK) and RNA was extracted according to standard protocols. RNA purification was performed using a Qiagen RNeasy kit (Qiagen, UK) according to the product protocol. RNA quality and quantity was assessed using Agilent bioanalyser (Agilent Technologies UK Limited, UK) and 3 μ g RNA was used for microarray analysis. Duplicate samples for each condition were sent to the CRUK GeneChip Microarray Facility (PICR, Manchester), samples were labeled using Affymetrix One Cycle Protocol V1.0 and hybridised to the Affymetrix human array, the U133 Plus 2.0 array.

Quantitative reverse transcription-polymerase chain reaction (Q-RT-PCR)

This technique is used to amplify and simultaneously quantify a targeted DNA molecule. It enables both detection and quantification of a specific sequence in a DNA sample.

Ramos cells in logarithmic growth phase were treated with SAHA and/or Rituximab. Samples were washed twice with ice cold PBS and maintained in RNase free conditions at all times. Cell pellets were treated with Trizol reagent (Invitrogen, UK) and RNA was extracted according to standard protocols. RNA was quantified using Spectrophotometer nano drop ND-1000 (Thermo Fisher scientific, USA) and 1µg RNA was used for cDNA synthesis. 1µg RNA was made upto 14µl with nuclease free water. This was mixed with 1µl oligo (dT) primer (500µg/ml, Promega, UK) and incubated for 5 minutes at 70°C in a thermal cycler (Techne, UK). Following this 5µl 5x buffer, 1.25µl 10mM dNTP (1/10 dilution of dATP (100mM), dNTP(100mM), dGTP(100mM), dCTP (100mM) made up in RNase free water, 0.625µl RNasin (40u/µl), 1µl M-MLV RT enzyme (200u/µl) (all Promega, UK) and 2.125µl water was added to each sample. Samples were mixed and incubated in a thermal cycler for 60 minutes at 42 °C. Samples were diluted to 85µl with RNase free water. Q-RT-PCR was performed in 96 well optical plates (Applied Biosystems, UK) duplicate wells were loaded with 5µl sample, 10µl PCR master mix (Applied Biosystems, UK), 4µl water and 1µl of appropriate taqman gene expression assay (Applied Biosystems, UK). All reactions were performed in duplicate using the ABI PRISM 7500 Sequence Detection system (Applied Biosystems) according to the following thermal cycle protocol: 94°C 10 mins, 94°C 15 secs followed by 60°C 1 min for 40 cycles and 60°C for 1 min. Control reactions with no cDNA were run on each plate for each Taqman gene Expression Assay used, no amplification was detected in any control reaction.

Gene	Assay ID	Accession number	Comments
β-actin	Hs99999903_m1	NM_001101.2	β-actin
PRG1	Hs01004159_m1	NM_002727.2	Proteoglycan 1, secretory granule
Fos	Hs00170630_m1	NM_005252.2	v-fos murine osteosarcoma viral oncogene homolog
CD69	Hs00156399_m1	NM_001781.1	CD69 molecule
Bcl2A1	Hs00187845_m1	NM_004049.2	BCL-2-related protein A1
LTA	Hs00236874_m1	NM_000595.2	lymphotoxin alpha (TNF superfamily, member 1)
Bcl-2L1	Hs00236329_m1	NM_138578.1	BCL-2-like 1, Bcl-X _L

Table 2-3 Gene Expression assays used for real time PCR:

2.2.6 HDAC assay

This Colorimetric HDAC Activity Assay uses an HDAC colorimetric substrate (Boc-lys(ac)-AMC), which comprises an acetylated lysine side chain.

Deacetylation of the substrate results in production of a chromophore which can be analysed using a spectrophotometer. SU-DHL-4 cells at 0.5×10^6 cells/ml in complete medium (2×10^4 cells/well) were plated in 96 well plates (Greiner, UK) and cultured for 2 hours in a humidified cell incubator (HERA Cell, Heraeus) at 37°C and 5% CO₂ with SAHA or SAHA and rituximab. Control wells were treated with corresponding concentrations of DMSO or rituximab alone. Boc-lys(ac)-AMC (chemicon, USA) was diluted to a stock concentration of 2 mM in complete media with 4 % DMSO. 10 µl of stock substrate is added to each well giving a final concentration of 200 µM in the well. The cells were then incubated for a further 3 hours at 37°C. Following this 100 µl of lysis buffer/developer mix (50 mM Tris-HCl pH8.0, 137 mM NaCl, 2.7 mM KCl, 1 mM MgCl₂, 1% v/v Nonidet-P40, 2 mg/ml trypsin, 10 µM TSA) was added and the cells were incubated overnight in a humidified cell incubator (HERA Cell, Heraeus) at 37°C and 5% CO₂. The plate was read at excitation 355 nM and emission 460 nM on a fluorescent plate reader (Varioskan flash, Thermo scientific).

2.2.7 Flow cytometry techniques

CD69 analysis

PBMCs extracted from whole blood were resuspended in complete medium at a concentration of 1×10^6 cells/ml. 1×10^6 cells were plated in 24 well plates (Greiner, UK) and treated with variable doses of SAHA and rituximab alone or in combination for variable durations. Following this cells were harvested and washed twice with PBS containing 1% BSA (v/v) (complete buffer). Cells were subsequently resuspended in 100µl complete buffer in Falcon tubes (BD, USA) and incubated in the dark on ice for 30 mins with 5µl CD69 and 5µl CD19. Control samples were incubated with equivalent concentrations of CD19 and IgG2a isotype control antibody [Table 2-4]. Samples were

subsequently washed twice and resuspended in 500µl complete buffer before being subjected to flow cytometric analysis (FACSCanto, BD, USA)

Ca flux assay

1x10⁷ cells (Ramos, Su-DHL-4) in logarithmic growth phase were treated with SAHA or a corresponding concentration of DMSO for 2 hours. They were then subjected to centrifugation at 1500 rpm for 5 minutes, and washed twice in 5mls of RPMI growth medium (Roswell Park Memorial Institute 1640 medium, Invitrogen, UK) supplemented with 2.0 mM L-glutamine (Invitrogen, UK) and 1.0 mM sodium pyruvate (serum free medium). Cell pellets were mixed with 10µM Indo-1-AM with 0.2% pluronic-F127, resuspended in 500µl serum free medium and incubated for 30 minutes in a humidified cell incubator (HERA Cell, Heraeus) at 37°C and 5% CO₂. Following this cells were washed twice in 5mls of serum free medium, resuspended in complete RPMI growth medium and allowed to rest in the dark in a humidified cell incubator (HERA Cell, Heraeus) at 37°C and 5% CO₂. Cells were subsequently divided into two samples and one sample was treated with rituximab 5µg/ml for 15 minutes. Samples were diluted to a flow rate of 100-200 cells/second and subjected to flow cytometric analysis (FACS vantage flow cytometer, BD Biosciences).

ERK phosphorylation

1x10⁷ SU-DHL-4 cells in logarithmic growth phase were treated with SAHA, Rituximab, B1 or the combination for 15 minutes. Control samples were incubated with a corresponding concentration of DMSO for 15 minutes. Following this an equal volume of buffered pH normal saline with 4% w/v paraformaldehyde (cytofix fixation buffer, BD, USA) was added. Cells were incubated at 37°C for 10 minutes, and collected by centrifugation. 1ml of 80% w/v methanol was added, and cells were incubated on ice for a further 30 minutes. Samples were washed twice and resuspended in 100µl complete buffer with 5 µl phosphoERK (cell signalling, UK) antibody [Table 2-4]. After 30 minute incubation at room temperature cells were washed again, resuspended in 200µl complete buffer and subjected to flow cytometric analysis.

Antibody to	Source	Type	Conjugate	Clone
pERK1/2	Cell signalling	IgG1	AlexaFluor-488	-
CD19	BD	IgG1	APC	HIB19
CD69	BD	IgG1	PE	FN50
CD20	Dr M Cragg	Rituximab	FITC	-
CD20	Dr M Cragg	B1	FITC	-
Isotype control	BD	IgG2a	FITC	G155-178
Isotype control	BD	IgG1	FITC	MOPC-21
Isotype control	BD	IgG1	R-PE	MOPC-21

Table 2-4 Antidodies used for flow cytometric analysis:

2.3 Statistical analysis

2.3.1 Dose response curves and IC50 calculations

These were performed using prism version 4.03 (GraphPad Software inc, USA). Analysis of synergy assays was performed using Calcsyn version 2.0 (Biosoft, UK) statistical software package. This program uses formulae developed from Chou's enzyme models of mass action and is routinely used to look at drug interactions [260]. A "combination index" value is derived which provides a quantification of the degree of drug interaction. Whereby a value less than 1 indicates a synergistic interaction and a value greater than 1 indicates an antagonistic interaction.

2.3.2 Microarray analysis

Bioinformatic input for analysis of microarray was received from Richard Mitter at the Cancer Research UK Bioinformatics service (London). Briefly Raw data was extracted from the MIAME VICE database (PICR, Manchester). The probe level data (Cel files) were normalized using Robust Multi-Array Average (RMA) (Bioconductor, Affymetrix, UK)

<http://bioconductor.org/packages/2.1/bioc/vignettes/affy/inst/doc/affy.pdf>)

Expression fold change was calculated from mean levels from duplicate samples and was compared to controls. A moderated t-test was used to assess differential expression and filtered on a false discovery rate adjusted *p* value of ≤ 0.05 , and an absolute fold change of ≥ 2 .

3 Project Aims and Outline of Investigation

Combining targeted therapies for the treatment of malignant disease is a well established strategy and the benefit of this approach has clearly been demonstrated with both HDI and CD20 mAb. When considering novel combinations two major considerations are important. Firstly a clear mechanistic rationale for combining agents must exist in order to potentiate their effects. Secondly it is paramount that when given in combination, therapeutic doses of both agents must be achievable without predictable toxicity based on the side effect profile of either agents given alone.

The published data discussed demonstrates that both HDI and CD20 mAb have shown some of their most promising activity when given in combination. Their ability to induce apoptosis and to modulate a number of important common survival pathways provides a clear rationale for investigating their effects together. With these factors in mind this project was conducted via three distinct approaches.

1. Firstly the ability of different HDI and CD20 mAb to induce cell death and apoptosis was investigated in a panel of CD20 positive B cell NHL cell lines, with the primary aim of establishing whether a synergistic effect was apparent and whether this was cell line or investigational agent specific.
2. Secondly the underlying mechanism for this effect was sought. Two approaches were used to do this. Initially the modulation of early biochemical responses to either class of agents was investigated prior to trying to elicit the effects of combination treatment on the intrinsic and extrinsic apoptotic pathways.
3. Thirdly gene expression analysis was performed to try to identify a cooperative transcriptional effect on previously described common survival pathways and to investigate novel interactions for further investigation. This technique was also utilised to try and identify a biomarker of HDI transcriptional effect.

4 Synergistic cell killing in B cell NHL cell lines

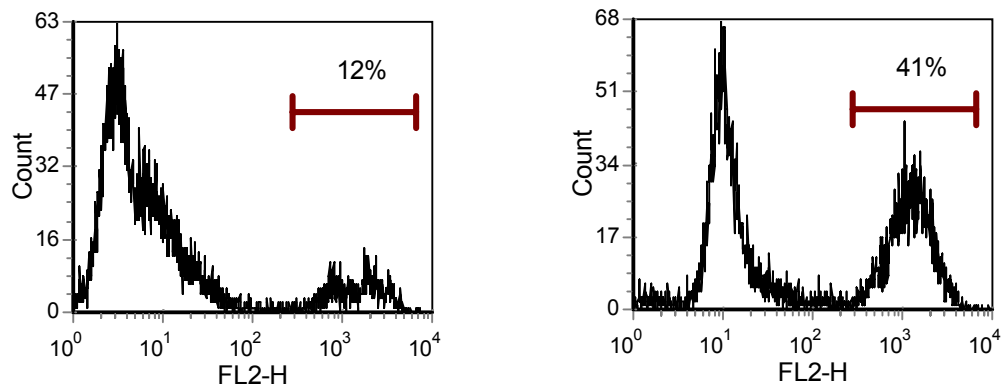
4.1 Introduction

The initial aim of this project was to investigate the induction of cell death by CD20 monoclonal antibodies and HDIs in a panel of B cell NHL cell lines. Despite the dramatic effect of rituximab in improving overall survival for patients with non Hodgkin's lymphoma [261], many patients relapse and new strategies are needed to try and overcome this problem. As has been discussed earlier one of the mechanisms employed by CD20 mAb is direct induction of cell death pathways following antibody binding. The induction of cell death was measured in B cell NHL cell lines following treatment with Rituximab and SAHA alone and in combination. Once a synergistic interaction had been observed the effect was investigated in different cell lines and with different combinations of CD20 mAb and HDI. A panel of 5 B cell non Hodgkin's lymphoma cell lines was chosen to investigate this interaction.

4.2 Effect of HDAC inhibitors

Prior to investigating a combination effect it was important to characterise the activity of two different classes of HDI. The hydroxamate SAHA and the cyclic tetrapeptide FK228 were chosen as they were two HDI in clinical development. The Ramos cell line was initially chosen to investigate the cytotoxic effect of the HDAC inhibitor SAHA. SAHA treatment resulted in dose dependent induction of cell death measured by propidium iodide staining and flow cytometric analysis [**Figure 4-1**]. Multiple data points were plotted using prism v4.03 software. The IC₅₀ was calculated as the concentration required to produce 50% of the maximal effect. The mean IC₅₀ was then calculated from multiple experiments. SAHA treatment resulted in induction of cell death in a dose dependent manner with an IC₅₀ of 5.5 (±1.4) µM.

A.



B.

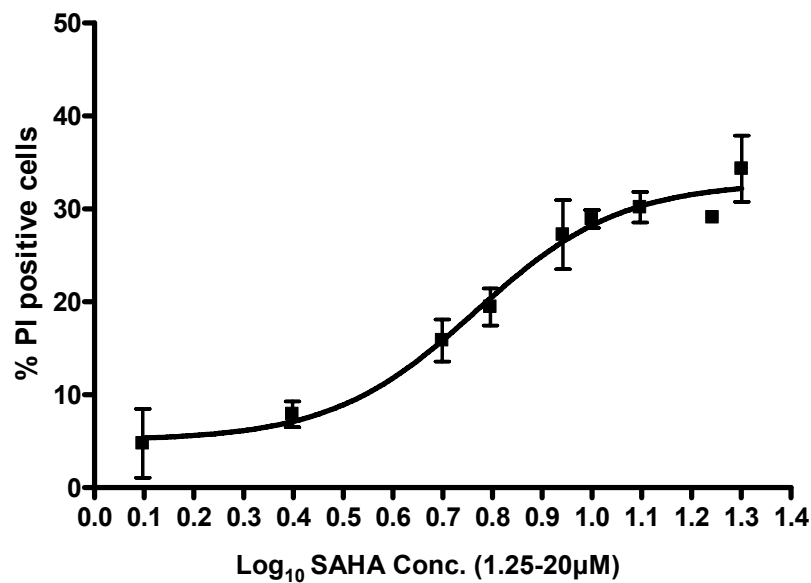


Figure 4-1 The effect of SAHA on Ramos cell survival:

(A) Ramos cells were treated with variable concentrations of SAHA (1.25-20 μ M) or left untreated as a control. After 2 days, the proportion of cells that failed to exclude PI was determined by flow cytometry. Representative histograms are shown with the percentage of PI positive cells in untreated (left) and 10 μ M SAHA treated (right) samples indicated.

(B) Ramos cells were treated with the indicated concentrations of SAHA. After 2 days the proportion of cells that failed to exclude PI was determined by flow cytometry. Data shown are the mean increase in the percentage of PI positive cells derived from duplicate determinations (\pm range) relative to untreated cells. Experiment shown is representative of three experiments.

This assay was repeated to investigate whether this effect was preserved across different B-cell NHL cell lines and with FK228. Figure 4-2 shows a representative dose response curve for Ramos cells treated with FK228. As was observed with SAHA this resulted in dose dependent cell killing, although FK228 was much more potent.

Table 4-1 shows IC₅₀s for the five cell lines treated with variable concentrations of SAHA and FK228. There was little variation in IC₅₀ between the cell lines with SAHA effective at micromolar concentrations, while FK228 was more potent with cell death induced at nanomolar concentrations. This data was consistent with reports from other investigators using solid tumour and lymphoid cell lines [262-264].

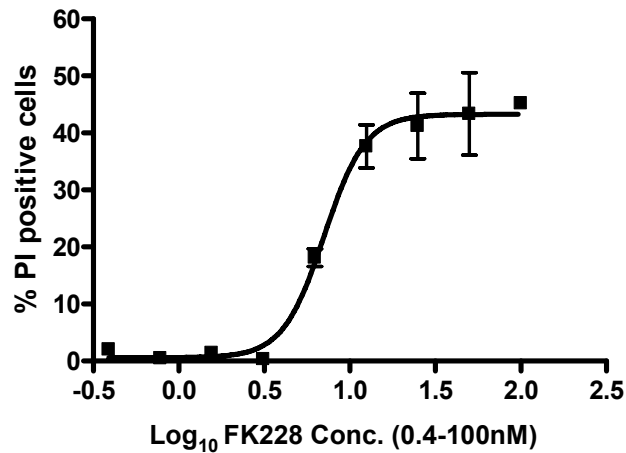


Figure 4-2 the effect of FK228 on Ramos cell survival:

Ramos cells were treated with variable concentrations of FK228 (0.4-100nM) or left untreated as a control. After 2 days, the proportion of cells that failed to exclude PI was determined by flow cytometry. Data shown are the mean increase in the percentage of PI positive cells derived from duplicate determinations (\pm range) relative to untreated cells. Experiment shown is representative of two experiments.

Cell line	SAHA				FK228			
	IC50 Concentration		Maximum cell death		IC50 Concentration		Maximum cell death	
	(μM)		(%)		(μM)		(%)	
	mean	SD	Mean	SD	mean	SD	mean	SD
Ramos	5.5	1.4	39.3	19.5	0.005	0.002	51.3	14.4
SU-DHL-4	2.8	1.0	63.6	26.6	0.005	0.0006	57.2	11.3
RL	3.2	0.6	33.0	8.1	0.006	0.0006	15.3	1.5
Akata	2.1	0.6	37.2	6.0	0.003	0.0002	47.2	2.3
Dohh2	0.9	0.0	41.1	1.0	0.006	0.0005	55.6	9.4

Table 4-1 Sensitivity of B cell NHL cell lines to HDI:

Summary of IC50's and maximum levels of PI positive cells for the panel of B cell NHL cell lines treated with SAHA or FK228. Data shown are the mean IC50 and % PI positive cells (±SD) from at least duplicate independent experiments for the cell lines and HDI indicated.

4.3 *Effect of CD20 monoclonal antibodies*

The effect of the CD20 monoclonal antibodies was again initially investigated in the Ramos cell line. Cells were treated with a range of concentrations of the type I antibody rituximab alone and in combination with an anti human IgG crosslinking agent, or the type II antibody B1. After 48 hours the levels of cell death were measured using a propidium iodide exclusion assay following incubation with Rituximab and B1 **[Figure 4-3]**. Both agents resulted in very low levels of cell killing in this assay with with no clear dose response relationship. Rituximab and B1 in the absence of crosslinking do not result in intracellular Ca^{2+} flux [99], so Ramos cells were also treated with Rituximab in combination with a crosslinking agent. The addition of crosslinking resulted in a small increase in the levels of cell death observed but no clear dose response relationship.

Data from Southampton, *Teeling et al* [265], has already demonstrated that CD20 receptor binding is saturated at concentrations greater than 0.5 $\mu\text{g}/\text{ml}$ mAb in cell lines with similar levels of surface CD20 to our panel of B cell lines. The assay was modified to investigate the effect of a saturating dose of mAb (10 $\mu\text{g}/\text{ml}$) simultaneously across the panel of B cell lines. Cells were treated for 48 hours with levels of cell death estimated with the PI exclusion assay. The percentage of PI positive cells observed in the 5 cell lines tested is shown **[Figure 4-4]**. Even at saturating concentrations low levels of cell death were observed with rituximab, B1 did result in higher levels of cell death in all the cell lines tested but the activity remained modest. This data emphasises the finding that CD20 mAb induce low levels intracellular signaling and cell death. Of note these assays were performed using heat inactivated fetal calf serum, which neutralizes any complement activity. Thus in the absence of functional ADCC and CDC; CD20 mAb demonstrate modest cytotoxic activity. This result suggested that mechanisms to enhance this effect would provide a promising strategy for improving the cytotoxic activity of these agents.

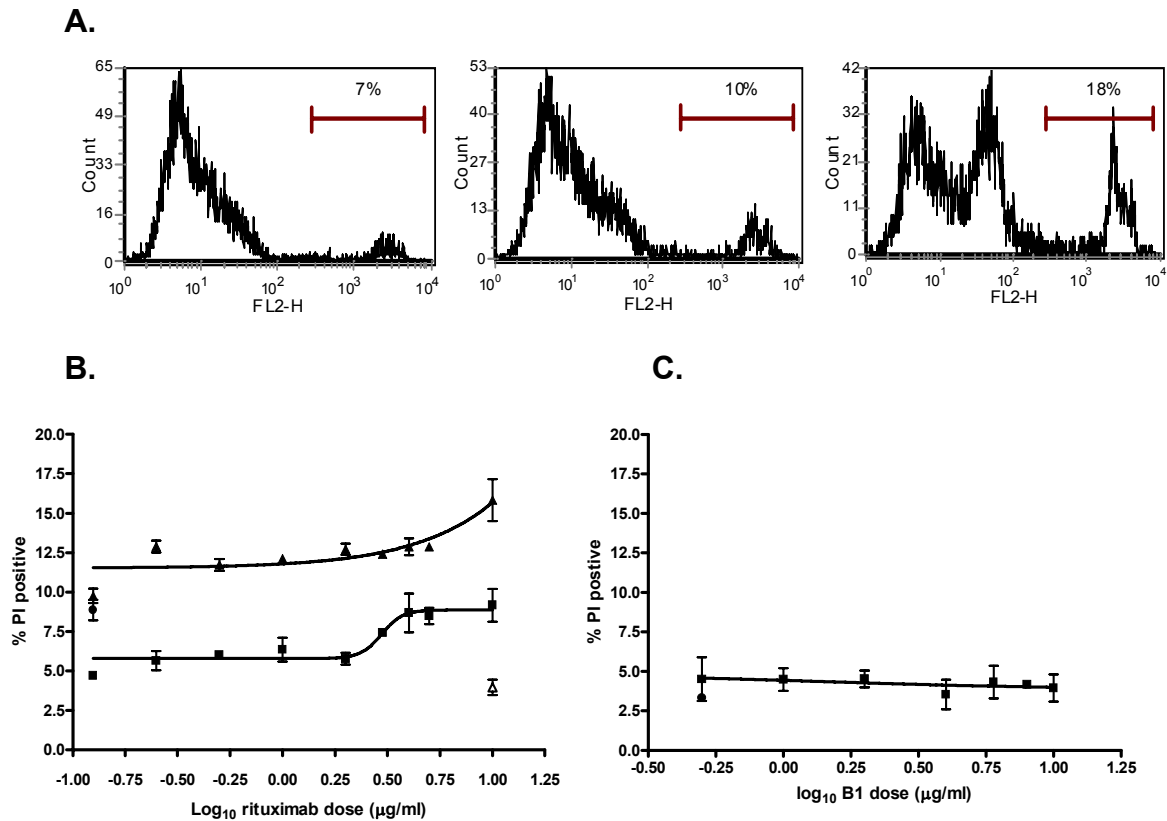


Figure 4-3 Effect of CD20 monoclonal antibodies in Ramos cell line:

Ramos cells were treated with variable concentrations of rituximab (0.125-10 μ g/ml) with or without crosslinking agent. After 2 days, the proportion of cells that failed to exclude PI was determined by flow cytometry. (A.) shows representative flow cytometry histograms for untreated (i), rituximab treated (ii) or crosslinked rituximab treated cells (iii). (B.) Shows the mean increase in the percentage of PI positive cells derived from duplicate determinations (\pm range) for rituximab with (▲) or without (■) crosslinking agent. Crosslinker only (Δ) and untreated cells (●) are also shown. Experiment shown is representative of two experiments. (C.) shows Ramos cells treated with variable concentrations of B1 (1-20 μ g/ml). After 2 days, the proportion of cells that failed to exclude PI was determined by flow cytometry. Data shown are the mean increase in the percentage of PI positive cells derived from duplicate determinations (\pm range) untreated cells are again shown as a control (●). Experiment shown is representative of two experiments.

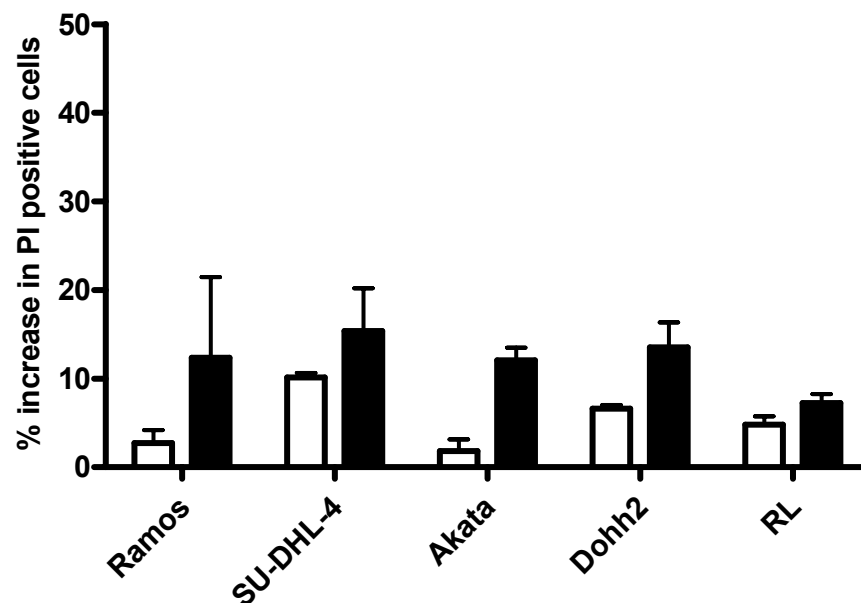


Figure 4-4 Effect of rituximab and B1 in a panel of B cell NHL cell lines:

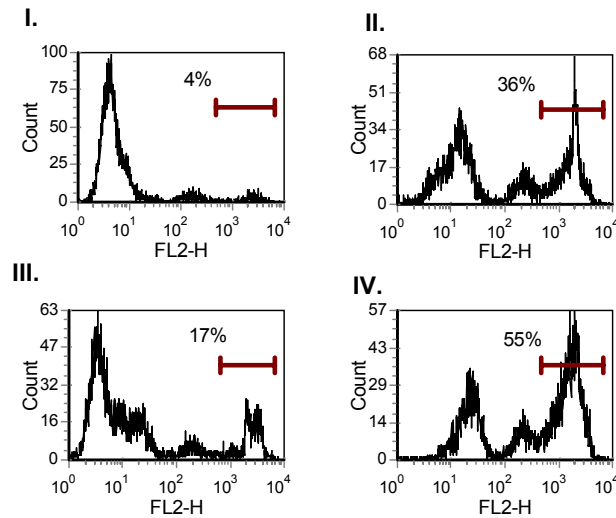
B cell NHL cells were treated with rituximab 10µg/ml (□) or B1 10µg/ml (■). After 2 days, the proportion of cells that failed to exclude PI was determined by flow cytometry. Data shown are the mean increase in the percentage of PI positive cells derived from triplicate determinations from two independent experiments (±range) relative to untreated cells.

4.4 Effect of combination treatment

The data already presented established working concentrations for CD20 mAb and HDI alone. To investigate the effect of combination treatment Ramos cells were treated with crosslinked rituximab and SAHA alone or in combination using the same assays. A saturating dose of rituximab was used with crosslinking as this achieved maximal effect with the weakly cytotoxic antibody, an active but sub optimal dose of SAHA was chosen to avoid maximal cell death with this agent. After 48 hours levels of cell death were measured by PI exclusion assay [**Figure 4-5**]. Combination treatment resulted in an increase in the percentage of PI positive cells compared to treatment with crosslinked rituximab or SAHA alone. An independent student's *t-test* comparing combination treatment demonstrated a significant increase in cell death compared to either treatment alone.

A similar effect was observed in Ramos cells treated with FK228 and rituximab [**Figure 4-6**]. This again resulted in a significantly higher level of cell death following combination treatment compared to either agent alone.

A.



B.

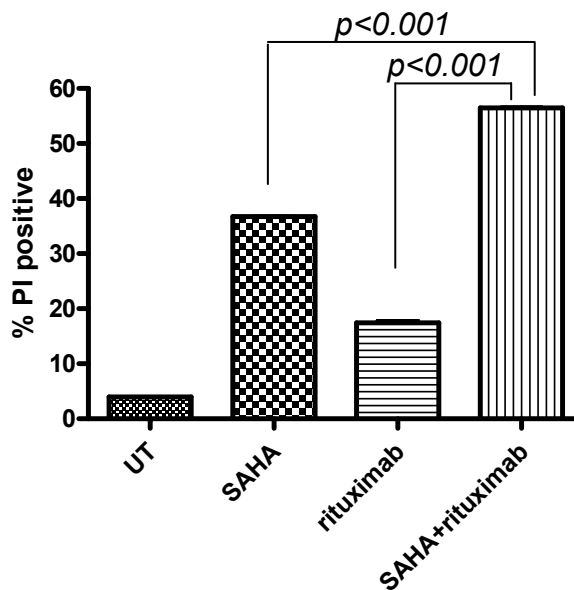


Figure 4-5 effect of SAHA in combination with rituximab in Ramos cell line:

(A) Ramos cells were (I.) untreated, (II.) treated with SAHA 2.5μM, (III.) treated with crosslinked rituximab 10μg/ml or (IV.) treated with both agents. After 2 days, the proportion of cells that failed to exclude PI was determined by flow cytometry. Representative histograms are shown.

(B) Ramos cells were treated with the indicated concentrations of SAHA, rituximab or the combination. After 2 days the proportion of cells that failed to exclude PI was determined by flow cytometry. Data shown are the mean increase in the percentage of PI positive cells derived from duplicate determinations (\pm range) relative to untreated cells. Experiment shown is representative of two experiments. Independent student's t-test was performed comparing combination treatment to either agent alone.

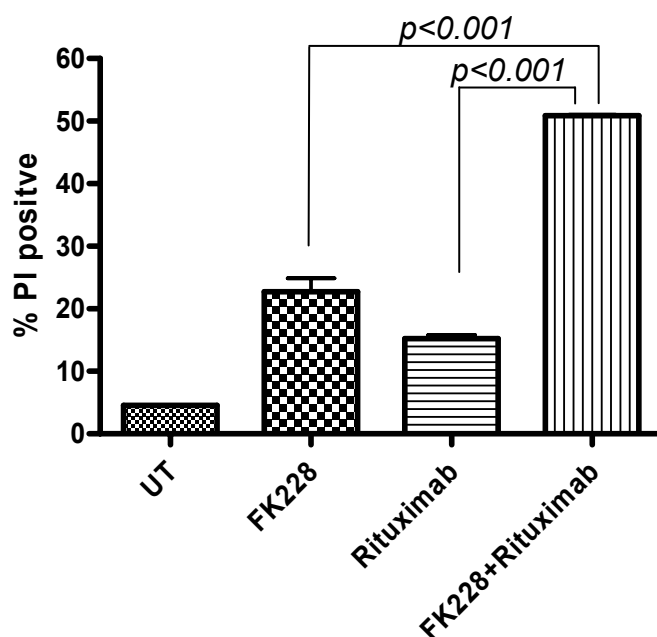


Figure 4-6 effect of FK228 and Rituximab in Ramos cell line:

Ramos cells were untreated or treated with 5.3nM FK228, rituximab 10µg/ml or the combination. After 2 days the proportion of cells that failed to exclude PI was determined by flow cytometry. Data shown are the mean increase in the percentage of PI positive cells derived from duplicate determinations (\pm range). Experiment shown is representative of two experiments. Independent student's t-test was performed comparing combination treatment to either agent alone.

To investigate this effect further the assay was repeated in different B-cell NHL cell lines using the same concentrations of SAHA and rituximab [**Figure 4-7**]. As was observed in Ramos cells there was a significant increase in the levels of cell death observed with combination treatment compared to either agent alone in 3 of the 4 additional cell lines investigated.

These data demonstrate that CD20 mAb and HDI in combination can produce significantly higher levels of cell death than when either agent is used alone but does not prove whether this effect is synergistic or simply additive.

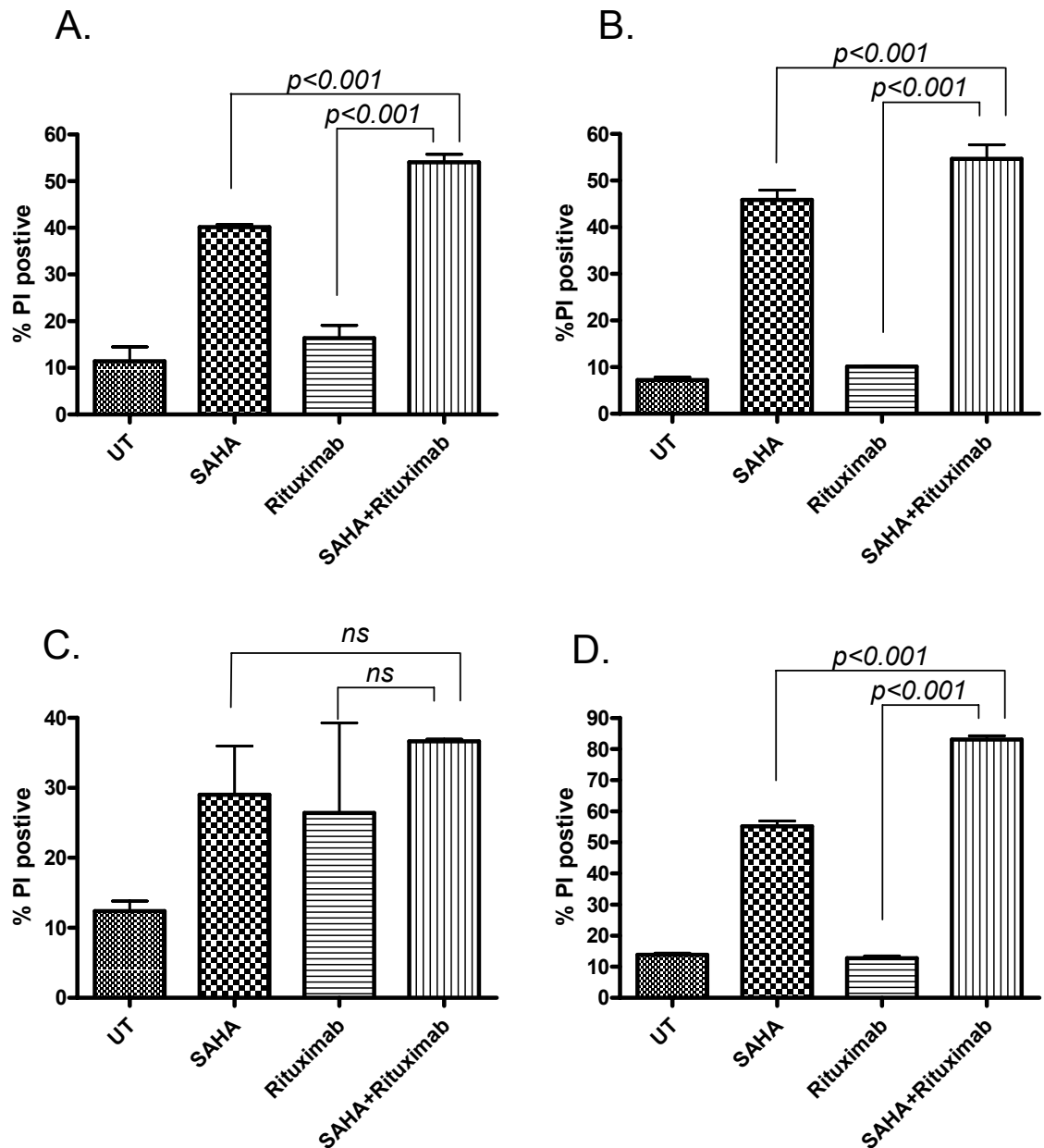


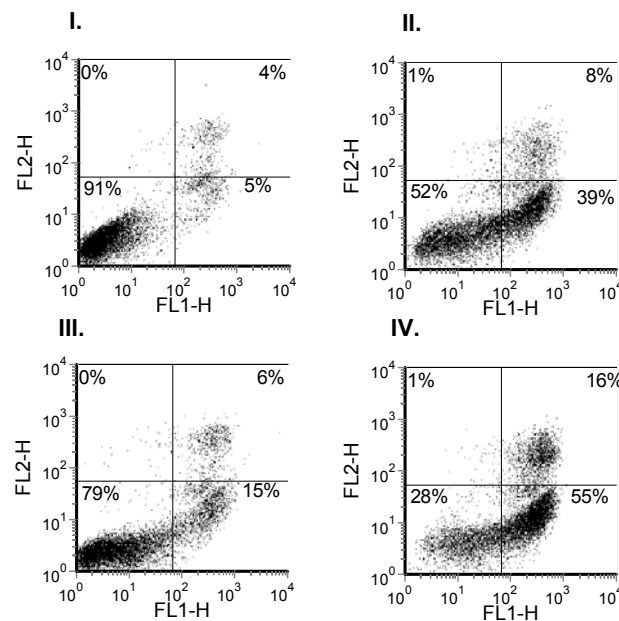
Figure 4-7 Effect of combination treatment in other cell lines:

(A.) Dohh2, (B.) Akata 6, (C.) RL, (D.) SU-DHL-4 cell lines were left untreated or treated with SAHA 2.5 μ M, rituximab 10 μ g/ml or a combination of the two agents. After 2 days the proportion of cells that failed to exclude PI was determined by flow cytometry. Data shown are the mean percentage of PI positive cells derived from duplicate or triplicate determinations (\pm range) and are representative of at least two independent experiments. Independent Student's t-test was performed comparing combination treatment to either agent alone.

4.5 Synergy calculations

The propidium iodide cell death assay used demonstrated cooperative cell killing but was limited by a number of factors. PI is a late marker of cell death requiring loss of membrane integrity and DNA binding to alter the fluorescence of the dye. Once cells have reached this stage, they are rapidly lysed. PI positive cells have short term viability in culture making detection of 100% positivity unfeasible. Another problem was the profile of PI staining (**Figure 4-3A**) which resulted in difficulty in gating true PI positive cells. Despite these limitations significant cooperative effect was seen, however it was important to determine whether this was an additive or synergistic effect. In this context synergy was defined as combination treatment resulting in greater levels of cell death than would be expected from the sum the effect of either agent alone. The experimental conditions were optimised prior to investigating whether this interaction was synergistic in nature. The initial aim was to investigate whether at an earlier time point induction of apoptotic pathways could be identified using annexin V staining and flow cytometry. Annexin V, is a 35-36 kDa, Ca^{2+} -dependent, phospholipid binding protein and is used to identify cells in the early stages of apoptosis. Cells are co stained with FITC conjugated Annexin V and PI allowing measurement of early and late apoptosis [**Figure 4-8**]. The percentage of apoptotic cells was analysed at the different timepoints with the most significant difference in levels of apoptosis between the treatments observed at 24 hours. On this basis 24 hours was chosen as the timepoint to investigate synergistic induction of apoptosis. The other important optimisation steps were to investigate the effect of scheduling and type of mAb. Scheduling, has previously been demonstrated to be important for the interaction between HDI and a number of other agents [235]. The effect of scheduling was investigated in Ramos and SU-DHL-4 cells with no significant effect observed (data not shown).

A.



B.

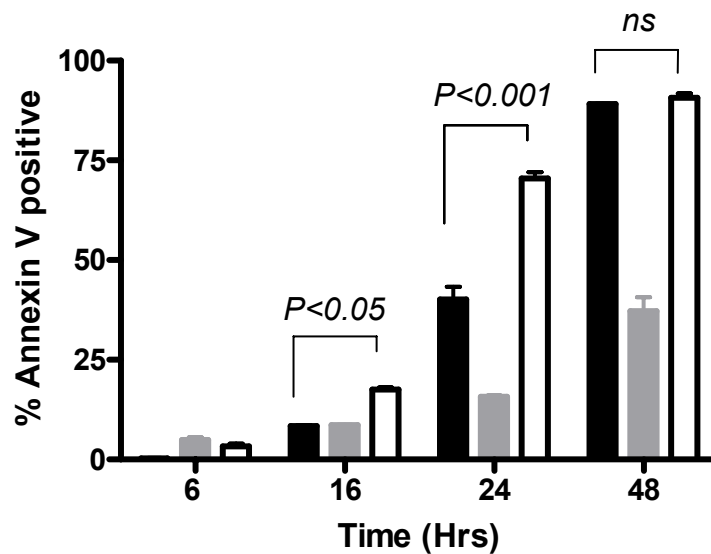


Figure 4-8 Induction of apoptosis in Ramos cell line:

(A) Ramos cells were (I.) untreated, (II.) treated with SAHA 5.5μM, (III.) treated with cross linked Rituximab 10μg/ml or (IV.) treated with both agents. Cells were harvested at 6, 16, 24 and 48 hours and co stained with annexin V and propidium iodide before being subjected to flow cytometric analysis. Representative dot plots for the 24 hour timepoint are shown with the % cells within each quadrant shown.

(B) Ramos cells were treated with the indicated concentrations of SAHA (■), Rituximab (■) or the combination (□). At variable time points the % of annexin V positive cells was determined by flow cytometry. Data shown are the mean increase in the percentage of annexin V positive cells derived from duplicate determinations (\pm range) relative to untreated cells. Experiment shown is representative of two experiments. Independent Student's *t*-test was performed comparing SAHA to combination treatment.

It was also important to investigate whether cooperative induction of apoptosis was specific to CD20 mAb or was simply part of a generalised response to mAb membrane binding. The effect of a panel of mAb, kindly provided by Dr M Cragg, alone or in combination with SAHA is shown **[Figure 4-9]**. The top panel shows the effect of CD20 mAb alone (clear bars) or with SAHA (black bars). As has previously been shown, combination treatment resulted in a significant increase in levels of apoptosis compared to SAHA treatment alone. The bottom graph shows the effect of irrelevant mAb (CD3) and isotype matched non CD20 specific mAb. These mAb did not result in any significant increase in the level of apoptosis seen compared to SAHA alone. Interestingly the anti BCR mAb (M15/8) resulted in higher levels of apoptosis than CD20 mAb alone and appeared to potentiate the effects of SAHA, although this effect was not statistically significant.

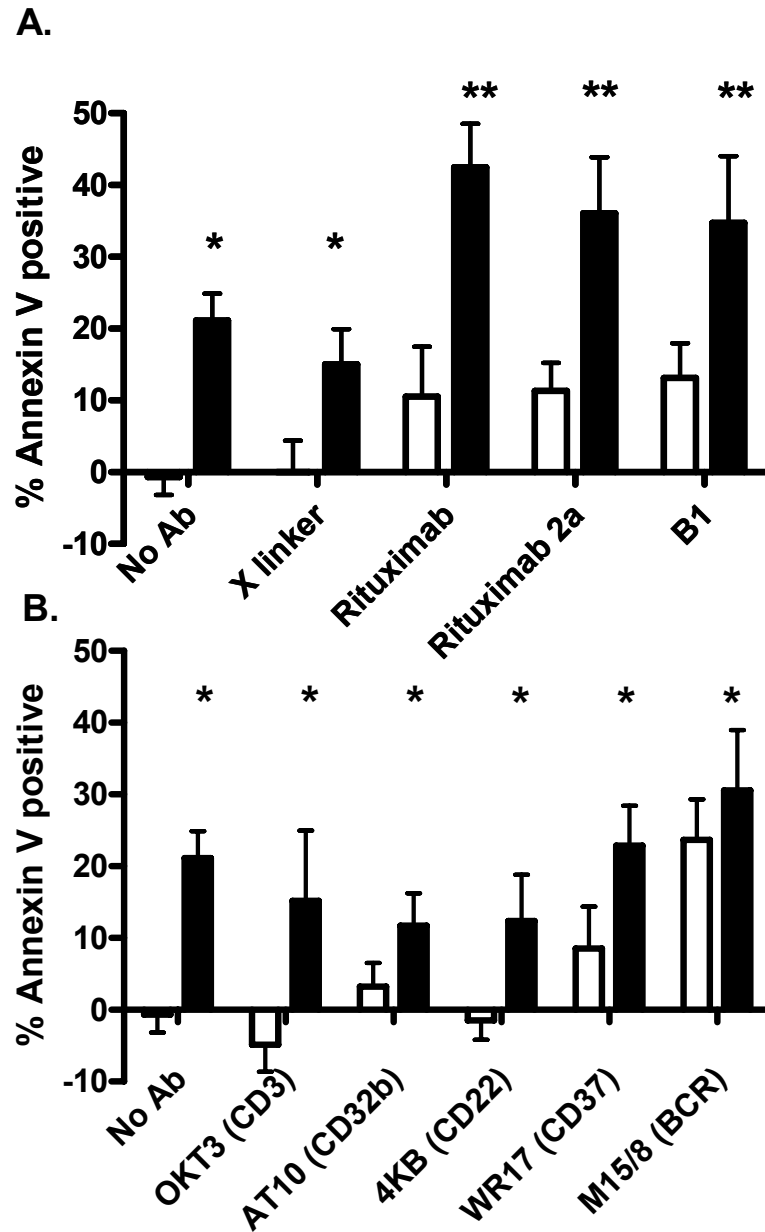
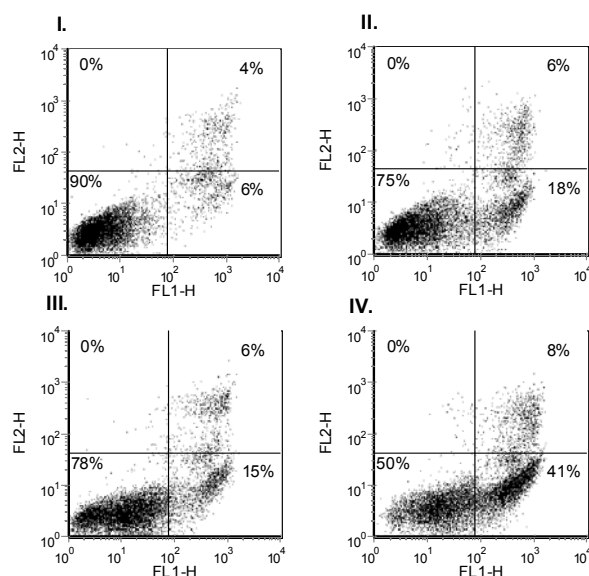


Figure 4-9 The specificity of CD20 mAb at inducing apoptosis:

Ramos cells were treated with SAHA (5.5 μ M) (■) or a corresponding concentration of DMSO (□) in combination with the mAb indicated (10 μ g/ml). After 24 hours cells were harvested and co stained with annexin V and propidium. The percentage of annexin V positive cells was determined by flow cytometry. Data shown are the mean increase in the percentage of annexin V positive cells derived from duplicate determinations from two independent experiments (\pm range) relative to untreated cells. Independent Student's *t*-test was performed comparing each combination to SAHA alone (* *ns*, ** *p*≤0.05).

Rigorous testing of the synergistic interaction between SAHA and rituximab was performed initially in the Ramos and SU-DHL-4 cell lines using the calcsyn statistical software package (Biosoft, UK). Ramos cells were treated with a range of concentrations of SAHA distributed around the IC₅₀ from the initial PI exclusion assays. A Rituximab dose range of 0.75–12 µg/ml was chosen. Combination treated samples were treated with either drug at a fixed ratio. The levels of apoptosis were measured following 24 hours incubation. A dose response curve is shown for the three experimental conditions in Ramos and SU-DHL-4 cell lines. Combination treatment results in higher levels of apoptosis at all dose levels compared to either agent alone [**Figure 4-10**]. The mean percentage of annexin V positive cells for each condition at each dose level was analysed using calcsyn and is shown below. Synergistic induction of apoptosis (CI <1) was seen across a wide dose range.

A.



B.

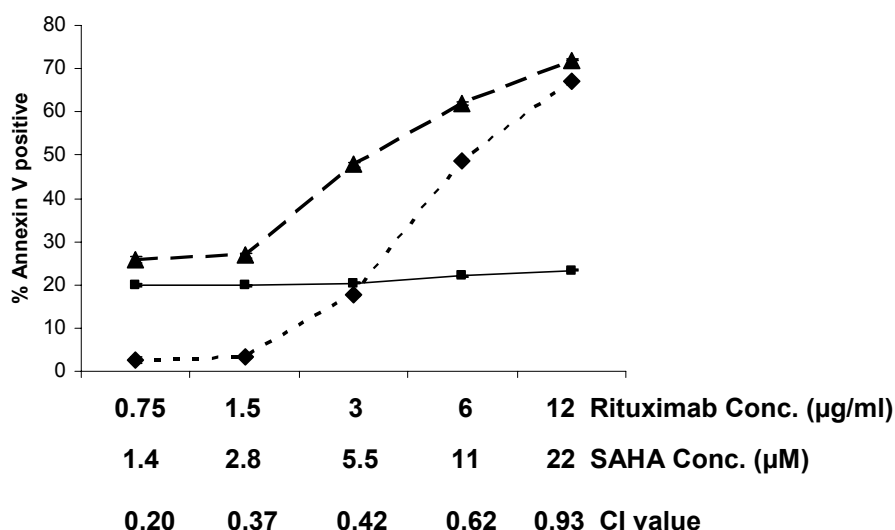


Figure 4-10 Synergistic induction of apoptosis in Ramos cell line:

Ramos cells were treated with a range of concentrations of SAHA, Rituximab or the combination. Cells were harvested at 24 hours and co stained with annexin V and propidium iodide before being subjected to flow cytometric analysis.

(A) Representative dot plots for Ramos cells (I.) untreated, (II.) treated with SAHA 5.5μM, (III.) treated with crosslinked rituximab 3μg/ml or (IV.) treated with both agents are shown with the % cells within each quadrant illustrated. Dose response curve **(B)** is shown. Data shown are the mean increase in the percentage of annexin V positive cells derived from duplicate determinations (±range) relative to untreated cells for SAHA (◆), Rituximab (■) or the combination (▲) treatments. CI value for each data point are shown. Results shown are representative of two independent experiments.

This assay was repeated initially in Ramos cells with uncrosslinked rituximab and B1 in combination with SAHA and subsequently with FK228 in combination with rituximab. The CI values at the IC₅₀ point for these combinations are shown in **Figure 4-11**. All combinations resulted in synergistic induction of apoptosis. The mean CI value at the IC₅₀ from duplicate experiments for other representative cell lines and treatment combinations is summarised in **Table 4-2**. Synergistic induction of apoptosis was observed across 4 of the 5 cell lines treated with SAHA in combination with rituximab. The Ramos and SU-DHL-4 cell lines were used to investigate the interaction between FK228 and rituximab and SAHA and B1. Synergistic induction of apoptosis was observed with all the different HDI CD20 mAb combinations tested.

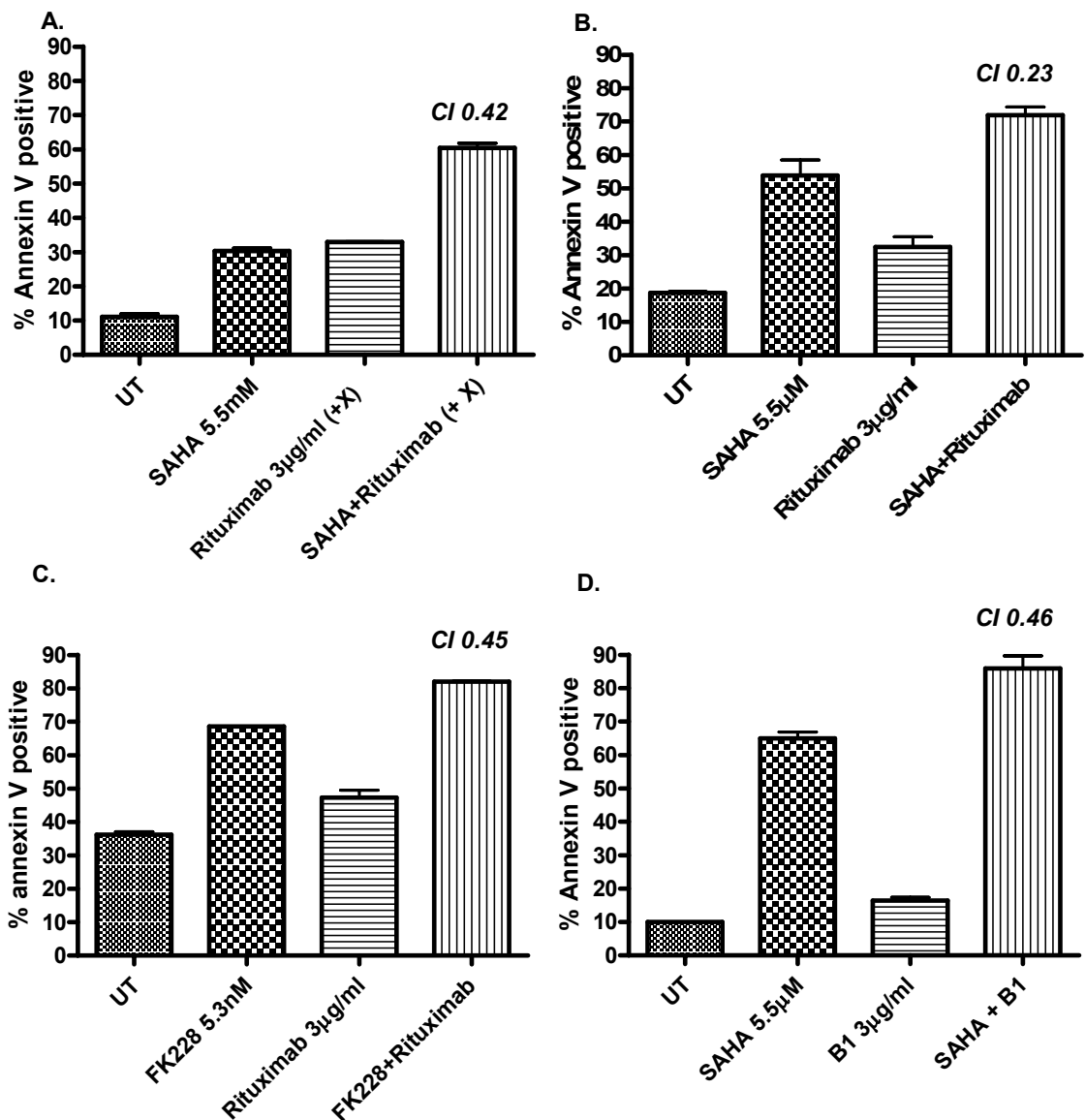


Figure 4-11 Synergistic interactions in Ramos cells.

Ramos cells were treated with SAHA±Cross linked Rituximab **(A)**, SAHA±Rituximab **(B)**, FK228±Rituximab **(C)** or SAHA±B1 **(D)**: Cells were harvested at 24 hours and co stained with annexin V and propidium iodide before being subjected to flow cytometric analysis. Bar charts show the mean increase in the percentage of annexin V positive cells derived from duplicate determinations (\pm range) at the IC50 for the treatments indicated. CI values derived used calcsyn software are shown.

cell line	HDI	mAb	CI
Ramos	SAHA 5.5µM	rituximab 3µg/ml	0.42
	FK228 5.3nM	rituximab 3µg/ml	0.45
	SAHA 5.5µM	B1 3µg/ml	0.58
SU-DHL-4	SAHA 2.8µM	rituximab 3µg/ml	0.06
	FK228 5nM	rituximab 3µg/ml	0.19
	SAHA 2.8µM	B1 3µg/ml	0.24
Dohh2	SAHA 0.9µM	rituximab 3µg/ml	0.26
Akata 6	SAHA 2.1µM	rituximab 3µg/ml	0.33
RL	SAHA 3.2µM	rituximab 3µg/ml	3.1x10 ⁶

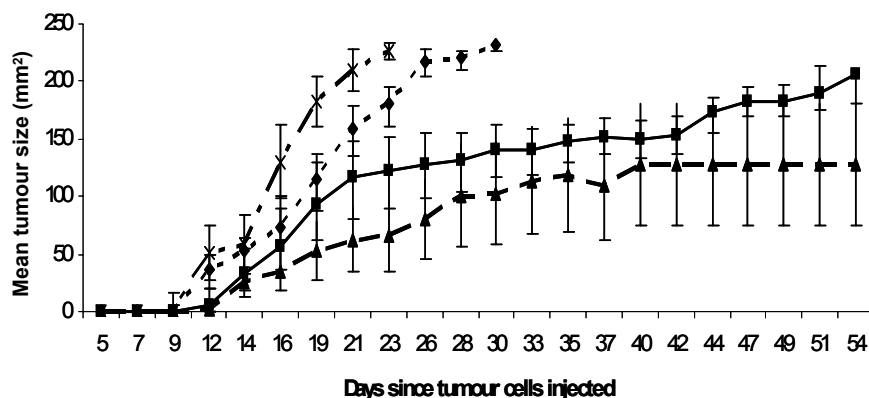
Table 4-2 Summary of combination index (CI) across panel of B cell NHL cell lines:

Mean CI values from duplicate experiments at the concentrations of HDI and CD20 mAb indicated are shown.

4.6 **Combination therapy in a xenograft model**

Having observed synergistic induction of apoptosis *in vitro*, a xenograft model was tested using subcutaneous Ramos tumours in severe combined immunodeficient mice (SCID). Published data using a prostate cancer xenograft model had demonstrated that doses of SAHA 25mg/kg-100mg/kg intraperitoneal (IP) daily were well tolerated [262]. Initial experiments utilised SAHA at a dose of 25mg/kg on day 7 for 7 days, rituximab 250µg/ml on day 7 or the combination of SAHA and rituximab at the above doses and schedule. Control animals received DMSO diluted in PBS on day 7 for seven days. **Figure 4-12 A.** shows rate of tumour growth for the different treatments, this approach resulted in large variation in tumour size between mice and although combination treatment resulted in the slowest rate of tumour growth this was not statistically better than rituximab treatment alone. The toxicity of the treatments was estimated by assessing the change in weight of mice during treatment, there appeared to be no measurable changes in weight observed between the treated groups (**Figure 4-12 B**). To establish that SAHA was producing a target effect, western blotting for histone acetylation was performed on tumours extracted from mice at different timepoints. 1.8 fold induction of histone acetylation was detectable six hours after intraperitoneal injection of SAHA (**Figure 4-13**). To optimise the model, treatment of established tumours was adopted. Based on a predicted tumour failure rate of 20%, thirty mice were inoculated with tumour and twenty mice were selected to receive treatment once tumours were measurable. The SAHA treatment schedule was also adapted. Initially mice were treated for 14 days with SAHA 25mg/kg, this still resulted in little activity in the SAHA alone treatment arm (data not shown). When the dose was increased to 50mg/kg, SAHA became poorly soluble over the duration of the experiment. **Figure 4-14** shows tumour growth against time for the established tumour model. Combination treatment again resulted in reduced tumour growth during treatment with SAHA, however this effect was lost once treatment was withdrawn.

A.



B.

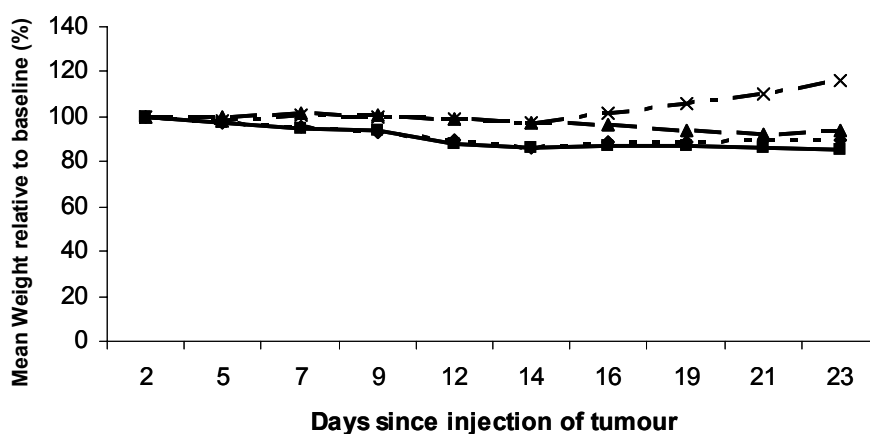


Figure 4-12 Ramos xenograft:

SCID mice were inoculated with 5×10^6 Ramos cells in the flank. Following 7 days mice were treated with DMSO for 7 days(x), SAHA 25mg/kg for 7 days (♦), Rituximab 250µg/ml on Day 7 (■) or the combination (▲). Tumour size in 2 dimensions and weight were estimated three times weekly. Data shown represents: (A.). Mean tumour size (+/-SEM) from surviving mice for each treatment (n=5), (B.). Mean change in weight (%) of mice from baseline for each treatment (n=5).

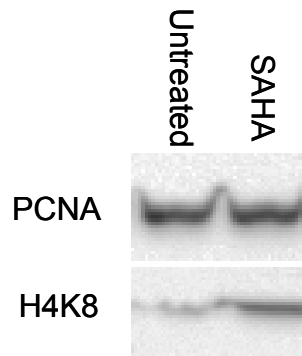


Figure 4-13 Western blot of tumours from Ramos xenografts:

SCID mice with established subcutaneous Ramos tumours were treated with SAHA 50mg/kg or a corresponding concentration of DMSO via intraperitoneal injection. After 6 hours the mice were culled and tumours were removed. and homogenised to create a single cell suspension. 1×10^6 cells were lysed in 70 μ l sample buffer (3x loading buffer, 30x DTT, H₂O) and sonicated. Samples were subjected to immunoblotting as described.

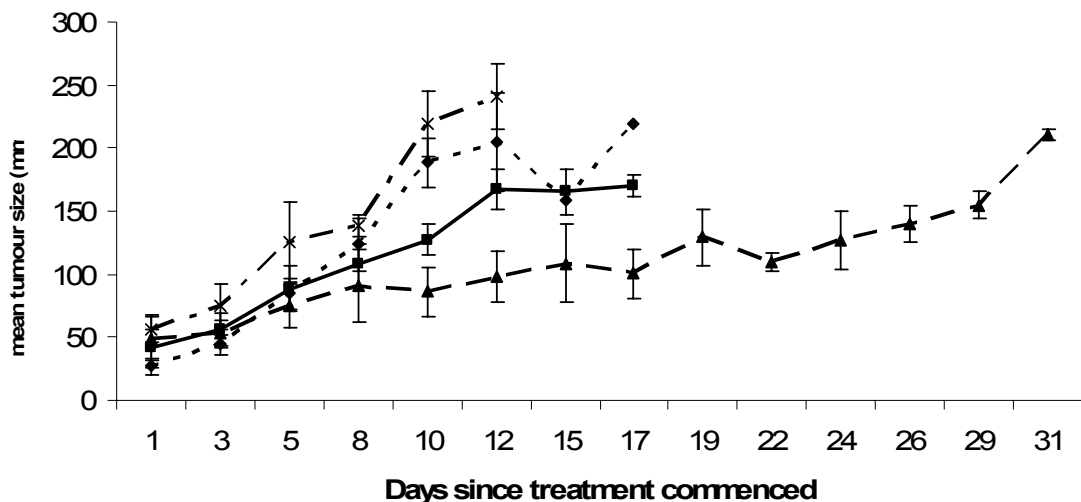


Figure 4-14 Rate of tumour growth in SCID mice with established tumours:

SCID mice were inoculated with 5×10^6 Ramos cells in the flank. Once tumours were palpable, mice were randomly assigned to treatment groups: DMSO/control (x), SAHA 25mg/kg for 14 days (♦), Rituximab 250 μ g/ml on Day 7 (■) or the combination (▲). Tumour size in 2 dimensions and weight were estimated three times weekly. Data shown represents: mean tumour size (+/-SEM) from surviving mice for each treatment (n=5).

The effect of the different treatments on survival is shown [Figure 4-15]. The Kaplan Meier plot shows the cumulative survival from 4 separate experiments. Combination treatment resulted in a statistically significant improvement in survival compared to control or SAHA treated animals ($p<0.001$). Across the entire duration of the experiments combination treatment showed an improved median overall survival compared to rituximab alone, but this was of borderline significance ($p=0.067$). When the survival curves were compared at an earlier timepoint closer to completion of SAHA dosing there was a statistically significant benefit for combination treatment over Rituximab alone ($p=0.017$). These data demonstrate the effect of combination treatment in a xenograft model, reinforcing the synergistic effect observed in vitro.

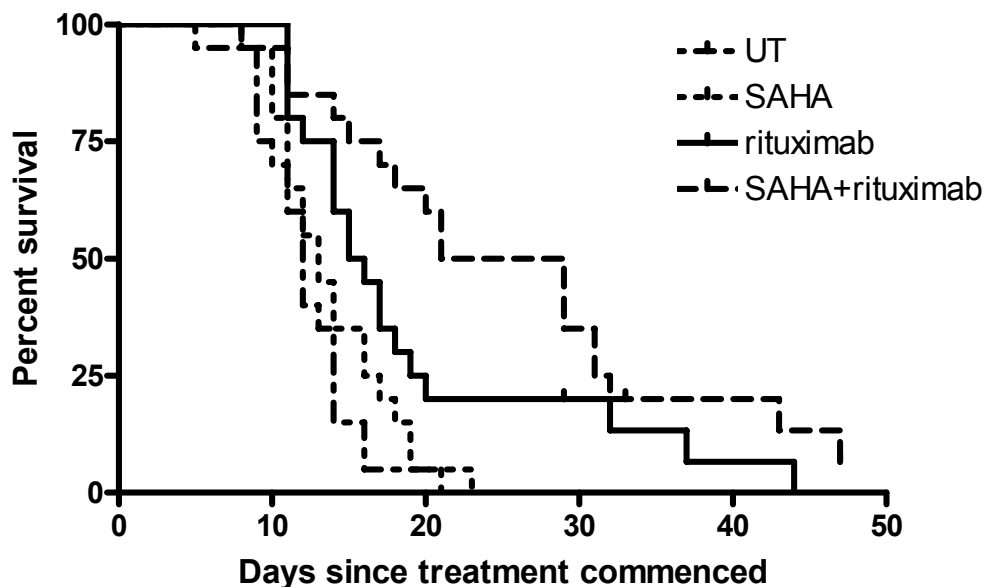


Figure 4-15 cumulative survival in xenograft model

Kaplan Meier analysis of cumulative survival of mice from 4 experiments are shown (n=80). Survival was measured from the first day of treatment for mice with established and non established tumours. All control mice received DMSO and PBS IP at concentrations corresponding to the active agents. Rituximab treated mice received 250µg on day 1. SAHA treatment arm includes mice who received SAHA 25mg/kg for 7 days, 50mg/kg for 14 days and 25mg/kg for 14 days. All control mice received. Both Rituximab and combination treated arms showed a significant survival benefit over the control arm ($p<0.05$). Combination treatment showed a trend towards improved median survival compared to rituximab alone (25 Vs15.5 days, $p=0.067$)

4.7 Discussion

The data presented in this chapter regarding the single agent activity of CD20 mAb and HDI are consistent with the published data for the activity of these agents in inducing cell death in non Hodgkin's lymphoma cell lines. It has been shown that treatment of B cell NHL cell lines with type I mAb (rituximab) results in little or no induction of cell death [84, 266] unless crosslinking is used. In subsequent studies *Shan et al* utilised Annexin V and PI staining and demonstrated induction of apoptosis without cross linking [85]. In the time course assay [Figure 4-8] cross linked rituximab resulted in 36% Annexin V positive cells after 48 hours treatment. Work in Southampton has concentrated on type II mAb (B1) which are more effective at inducing cell death than type I mAb [87], as shown here [Figure 4-4]. It appears that type II mAb utilise different mechanisms for inducing cell death to type I mAb. In the case of type II mAb this cell death is independent of caspase activity and only partially blocked by overexpressing Bcl-2 [71, 87, 90]. Type I mAb appear to utilise classical apoptotic pathways with PARP cleavage and DNA fragmentation [85, 88, 267]. Despite persisting debate about the exact mechanism of action of these agents, they have proven most effective in clinical use when given in combination with other agents. This cooperative activity is underpinned by mechanistic data supporting the importance of intracellular signaling events in these interactions. *Demidem et al* [268] observed that cell lines resistant to chemotherapeutic agents (doxorubicin and cisplatin) could be resensitised by pre treatment with CD20 mAb. Further studies by this group have suggested that downregulation of BclxL and Bcl-2 are responsible for this effect [68]. They have been able to show that rituximab modulates a number of key upstream pathways responsible for regulating these Bcl-2 family proteins. Initially they assessed the effect of rituximab on the ERK 1/2 pathway. They showed that monomeric rituximab inhibited ERK 1/2 phosphorylation resulting in downregulation of BclxL [102]. Inhibition of the NFkB pathway was also observed using EMSA, with time dependent downregulation of Bcl-X_L expression demonstrated with western blotting [269]. Regulation of STAT

pathways have also been implicated in the generation of a chemosensitive phenotype by rituximab via down regulation of IL-10 and STAT3 phosphorylation [270].

The ability of HDI to induce cell death in a dose dependent manner has been well described with other investigators demonstrating this effect at similar concentrations to those illustrated here [262-264]. The data in this chapter demonstrates that 2 clinically relevant HDI induce apoptosis in a dose and time dependent fashion in a panel of B cell NHL cell lines. It also illustrates that this effect is not dependent on the inhibition of class II HDAC enzymes as the effect is observed with FK228 which is a specific inhibitor of class I HDACs [201].

Despite their ability to induce cell death in a wide range of haematological and solid tumour cell lines, the exact mechanism of action of HDIs remains elusive. Their ability to induce apoptosis was reported in 1999 by *Vrana et al* [214]. They observed that treatment of U937 leukaemia cell line with SAHA resulted in PARP cleavage and induction of caspase 3 activity. They also demonstrated that this effect could be overcome by overexpression of Bcl-2 and Bcl-X_L and required an intact c-Jun/AP1 axis. Subsequent studies have mapped the apoptotic pathways induced more clearly; *Henderson et al* [271] used an MCF7 cell line expressing a dominant negative form of Caspase 9. They observed that although processing of other caspases occurred following TSA treatment, over expression of the aberrant caspase 9 blocked this effect. They postulated that caspase 9 was activated by release of cytochrome C in a Bcl-2 dependent fashion. The role of cytochrome C release is supported by other investigators [272], although this group showed that caspase activity was dispensable, albeit in a different cell line. Taken together this data suggests that the effects seen may be cell line and HDI specific.

Despite the ability of HDI to induce apoptosis, their most promising activity has been observed in combination with other agents. They have shown promising activity in combination with the monoclonal antibody trastuzumab resulting in synergistic induction of apoptosis [238, 242]. Synergy may result from counteracting HER2 over expression as HDAC inhibition reduced HER2 mRNA transcript expression and induced HER2 protein degradation

[242, 243]. The latter mechanism occurred via acetylation of heat shock protein (HSP) 90 causing its inactivation and loss of multiple HSP90 client proteins. HSP90 acetylation decreased ATP binding inducing a shift from HER2 binding with HSP90 to HSP70, resulting in HER2 targeting for ubiquitination and proteasomal degradation [242]. This example demonstrates the ability of HDI to interact with monoclonal antibodies to potentiate their activity. Perhaps more relevant to combination with rituximab is the cooperative effect observed with the proteasome inhibitor bortezomib [273]. In this study combination treatment resulted in synergistic induction of classical apoptosis with caspase activation. Of particular relevance was the observation that combination treatment resulted in inhibition of NF κ B signaling, a mechanism that may be important for combination with CD20 mAb [273].

The ability of SAHA and rituximab to produce synergistic induction of apoptosis has also been described [274]. In this study SU-DHL-4 and Daudi cell lines were used to show synergistic growth inhibition as well as induction of apoptosis. The data presented in this chapter demonstrates this effect across a wider range of cell lines and with different combinations of mAb and HDI. These differences are important as they help to probe some of the potential mechanisms underlying this interaction.

All except one of the cell lines tested resulted in synergistic induction of apoptosis despite a broad spectrum of expression of Bcl-2 and STAT family proteins (data not shown). Of note the RL cell line has high levels of Bcl-2, Bcl X_L and STAT3 all of which have been implicated in resistance to HDI mediated induction of apoptosis. Type I and II mAb appear to utilise different cell death pathways yet both agents synergise with HDI. The assays utilised in this chapter are not specific for the different apoptotic pathways, but it seems clear that synergistic activity results in translocation of PS to the cell membrane and ultimately loss of membrane integrity. Further investigation of the apoptotic mechanisms involved will be discussed in chapter 5. It is clear from the literature that type II mAb do not invoke intracellular Ca²⁺ flux [99], yet synergistic induction of apoptosis was still observed with SAHA suggesting that this is irrelevant for synergistic killing.

5 Mechanisms underlying cytotoxicity

5.1 Introduction

With the mechanism of action of both agents *in vivo* unclear, investigations initially explored simple interactions that might account for the synergistic induction of apoptosis observed. The effect of combination treatment on levels of histone acetylation, surface CD20 expression and intracellular Ca^{2+} flux were assessed. Subsequently the effect of treatment on Bcl-2 family protein expression was examined. Having demonstrated that combination treatment resulted in induction of apoptosis, western blotting was used to investigate processing of caspases and poly ADP ribose polymerase (PARP). Subsequently overexpression of Bcl-2 and caspase inhibitors were utilised to explore this interaction.

5.2 Induction of histone acetylation

Induction of histone acetylation is one of the best described direct biochemical responses following treatment with HDAC inhibitors. Two assays were performed to identify whether combination treatment with HDAC inhibitors and CD20 mAb resulted in changes in the dynamics of histone acetylation compared to HDAC inhibitors alone. Initially timecourse assays were performed to examine the dynamics of histone acetylation in Ramos cells treated with SAHA. Cells were treated at the IC₅₀ from previously performed cell death assays with or without crosslinked rituximab. This concentration was chosen as it had induced robust synergistic apoptosis. Acetylation was increased within 2 hours and was not affected by the addition of Rituximab which had no effect on histone acetylation [**Figure 5-1**]. To investigate this effect further western blotting was performed in the RL cell line, which had not shown synergistic induction of apoptosis with the combination. [**Figure 5-2**]. This again demonstrates that Rituximab treatment resulted in no change in the dynamics of histone acetylation resulting from treatment with SAHA

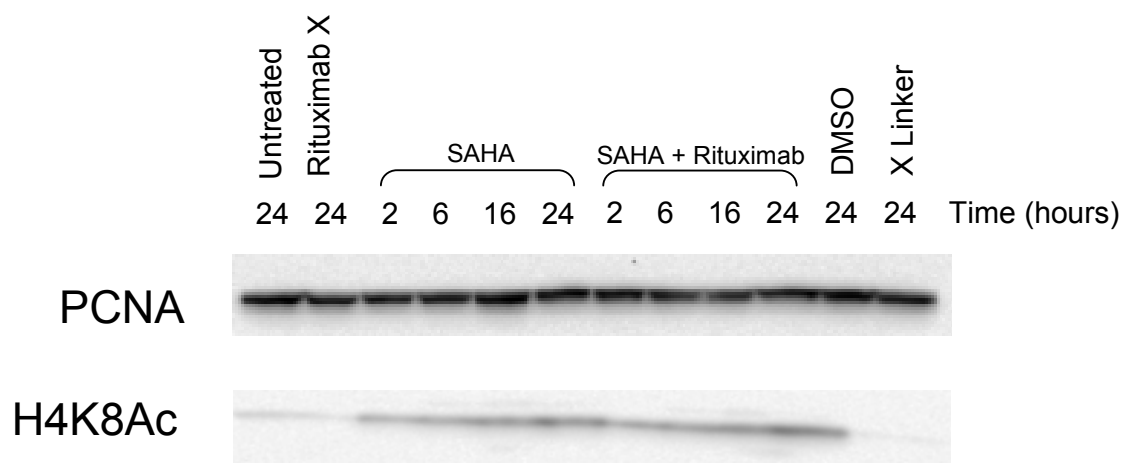


Figure 5-1 Histone acetylation in Ramos cells:

Ramos cells at $0.5 \times 10^6/\text{ml}$ were plated in 24 well plates. Cells were treated with SAHA ($5.5 \mu\text{M}$) alone or in combination with crosslinked Rituximab ($3 \mu\text{g}/\text{ml}$). Control samples were left untreated, treated with crosslinked Rituximab ($3 \mu\text{g}/\text{ml}$), X linker alone or an equivalent concentration of DMSO. At the time points indicated cells were harvested and whole cell lysates were prepared for western blotting as described above. Results shown are representative of two independent experiments.

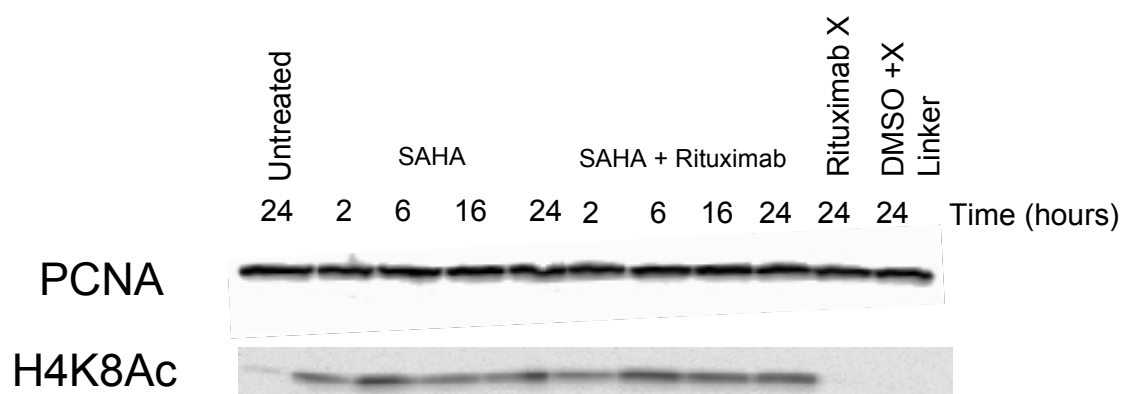


Figure 5-2 Histone acetylation in RL cells:

RL cells at $0.5 \times 10^6/\text{ml}$ were plated in 24 well plates. Cells were treated with SAHA ($3.2 \mu\text{M}$) alone or in combination with crosslinked Rituximab ($3 \mu\text{g}/\text{ml}$). Control samples were left untreated, treated with crosslinked Rituximab ($3 \mu\text{g}/\text{ml}$), or an equivalent concentration of DMSO with X linker. At the time points indicated cells were harvested and whole cell lysates were prepared for western blotting as described above. Results shown are representative of two independent experiments.

To quantify the effect of the various treatment combinations on the levels of histone acetylation, western blotting was repeated at the 24 hour timepoint with SAHA alone or in combination with Rituximab or B1. Quantification of band intensity was performed from duplicate immunoblots. Figure 5-3, shows a representative blot from Ramos cells with levels of histone acetylation shown in the bar chart. There was no significant difference in the levels of histone acetylation observed in SAHA or combination treated cells. This effect was also observed in the SU-DHL-4 cell line **[Figure 5-4]**.

Western blotting with quantification of levels of histone acetylation is widely used as a measure of HDI activity. As already discussed histone acetylation occurs as a result of the balance between HDAC and HAT activity. An HDAC enzyme inhibition study was performed with a dose range of SAHA alone or in combination with Rituximab to specifically analyse enzyme inhibition. This colorimetric HDAC enzyme activity assay uses colorimetric HDAC substrate with an acetylated lysine side chain. Deacetylation of the substrate results in production of a chromophore. This can be measured using a spectrophotometer, to determine HDAC enzyme activity. This assay was performed in the SU-DHL-4 cell line as a representative cell line to corroborate the findings from western blotting. Cells were treated for 2 hours with increasing concentrations of SAHA alone or in combination with Rituximab. This timepoint was chosen as western blotting had confirmed histone acetylation and cells would remain viable. The addition of Rituximab had no effect on the dose response curve for the HDAC enzyme inhibition of SAHA **[Figure 5-5]**. Taken together these data demonstrate that SAHA produces HDAC enzyme inhibition in a dose dependent fashion with time dependent accumulation of acetylated core histones, as measured by histone 4 lysine 8 acetylation. The addition of CD20 mAb does not appear to affect the modulation of this specific HDAC target.

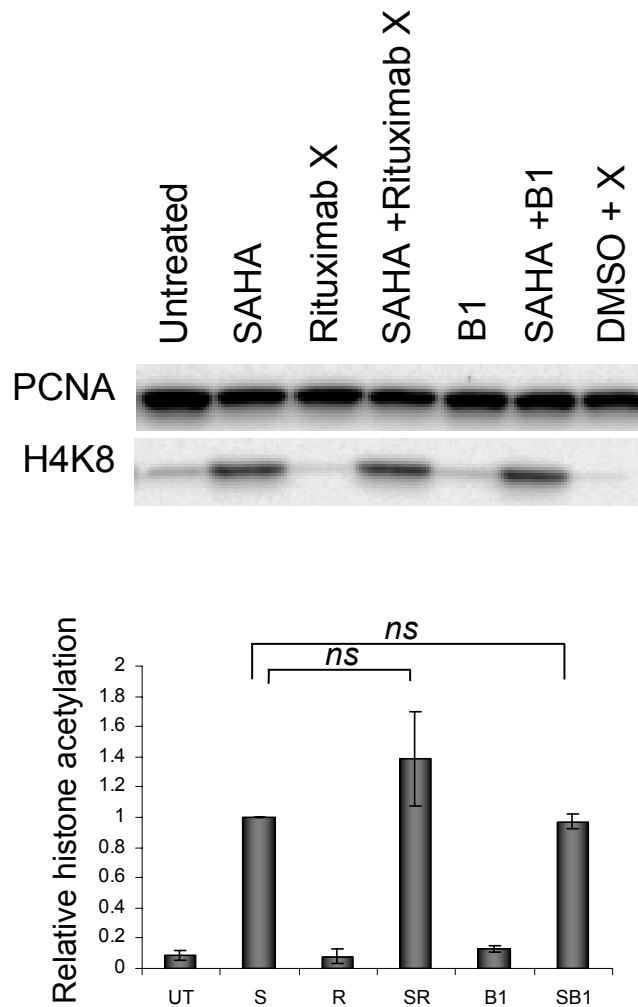


Figure 5-3 Histone acetylation in Ramos cells:

Ramos cells at $0.5 \times 10^6/\text{ml}$ were plated in 24 well plates. Cells were treated with SAHA ($5.5 \mu\text{M}$) alone or in combination with crosslinked Rituximab ($3 \mu\text{g}/\text{ml}$) or B1 ($3 \mu\text{g}/\text{ml}$). Control samples were left untreated, treated with crosslinked Rituximab ($3 \mu\text{g}/\text{ml}$), or B1 ($3 \mu\text{g}/\text{ml}$). After 24Hrs cells were harvested and whole cell lysates were prepared for western blotting. Results shown are representative of two independent experiments. Bar chart shows mean level of H4K8Ac (\pm range) from duplicate blots normalised to PCNA loading control, relative to SAHA treated cells (set to 1.0). Independent Student's t-test was performed comparing SAHA to combination treatment.

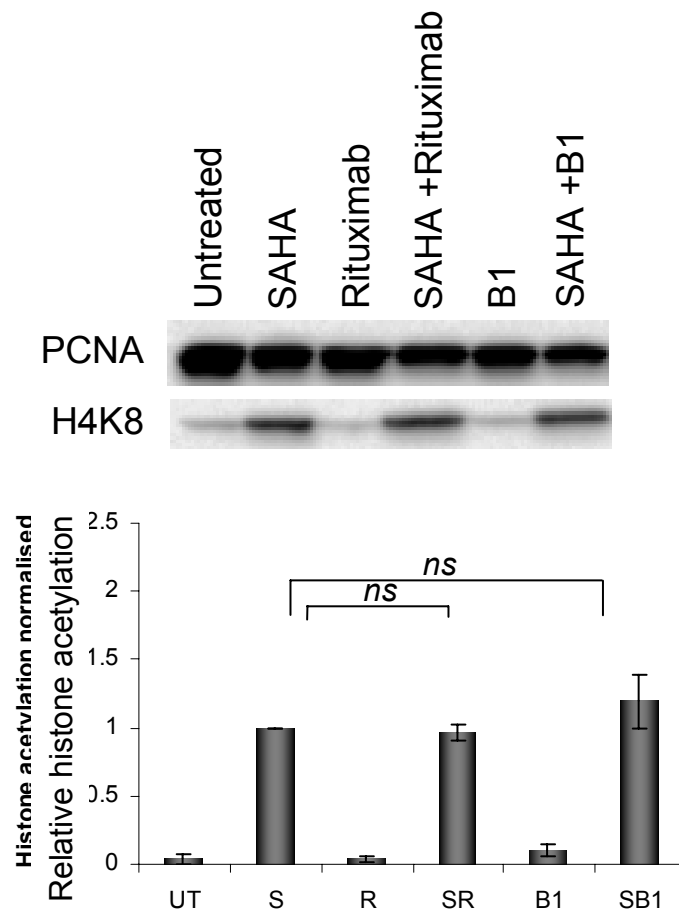


Figure 5-4 Histone acetylation in SU-DHL-4 cell line:

SU-DHL-4 cells at 0.5×10^6 /ml were plated in 24 well plates. Cells were treated with SAHA ($2.4 \mu\text{M}$) alone or in combination with Rituximab ($3 \mu\text{g/ml}$) or B1 ($3 \mu\text{g/ml}$). Control samples were treated with DMSO, Rituximab ($3 \mu\text{g/ml}$), or B1 ($3 \mu\text{g/ml}$). After 24Hrs cells were harvested and whole cell lysates were prepared for western blotting. Results shown are representative of two independent experiments. Bar chart shows mean level of H4K8Ac (\pm range) from duplicate blots normalised to PCNA loading control, relative to SAHA treated cells (set to 1.0). Independent Student's t-test was performed comparing SAHA to combination treatment.

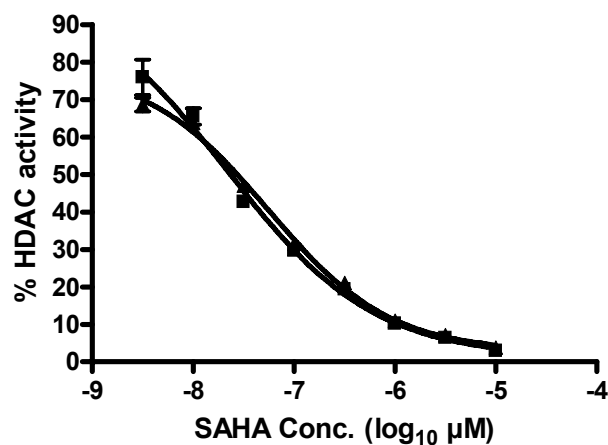


Figure 5-5 HDAC enzyme assay in SU-DHL-4 cell line:

SU-DHL-4 cells at 0.5×10^6 cells/ml were plated in 96 well plates and cultured for 2 hours with SAHA (0.075-10 μM) (■) or SAHA and Rituximab (3 $\mu\text{g/ml}$) (▲). Control wells were treated with corresponding concentrations of DMSO or rituximab alone. HDAC enzyme assay was performed. Graph shows a dose response curve for mean percentage enzyme activity (\pm -range), normalised to control wells (DMSO) for triplicate samples from a representative experiment.

5.3 Modulation of CD20 expression

Having excluded modifications of HDAC inhibitor associated histone acetylation, it was important to exclude that SAHA was upregulating surface CD20 expression or modifying CD20 association with Triton X insoluble lipid rafts. Initially the baseline level of CD20 expression was assessed in the panel of B cell NHL cell lines already utilised. There was a large range of CD20 expression, and RL cells which had not shown synergistic killing displayed high levels of surface CD20 compared to cell lines which had displayed strong synergy [**Figure 5-6**].

The Ramos cell line, with a moderately high surface CD20 level, was again chosen to examine the effect of treatment on CD20 expression. This was assessed in two ways using a flow cytometry assay. Firstly the global levels of surface CD20 expression were assessed with and without pretreatment with SAHA. This appeared to have no effect on FITC labelled Rituximab or B1 binding at the time points utilised [**Figure 5-7**]. Secondly the extent of CD20 lipid raft redistribution was examined. It has already been described that type I, but not type II CD20 mAb induce CD20 lipid raft redistribution [87]. In these experiments lipid rafts were defined by their confinement to the Triton X-100 insoluble membrane portion. In the Triton X-100 insoluble fraction Rituximab had resulted in accumulation of CD20, with binding $\geq 100\%$ of the whole membrane fraction. The type II mAb had not resulted in translocation of CD20 to Tx-100 insoluble lipid rafts with binding reduced to $\leq 40\%$ of the whole membrane fraction consistent with published data. This effect on CD20 was not influenced with pretreatment with SAHA for the timepoint indicated [**Figure 5-7**]. In conclusion this data suggested that synergy was observed in cell lines with a range of CD20 expression and that treatment with SAHA did not result in modulation of CD20 or influence redistribution patterns at early timepoints following CD20 mAb ligation.

Having demonstrated that the synergy observed was not due to alterations in the putative targets of HDI or CD20 mAb, further investigation concentrated on the effect of either agent on induction of apoptotic pathways.

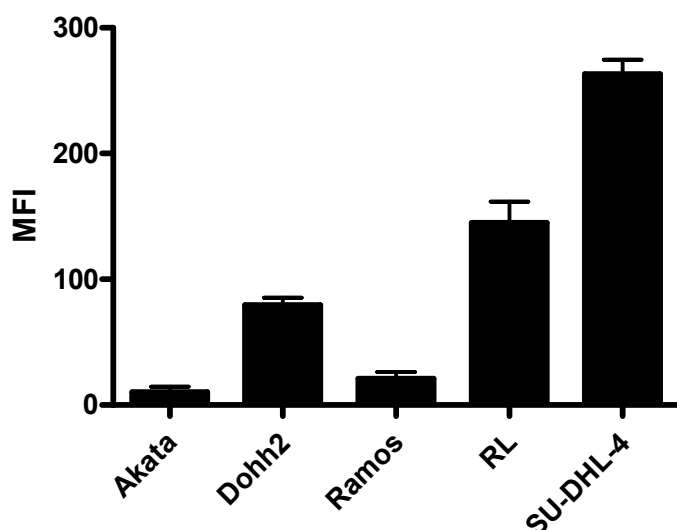


Figure 5-6 CD20 expression in panel of B cell NHL cell lines:

0.5x10⁶ cells from each cell line was placed in a FACS tube and washed in FACS buffer, cells were resuspended in 50µl FACS buffer with FITC labelled rituximab or FITC labelled IgG1 isotype control antibody. Cells were incubated on ice for 30 minutes, then washed twice in FACS buffer. Cells were resuspended and analysed by flow cytometric analysis. Graph shows mean MFI (±range) relative to Isotype control for each cell line from two independent experiments.

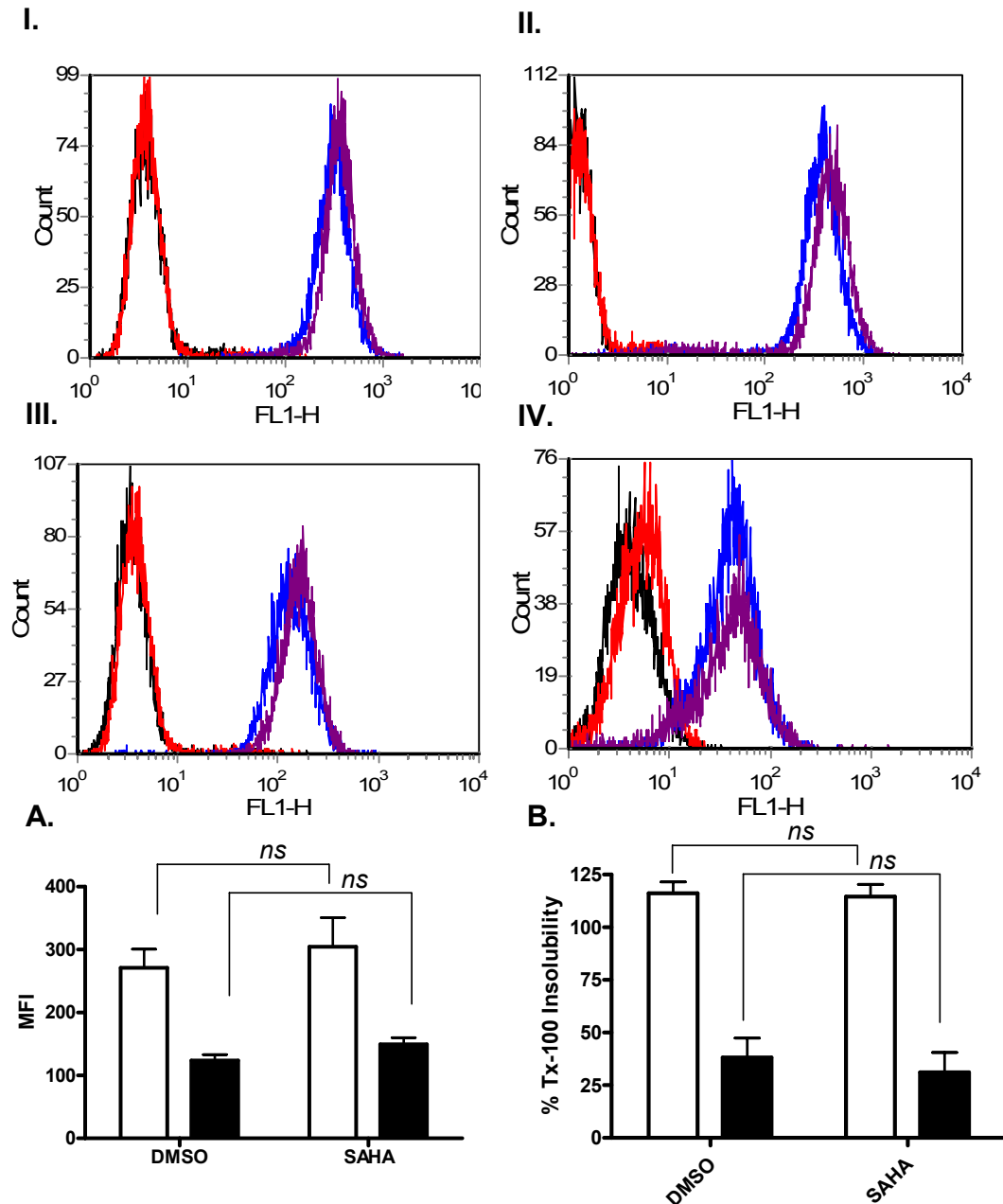


Figure 5-7 Effect of SAHA on CD20 expression in Ramos cells:

Ramos cells at 0.5×10^6 were treated overnight with $5.5 \mu\text{M}$ SAHA or a corresponding concentration of DMSO. Cells were harvested and washed in FACS buffer, and incubated on ice with $10 \mu\text{g/ml}$ FITC labelled rituximab or B1 for 30 minutes. At this point samples were split, 1 part was incubated with Triton X100 for 30 minutes (III, IV), 1 part remained on ice (I, II). All samples were washed twice and resuspended with FACS buffer.

Representative histograms are shown with isotype control DMSO (■), SAHA (■) and rituximab plus DMSO (■), SAHA (■) in I and III. B1 DMSO (blue) and SAHA (purple) in II and IV. Bar charts show (A) mean CD20 binding (\pm range) with Rituximab (□) and B1 (■) for DMSO or SAHA pretreated cells from duplicate experiments. (B). mean percentage Tx-100 insoluble CD20 binding (\pm range) with Rituximab (□) and B1 (■) for DMSO or SAHA pretreated cells from duplicate experiments.

5.4 Measurement of Ca^{2+} flux and ERK phosphorylation

In contrast to histone acetylation one of the earliest events occurring after mAb binding is Ca^{2+} fluxing. Therefore flow cytometric analysis of Ca^{2+} fluxing following Rituximab binding was performed in Ramos cells in the presence or absence of SAHA pretreatment to elucidate whether Ca^{2+} flux was potentiated by combination treatment [**Figure 5-8**]. In the absence of Rituximab no Ca^{2+} flux occurs even with the addition of crosslinking agent. Rituximab only results in Ca^{2+} fluxing after the addition of the crosslinking agent. This effect is not changed by pretreatment with SAHA. The histogram shows mean values for the FL5/FL4 ratio against time for untreated and SAHA pretreated samples. This result demonstrates that the synergistic killing observed is not due to changes in Ca^{2+} fluxing following Rituximab treatment.

Another well described downstream sequelae of Rituximab binding to the CD20 receptor is ERK 1/2 phosphorylation. A flow cytometry assay was performed to investigate whether SAHA affected ERK 1/2 phosphorylation. The SU-DHL-4 cell line was chosen as ERK 1/2 phosphorylation occurs in this cell line following CD20 ligation in the absence of crosslinking. Consistent with published literature type I but not type II CD20 mAb induce ERK 1/2 phosphorylation, this is unaffected by the addition of SAHA [**Figure 5-9**].

These two experiments do not support the hypothesis that SAHA modulates early intra cellular signalling events following type I mAb ligation.

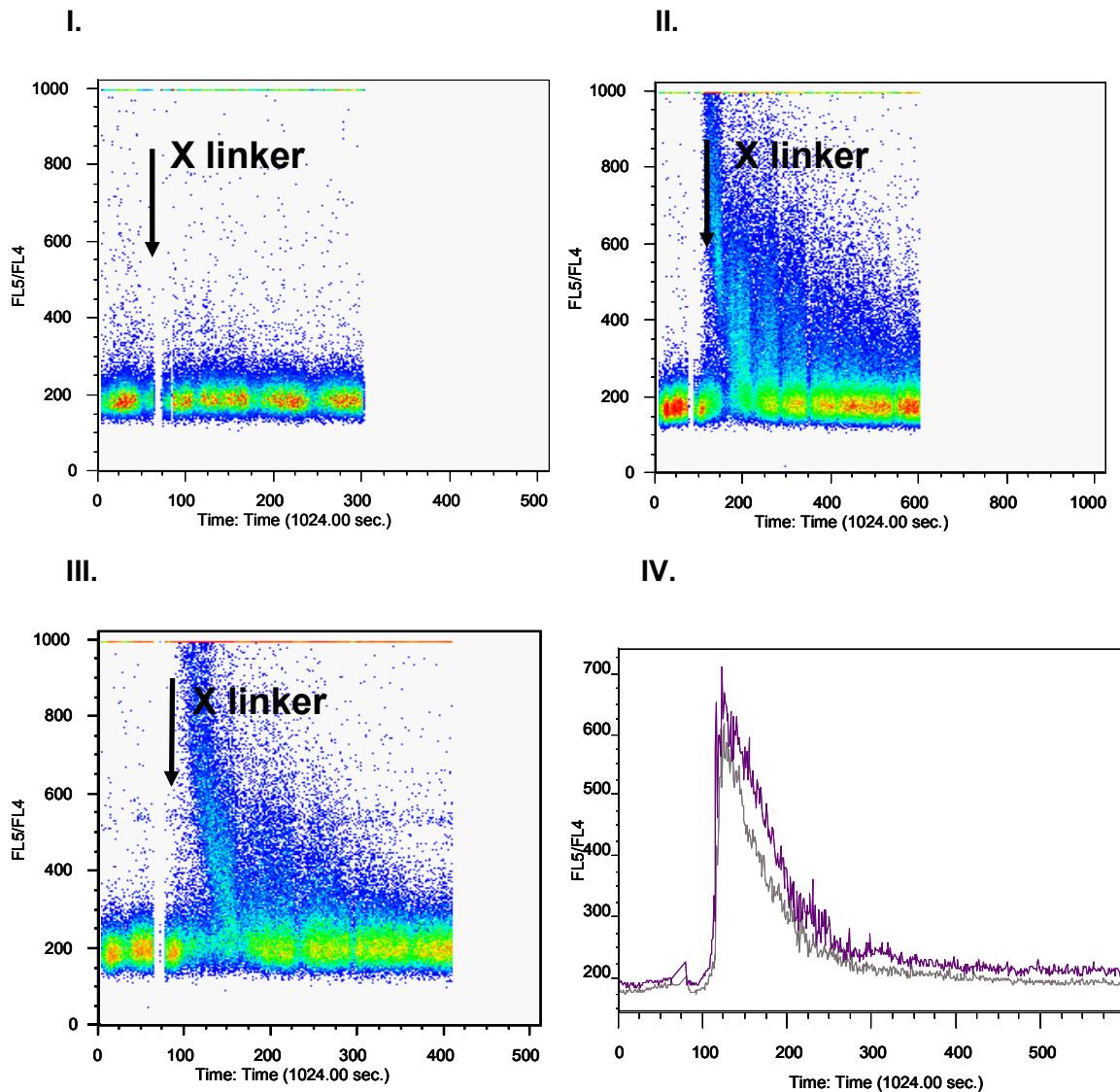


Figure 5-8 Ca^{2+} flux following Rituximab treatment in Ramos cells
 1×10^7 Ramos cells were treated with $5.5 \mu\text{M}$ SAHA or a corresponding concentration of DMSO for 2 hours and stained for Ca^{2+} measurement as described. Cells were subsequently divided into two samples and one sample was treated with rituximab $5 \mu\text{g}/\text{ml}$ and one treated with a corresponding concentration of PBS for 15 minutes. Ca^{2+} flux was measured for 60 seconds before addition of crosslinking agent. Dot plots are shown for cells treated with I. PBS, II. Rituximab and III. SAHA and Rituximab. IV. Shows mean FL5/FL4 ratio for Rituximab treated (■) and SAHA + Rituximab (■) treated cells. Data shown are representative of two independent experiments.

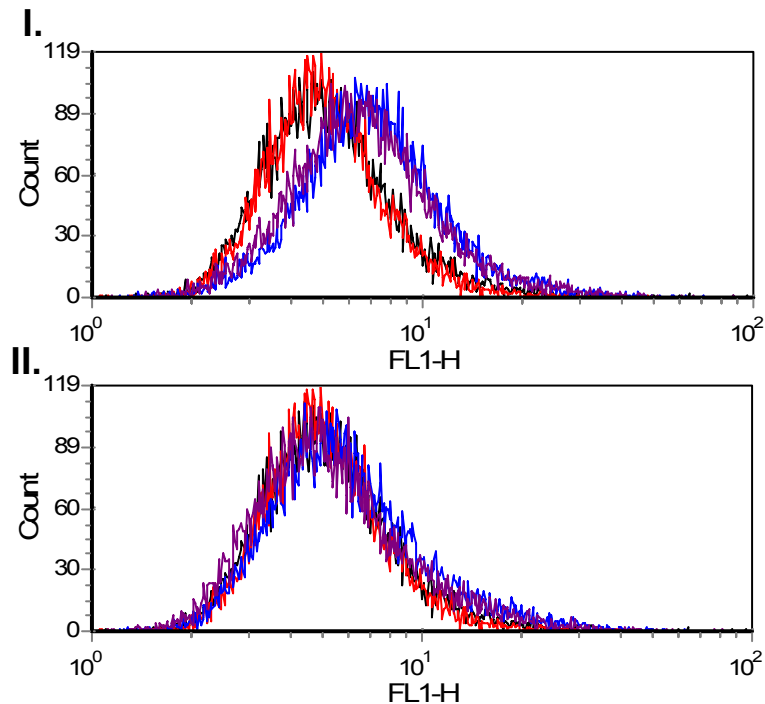


Figure 5-9 ERK phosphorylation in SU-DHL-4 cell line

1×10^6 SU-DHL-4 cells were treated incubated with Rituximab or B1 with or without SAHA. Control samples were treated with SAHA alone or a corresponding concentration of DMSO. After 15 minutes cells were harvested, permeabilised and stained with pERK antibody for 30 minutes. Samples were washed twice and resuspended in FACS buffer. I. shows untreated (■) and SAHA treated controls (■) and Rituximab (■) and combination treated samples (■). II. Shows untreated (■) and SAHA treated controls (■) and B1 (■) and combination treated samples (■). Data shown are representative of two independent experiments.

5.5 *Mechanisms of cell death*

With clear evidence of synergistic cell killing demonstrated with flow cytometry using Annexin V and PI staining and no evidence that this was due to changes in CD20 expression, Ca^{2+} flux, ERK phosphorylation, or histone acetylation, investigation turned to the mechanism of cell death.

Published data suggest that cell death due to HDAC inhibitors is via caspase dependent apoptotic pathways with regulation of genes from the intrinsic apoptotic pathway [211]. The role of the intrinsic pathway is supported by other investigators [214, 215]. These observations are not universally observed with evidence of modulation of the extrinsic pathway [216]. Thus it appears that their ability to induce apoptosis appears to be cell line and HDI specific. In Ramos cells treated with SAHA time dependent induction of apoptosis occurs [Figure 5-10]. PARP cleavage was observed after 16 hours incubation with cleavage of effector caspase 3 at the same timepoints. Processing of the intrinsic initiator caspase 9, appeared to precede these events, implying it was an upstream event. The effect on caspase 8 was also investigated and there did not appear to be any processing visible.

In contrast to this the mechanisms adopted by CD20 mAb are much more controversial. In Burkitt lymphoma cell lines CD20 mAb can induce apoptosis [85]. This effect is usually dependent on the addition of an Fc region cross-linking agent or Fc-receptor-bearing accessory cells [85, 98]. The mechanisms of cell death resulting from mAb binding appear to differ depending on the class of mAb used (review [83]). Rituximab treatment in the presence of crosslinking results in classical apoptosis with caspase activation and PARP cleavage [84, 85]. In Ramos cells incubation with a saturating concentration of CD20 mAb produced apoptosis [Figure 5-11]. Western blotting from these experiments showed that this level of cell death was not accompanied by PARP cleavage or caspase 9 processing following incubation with the type II mAb B1. The addition of hypercrosslinking resulted in a small increase in the level of apoptosis and induction of PARP cleavage and caspase 9 processing.

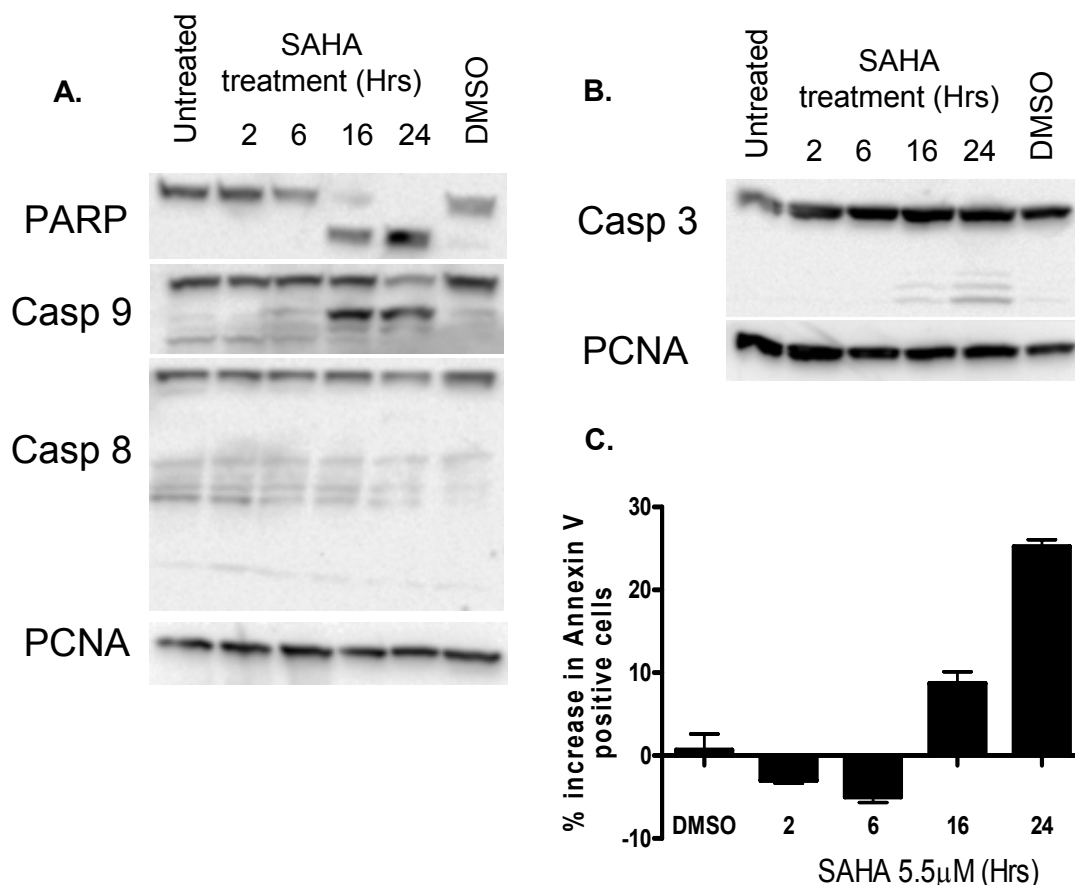


Figure 5-10 Apoptosis following SAHA treatment:

Ramos cells at 0.5×10^6 cells/ml were plated in 6 well plates and treated with SAHA (5.5 μ M). Control samples were left untreated or treated with an equivalent concentration of DMSO. At the timepoints indicated cells were harvested. Duplicate samples from each well were prepared for flow cytometric analysis using Annexin V/PI staining. The remainder was resuspended in a RIPA lysis buffer. Following quantification, 20 μ g of protein per sample was used for immunoblotting. **(A.)** shows PARP, Caspase 9 and 8, with PCNA as a loading control. **(B.)** Shows caspase 3 processing with PCNA loading control. **(C.)** Shows mean % increase in annexin V positive cells (\pm range) compared to untreated cells from the same experiment. Data shown are representative of two independent experiments.

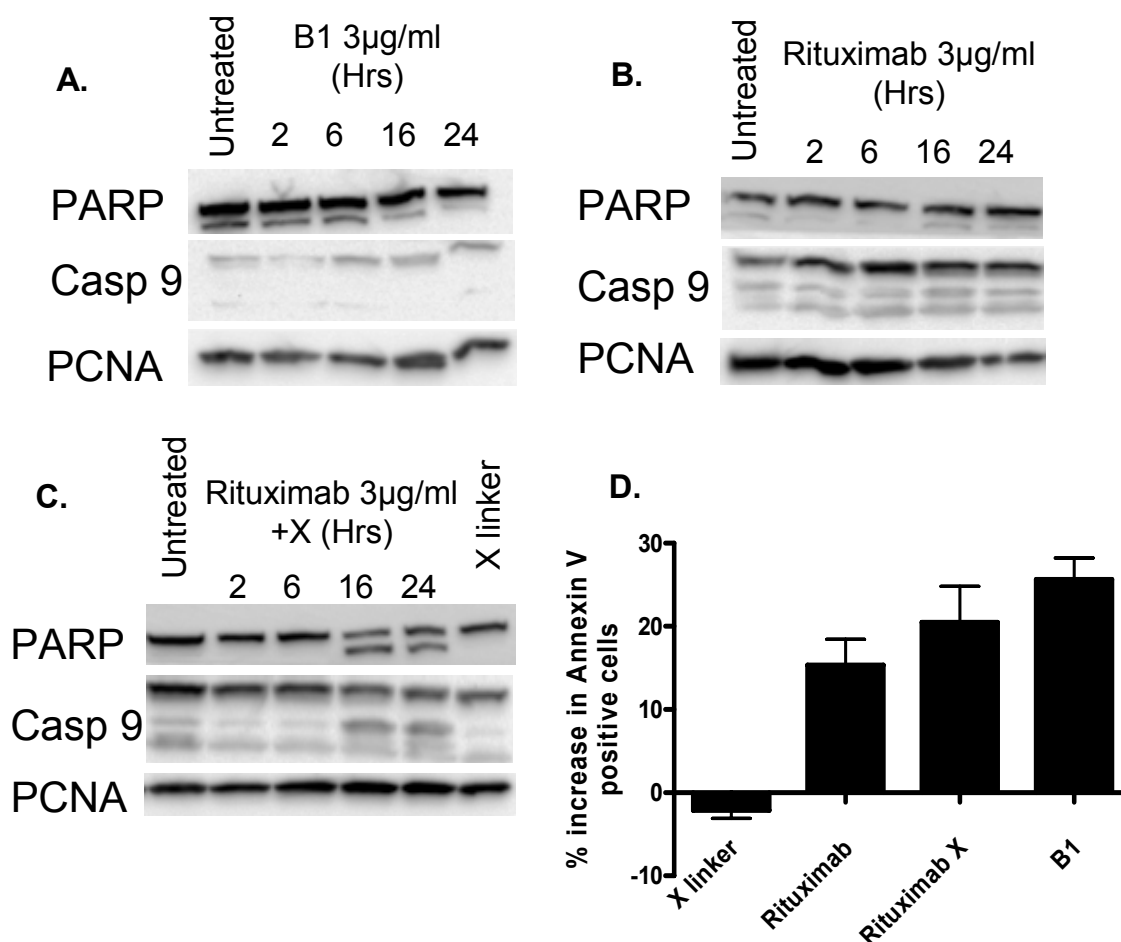


Figure 5-11 Mechanism of induction of cell death with CD20 mAb in Ramos cells:

Ramos cells at 0.5×10^6 cells/ml were plated in 6 well plates and treated with Rituximab (3μg/ml) alone or with a crosslinking agent (X), or B1 (3μg/ml). Control samples were left untreated or treated with a corresponding concentration of crosslinking agent. At the timepoints indicated cells were harvested. Duplicate samples from each well were prepared for flow cytometric analysis using Annexin V/PI staining. The remainder was resuspended in a RIPA lysis buffer. Following quantification, 20μg of protein per sample was used for immunoblotting. **(A.)** shows B1 treated cells, **(B.)** Rituximab and **(C.)** Crosslinked Rituximab. **(D.)** Shows mean % increase in annexin V positive cells following 24 hours treatment (\pm range) compared to untreated cells from 2 independent experiments. Data shown are representative of 2 independent experiments.

The effect of combination treatment was investigated in three B cell NHL cell lines. Compared to SAHA alone combination treatment appeared to induce higher levels of PARP cleavage in Ramos and SU-DHL-4 cells [**Figure 5-12**]. Treatment of RL cells with either SAHA or Rituximab alone or in combination did not result in induction of PARP cleavage, this was consistent with the low levels of cell death observed in previously shown cell death assays.

These timecourse studies did not allow simultaneous comparison of type I and type II CD20 mAb in combination with SAHA, so the experiment was redesigned. Ramos and SU-DHL-4 cells were incubated for 24 hours in the presence of SAHA, Rituximab and B1 alone and in combination [**Figure 5-13**]. Quantification of the levels of PARP cleavage induced by the treatment conditions was performed from duplicate blots using “quantity one” software. The levels of PARP cleavage are shown in the bar charts. There was a modest but significant increase in the levels of cleaved PARP in both cell lines following combination treatment compared to SAHA alone. This data supports the Annexin V/PI cell death analysis and suggests that the synergistic interaction observed is feasibly through activation of apoptotic pathways culminating in PARP cleavage.

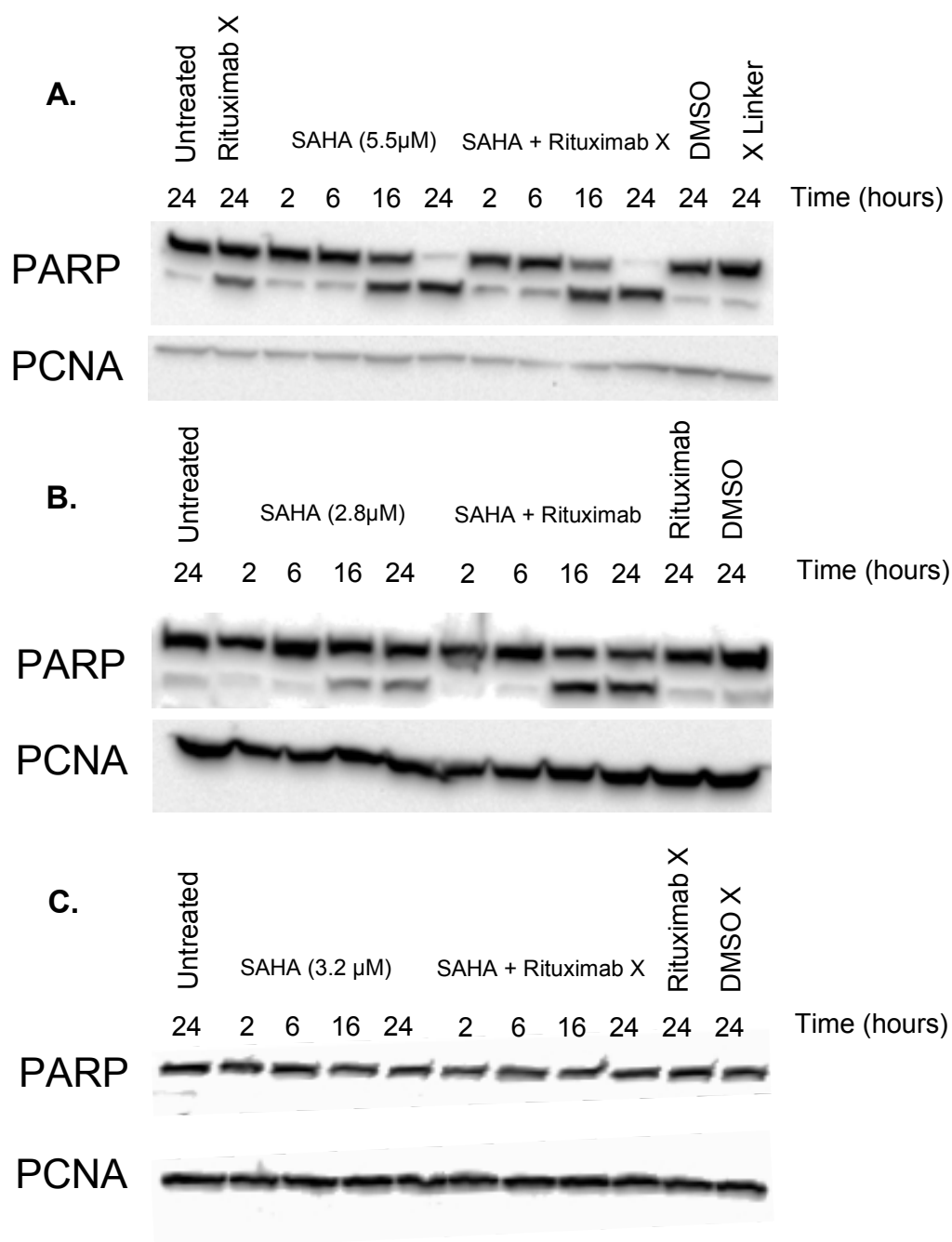


Figure 5-12 Combination treatment in B cell NHL cell lines:

B cell NHL cells at 0.5×10^6 /ml were plated in 24 well plates. Cells were treated with SAHA, at the concentration shown, alone or in combination with Rituximab (3 μ g/ml).. Control samples were left untreated, treated with crosslinked Rituximab (3 μ g/ml), or an equivalent concentration of DMSO and/or crosslinking agent. At the time points indicated cells were harvested and whole cell lysates were prepared for western blotting as described above. Results shown for **(A)** Ramos, **(B)** SU-DHL-4 and **(C)** RL cell lines are representative of two independent experiments.

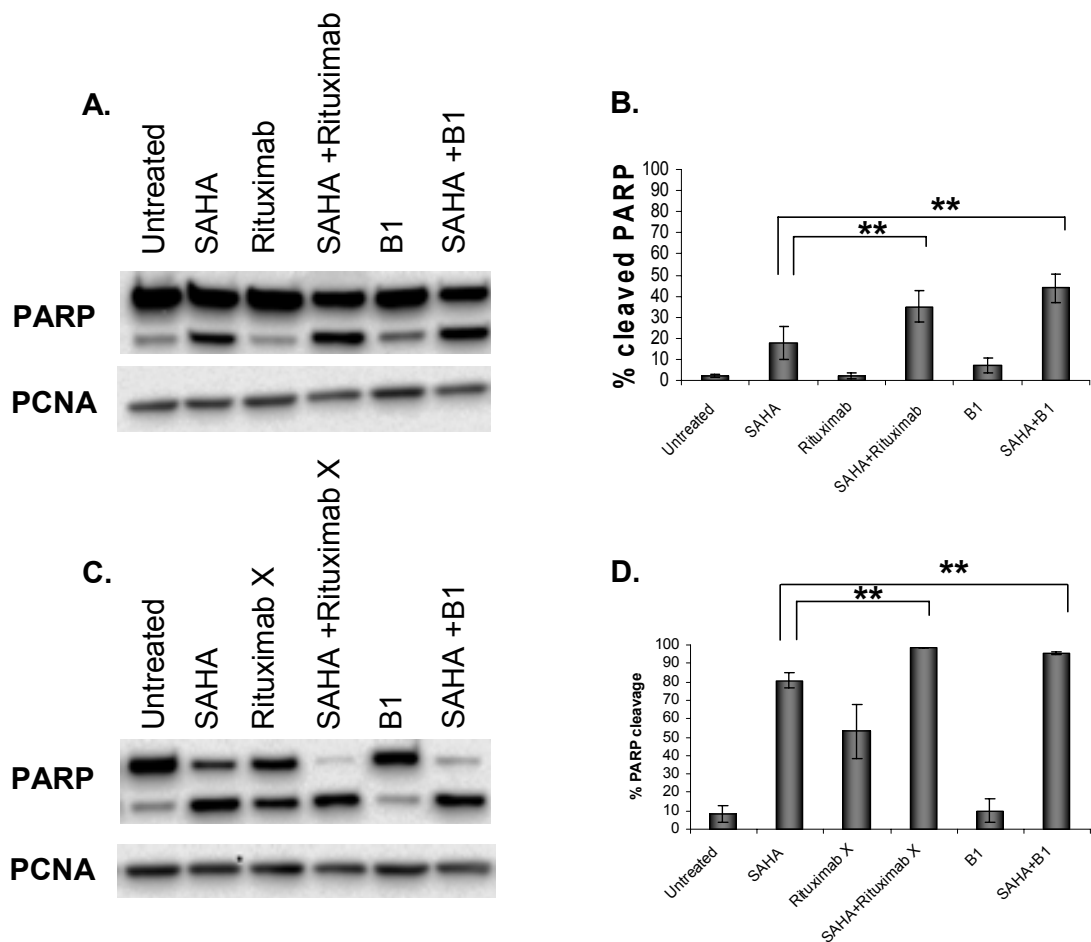
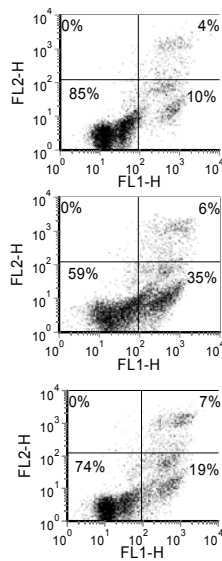


Figure 5-13 Induction of PARP cleavage following combination treatment:

Ramos or SU-DHL-4 cells at $0.5 \times 10^6/\text{ml}$ were plated in 24 well plates. Cells were treated with SAHA ($5.5 \mu\text{M}$ Ramos, $2.8 \mu\text{M}$ SU-DHL-4) alone or in combination with Rituximab ($3 \mu\text{g}/\text{ml}$) or (B1 $3 \mu\text{g}/\text{ml}$). Control samples were treated with an equivalent concentration of DMSO. After 24Hrs cells were harvested and whole cell lysates were prepared for western blotting as described above. Results shown are representative of two independent experiments from (A) SU-DHL-4 and (C) Ramos cells. Bar charts show mean level of cleaved PARP (\pm range) from duplicate blots for (B) SU-DHL-4 and (D) Ramos cells. Independent Student's *t*-test was performed for mean level of cleaved PARP in SAHA compared to combination treated samples. (** $p \leq 0.05$)

To investigate whether caspase processing was necessary for the induction of apoptosis observed following combination treatment, Ramos cells were again incubated with SAHA, Rituximab and B1 alone and in combination in the presence and absence of the pan caspase inhibitor QVD-oph (MP Biomedicals, Aurora, Ohio, USA). SAHA and combination induced apoptosis was inhibited by caspase inhibition [**Figure 5-14**]. The Addition of QVD-oph had no significant effect on levels on annexin V positive cells in Rituximab treated cells, consistent with the observation that caspase activity is not necessary for this effect. Importantly the addition of the pan caspase inhibitor abolished any cooperative effect seen with combination treatment. A similar effect was seen with B1 (data not shown). To establish whether the abolition of cooperative induction of apoptosis observed was through inhibition of caspase processing samples were also prepared for western blotting. Induction of PARP cleavage and caspase 3 and 9 processing was seen, the addition of QVD-oph abolished this effect [**Figure 5-15**]. Taken together these observations support the hypothesis that the synergistic cell death observed is dependent on caspase processing and ultimately PARP cleavage.

A.

untreated

SAHA (5.5µM)

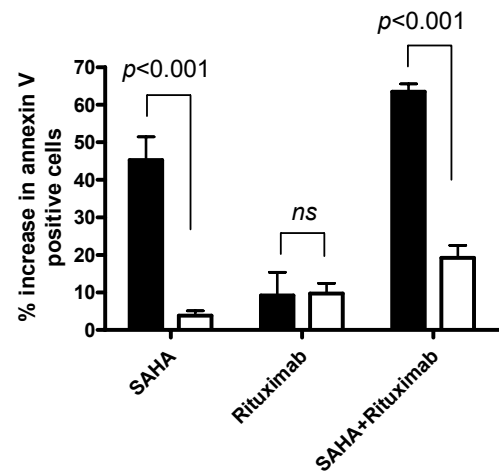
SAHA (5.5µM) +
QVD-oph (12.5µM)**B.**

Figure 5-14 Effect of caspase inhibitor on induction of apoptosis in Ramos cell line:

Ramos cells at 0.5×10^6 cells/ml were suspended in complete medium with QVD-oph (12.5µM) (□) or an equivalent concentration of DMSO (■). Cells were then plated in triplicate in 96 well plates and incubated with SAHA (5.5µM) or Rituximab (3µg/ml) alone or in combination, control samples were treated with an equivalent concentration of DMSO. After 24 hours cells were harvested and prepared for flow cytometric analysis using Annexin V/PI staining. **(A.)** shows representative flow cytometry dot plots. **(B.)** Shows mean % increase in annexin V positive cells (\pm range) from a representative experiment compared to untreated cells. Independent Student's *t*-test was performed comparing presence or absence of QVD-oph. Data shown are representative of two independent experiments.

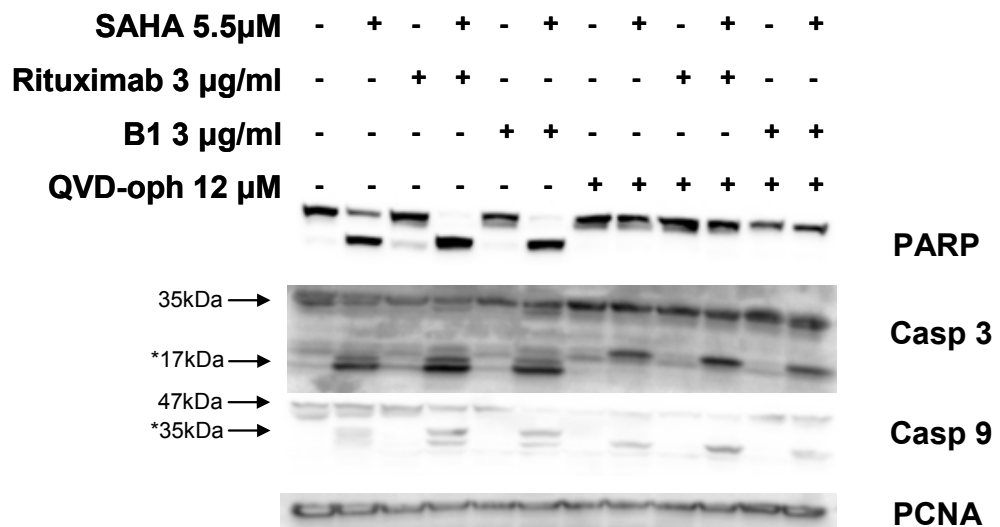


Figure 5-15 Effect of QVD-oph on caspase processing in Ramos cell line:

Ramos cells at 0.5×10^6 cells/ml were suspended in complete medium with QVD-oph (12.5μM) or an equivalent concentration of DMSO. Cells were plated in 6 well plates and incubated with SAHA (5.5μM), Rituximab (3μg/ml) and B1 (3μg/ml) indicated for 24 hours. Control samples were treated with an equivalent concentration of DMSO. Cells were harvested by centrifugation and resuspended in a RIPA lysis buffer. Following quantification, 20μg of protein per sample was used for immunoblotting. Results for PARP, caspase 9 and caspase 3 (*denotes activated cleaved caspase) are shown and are representative of 2 independent experiments.

The synergy data presented in chapter 4 demonstrated that there was variability in the extent of synergistic induction of apoptosis seen across the panel of B cell NHL cell lines. In particular the RL cell line showed no synergistic activity, with only low levels of apoptosis following HDI treatment. In attempting to explain this, the baseline expression of Bcl-2 family proteins was examined. The RL cell line was found to express high levels of Bcl-2 [Figure 5-16].

To further investigate whether this was important the assay was repeated in Ramos cells which were stably transfected to overexpress Bcl-2. This cell line was kindly provided by Dr Mark Cragg. Published data by *Chan et al* [87] had already demonstrated that overexpression of Bcl-2 in these cells was able to inhibit the intrinsic apoptotic pathway. Overexpression of Bcl-2 appeared to result in lower levels of apoptosis following treatment with SAHA compared to the same concentration in standard Ramos. As would be expected there was little effect seen on Rituximab or B1 alone. Following combination treatment overexpression of Bcl-2 results in loss of the synergistic induction of apoptosis seen with SAHA and Rituximab, but not B1 [Figure 5-17]. The addition of QVD-opf resulted in loss of this cooperative activity. Western blotting was also performed and immunoblots for PARP, caspase 3 and 9 are shown [Figure 5-18]. Caspase processing and PARP cleavage was still observed in SAHA treated samples but did not appear to be increased with combination treatment. Once again the addition of the pan caspase inhibitor completely inhibited PARP cleavage.

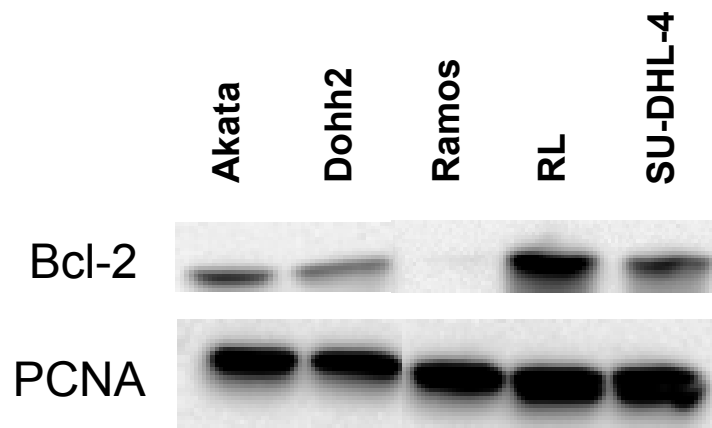


Figure 5-16 Expression of Bcl-2 in B cell NHL cell lines:

0.5x10⁶ cells were harvested by centrifugation and whole cell lysates were prepared as described. 15µl of each sample was loaded and gel electrophoresis was performed as described. Immunoblots for Bcl-2 are shown with PCNA as a loading control. Data shown are representative of two independent experiments.

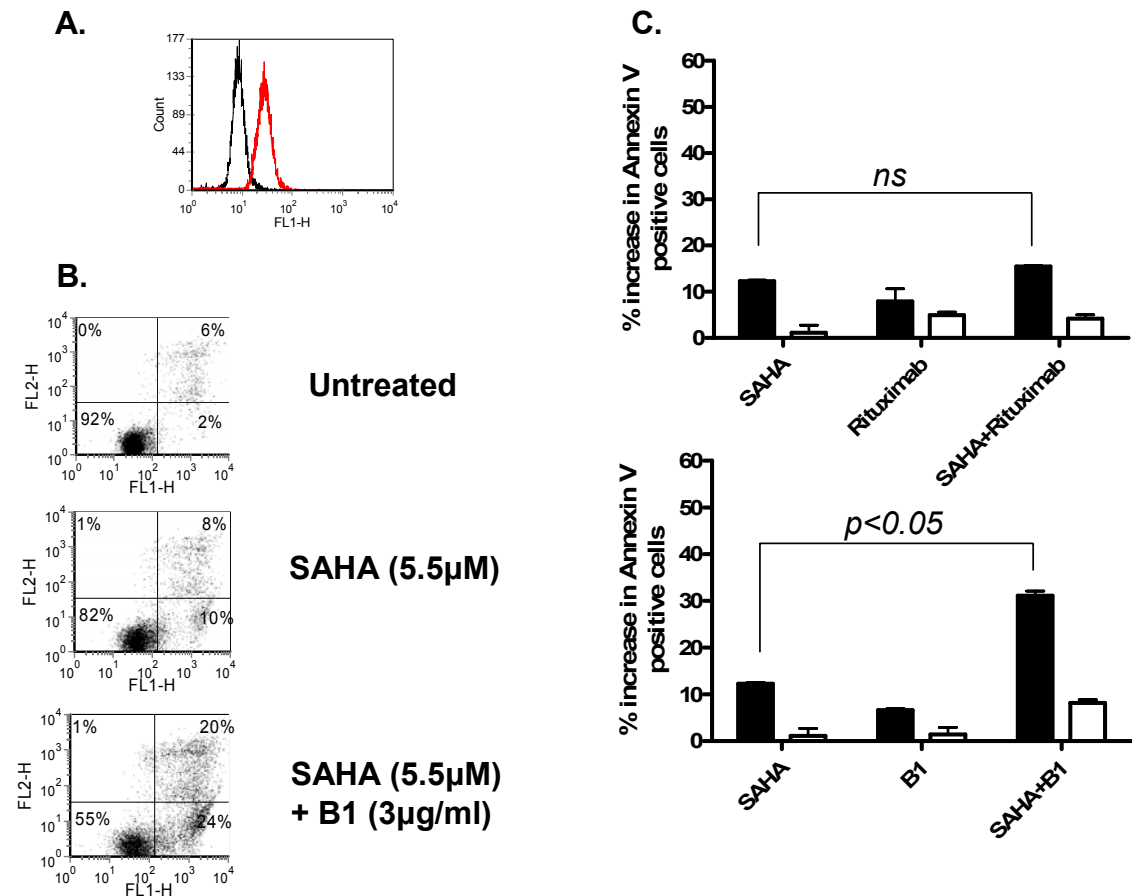


Figure 5-17 Induction of apoptosis in Bcl-2 overexpressing Ramos: Bcl-2 overexpressing Ramos cells at 0.5×10^6 cells/ml were suspended in complete medium with $12.5 \mu\text{M}$ QVD-op or a corresponding concentration of DMSO. Cells were then plated in triplicate in 96 well plates and incubated with SAHA $5.5 \mu\text{M}$, Rituximab $3 \mu\text{g/ml}$ or B1 $3 \mu\text{g/ml}$ alone or in combination, control samples were treated with a corresponding concentration of DMSO. After 24 hours cells were harvested and prepared for flow cytometric analysis using Annexin V/PI staining. **(A.)** Shows clonal Bcl-2 overexpression (■) compared to isotype control antibody (■). **(B.)** shows representative flow cytometry dot plots **(C.)** Shows mean % increase in annexin V positive cells for QVD-op treated (□) and untreated (■) cells (\pm range) compared to untreated cells. Independent student's *t*-test was performed comparing SAHA to combination treated samples. Data shown are representative of two independent experiments.

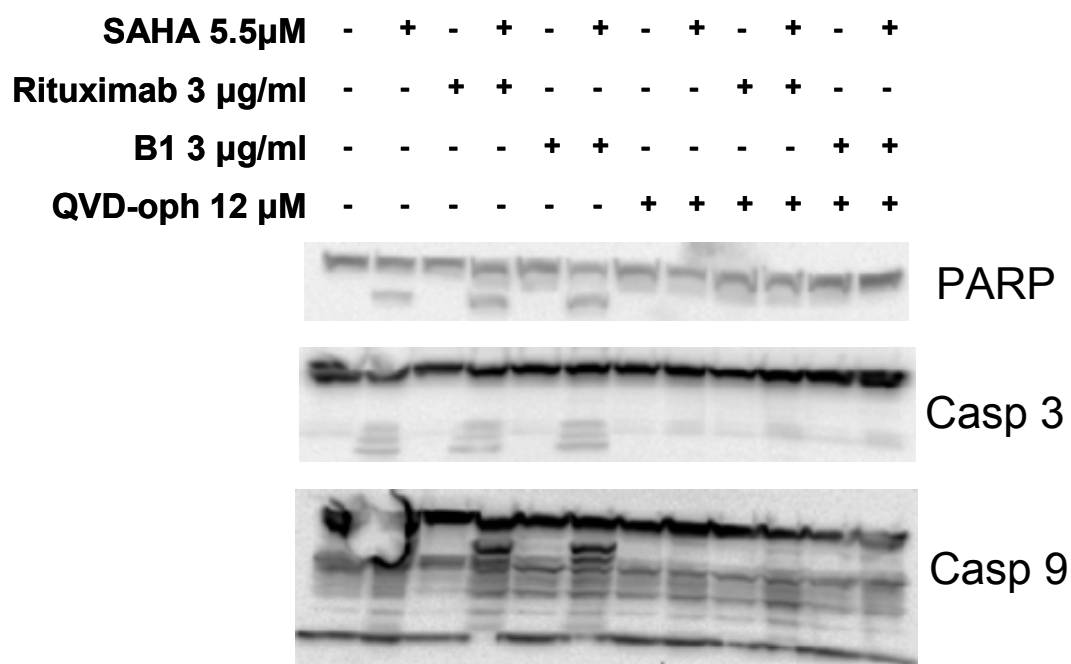


Figure 5-18 Capase processing in Bcl-2 Ramos:

Bcl-2 overexpressing Ramos cells at 0.5×10^6 cells/ml were suspended in complete medium with 12.5μM QVD-opb or a corresponding concentration of DMSO. Cells were plated in 6 well plates and incubated with the concentrations of SAHA, Rituximab and B1 indicated for 24 hours. Control samples were treated with a corresponding concentration of DMSO. Cells were harvested by centrifugation and resuspended in a RIPA lysis buffer and prepared as described above. Following quantification, 20μg of protein per sample was used for immunoblotting. Immunoblot for PARP, caspase 9 and caspase 3 is shown and is representative of two independent experiments.

5.6 Discussion

The data presented in this chapter illustrates two key points. Firstly the synergistic induction of apoptosis following combination treatment occurs without changes in the early biochemical responses to either agent alone. Secondly there is strong evidence that the intrinsic apoptotic pathway is necessary for the activity of HDI but not CD20 mAb. The synergistic activity demonstrated in chapter 4 appears to be dependent on this pathway.

Rituximab is well known to cause lipid raft formation [81, 82]. This results in altered composition of the cell membrane. This has been shown by a number of investigators to alter the activity of p-glycoprotein and hence reverse multi drug resistance phenotypes [275]. Thus it was important to test the hypothesis that Rituximab altered the intracellular levels of HDI. Histone acetylation is the classically used biomarker of target effect in cells following incubation with HDAC inhibitors, and western blotting for histone 4 acetylation is commonly used to demonstrate this [217]. Robust histone acetylation was detected within 2 hours and persisted upto 24 hours in Ramos and RL cells and did not appear to be affected by the addition of Rituximab. Using a late timepoint, levels of histone acetylation were quantified. This demonstrated that there was no significant difference between SAHA alone and in combination with either Rituximab or B1. A single timepoint of 24 hours incubation was chosen as synergy had already been demonstrated at this timepoint, as had high levels of histone acetylation. These experiments were able to demonstrate that time dependent histone acetylation was not influenced by combination treatment. Western blotting did not however differentiate between reduced HDAC activity or increased HAT activity. To investigate the effect on direct enzymatic activity an *in vitro* enzyme assay was used. The dose response curves for SAHA and combination treated cells were super imposable confirming that there was no interaction. Reassuringly the IC₅₀ for SAHA in this cell line was approximately 10 fold higher than the IC₅₀ for induction of apoptosis.

Having identified that CD20 mAb do not effect HDI pharmacokinetics, the effect of HDI on CD20 expression and CD20 lipid raft redistribution was investigated. There was a wide range of CD20 expression across the cell lines used and this did not seem to have an effect on the levels of cell death observed or synergistic activity. There is some preliminary data to suggest that down regulation of surface CD20 expression may be a mechanism of resistance to Rituximab. This was initially suggested following the observation that CD20 negative clones can be detected in patients with CD20 positive NHL who have received multiple treatments with Rituximab [276, 277]. These observations have been recapitulated in *in vitro* models of rituximab resistance [278, 279]. Czuczman *et al* [279] have demonstrated that this down regulation is possibly due to post transcriptional regulatory mechanisms. There are also some preliminary data demonstrating that HDI can upregulate CD20 mRNA expression [280]. The effect of treatment with SAHA on CD20 expression, and more specifically Rituximab and B1 binding was investigated in Ramos cells. Overnight incubation with SAHA was chosen as it facilitated assessment of transcriptional and post transcriptional regulatory mechanisms yet yielded high levels of cell viability. Surface CD20 expression was measured with FITC conjugated Rituximab and B1 mAb. At the timepoints chosen it was not possible to detect significant changes in the level of surface or triton X insoluble compartment CD20 expression. As would be expected rituximab showed a 2:1 binding ratio compared to B1 [265], and this was unaffected by pre incubation with SAHA. Although the data from these assays are convincing with measurement of CD20 expression occurring at timepoints already shown to result in induction of synergistic apoptosis, they do not exclude an effect at earlier timepoints. To investigate the early sequelae of CD20 mAb binding in combination with SAHA, flow cytometry was used to measure intracellular Ca^{2+} flux and ERK phosphorylation. It was chosen to incubate Ramos cells with SAHA or an equivalent concentration of DMSO for 2 hours as this timepoint had been previously identified as sufficient to allow intracellular accumulation of SAHA as measured by histone acetylation. Hypercrosslinking produced rapid induction of intracellular Ca^{2+} fluxing. This event was not affected by pre treatment with SAHA. The effect of SAHA on the type II mAb B1 was not

assessed as data already published by Walshe *et al* had shown that type II mAb did not induce Ca^{2+} fluxing [99]. To corroborate these findings flow cytometric analysis of ERK 1/2 phosphorylation was performed in SU-DHL-4 cells. This cell line was chosen as it was known that rituximab could induce ERK 1/2 phosphorylation without the hypercrosslinking allowing direct comparison of type I and II mAb. Consistent with published reports rituximab induced ERK phosphorylation within 15 minutes, but no effect was seen with B1. Once again these early CD20 mAb induced molecular events were unaffected by the addition of SAHA. Taken together these data demonstrates that the cooperative cell death observed with the combination of these agents is not due to effects on the early signaling events known to occur following CD20 mAb binding.

As discussed earlier it was important to clarify the effects of these agents at inducing apoptosis. Time dependent induction of PARP cleavage following incubation of cells with SAHA was seen. This corresponded with the induction of Annexin V positive cells. Caspase 9 processing appeared to precede this, suggesting that in this cell line SAHA induces apoptosis through caspase 9 processing, possible as a result of mitochondrial cytochrome C release. In support of this hypothesis; there was no caspase 8 processing and the pan caspase inhibitor QVD-oph blocked SAHA induced apoptosis as did overexpression of Bcl-2.

The data for CD20 mAb are less clear. The data presented here show that in the absence of cross linking, PS translocation occurs without caspase processing or PARP cleavage. This is consistent with the majority of published data [87, 281]. The addition of crosslinking to Rituximab results in PARP cleavage and caspase 9 processing, again a common finding in the literature [266, 282]. The differences between type I and II mAb is further demonstrated in cells overexpressing Bcl-2. This abrogates any cooperative effect seen with rituximab but not with B1, suggesting that the B1/SAHA cooperative effect is not Bcl-2 dependent. Interestingly western blotting of the cell lines used demonstrated that the RL cell line, which did not show synergy, had a high level of Bcl-2 expression, supporting the hypothesis that this mechanism confers resistance to SAHA/Rituximab induced apoptosis.

The role of pharmacological caspase inhibition in blocking synergistic induction of apoptosis is clear. The addition of QVD-OPh inhibited all caspase processing, PARP cleavage and PS translocation in all the experimental conditions tested. This observation supports the hypothesis that apoptosis induced by SAHA/Rituximab is caspase and Bcl-2 dependent. A model for this interaction is shown in **[Figure 5-19]**.

However, the fact that the cooperative effect seen with SAHA/B1 in Bcl-2 overexpressing Ramos is blocked by caspase inhibition is harder to explain and might be due to the fact that QVD-oph is not completely specific. It may be that apoptosis is induced in these cells by non Bcl-2 dependent apoptotic mechanisms, which are inhibited by QVD-oph. Caspase 8 cleavage was not seen following treatment with SAHA or with combination treatment (data not shown), suggesting the 'extrinsic apoptotic pathway' is not involved. It is possible that other Bcl-2 independent mechanisms such as calpain activation are involved. It has been shown that cross talk between these pathways occurs and may explain why caspase inhibitors also block this mechanism [283].

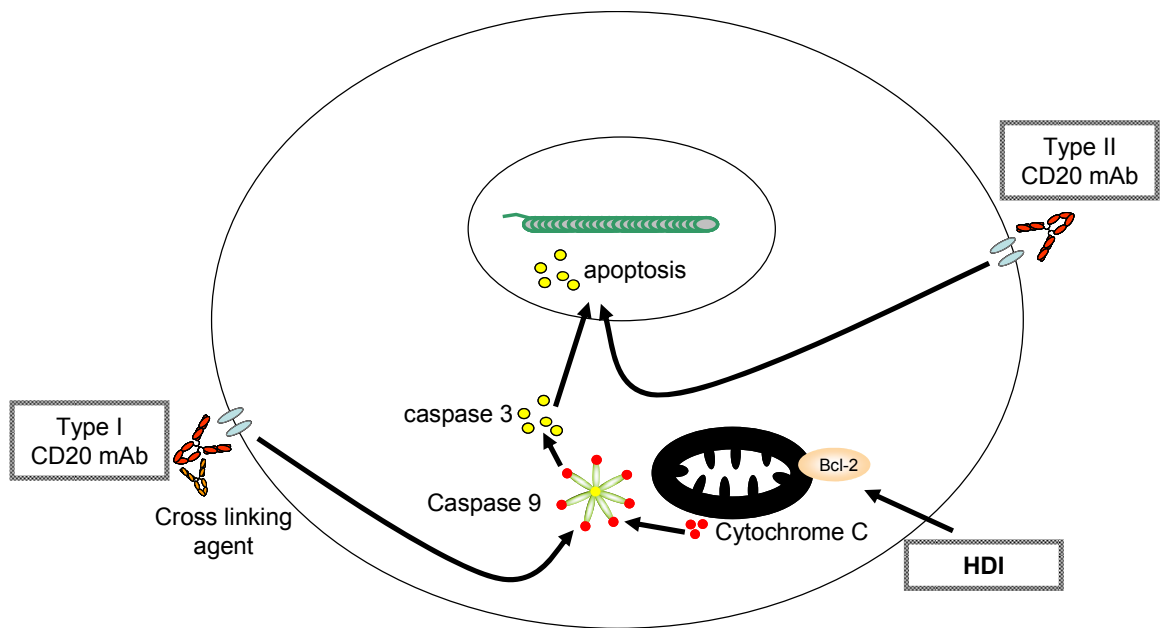


Figure 5-19 Model of interaction between HDI and type I and II CD20 mAb:

6 Transcriptional mechanisms for cooperative activity.

6.1 Introduction

With data showing clear synergistic cell killing with HDI in combination with CD20 mAb and evidence of induction of apoptotic pathways, investigation turned to transcriptional regulation. HDI exert their effects through the regulation of genes and understanding the transcriptional consequences of their effect was potentially important for understanding how they interacted with CD20 mAb. As discussed earlier, HDI mediated acetylation of core histone proteins results in conformational change in chromatin. This allows access of transcription factors to previously 'condensed regions' of DNA as well as facilitating binding of cofactors to docking sites. HDI also modulate gene expression through the post transcriptional regulation of a host of transcription factors and DNA binding proteins. Although CD20 mAb produce little direct effect on transcription, ligation of CD20 receptor has been shown to induce intracellular signalling with modulated expression of a number of genes, including Bcl-2 family apoptotic regulators.

Recent advances in gene expression profiling have facilitated investigation of the regulation of gene transcription across the entire genome. To investigate the role of transcriptional modulation in this cooperative effect gene expression profiling was performed in Ramos cells following incubation with SAHA and Rituximab alone or in combination. RT-Q-PCR was used to confirm changes observed in individual genes and geneset enrichment analysis was performed to assess the regulation of NF κ B target genes and to explore for enrichment of genes with functional associations. The secondary aim of these experiments was to identify biomarkers that could be utilised to confirm transcriptional target effect of HDIs. Clinical trials of HDIs have utilised histone acetylation as a marker of biological effect. This approach has proved problematic for a number of reasons. In one of the defining phase I studies although they were able to demonstrate histone acetylation in PBMC, there was no correlation with dose [205], a finding that has been

mirrored in other studies. Histone acetylation is a result of the enzyme inhibitory activity of HDI, but needs to be sustained in order to achieve transcriptional regulation.

6.2 Microarray design and sample preparation

This analysis was performed using the Affymetrix human U133 plus2.0 gene expression profiling platform, to analyse over 47,000 transcripts. Two time points were chosen to investigate early (6 hours) and later (16 hours) transcriptional effects. It was decided to use concentrations of SAHA and crosslinked Rituximab that had resulted in strong synergistic activity in earlier assays. Samples were prepared in triplicate, at each time point. RNA was extracted using TRIzol reagent, followed by an RNA cleanup protocol using Qiagen RNA columns. The experimental design with representative electrophoresis and electropherogram images is shown [**Figure 6-1**]. Duplicate samples with the best quality RNA traces were selected and couriered on dry ice to the PICR Microarray facility, Manchester, UK.

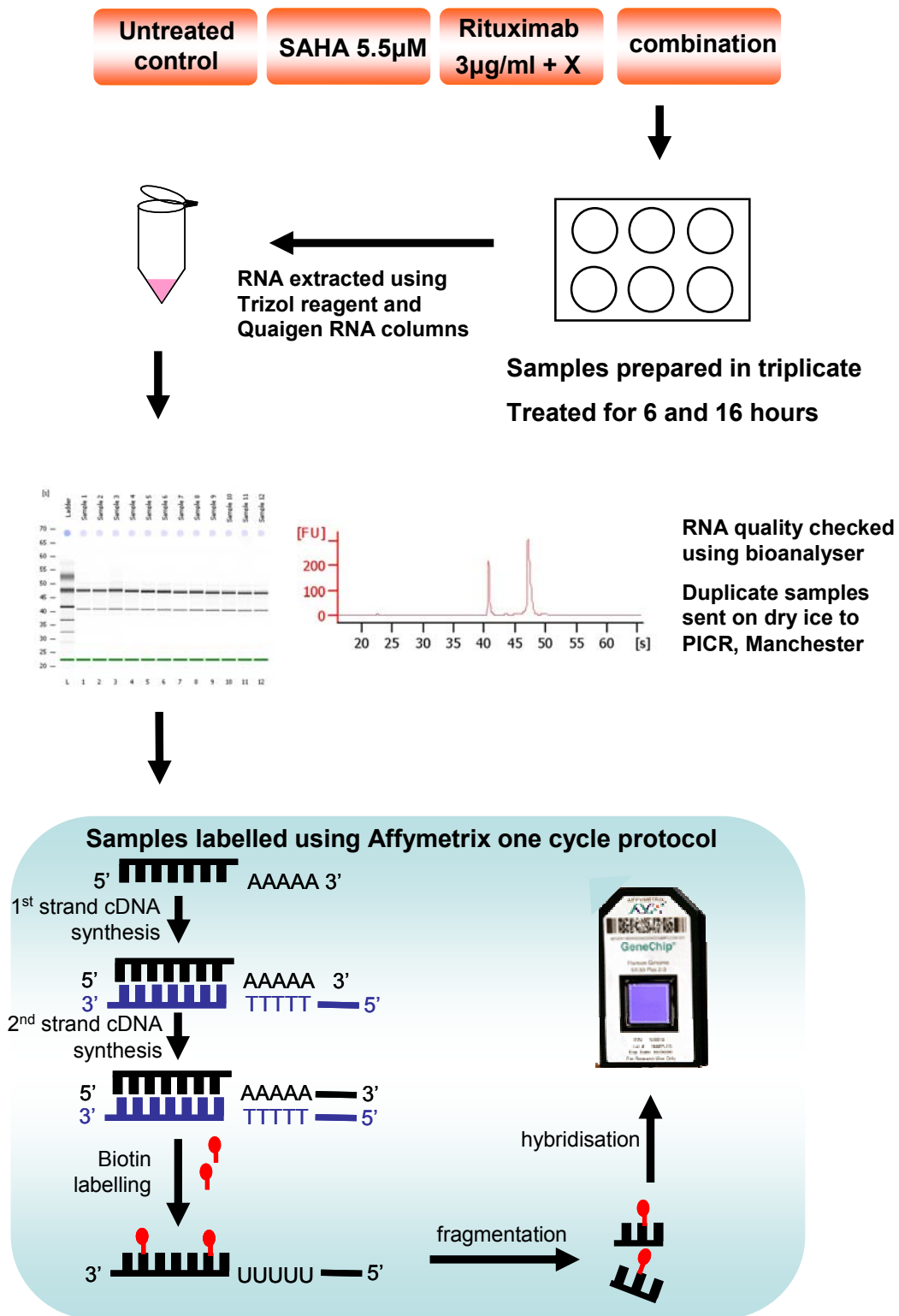


Figure 6-1 Microarray sample preparation:

Ramos cells at $0.5 \times 10^6/\text{ml}$ were plated in triplicate in 6 well plates as indicated. After six and sixteen hours incubation cells were harvested by centrifugation and RNA was extracted using TRIzol reagent, and purified using qiagen RNA columns. RNA quality was checked using bioanalyzer and duplicate samples were labelled and hybridised to Affymetrix u133 plus2.0 array.

Target cRNA was synthesized using the Affymetrix one cycle labelling protocol (http://bioinformatics.picr.man.ac.uk/mbcf/One_Cycle_Target_Prep_Protocol_PICR_v1-0.pdf). Following this RNA quality was rechecked using a standard Agilent bioanalyzer protocol. Labelled RNA was hybridized to human 133 plus 2.0 chips. Probe level data (Cel files) were normalised using Robust Multi-Array Average (RMA) (Bioconductor, Affymetrix, UK). This analysis was performed by Richard Mitter from the Cancer Research UK bioinformatics service (Lincolns Inn Field, London, UK). For initial analysis of the data set expression fold change was calculated from the mean of duplicate samples and was compared to controls. A moderated t-test was used to identify differential expression and filtered on a false discovery rate adjusted *p* value of ≤ 0.05 , and an absolute fold change of ≥ 2 . The total number of transcripts for each experimental condition meeting these criteria are summarised with number of up/down regulated and unchanged genes shown [Table 6-1].

Comparison of control samples at the two timepoints revealed close concordance in the gene expression patterns, with only 34 genes with differential expression identified. This confirms the robustness of the whole experimental procedure and RMA normalisation. For all future analysis all the untreated samples were combined and used as comparators for the different treatment conditions. Consistent with published data, treatment with SAHA resulted in the significant regulation of approximately 3% of genes at both time points. Rituximab resulted in very modest transcriptional effects. Combination treatment resulted in a larger number of genes than either agent alone.

Cluster dendrograms graphically present the relationship between duplicate samples and the different treatment conditions. Horizontal lines depict the level of clustering of samples, whilst vertical lines represent the differences between samples. There was tight clustering of the duplicates for each sample. Rituximab treated samples also clustered with control samples. The SAHA transcriptional signature clustered closely with combination treated samples, confirming the dominance of the HDI transcriptional signature. There was tight clustering of the duplicates for each sample, although with such a weak transcriptional signature

duplicate variance was greater with Rituximab treated samples than SAHA treated. The highest level of clustering was between samples incubated with or without SAHA. The next most striking feature was that the SAHA transcriptional signature clustered closely with combination treated samples, confirming the dominance of the HDI transcriptional signature [**Figure 6-2**].

	6 hours			16 hours			
	SAHA	Rituximab	Combined	SAHA	Rituximab	Combined	Control 6 hrs
Downregulated	1351	101	1655	1400	17	2295	8
Unchanged	51689	54386	51343	51290	54432	49359	54641
Upregulated	1635	188	1677	1985	226	3021	26

Table 6-1 Differentially expressed transcripts:

FDR ≤ 0.05 , fold change ≥ 2 . total number of differentially expressed genes for each time point compared to controls at that timepoint are shown.

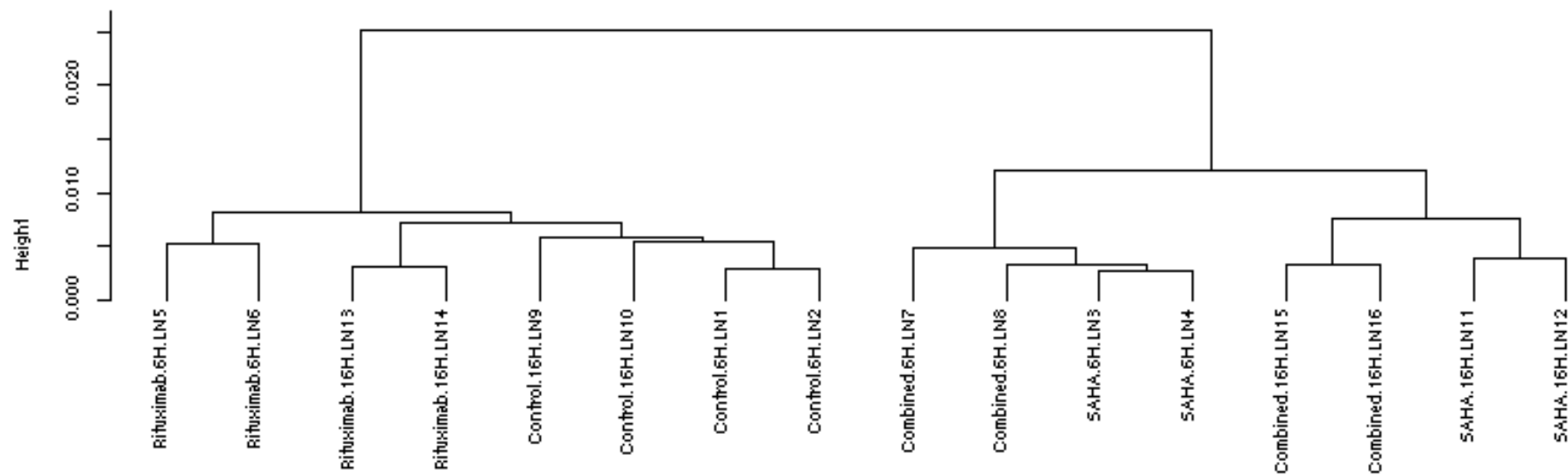


Figure 6-2 Cluster dendrogram of Ramos cells gene expression analysis:

To examine the effect of each experimental condition on the expression of all the genes examined, the expression level of gene transcripts was expressed as a linear fold change induction (positive values) or down regulation (negative values) relative to control samples. All genes which reached statistical significance with a false discovery rate (FDR) of $p \leq 0.05$ were included in this analysis. Genes were ranked according to fold change induction in SAHA treated samples and this 'gene expression signature' for the three experimental conditions is shown [**Figure 6-3**]. As was demonstrated with the cluster dendrogram, the combination signature was dominated by the effect of SAHA. There were only 736 genes differentially expressed by combination treatment alone and 163 genes regulated solely by Rituximab. Within the combination gene signature there were genes which were differentially expressed compared to SAHA or Rituximab alone. For example CD69 was upregulated 8.6 fold with SAHA and 15.8 fold with combination treatment.

To systematically identify genes which might be responsible for the cooperative effect observed in apoptotic assays, the subset of genes which was significantly regulated in combination treated samples compared to SAHA following six hours incubation was identified [**Figure 6-4**], [**Table 6-2**]. This analysis revealed a subset of 64 genes. This data set was notable for containing 8 well described NF κ B target genes (CD69, TRAF1, BLR1, BCL2A1, CD83, CCR7, and CCL3). This observation was important as it suggested that combination treatment was able to modulate NF κ B target genes independently of either agent alone.

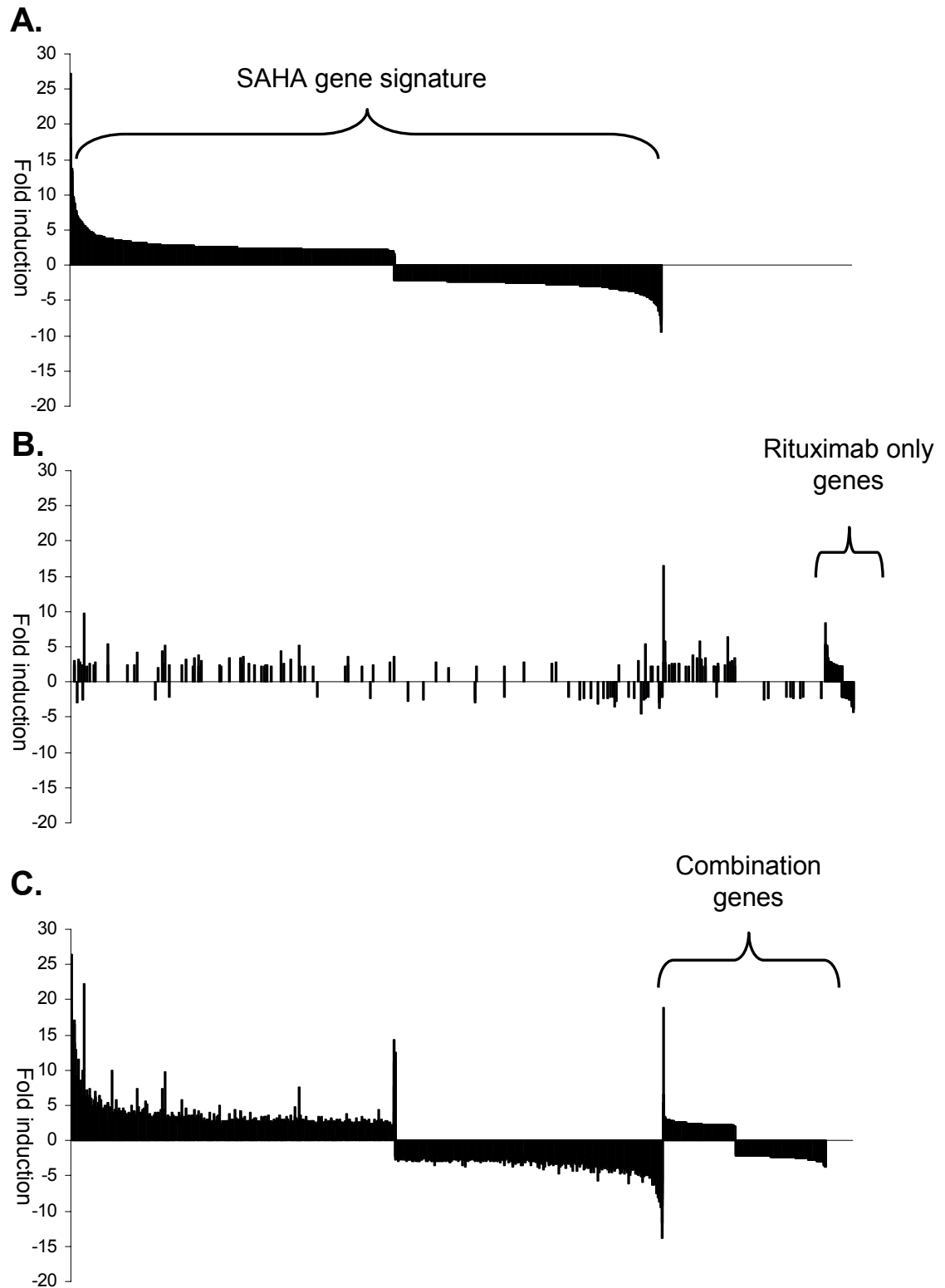


Figure 6-3 expression of all significant genes compared to control: Bar charts shows the genes which were statistically significantly regulated (FDR $p \leq 0.05$, Fold change $\leq \geq 2$) for any treatment condition compared to controls following 6 hours incubation. Each bar represents the fold change of a single gene transcript, derived from the mean of duplicate samples compared to controls for **(A.)** SAHA, **(B.)** Rituximab or **(C.)** the combination.

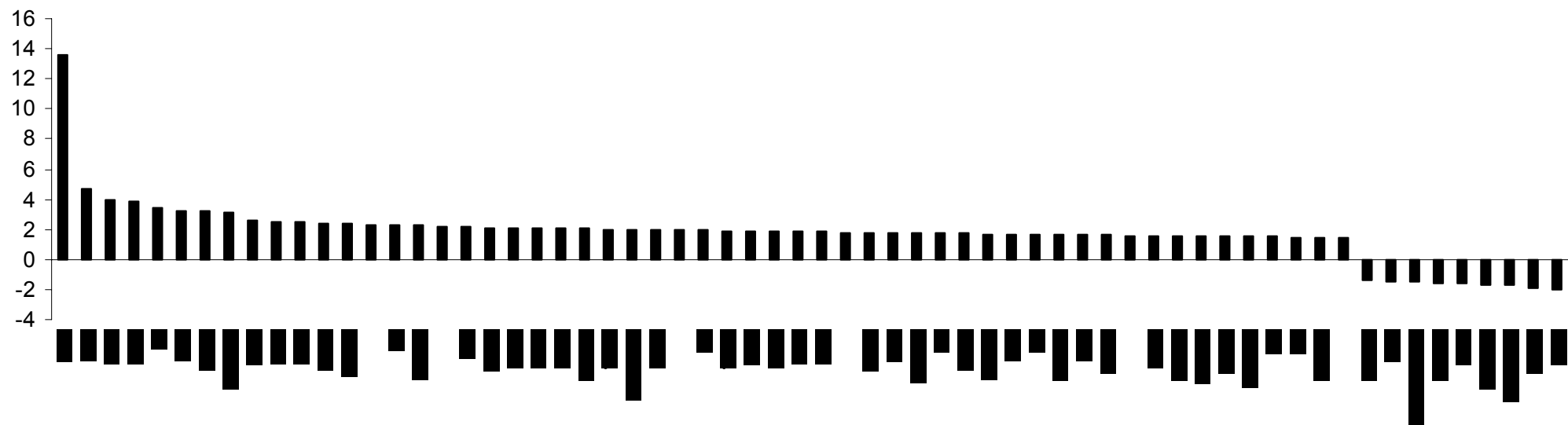


Figure 6-4 Differentially expressed genes following combination treatment:

All 64 differentially expressed genes in combination treated samples compared to SAHA following six hours incubation are shown ($p \leq 0.05$, any FC). Genes are ranked according to fold change induction. Each bar represents the fold change of a single gene transcript, derived from the mean of duplicate samples. For example BIK is upregulated 3.9 fold compared to SAHA alone.

CCL3	chemokine (C-C motif) ligand 3	CD69	CD69 molecule
RGS1	regulator of G-protein signalling 1		NA
CCR7	chemokine (C-C motif) receptor 7	DUSP2	dual specificity phosphatase 2
EGR2	early growth response 2 (Krox-20 homolog, Drosophila)	ATF3	activating transcription factor 3
BIK	BCL2-interacting killer (apoptosis-inducing)	MAP3K8	mitogen-activated protein kinase kinase kinase 8
RGS1	regulator of G-protein signalling 1	GLS	glutaminase
KCNJ2	potassium inwardly-rectifying channel, subfamily J, member 2	FCRL4	Fc receptor-like 4
FAM102A	family with sequence similarity 102, member A	CLEC2D	C-type lectin domain family 2, member D
SRGN	serglycin	LPIN1	lipin 1
CD83	CD83 molecule	GLS	glutaminase
EGR3	early growth response 3	HOMER1	homer homolog 1 (Drosophila)
NR4A1	nuclear receptor subfamily 4, group A, member 1	LPIN1	lipin 1
BCL2A1	BCL2-related protein A1	EIF2C2	eukaryotic translation initiation factor 2C, 2
	NA		NA
BIC	BIC transcript	RGS14	regulator of G-protein signalling 14
SQSTM1	sequestosome 1	HOMER1	homer homolog 1 (Drosophila)
	NA	SLCO4A1	solute carrier organic anion transporter family, member 4A1
BLR1	Burkitt lymphoma receptor 1, GTP binding protein (chemokine (C-X-C motif) receptor 5)	ABCC5	ATP-binding cassette, sub-family C (CFTR/MRP), member 5
MCTP1	multiple C2 domains, transmembrane 1	ANKRD10	ankyrin repeat domain 10
CREM	cAMP responsive element modulator	SGK	serum/glucocorticoid regulated kinase
CREM	cAMP responsive element modulator	GLA	galactosidase, alpha
CREM	cAMP responsive element modulator	C21orf91	chromosome 21 open reading frame 91
ADARB1	adenosine deaminase, RNA-specific, B1 (RED1 homolog rat)		NA
TRAF1	TNF receptor-associated factor 1	C21orf57	chromosome 21 open reading frame 57
LOC283454	hypothetical protein LOC283454	RGS5	regulator of G-protein signalling 5
CREM	cAMP responsive element modulator	DKFZp667G2110	hypothetical protein DKFZp667G2110
	NA	FLJ13195	stromal antigen 3-like
LY9	lymphocyte antigen 9	DIDO1	death inducer-obliterators 1
TRAF1	TNF receptor-associated factor 1	HIST1H2BI	histone cluster 1, H2bi
KLHL6	kelch-like 6 (Drosophila)	LOC339929	hypothetical protein LOC339929
VGLL4	vestigial like 4 (Drosophila)	UBE3C	ubiquitin protein ligase E3C
JUND	jun D proto-oncogene	GRAP	GRB2-related adaptor protein

Table 6-2: Differentially expressed genes following 6 hours combination treatment

All differentially expressed genes in combination treated samples compared to SAHA are shown ($p \leq 0.05$, any FC).

6.3 Validation

As an initial validation step the 'gene expression signatures' seen were compared with available data sets. For Rituximab effect *Cittera et al* had published data using Affymetrix HG-U95av2 chips [284]. They identified no genes significantly downregulated greater than two fold and only 16 and 12 genes upregulated in DHL-4 and BJAB respectively ($P \leq 0.0025$). Geneset enrichment analysis, Performed by Richard Mitter, of the Rituximab treated data set from this experiment confirmed significant enrichment of these previously identified genes within our larger data set ($p \leq 0.0001$). By superimposing these genes onto the Rituximab Vs. control 6 hour data set it can be seen how the genes with the greatest fold induction in our data set showed concordance with those previously identified [**Figure 6-5**].

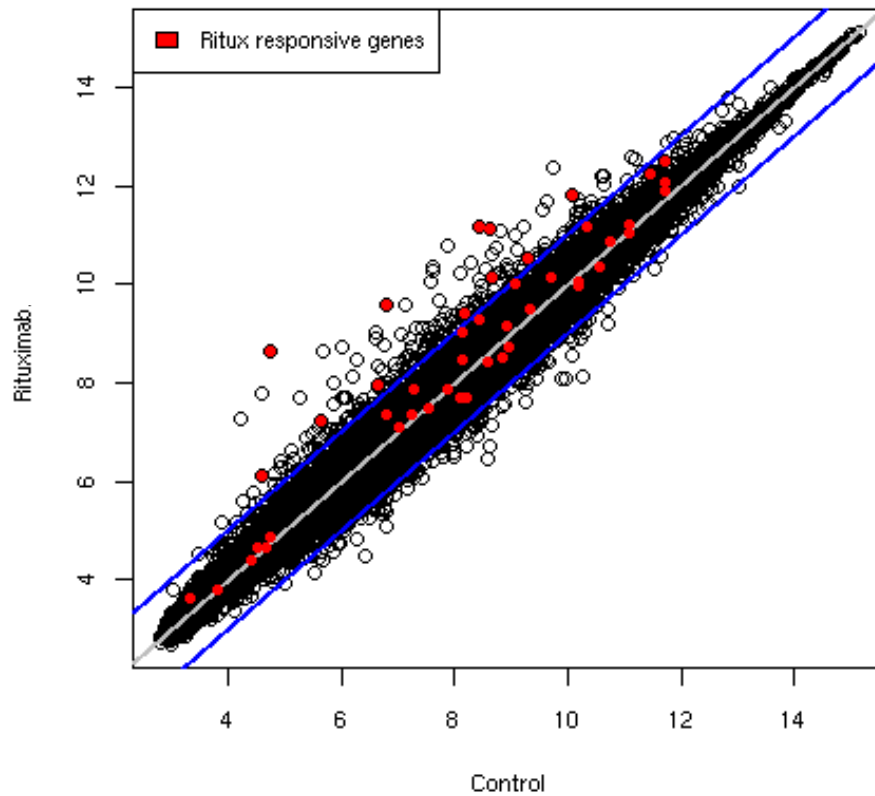


Figure 6-5: Scatter plot of Rituximab regulated genes.

This scatter plot shows all the genes significantly differentially regulated by Rituximab following six hours incubation (○) ($FDR \leq 0.05$, $FC \leq 2$) compared to controls. Genes identified by citerra *et al* [284] (●) are shown superimposed on this data set. Non significant genes are also shown (●). Blue line depicts the linear 2 fold induction/down regulation cut off.

Validation of the SAHA data was performed using the Connectivity Map (<http://www.broad.mit.edu/cmap/displayServlet?servletAction=mainMenu>). This web-based tool allows comparison of gene expression profiles to a database generated through responses to small molecules in the MCF7 breast cancer cell line. The top 1000 up or down regulated genes from the SAHA gene signature were used to query this database. The top ranked molecules, based on connectivity score are shown, all 10 were HDAC inhibitors [**Table 6-3**].

These validation steps demonstrated the reproducibility of the gene expression signatures generated with either agent alone, and serve to validate the signature observed with combination treatment. Of particular note is the strong connectivity score for HDI of different classes across different cell lines, once again confirming the regulatory effects of HDI on a number of core genes [210].

rank	batch	cmap name	dose	cell	Connectivity score
1	506	trichostatin A	1 μ M	MCF7	1
2	506	vorinostat	10 μ M	MCF7	0.989
3	502	trichostatin A	1 μ M	MCF7	0.958
4	505	HC toxin	100 nM	MCF7	0.952
5	506	trichostatin A	100 nM	MCF7	0.941
6	504	trichostatin A	1 μ M	MCF7	0.933
7	513	vorinostat	10 μ M	MCF7	0.909
8	513	trichostatin A	100 nM	MCF7	0.905
9	513	trichostatin A	1 μ M	MCF7	0.901
10	44	valproic acid	10 mM	HL60	0.871

Table 6-3 Connectivity score for SAHA dataset compared to Cmap database:

The top 1000 up or down regulated genes from the SAHA gene signature was entered into the Cmap database. Listed are the top ten ranked matches based on connectivity score.

To validate the effect on individual genes RT-Q-PCR was performed from excess RNA samples from the same experiment. It was decided to select genes which had been significantly upregulated in the combination treated data set compared to control samples. Two gene probes with the highest levels of differential expression were selected; proteoglycan 1, serglycin, secretory granule (PRG1, NM_002727) and v-fos FBJ murine osteosarcoma viral oncogene homolog (FOS, NM_005252). RT-Q-PCR for these transcripts is shown [Figure 6-6].

As with the microarray analysis there was significant upregulation with combination treatment and SAHA alone compared to control samples. The mean fold change for each sample from the microarray analysis was plotted against the fold change for RT-Q-PCR analysis, Statistical analysis using Pearson's correlation demonstrated a highly significant relationship ($p \leq 0.001$). Of note the magnitude of fold change induction observed with RT-Q-PCR was consistently higher than was seen in the microarray analysis.

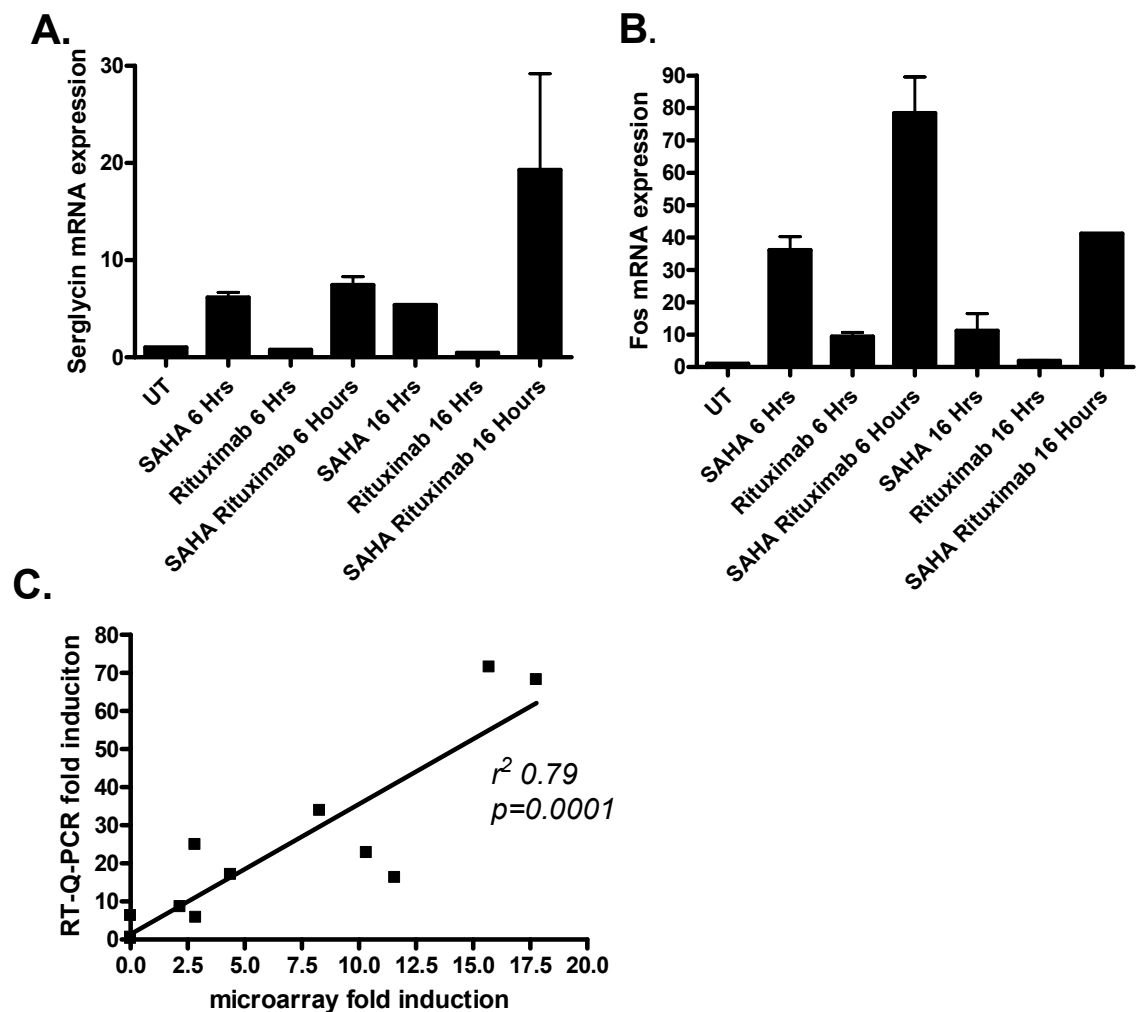


Figure 6-6 RT-Q-PCR validation of microarray:

Ramos cells at 0.5×10^6 cells/ml were plated in duplicate in 6 well plates and treated with SAHA $5.5 \mu\text{M}$, Rituximab $3 \mu\text{g/ml}$ with crosslinking agent or the combination. Control samples were left untreated (UT). At the timepoints indicated cells were harvested and RNA was extracted using TRIzol reagent, and purified using Qiagen RNA columns. Oligo dT primed cDNA was prepared from $1 \mu\text{g}$ RNA and duplicate wells were loaded with $5 \mu\text{l}$ cDNA, $15 \mu\text{l}$ PCR master mix and appropriate taqman gene expression assay. Q-RT-PCR was performed as previously described. **(A.)** and **(B.)** show mRNA expression level relative to β actin for the probes described, data shown are mean (\pm range) from two independent experiments. **(C.)** Shows correlation between microarray fold induction and RT-Q-PCR for these probes, each data point represents a condition where fold induction data was available from both experimental techniques. Pearsons correlation coefficient was calculated with the r^2 and p value shown.

6.4 Functional annotation clustering analysis

Functional annotation clustering analysis was performed using an online bioinformatics tool (The Database for Annotation, Visualization and Integrated Discovery (DAVID) <http://david.abcc.ncifcrf.gov/home.jsp>) [285].

This web based software uses a modified Fisher Exact test to determine whether the proportions of genes, from an uploaded dataset, falling into each category differs by group. The Fisher Exact test is adopted to measure the gene-enrichment within annotation terms. The genelist was ranked by fold change in combination treated samples and the top 100 genes were selected and uploaded for analysis. The top 3 functional groups are shown with gene ontology (GO) [286] functional annotation, percentage of genes and *p* value [Table 6-4]. These 3 functional groups were related to lymphocyte activation and immunomodulatory function and their constituent genes are shown [Table 6-5].

Functional Group 1	%	PValue
Term		
GO:0050896~response to stimulus	27%	0.009
GO:0006955~immune response	12%	0.014
GO:0002376~immune system process	13%	0.019
Functional Group 2		
GO:0046649~lymphocyte activation	6%	0.007
GO:0045321~leukocyte activation	6%	0.011
GO:0001775~cell activation	6%	0.016
GO:0051239~reg. of multicellular organismal process	6%	0.032
Functional Group 3		
GO:0006952~defense response	12%	0.001
GO:0042221~response to chemical stimulus	10%	0.012
GO:0009605~response to external stimulus	10%	0.016
GO:0006950~response to stress	12%	0.031
GO:0006954~inflammatory response	6%	0.035
GO:0007610~behavior	6%	0.046
GO:0007626~locomotory behavior	5%	0.048

Table 6-4 Functional annotation clustering analysis:

Gene Name
PROSTAGLANDIN E RECEPTOR 4 (SUBTYPE EP4)
PROTEOGLYCAN 1, SECRETORY GRANULE
BURKITT LYMPHOMA RECEPTOR 1, GTP BINDING PROTEIN (CHEMOKINE (C-X-C MOTIF) RECEPTOR 5)
HISTONE 1, H2BD
CD69 ANTIGEN (P60, EARLY T-CELL ACTIVATION ANTIGEN)
HEAT SHOCK 70KDA PROTEIN 1A
TUMOR PROTEIN P53 INDUCIBLE NUCLEAR PROTEIN 1
EARLY GROWTH RESPONSE 2 (KROX-20 HOMOLOG, DROSOPHILA)
CD24 ANTIGEN (SMALL CELL LUNG CARCINOMA CLUSTER 4 ANTIGEN)
TUMOR NECROSIS FACTOR (LIGAND) SUPERFAMILY, MEMBER 9
CYCLIN-DEPENDENT KINASE INHIBITOR 2B (P15, INHIBITS CDK4)
CHEMOKINE (C-C MOTIF) LIGAND 3
CD1D ANTIGEN, D POLYPEPTIDE
LYSOSOMAL TRAFFICKING REGULATOR
CHEMOKINE (C-C MOTIF) RECEPTOR 7
CHEMOKINE (C-C MOTIF) LIGAND 3-LIKE 1
REGULATOR OF G-PROTEIN SIGNALLING 1
PROTEIN PHOSPHATASE 3 (FORMERLY 2B), CATALYTIC SUBUNIT, ALPHA ISOFORM (CALCINEURIN A ALPHA)
V-FOS FBJ MURINE OSTEOSARCOMA VIRAL ONCOGENE HOMOLOG
UL16 BINDING PROTEIN 2
CD83 ANTIGEN (ACTIVATED B LYMPHOCYTES, IMMUNOGLOBULIN SUPERFAMILY)
SELENOPROTEIN P, PLASMA, 1
F11 RECEPTOR
CD274 ANTIGEN

Table 6-5: top ranked functionally associated genes.

This gene list was notable for containing well described NFκB target genes including CCR3, CCR7, CD83 and CD69.

The NFκB pathway was a known target of both agents and geneset enrichment analysis for NFκB target genes was performed. This is a bioinformatic tool for testing for differential regulation of gene sets of pre defined biological relevance as opposed to single genes and was first described in 2003 [287]. A list of validated NFκB target genes was obtained (<http://bioinfo.lifl.fr/NF-KB/NM-human.txt>) from a web based search. Analysis was performed, by Richard Mitter, for enrichment of this geneset in treated samples compared to control samples using GeneSetTest software package [288] [Table 6-6].

Within the 'Rituximab geneset' there was significant enrichment of NFκB targets at both 6 and 16 hours. 'Combination genesets' were also enriched for NFκB targets when compared to SAHA alone. To further examine this effect the fold change in mRNA expression for each gene probe that reached significance ($FDR\ p\leq 0.05$) following six hours incubation was plotted [Figure 6-7]. This shows that the gene expression profile of NFκB target genes is very complex, reinforcing the hypothesis that interpretation of effects on this pathway cannot be made by looking at individual genes. Combination treatment appeared to induce the expression of a number of genes independently of either agent alone as well as showing enhanced effect on genes regulated by either agent independently. For example the TNF superfamily member, lymphotoxin alpha, was upregulated 2.2 fold following Rituximab treatment but down regulated by SAHA alone or in combination. Whereas Chemokine (c-c motif) ligand 3 (CCL3) was upregulated 14.9 fold by Rituximab and 16.2 fold by combination but was unaffected by SAHA alone.

Treatment duration	Data set	P value
6 Hours	SAHA Vs. Control	<i>ns</i>
	Rituximab Vs. Control	0.0001
	Combined Vs. Control	<i>ns</i>
	Combined Vs. SAHA	0.0001
	Combined Vs. Rituximab	<i>ns</i>
	SAHA Vs. Control	<i>ns</i>
16 Hours	Rituximab Vs. Control	0.0001
	Combined Vs. Control	0.0926
	Combined Vs. SAHA	0.0002
	Combined Vs. Rituximab	0.0023

Table 6-6 Geneset enrichment analysis:

GeneSetTest software package was used to probe differentially expressed genes from the data sets indicated for enrichment of genes known to be NF κ B targets.

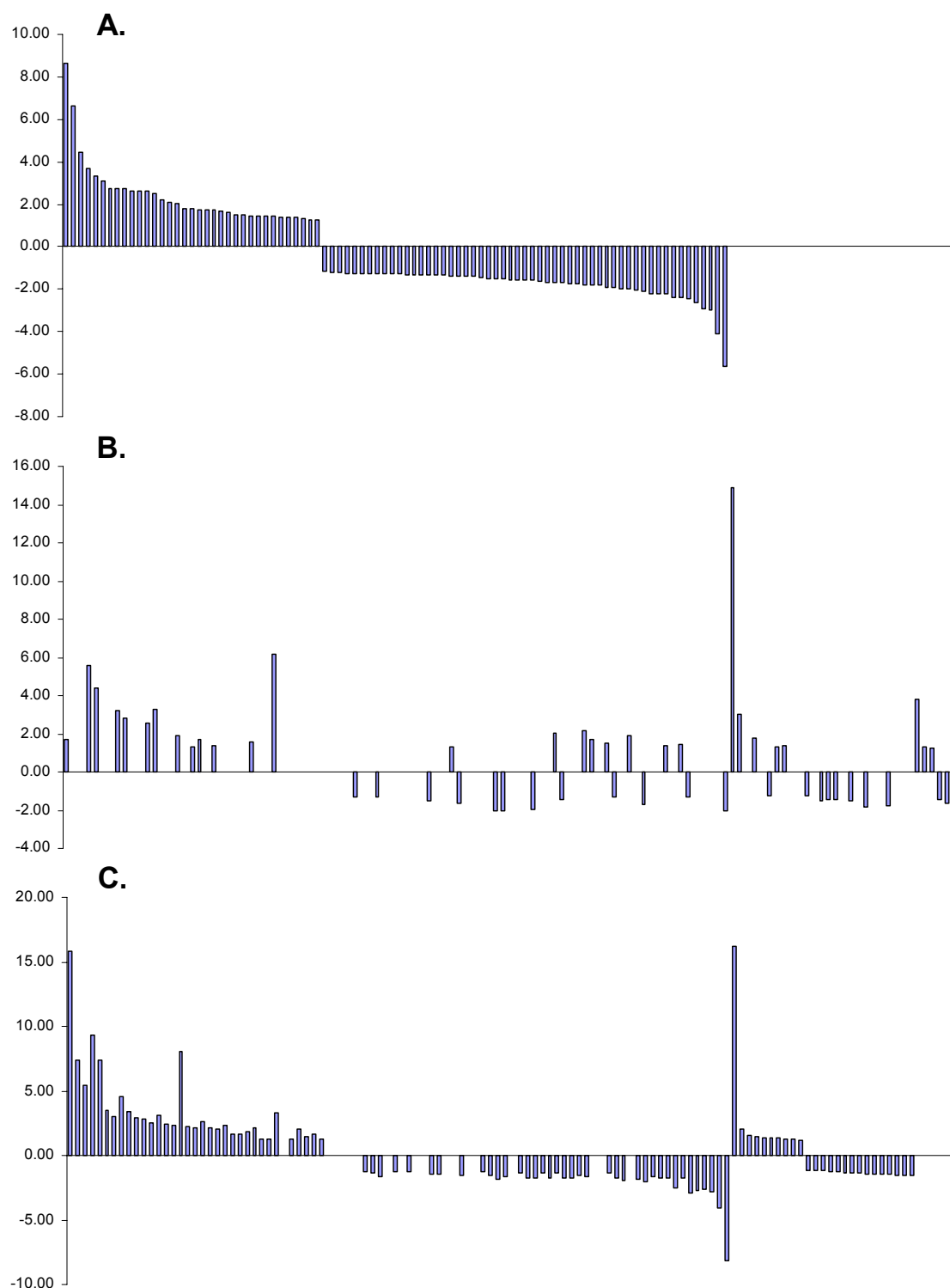


Figure 6-7 Regulation of NFκB target genes:

Bar charts show the genes which were statistically significantly regulated (FDR $p \leq 0.05$) for any treatment condition compared to controls following 6 hours incubation. Each bar represents the fold change of a single NFκB target gene transcript, derived from the mean of duplicate samples compared to controls for (A.) SAHA, (B.) Rituximab or (C.) the combination.

6.5 RT-Q-PCR analysis of NF κ B target genes

To confirm the effect of combination treatment on individual NF κ B target genes RT-Q-PCR was performed using cDNA prepared from duplicate experiments. Taqman gene expression assays were performed using BclX_L, Bcl2A1, CD69 and LTA.

Previous studies have used the anti apoptotic Bcl-2 family protein BclX_L as a marker of NF κ B activity so this was initially analysed [274]. In the earlier microarray analysis there had been no significant effect on BclX_L following SAHA and a low level of downregulation following either Rituximab or combination treatments (-1.46, -1.29 fold respectively). In Ramos cells timecourse analysis following treatment with Rituximab demonstrated downregulation of BclX_L within 2 hours. SAHA appeared to have no significant effect on this target in Ramos cells at the timepoints investigated [Figure 6-8]. This observation is important because it reinforces the hypothesis that individual NF κ B target gene regulation cannot be looked at in isolation.

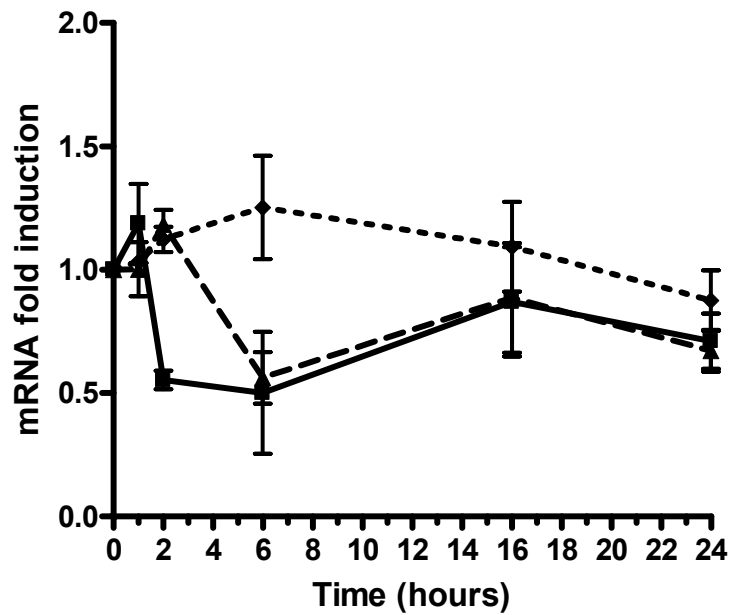


Figure 6-8 RT-Q-PCR timecourse of BclX_L regulation:

Ramos cells at 0.5×10^6 cells/ml were plated in duplicate in 6 well plates and treated with SAHA (5.5μM) (◆), Rituximab (3μg/ml) with crosslinking agent (■) or the combination (▲). Control samples were left untreated. At the timepoints indicated cells were harvested and RNA was extracted using TRIzol reagent, and purified using qiagen RNA columns. Oligo dT primed cDNA was prepared from 1μg RNA and duplicate wells were loaded with 5μl cDNA, 15μl PCR master mix and appropriate taqman gene expression assay. Q-RT-PCR was performed as previously described. Data shown are mean (±range) from two independent experiments.

Using the six and sixteen hour time points the effect on the other biologically relevant targets was investigated [**Figure 6-9**].

Bcl2A1 is an antiapoptotic Bcl-2 family protein which is known to protect cells from BCR mediated cell death [289]. In the microarray analysis Rituximab treatment resulted in 6.16 fold induction an effect that was partially blocked by combination treatment at 6 hours (3.34 fold) with a similar effect seen at 16 hours. RT-Q-PCR at these timepoints shows a similar effect. The modulation of Rituximab mediated Bcl2A1 upregulation with combination treatment demonstrates how SAHA may inhibit an NF κ B mediated defence mechanism to mitogenic stimuli, and hence sensitise cells. These data taken together, show how combination treatment can result in subtle changes in the way that Ramos cells respond to either agent alone and demonstrate how the balance of Bcl-2 family proteins may be influenced to promote apoptosis following combination treatment.

The effect on LTA, another well described NF κ B target was also investigated [290]. LTA acts as a growth factor on B cells and is known to be upregulated by IL4 through NF κ B binding to its promoter. The effect on LTA was similar to that on Bcl2A1, SAHA blocked the Rituximab mediated upregulation observed. This again demonstrates how combination treatment results in modulation of the gene expression changes observed with Rituximab alone [**Figure 6-9**].

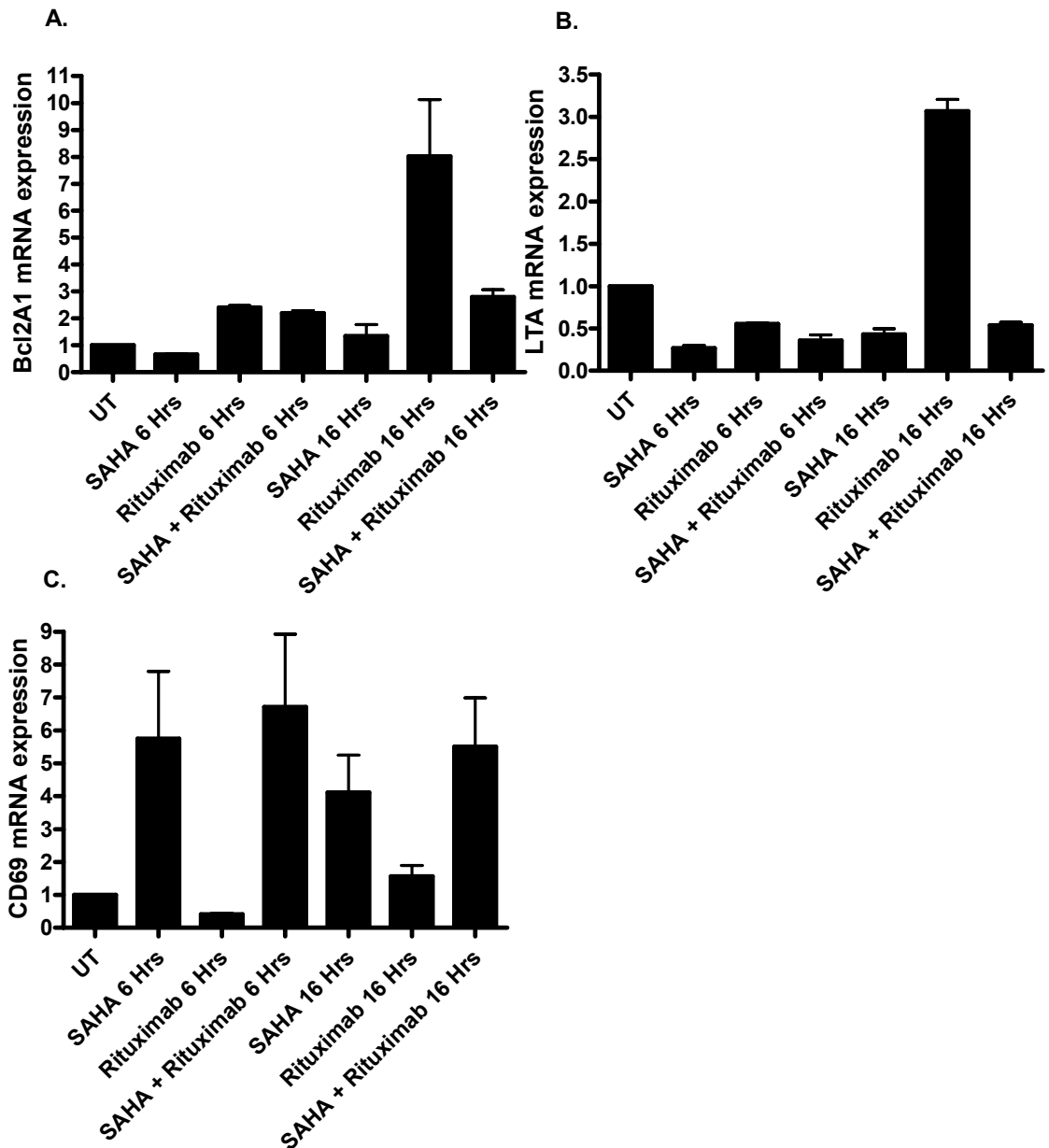


Figure 6-9 RT-Q-PCR of NFκB target genes in Ramos cells:

Ramos cells at 0.5×10^6 cells/ml were plated in duplicate in 6 well plates and treated with SAHA 5.5μM, Rituximab 3μg/ml with crosslinking agent or the combination. Control samples were left untreated. At the timepoints indicated cells were harvested and RNA was extracted using TRIzol reagent, and purified using qiagen RNA columns. Oligo dT primed cDNA was prepared from 1μg RNA and duplicate wells were loaded with 5μl cDNA, 15μl PCR master mix and appropriate taqman gene expression assay. Q-RT-PCR was performed as previously described. Data shown are mean (\pm range) from two independent experiments.

The effect on CD69 is different to this and demonstrates how combination treatment can serve to enhance activation of NF κ B targets. In the microarray analysis CD69 was ranked as one of the most differentially expressed genes following SAHA treatment (8.6 fold upregulation at 6 hours) and this effect was enhanced further with combination treatment (15.8 fold induction at 6 hours) despite little effect of Rituximab alone (1.7 fold induction at 6 hours). This effect was again confirmed with RT-Q-PCR analysis.

6.6 CD69 as a Biomarker of HDI transcriptional regulation

As discussed earlier the secondary aim of the gene expression analysis was to identify potential biomarkers indicative of transcriptional regulation occurring from HDAC inhibition.

CD69 is an early activation marker and was identified by *Sanchez-Mateos et al* as a 27/33 kDa homodimeric glycoprotein expressed on the surface of lymphoid cells [291]. Genomic analysis of human and murine CD69 gene has suggested it is a member of the Ca^{2+} dependent lectin superfamily and is expressed on the surface of T and B lymphocytes and NK cells upon activation [292]. It has no known ligand but appears to be upregulated through transcriptional mechanisms in response to a number of stimuli. Analysis of the promoter has identified binding sites for a number of transcription factors including NF κ B and AP1 [293]. The upregulation of CD69 mRNA observed in Ramos cells following SAHA treatment suggests that NF κ B is being activated resulting in transcriptional upregulation of this B cell activation marker. This effect was also observed with RT-Q-PCR in Ramos cells [**Figure 6-9**]. To investigate this effect further RT-Q-PCR was performed in SU-DHL-4 cells, this analysis was performed with summer student Alison Donlevy. There was robust induction of CD69 mRNA expression following six hours incubation with SAHA with significant further upregulation seen with combination treatment. The effect of HDI on CD69 mRNA expression was also confirmed in the HBL cell line and in human PBMC treated *ex vivo* (data not shown).

It seemed plausible that this could be used as a pharmacodynamic endpoint to establish a transcriptional target effect of HDI. To further examine this the regulation of cell surface CD69 was examined using flow cytometry initially in B cell NHL cell lines and subsequently in peripheral blood mononuclear cells (PBMC) treated *ex vivo*. Measurement of the regulation of other B cell activation markers was investigated to establish whether this effect was as part of a generalised B cell activation.

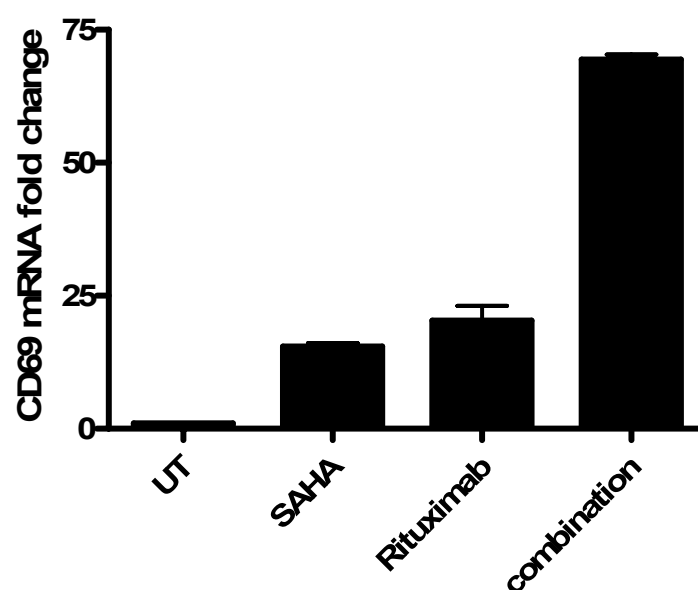


Figure 6-10 CD69 upregulation in SU-DHL-4 cell line

SU-DHL-4 cells at 0.5×10^6 cells/ml were plated in duplicate in 6 well plates and treated with SAHA (2.8 μ M), Rituximab (3 μ g/ml) or the combination. Control samples were left untreated. At the timepoints indicated cells were harvested and RNA was extracted using TRIzol reagent, and purified using qiagen RNA columns. Oligo dT primed cDNA was prepared from 1 μ g RNA and duplicate wells were loaded with 5 μ l cDNA , 15 μ l PCR master mix and appropriate taqman gene expression assay. Q-RT-PCR was performed as previously described. Data shown are mean (\pm range) from two independent experiments.

6.7 Up regulation of surface CD69 expression

Microarray analysis and RT-Q-PCR had demonstrated upregulation of CD69 mRNA expression. A flow cytometry assay was developed to investigate whether this resulted in upregulation of cell surface protein expression. This assay was initially performed in human peripheral blood lymphocytes (PBMC) treated ex vivo. Following 16 hours incubation with SAHA or Rituximab alone or in combination the percentage of CD69 positive, CD19 positive PBMC was determined [Figure 6-11]. There was a low but detectable level of CD69 positive B lymphocytes in control samples compared to an isotope matched antibody. Consistent with the changes observed in mRNA expression in cell lines, there was reproducible up regulation of CD69 cell surface expression with both SAHA and combination treatment. The effect of SAHA was also investigated in primary NHL samples. There was upregulation of surface CD69 expression observed in 3 NHL primary samples examined. Cells were again treated overnight and CD19 was used to identify B cells within the population. There was modest but reproducible upregulation of CD69 with the 2 concentrations of SAHA utilised [Figure 6-12].

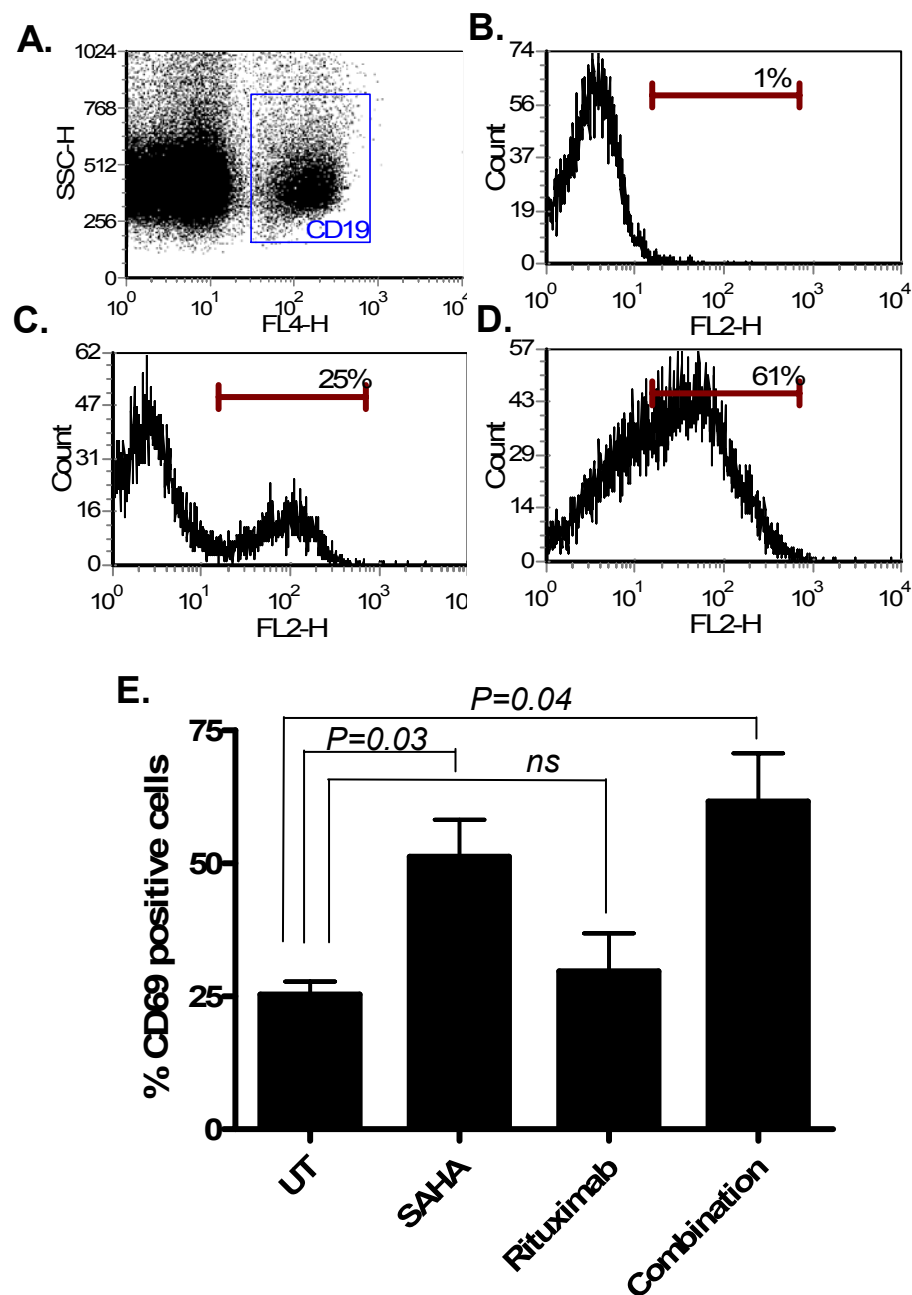


Figure 6-11 cell surface upregulation of CD69 in CD19 positive PBMC

PBMC were extracted from whole blood by centrifugation using lymphoprep reagent. After washing cells were resuspended in complete media with SAHA ($1\mu\text{M}$) or Rituximab ($10\mu\text{g/ml}$) alone or in combination, control samples were treated with DMSO alone. (A.) shows a representative dot plot demonstrating CD19 staining. (B.) shows a representative histogram for PE labelled IgG1 isotype control antibody. (C.) and (D.) show representative histograms for control and SAHA treated cells respectively. (E.) shows mean percentage CD69 positive cells (\pm range) from 3 independent experiments. Independent student's ttest was performed comparing untreated cells with the other conditions.

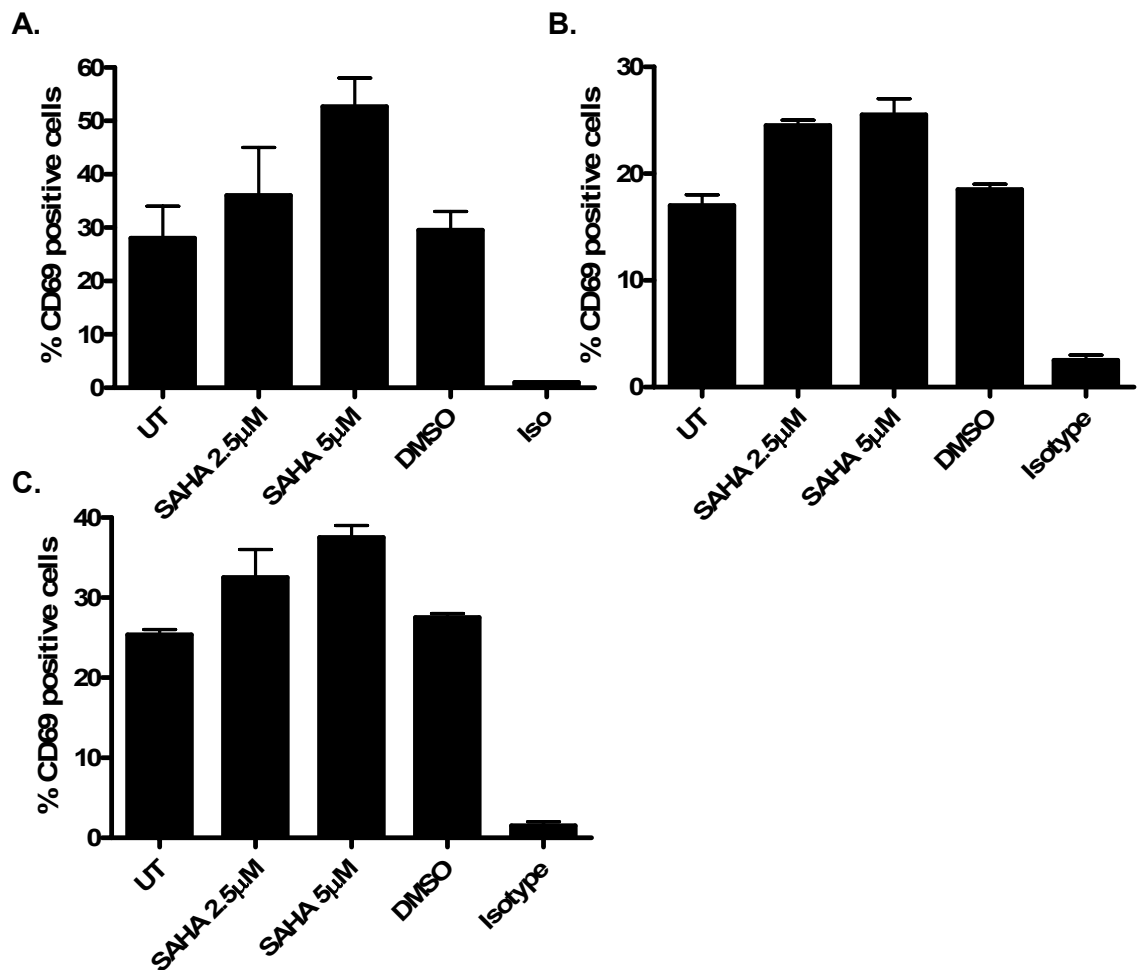


Figure 6-12 CD69 upregulation in primary cells:

Primary B cell NHL cells from the Southampton University tumour bank were resuspended in complete media and incubated overnight (16 Hrs) with the concentration of SAHA indicated. Control samples were left untreated or incubated with DMSO. Cells were harvested by centrifugation and resuspended in FACS buffer with APC conjugated CD19 and PE conjugated CD69 antibodies. Control samples were incubated with CD19 and an IgG1 isotype control antibody. Data shown are mean percentage of CD69 positive cells (\pm range) from two separate experiments for (A., B.) Follicular NHL and (C.) DLBCL.

These experiments established that SAHA could induce upregulation of CD69 expression at both an mRNA and protein level. The effect of HDI was investigated further by repeating the same assay with a range of concentrations of SAHA and FK228 [**Figure 6-13**]. Both these HDI resulted in dose dependent upregulation of CD69 expression, confirming that this effect was dose dependent. These data also demonstrate that the effect is not due to inhibition of class 2 HDACs only.

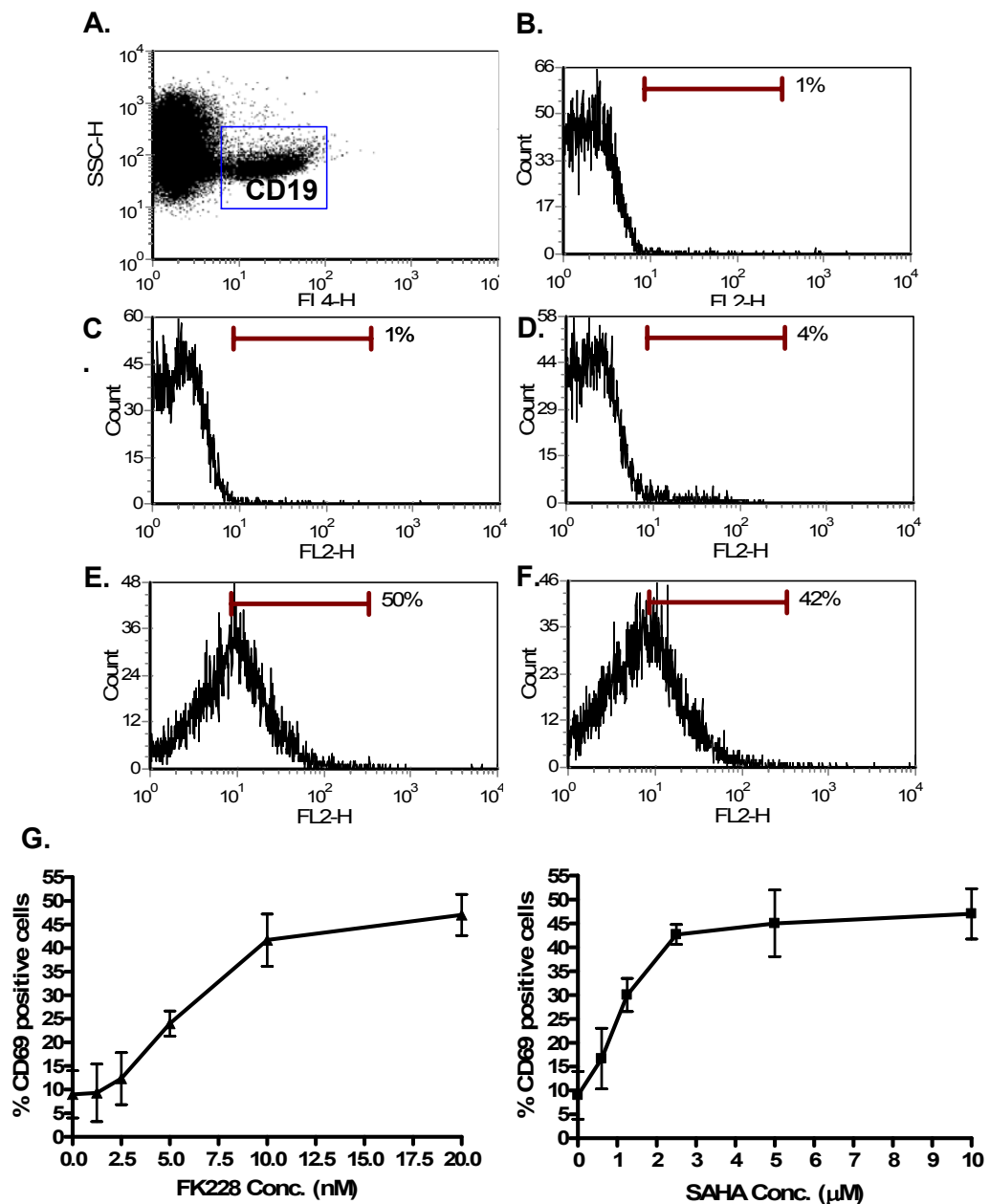


Figure 6-13 Induction of CD69 in a dose dependent manner by HDI
 PBMC were extracted from whole blood by centrifugation using lymphoprep reagent. After washing cells were resuspended in complete media and incubated for 16 hours with a range of concentrations of SAHA (0.07-10 μ M) or FK228 (1.25-20nM), control samples were treated with DMSO alone. (A.) shows a representative dot plot demonstrating CD19 staining. (B.) and (C.) show representative histograms of untreated and SAHA (10 μ M) treated cells stained with PE labelled IgG1 isotype control. (D.) shows a representative histogram of CD69 expression in untreated cells, with percentage of positive cells shown. (E.) and (F.) show representative histograms of CD69 expression in SAHA (5 μ M) and FK228 (10nM) treated cells. (G.) shows dose response curves for mean percentage (\pm range) of CD69 positive cells against concentration for SAHA and FK228 respectively. Data shown are from 3 independent experiments.

Having confirmed that incubation of PBMC with HDI resulted in dose dependent upregulation of CD69 expression, cells were incubated in the presence or absence of an NF κ B inhibitor to examine whether this effect occurred as a result of activation of the NF κ B pathway. Co-incubation with the IK β inhibitor, Bay 11-7082, resulted in inhibition of this upregulation confirming that this effect may be NF κ B mediated [**Figure 6-14**].

To investigate whether this was the result of a specific transcriptional effect of HDIs, rather than as part of a generalised B cell activation the effect of SAHA on another B cell activation marker was investigated. Incubation with CPG resulted in upregulation of CD69 and CD23, however SAHA only induced upregulation of CD69.

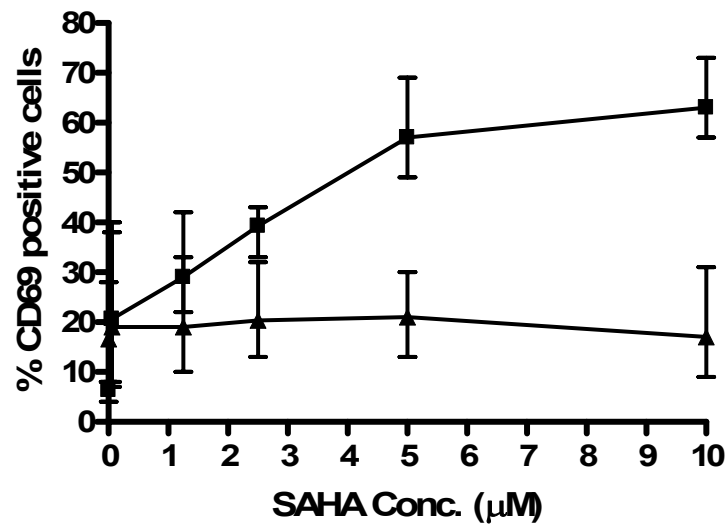


Figure 6-14 Effect of NFκB inhibition on CD69 upregulation:

PBMC were extracted from whole blood by centrifugation using lymphoprep reagent. After washing cells were resuspended in complete media and incubated for 16 hours in the presence (▲) or absence (■) of the IKβ kinase inhibitor Bay11-7082 (1.25μM) and a range of concentrations of SAHA (0.07-10μM), control samples were treated with DMSO alone or DMSO plus Bay 11-7082. data shown are mean percentage of CD69 positive cells (±range) from 3 independent experiments.

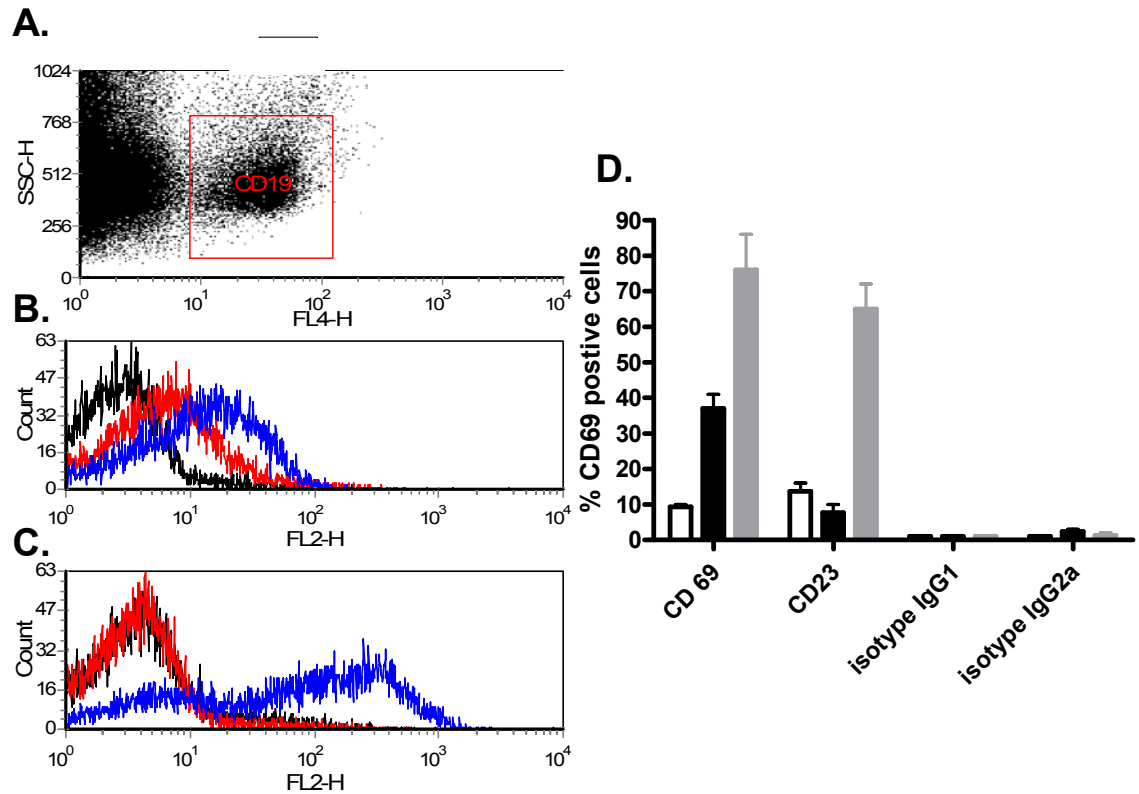


Figure 6-15 specific upregulation of CD69:

PBMC were extracted from whole blood by centrifugation using lymphoprep reagent. After washing cells were resuspended in complete media with SAHA ($1\mu\text{M}$) or CpG, control samples were treated with DMSO. **(A.)** shows a representative dot plot demonstrating CD19 staining. **(B.)** shows a representative histograms for CD69 expression in control (-), SAHA (-) or CpG (-) treated cells **(C.)** shows a representative histograms for CD23 expression in control (-), SAHA (-) or CpG (-) treated cells. **(D.)** shows mean percentage CD69 positive cells (\pm range) for control (□), SAHA (■) or CpG(■), treated samples from 3 independent experiments.

6.8 Discussion

Microarray gene expression analysis allows for the analysis of genome wide changes and provides a unique platform for evaluating the transcriptional response to anticancer therapies.

Transcriptional effect of Rituximab

There is little published data surrounding the transcriptional consequences of ligation by CD20 mAb. *Cittera et al* treated DHL-4 and BJAB cells with 10µg/ml Rituximab (without cross linking) for 2, 4 and 8 hours [284]. They observed little transcriptional activity with only 16 genes in DHL4 and 12 genes in BJAB upregulated greater than two fold, and no genes downregulated. The u133 plus2.0 chip used for the experiments presented here has a much higher number of probes than this earlier array, was conducted in the presence of crosslinking and analysed using a different FDR ($p \leq 0.05$) which may explain the higher number of differentially expressed genes. Despite these differences 7 genes (CD83, CCL3, CCL4, SGK, RGS2, FOS, ZFP36L) were identified which were differentially expressed across both experiments, including CCL3 which was the top ranked gene from our dataset.

It has been well documented that in some circumstances CD20 mAb can induce intracellular signalling [294]. Data from earlier experiments has also shown that in this cell line cross linked Rituximab results in Ca^{2+} flux and phosphorylation of ERK1/2, with published data showing this effect appears to be through utilization of the B cell receptor (BCR) signalling pathway [99]. The timepoint utilised in the microarray experiment was not likely to show these early events which do not occur at a transcriptional level.

The ability of Rituximab to inhibit NFκB activation is controversial with the only published data confirming this from Professor Bonavida's group [68, 102, 269, 270, 294]. The majority of these data were generated without crosslinking making comparison difficult. Using a single representative target gene such as BclX_L to establish 'inhibition of NFκB', then the data presented in this chapter is entirely consistent with this.

However, modulation of this pathway cannot be understood by assessment of a solitary gene. The gene expression profile of NF κ B target genes following Rituximab does not show down regulation of other anti apoptotic Bcl-2 family members. This is consistent with the observation that caspase processing is not necessary to induce Annexin V positivity and that Bcl-2 overexpression does not block the cell death seen. Based on the hypothesis that Rituximab induces intracellular signalling through BCR it is not surprising that there was upregulation of a number of targets associated with lymphocyte activation (CD83, CD69) and intracellular signalling (TRAF, TNF)

Transcriptional effect of SAHA

In contrast to this the transcriptional effects of HDAC inhibitors are well described with differential regulation of between 2 and 10% of genes observed [207-209]. A number of groups have investigated the gene expression profiles of structurally different HDI across different cell lines [210, 211]. It seems clear that although different experimental conditions result in regulation of distinct genes, there is a subset of 'core genes' which can be used to define an HDI transcriptional response. For example differential expression of TOB1, MXI1, and p21^{cip1} with downregulation of MYC were observed in all these studies and also in this experiment. This factor allowed the use of the connectivity map to validate the gene expression signature observed in the microarray experiment presented in this thesis. Peart *et al* observed that SAHA and FK228 modulated the expression of Bcl-2 family proteins in a complex fashion and argued that the overall effect coupled with upregulation of Apaf-1 was to induce activation of the intrinsic apoptotic pathway [211]. I observed that following 6 hours treatment with SAHA in Ramos cells there was also upregulation of Apaf-1 (4.4 fold) as well as significant changes in pro and anti apoptotic Bcl-2 proteins, however down regulation of BclX_L was not seen. This, coupled with the effects of over expressing Bcl-2 in Ramos cells suggest that the apoptosis seen in Ramos cells and the other B cell NHL cell lines is occurring via transcriptional modulation of the intrinsic apoptotic pathway. Modulation of other well described pathways were also observed including cell proliferation regulating genes (TOB1, BTG1, MYC, and GADD45 β). In contrast to these studies the

use of a B lymphocyte cell line allowed insight into effects on B cell activation and localisation genes. A striking feature of the functional annotation clustering analysis was that there appeared to be evidence B cell activation and immune modulation. The role of HDI in immune modulation is becoming increasingly well described with both pro and anti inflammatory effects observed [295, 296]. One of the key regulators of inflammatory responses and the intrinsic apoptotic pathway is the NF κ B transcription factor family. As discussed earlier HDI exert their transcriptional effects through; accumulation of acetylated core histones resulting in access of transcription factors to previously inaccessible promoter regions of genes [157, 297, 298]; and by directly influencing the acetylation of DNA binding proteins [146, 162, 163]. Both these mechanisms are pertinent to the HDI mediated regulation of NF κ B which is extremely complex with many gene specific interactions. HDAC3 promotes deacetylation of RelA and TSA promotes its DNA binding through acetylation [55], Chen *et al* have also shown that acetylation of K221 promotes DNA binding whilst acetylation of K310 is required for full transcriptional activity. In contrast to this there are also data suggesting that HDI can inhibit proteasome dependent NF κ B activation [299]. To try and understand the effect of SAHA on NF κ B targets in Ramos cells, the effect on well recognised targets was examined. SAHA induced both up and down regulation of targets with almost equal frequency. There was up regulation of pro apoptotic and down regulation of antiapoptotic Bcl-2 family members. However upregulation of Bcl-2 antiapoptotic transcripts (Bcl-2, Bcl2A1) with very low level downregulation of proapoptotic genes (BFLAR) was also seen. Despite this there was strong evidence of a transcriptional effect on many target genes important for regulation of apoptosis and lymphocyte activation and signalling.

Transcriptional effect of combination

The combination treatment effect is dominated by the SAHA transcriptional response. The small subset of genes differentially expressed with combination treatment compared to SAHA, predominantly with upregulation allowed insight into combination effects. Geneset enrichment analysis of this data set confirms that there is enrichment for NF κ B target genes (CD69,

Bcl2A1, CD83, CCL3, CCR7, BLR1, TRAF1) suggesting the importance of this transcription factor family in cooperative activity. The differential regulation of NF κ B target genes following combination treatment is again dominated by the effect of SAHA. However there are clear examples of gene expression changes in the combination resulting from Rituximab. For example CCL3 is up regulated 14.9 fold by Rituximab and 16.2 fold following combination, but unaffected by SAHA alone. CD69 and CD83 are both associated with activation of B cells and demonstrate that both agents may be acting together to induce B cell activation at a transcriptional level via NF κ B activation. The effect on Bcl2A1 in contrast to this demonstrates how SAHA can reduce the upregulation of an anti apoptotic Bcl-2 family member. Although this effect in isolation may not be important, it is occurring in combination with modulation of other apoptotic regulatory molecules and may be part of an alteration of the balance of pro and anti apoptotic signalling. If this effect is combined with the downregulation of BclX_L observed following Rituximab and combination treatments, a plausible hypothesis that 'modulation of Bcl-2 family proteins could enhance the induction of apoptosis through the intrinsic pathway' develops. Data already presented in earlier chapters has shown that induction of intrinsic apoptotic pathways is necessary for co operative effect, and this genomic level data is consistent with this.

7 Discussion and future work

The work presented here has specifically addressed the three main aims of the project.

The first aim was to investigate the ability of different HDI and CD20 mAb to induce cell death and apoptosis in a panel of CD20 positive B cell NHL cell lines, with the primary aim of establishing whether a synergistic effect was apparent and whether this was cell line or investigational agent specific. Using Annexin V/PI staining and flow cytometric analysis synergistic induction of apoptosis has been shown in a panel of CD20 positive B cell NHL cell lines. This synergistic killing appears to be specific to CD20 mAb, with a panel of other mAb not demonstrating this effect. It appears that to a degree synergy is dependent on levels of Bcl-2 expression, and can be blocked by pharmacological caspase inhibition. This effect has been recapitulated in a Ramos cell xenograft model, with significantly prolonged survival and reduced subcutaneous tumour growth.

The second aim was to identify the underlying mechanism for this effect. Two approaches were used to do this. Initially simple drug interactions were investigated prior to trying to elicit the effects of combination treatment on the intrinsic and extrinsic apoptotic pathways. Some of the underlying mechanisms have been demonstrated. Importantly it appears that the synergy observed is not simply due to changes in the early biochemical responses to HDI or CD20 mAb. Western blotting has shown that HDI require caspase processing for their activity in these cells. This does not seem to be the case with CD20 mAb. Synergy requires caspase processing and for type I mAb can be overcome by high levels of Bcl-2 expression. The synergy seen with type II mAb does not seem to depend on levels of Bcl-2 expression. This implies that the mechanism of this interaction occurs downstream of Bcl-2 in the apoptotic pathway, and may be subtly different for type I and II mAb.

The third aim was to utilise gene expression analysis to try to identify a cooperative transcriptional effect on previously described common survival

pathways and to investigate novel interactions for further investigation. This technique was also utilised to try and identify a biomarker of HDI transcriptional effect. Gene expression analysis has demonstrated that SAHA induces a robustly reproducible gene expression profile. Despite the very modest transcriptional effects of Rituximab, combination treatment results in significant changes in a number of genes compared to SAHA alone. This in itself demonstrates that the combination results in changes in gene expression that are independent of either agent alone. Gene set enrichment analysis and RT-Q-PCR analyses have demonstrated differential regulation of NFκB target genes and in particular members of the Bcl-2 family. These changes may be responsible for the synergistic apoptotic effects seen, but are extremely complex in nature. Alongside this we have identified the activation marker CD69 as a specific transcriptional target of SAHA in B cell NHL cell lines, and have demonstrated upregulation of cell membrane protein expression in human B cells treated *ex vivo*. This novel biomarker is potentially exploitable as an endpoint in clinical trials of HDI to demonstrate biological effect.

Taken together these observations provide compelling evidence for the potential of combining these agents as a novel treatment of B cell NHL. However they also demonstrate the complexity of this interaction raising many potential new avenues for investigation.

The logical future direction for this combination would be in an early phase clinical trial. A protocol for this has been developed and funding for this clinical trial is currently being sought.

This study is planned as an initial dose escalation phase I study and an expanded phase II cohort treated at a dose defined in the phase I study. It is proposed that patients will receive vorinostat (SAHA) orally starting at a dose of 200mg. After 14 days this will be given in combination with Rituximab at a standard dose of 375mg/m² weekly for 4 weeks. This will be followed by a further 4 weeks of SAHA to maximise the exposure to the combination. SAHA will be dose escalated up to the expected MTD derived from previous phase I studies as a single agent. The primary endpoint of the phase I study

will be to establish a safe and biologically effective dose for the phase II study. The primary end point of the phase II study will be to determine anti-tumour at a BED, the secondary endpoint will be toxicity. We have proposed using a flow cytometry assay of CD69 expression in B lymphocytes, alongside western blotting for histone acetylation to confirm biological effect.

In trying to further understand the interactions *in vitro* it would be important to explore the effects of HDI and the combination on gene specific promoters, particularly of NFκB target genes. It has already been described how epigenetic regulation of NFκB subunits can influence the gene expression patterns of NFκB target genes, without altering its DNA binding properties [55, 300]. It is possible that this mechanism could account for some of the gene expression changes described earlier. The NFκB promoter binding regions for a number of the differentially expressed genes have already been described [293, 301]. Using chromatin immunoprecipitation assay (ChIP) it would be possible to identify whether HDI or the combination resulted in alterations in the promoter occupation of these genes. This would help to demonstrate a link between HDI mediated modulation of NFκB activity and consequently the expression of target genes implicated in the initiation and regulation of the intrinsic apoptotic pathway.

The importance of the tumour microenvironment in developing and maintaining tumourigenesis has been well described [23]. This has not been exploited by conventional cytotoxic treatments, but may be a potential target for novel therapies. As discussed earlier the ability of Rituximab to recruit effector cells through Fc receptor interactions, is likely to be very important for its clinical efficacy [84]. This mechanism has not been investigated in the data presented. All *in vitro* assays were performed in the absence of these cells. It is interesting that in the xenograft studies, where macrophages were present, Rituximab appeared more effective than in the *in vitro* assays. This suggests that potentiation of Fc receptor interactions may be another important mechanism for the combination effect. Recent data defining the epigenetic regulation of macrophage activation further strengthens this hypothesis [302]. Ishii *et al* have shown that alternatively activated

macrophage (M2) are characterised by a number of marker genes and that these are epigenetically regulated. This provides another potential avenue for future investigations.

In summary the data presented from this project have demonstrated how the combination of HDI and CD20 mAb result in synergistic induction of apoptosis in B cell NHL cells. The mechanism of interaction between type I and type II mAb appear to be different consistent with their known mechanisms of action as single agents. The gene expression analysis has demonstrated how a complex effect on NF κ B target genes occurs, which may be acting to influence the apoptotic response to this combination. It will be interesting to see whether clinical trials of this combination can recapitulate this pre clinical data.

References

1. Jemal, A., et al., *Cancer Statistics, 2008*. CA Cancer J Clin, 2008. 58(2): p. 71-96.
2. Naresh, K.N., V. Srinivas, and C.S. Soman, *Distribution of various subtypes of non-Hodgkin's lymphoma in India: a study of 2773 lymphomas using R.E.A.L. and WHO Classifications*. Ann Oncol, 2000. 11 Suppl 1: p. 63-7.
3. Groves, F.D., et al., *Cancer Surveillance Series: Non-Hodgkin's Lymphoma Incidence by Histologic Subtype in the United States From 1978 Through 1995*. J. Natl. Cancer Inst., 2000. 92(15): p. 1240-1251.
4. Coiffier, B., et al., *CHOP chemotherapy plus rituximab compared with CHOP alone in elderly patients with diffuse large-B-cell lymphoma*. N Engl J Med, 2002. 346(4): p. 235-42.
5. Czuczman, M.S., et al., *Prolonged Clinical and Molecular Remission in Patients With Low-Grade or Follicular Non-Hodgkin's Lymphoma Treated With Rituximab Plus CHOP Chemotherapy: 9-Year Follow-Up*. J Clin Oncol, 2004. 22(23): p. 4711-4716.
6. Schatz, D.G., M.A. Oettinger, and D. Baltimore, *The V(D)J recombination activating gene, RAG-1*. Cell, 1989. 59(6): p. 1035-48.
7. Melchers, F., et al., *The surrogate light chain in B-cell development*. Immunol Today, 1993. 14(2): p. 60-8.
8. Kuppers, R., *Mechanisms of B-cell lymphoma pathogenesis*. Nat Rev Cancer, 2005. 5(4): p. 251-262.
9. Vaux, D.L., S. Cory, and J.M. Adams, *Bcl-2 gene promotes haemopoietic cell survival and cooperates with c-myc to immortalize pre-B cells*. Nature, 1988. 335(6189): p. 440-2.
10. Leroux, D., et al., *Non-Hodgkin's lymphomas with t(11;14)(q13;q32): a subset of mantle zone/intermediate lymphocytic lymphoma?* Br J Haematol, 1991. 77(3): p. 346-53.
11. Showe, L.C., et al., *Cloning and sequencing of a c-myc oncogene in a Burkitt's lymphoma cell line that is translocated to a germ line alpha switch region*. Mol Cell Biol, 1985. 5(3): p. 501-9.

12. Baron, B.W., et al., *Identification of the gene associated with the recurring chromosomal translocations t(3;14)(q27;q32) and t(3;22)(q27;q11) in B-cell lymphomas*. Proc Natl Acad Sci U S A, 1993. 90(11): p. 5262-6.
13. Yang, X., et al., *Association of Ig/BCL6 translocations with germinal center B lymphocytes in human lymphoid tissues: implications for malignant transformation*. Blood, 2006. 108(6): p. 2006-2012.
14. Alizadeh, A.A., et al., *Distinct types of diffuse large B-cell lymphoma identified by gene expression profiling*. Nature, 2000. 403(6769): p. 503-11.
15. Rosenwald, A., et al., *The use of molecular profiling to predict survival after chemotherapy for diffuse large-B-cell lymphoma*. N Engl J Med, 2002. 346(25): p. 1937-47.
16. Lenz, G., et al., *Molecular subtypes of diffuse large B-cell lymphoma arise by distinct genetic pathways*. Proc Natl Acad Sci U S A, 2008. 105(36): p. 13520-5.
17. Davis, R.E., et al., *Constitutive nuclear factor kappaB activity is required for survival of activated B cell-like diffuse large B cell lymphoma cells*. J Exp Med, 2001. 194(12): p. 1861-74.
18. Ngo, V.N., et al., *A loss-of-function RNA interference screen for molecular targets in cancer*. Nature, 2006. 441(7089): p. 106-110.
19. Lenz, G., et al., *Oncogenic CARD11 mutations in human diffuse large B cell lymphoma*. Science, 2008. 319(5870): p. 1676-9.
20. Pezzella, F., et al., *Expression of the bcl-2 oncogene protein is not specific for the 14;18 chromosomal translocation*. Am J Pathol, 1990. 137(2): p. 225-32.
21. Liu, Y.J., et al., *Germinal center cells express bcl-2 protein after activation by signals which prevent their entry into apoptosis*. Eur J Immunol, 1991. 21(8): p. 1905-10.
22. Craxton, A., et al., *The CD40-inducible Bcl-2 family member A1 protects B cells from antigen receptor-mediated apoptosis*. Cell Immunol, 2000. 200(1): p. 56-62.
23. Hanahan, D. and R.A. Weinberg, *The hallmarks of cancer*. Cell, 2000. 100(1): p. 57-70.

24. Chipuk, J.E. and D.R. Green, *How do BCL-2 proteins induce mitochondrial outer membrane permeabilization?* Trends in Cell Biology, 2008. 18(4): p. 157-164.
25. Li, P., et al., *Cytochrome c and dATP-Dependent Formation of Apaf-1/Caspase-9 Complex Initiates an Apoptotic Protease Cascade.* Cell, 1997. 91(4): p. 479-489.
26. Tewari, M., et al., *Yama/ CPP32 beta, a mammalian homolog of CED-3, is a CrmA-inhibitable protease that cleaves the death substrate poly(ADP-ribose) polymerase.* Cell, 1995. 81(5): p. 801-9.
27. Nicholson, D.W., et al., *Identification and inhibition of the ICE/CED-3 protease necessary for mammalian apoptosis.* Nature, 1995. 376(6535): p. 37-43.
28. Fulda, S. and K.M. Debatin, *Extrinsic versus intrinsic apoptosis pathways in anticancer chemotherapy.* Oncogene. 25(34): p. 4798-4811.
29. Kischkel, F.C., et al., *Cytotoxicity-dependent APO-1 (Fas/CD95)-associated proteins form a death-inducing signaling complex (DISC) with the receptor.* EMBO J, 1995. 14(22): p. 5579-88.
30. Scaffidi, C., et al., *Two CD95 (APO-1/Fas) signaling pathways.* EMBO J, 1998. 17(6): p. 1675-87.
31. Scaffidi, C., et al., *Differential modulation of apoptosis sensitivity in CD95 type I and type II cells.* J Biol Chem, 1999. 274(32): p. 22532-8.
32. Ashkenazi, A., *Targeting death and decoy receptors of the tumour-necrosis factor superfamily.* Nat Rev Cancer, 2002. 2(6): p. 420-430.
33. Yang, E. and S.J. Korsmeyer, *Molecular thanatopsis: a discourse on the BCL2 family and cell death.* Blood, 1996. 88(2): p. 386-401.
34. Zha, H., et al., *Proapoptotic protein Bax heterodimerizes with Bcl-2 and homodimerizes with Bax via a novel domain (BH3) distinct from BH1 and BH2.* J Biol Chem, 1996. 271(13): p. 7440-4.
35. Tanaka, S., K. Saito, and J.C. Reed, *Structure-function analysis of the Bcl-2 oncoprotein. Addition of a heterologous transmembrane domain to portions of the Bcl-2 beta protein restores function as a regulator of cell survival.* J Biol Chem, 1993. 268(15): p. 10920-6.
36. Hockenbery, D.M., et al., *Bcl-2 functions in an antioxidant pathway to prevent apoptosis.* Cell, 1993. 75(2): p. 241-51.

37. Letai, A., et al., *Distinct BH3 domains either sensitize or activate mitochondrial apoptosis, serving as prototype cancer therapeutics*. Cancer Cell, 2002. 2(3): p. 183-92.
38. Adams, J.M. and S. Cory, *The Bcl-2 apoptotic switch in cancer development and therapy*. Oncogene, 2007. 26(9): p. 1324-37.
39. Chen, L., et al., *Differential targeting of prosurvival Bcl-2 proteins by their BH3-only ligands allows complementary apoptotic function*. Mol Cell, 2005. 17(3): p. 393-403.
40. Willis, S.N., et al., *Proapoptotic Bak is sequestered by Mcl-1 and Bcl-xL, but not Bcl-2, until displaced by BH3-only proteins*. Genes Dev, 2005. 19(11): p. 1294-305.
41. Chang, B.S., et al., *Identification of a novel regulatory domain in Bcl-X(L) and Bcl-2*. EMBO J, 1997. 16(5): p. 968-77.
42. Zha, J., et al., *Serine Phosphorylation of Death Agonist BAD in Response to Survival Factor Results in Binding to 14-3-3 Not BCL-XL*. Cell, 1996. 87(4): p. 619-628.
43. Fukuhara, S., et al., *Chromosome abnormalities in poorly differentiated lymphocytic lymphoma*. Cancer Res, 1979. 39(8): p. 3119-28.
44. Yunis, J.J., et al., *bcl-2 and other genomic alterations in the prognosis of large-cell lymphoma*. N Engl J Med, 1989. 320(16): p. 1047-54.
45. McDonnell, T.J., et al., *bcl-2-immunoglobulin transgenic mice demonstrate extended B cell survival and follicular lymphoproliferation*. Cell, 1989. 57(1): p. 79-88.
46. Tagawa, H., et al., *Genome-wide array-based CGH for mantle cell lymphoma: identification of homozygous deletions of the proapoptotic gene BIM*. Oncogene, 2005. 24(8): p. 1348-58.
47. Michalak, E.M., et al., *Puma and to a lesser extent Noxa are suppressors of Myc-induced lymphomagenesis*. Cell Death Differ, 2009. 16(5): p. 684-696.
48. Gilmore, T.D., *Introduction to NF-kappaB: players, pathways, perspectives*. Oncogene, 2006. 25(51): p. 6680-4.
49. Sen, R. and D. Baltimore, *Inducibility of kappa immunoglobulin enhancer-binding protein Nf-kappa B by a posttranslational mechanism*. Cell, 1986. 47(6): p. 921-8.

50. Gonzalez-Crespo, S. and M. Levine, *Related target enhancers for dorsal and NF-kappa B signaling pathways*. Science, 1994. 264(5156): p. 255-258.
51. Fujita, T., et al., *The candidate proto-oncogene bcl-3 encodes a transcriptional coactivator that activates through NF-kappa B p50 homodimers*. Genes Dev, 1993. 7(7B): p. 1354-63.
52. Zhong, H., et al., *The phosphorylation status of nuclear NF-kappa B determines its association with CBP/p300 or HDAC-1*. Mol Cell, 2002. 9(3): p. 625-36.
53. Arenzana-Seisdedos, F., et al., *Inducible nuclear expression of newly synthesized I kappa B alpha negatively regulates DNA-binding and transcriptional activities of NF- kappa B*. Mol. Cell. Biol., 1995. 15(5): p. 2689-2696.
54. Perkins, N.D., *Post-translational modifications regulating the activity and function of the nuclear factor kappa B pathway*. Oncogene, 2006. 25(51): p. 6717-30.
55. Chen, L.F., Y. Mu, and W.C. Greene, *Acetylation of RelA at discrete sites regulates distinct nuclear functions of NF-kappaB*. EMBO J, 2002. 21(23): p. 6539-48.
56. Kim, J.H., et al., *Transcriptional regulation of a metastasis suppressor gene by Tip60 and beta-catenin complexes*. Nature, 2005. 434(7035): p. 921-6.
57. Packham, G., *The role of NF-kappaB in lymphoid malignancies*. Br J Haematol, 2008. 143(1): p. 3-15.
58. Pahl, H.L., *Activators and target genes of Rel/NF-kappaB transcription factors*. Oncogene, 1999. 18(49): p. 6853-66.
59. Beg, A.A., et al., *Embryonic lethality and liver degeneration in mice lacking the RelA component of NF-kappa B*. Nature, 1995. 376(6536): p. 167-70.
60. Alcamo, E., et al., *Targeted mutation of TNF receptor I rescues the RelA-deficient mouse and reveals a critical role for NF-kappa B in leukocyte recruitment*. J Immunol, 2001. 167(3): p. 1592-600.
61. Doi, T.S., et al., *NF-kappa B RelA-deficient lymphocytes: normal development of T cells and B cells, impaired production of IgA and IgG1 and reduced proliferative responses*. J Exp Med, 1997. 185(5): p. 953-61.

62. **Gilmore, T.D., et al., *The c-Rel transcription factor and B-cell proliferation: a deal with the devil*. Oncogene, 2004. 23(13): p. 2275-86.**
63. **Courtois, G. and T.D. Gilmore, *Mutations in the NF-kappaB signaling pathway: implications for human disease*. Oncogene, 2006. 25(51): p. 6831-43.**
64. **Rayet, B. and C. Gelinas, *Aberrant rel/nfkb genes and activity in human cancer*. Oncogene, 1999. 18(49): p. 6938-47.**
65. **Fisher, R.I., et al., *Comparison of a Standard Regimen (CHOP) with Three Intensive Chemotherapy Regimens for Advanced Non-Hodgkin's Lymphoma*. N Engl J Med, 1993. 328(14): p. 1002-1006.**
66. **Johnson, P.W., et al., *Patterns of survival in patients with recurrent follicular lymphoma: a 20-year study from a single center*. J Clin Oncol, 1995. 13(1): p. 140-147.**
67. **Gall EA, M.T., *Malignant lymphoma: A clinico-pathologic survey of 618 cases*. Am J Pathol, 1942. 18: p. 281-429.**
68. **Jazirehi, A.R. and B. Bonavida, *Cellular and molecular signal transduction pathways modulated by rituximab (rituxan, anti-CD20 mAb) in non-Hodgkin's lymphoma: implications in chemosensitization and therapeutic intervention*. Oncogene, 2005. 24(13): p. 2121-43.**
69. **Tedder, T.F., et al., *Isolation and structure of a cDNA encoding the B1 (CD20) cell-surface antigen of human B lymphocytes*. Proc Natl Acad Sci U S A, 1988. 85(1): p. 208-12.**
70. **Einfeld, D.A., et al., *Molecular cloning of the human B cell CD20 receptor predicts a hydrophobic protein with multiple transmembrane domains*. Embo J, 1988. 7(3): p. 711-7.**
71. **Cragg, M.S., et al., *The biology of CD20 and its potential as a target for mAb therapy*. Curr Dir Autoimmun, 2005. 8: p. 140-74.**
72. **Petrie, R.J. and J.P. Deans, *Colocalization of the B cell receptor and CD20 followed by activation-dependent dissociation in distinct lipid rafts*. J Immunol, 2002. 169(6): p. 2886-91.**
73. **O'Keefe, T.L., et al., *Mice carrying a CD20 gene disruption*. Immunogenetics, 1998. 48(2): p. 125-32.**

74. Bubien, J.K., et al., *Transfection of the CD20 cell surface molecule into ectopic cell types generates a Ca²⁺ conductance found constitutively in B lymphocytes*. J Cell Biol, 1993. 121(5): p. 1121-32.
75. Li, H., et al., *Store-operated cation entry mediated by CD20 in membrane rafts*. J Biol Chem, 2003. 278(43): p. 42427-34.
76. Stamenkovic, I. and B. Seed, *Analysis of two cDNA clones encoding the B lymphocyte antigen CD20 (B1, Bp35), a type III integral membrane protein*. J Exp Med, 1988. 167(6): p. 1975-80.
77. Tedder, T.F. and P. Engel, *CD20: a regulator of cell-cycle progression of B lymphocytes*. Immunol Today, 1994. 15(9): p. 450-4.
78. Genot, E., et al., *Hyperphosphorylation of CD20 in hairy cells. Alteration by low molecular weight B cell growth factor and IFN-alpha*. J Immunol, 1991. 146(3): p. 870-8.
79. Genot, E.M., et al., *Phosphorylation of CD20 in cells from a hairy cell leukemia cell line. Evidence for involvement of calcium/calmodulin-dependent protein kinase II*. J Immunol, 1993. 151(1): p. 71-82.
80. Kuijpers, T.W., et al., *CD20 deficiency in humans results in impaired T cell-independent antibody responses*. The Journal of Clinical Investigation. 120(1): p. 214-222.
81. Cragg, M.S., et al., *Complement-mediated lysis by anti-CD20 mAb correlates with segregation into lipid rafts*. Blood, 2003. 101(3): p. 1045-52.
82. Deans, J.P., et al., *Rapid redistribution of CD20 to a low density detergent-insoluble membrane compartment*. J Biol Chem, 1998. 273(1): p. 344-8.
83. Glennie, M.J., et al., *Mechanisms of killing by anti-CD20 monoclonal antibodies*. Mol Immunol, 2007. 44(16): p. 3823-37.
84. Shan, D., J.A. Ledbetter, and O.W. Press, *Apoptosis of malignant human B cells by ligation of CD20 with monoclonal antibodies*. Blood, 1998. 91(5): p. 1644-52.
85. Shan, D., J.A. Ledbetter, and O.W. Press, *Signaling events involved in anti-CD20-induced apoptosis of malignant human B cells*. Cancer Immunol Immunother, 2000. 48(12): p. 673-83.
86. Glennie, M.J. and P.W. Johnson, *Clinical trials of antibody therapy*. Immunol Today, 2000. 21(8): p. 403-10.

87. Chan, H.T., et al., *CD20-induced lymphoma cell death is independent of both caspases and its redistribution into triton X-100 insoluble membrane rafts*. Cancer Res, 2003. 63(17): p. 5480-9.
88. Deans, J.P., H. Li, and M.J. Polyak, *CD20-mediated apoptosis: signalling through lipid rafts*. Immunology, 2002. 107(2): p. 176-82.
89. Li, H., et al., *The CD20 calcium channel is localized to microvilli and constitutively associated with membrane rafts: antibody binding increases the affinity of the association through an epitope-dependent cross-linking-independent mechanism*. J Biol Chem, 2004. 279(19): p. 19893-901.
90. Cragg, M.S. and M.J. Glennie, *Antibody specificity controls in vivo effector mechanisms of anti-CD20 reagents*. Blood, 2004. 103(7): p. 2738-43.
91. Di Gaetano, N., et al., *Complement activation determines the therapeutic activity of rituximab in vivo*. J Immunol, 2003. 171(3): p. 1581-7.
92. Smith, M.R., *Rituximab (monoclonal anti-CD20 antibody): mechanisms of action and resistance*. Oncogene. 22(47): p. 7359-7368.
93. Treon, S.P., et al., *Tumor cell expression of CD59 is associated with resistance to CD20 serotherapy in patients with B-cell malignancies*. J Immunother, 2001. 24(3): p. 263-71.
94. Fridman, W.H., *Fc receptors and immunoglobulin binding factors*. FASEB J, 1991. 5(12): p. 2684-90.
95. Reff, M.E., et al., *Depletion of B cells in vivo by a chimeric mouse human monoclonal antibody to CD20*. Blood, 1994. 83(2): p. 435-445.
96. Clynes, R.A., et al., *Inhibitory Fc receptors modulate in vivo cytotoxicity against tumor targets*. Nat Med, 2000. 6(4): p. 443-6.
97. Cartron, G., et al., *Therapeutic activity of humanized anti-CD20 monoclonal antibody and polymorphism in IgG Fc receptor Fcgamma RIIa gene*. Blood, 2002. 99(3): p. 754-758.
98. Ghetie, M.A., H. Bright, and E.S. Vitetta, *Homodimers but not monomers of Rituxan (chimeric anti-CD20) induce apoptosis in human B-lymphoma cells and synergize with a chemotherapeutic agent and an immunotoxin*. Blood, 2001. 97(5): p. 1392-8.

99. Walshe, C.A., et al., *Induction of cytosolic calcium flux by CD20 is dependent upon B Cell antigen receptor signaling*. J Biol Chem, 2008. 283(25): p. 16971-84.
100. Ivanov, A., et al., *Monoclonal antibodies directed to CD20 and HLA-DR can elicit homotypic adhesion followed by lysosome-mediated cell death in human lymphoma and leukemia cells*. J Clin Invest, 2009. 119(8): p. 2143-59.
101. Jazirehi, A.R., et al., *Inhibition of the Raf-MEK1/2-ERK1/2 signaling pathway, Bcl-xL down-regulation, and chemosensitization of non-Hodgkin's lymphoma B cells by Rituximab*. Cancer Res, 2004. 64(19): p. 7117-26.
102. Jazirehi, A.R., et al., *Rituximab (chimeric anti-CD20 monoclonal antibody) inhibits the constitutive nuclear factor- κ B signaling pathway in non-Hodgkin's lymphoma B-cell lines: role in sensitization to chemotherapeutic drug-induced apoptosis*. Cancer Res, 2005. 65(1): p. 264-76.
103. Stolz, C., et al., *Targeting Bcl-2 family proteins modulates the sensitivity of B-cell lymphoma to rituximab-induced apoptosis*. Blood, 2008. 112(8): p. 3312-21.
104. Maloney, D.G., et al., *Monoclonal anti-idiotypic antibody therapy of B-cell lymphoma: the addition of a short course of chemotherapy does not interfere with the antitumor effect nor prevent the emergence of idiotype-negative variant cells*. Blood, 1992. 80(6): p. 1502-10.
105. Reff, M.E., et al., *Depletion of B cells in vivo by a chimeric mouse human monoclonal antibody to CD20*. Blood, 1994. 83(2): p. 435-45.
106. Maloney, D.G., et al., *Phase I clinical trial using escalating single-dose infusion of chimeric anti-CD20 monoclonal antibody (IDEC-C2B8) in patients with recurrent B-cell lymphoma*. Blood, 1994. 84(8): p. 2457-2466.
107. Maloney, D.G., et al., *IDEC-C2B8 (Rituximab) Anti-CD20 Monoclonal Antibody Therapy in Patients With Relapsed Low-Grade Non-Hodgkin's Lymphoma*. Blood, 1997. 90(6): p. 2188-2195.
108. McLaughlin, P., et al., *Rituximab chimeric anti-CD20 monoclonal antibody therapy for relapsed indolent lymphoma: half of patients respond to a four-dose treatment program*. J Clin Oncol, 1998. 16(8): p. 2825-2833.
109. Czuczman, M.S., et al., *Treatment of Patients With Low-Grade B-Cell Lymphoma With the Combination of Chimeric Anti-CD20 Monoclonal Antibody and CHOP Chemotherapy*. J Clin Oncol, 1999. 17(1): p. 268-.

110. Czuczman, M.S., et al., *Rituximab in Combination With Fludarabine Chemotherapy in Low-Grade or Follicular Lymphoma*. J Clin Oncol, 2005. 23(4): p. 694-704.
111. Marcus, R., et al., *Phase III study of R-CVP compared with cyclophosphamide, vincristine, and prednisone alone in patients with previously untreated advanced follicular lymphoma*. J Clin Oncol, 2008. 26(28): p. 4579-86.
112. Hiddemann, W., et al., *Frontline therapy with rituximab added to the combination of cyclophosphamide, doxorubicin, vincristine, and prednisone (CHOP) significantly improves the outcome for patients with advanced-stage follicular lymphoma compared with therapy with CHOP alone: results of a prospective randomized study of the German Low-Grade Lymphoma Study Group*. Blood, 2005. 106(12): p. 3725-32.
113. Herold, M., et al., *Rituximab Added to First-Line Mitoxantrone, Chlorambucil, and Prednisolone Chemotherapy Followed by Interferon Maintenance Prolongs Survival in Patients With Advanced Follicular Lymphoma: An East German Study Group Hematology and Oncology Study*. J Clin Oncol, 2007. 25(15): p. 1986-1992.
114. van Oers, M.H., et al., *Rituximab maintenance improves clinical outcome of relapsed/resistant follicular non-Hodgkin lymphoma in patients both with and without rituximab during induction: results of a prospective randomized phase 3 intergroup trial*. Blood, 2006. 108(10): p. 3295-301.
115. Forstpointner, R., et al., *Maintenance therapy with rituximab leads to a significant prolongation of response duration after salvage therapy with a combination of rituximab, fludarabine, cyclophosphamide, and mitoxantrone (R-FCM) in patients with recurring and refractory follicular and mantle cell lymphomas: Results of a prospective randomized study of the German Low Grade Lymphoma Study Group (GLSG)*. Blood, 2006. 108(13): p. 4003-8.
116. Ghielmini, M., et al., *Prolonged treatment with rituximab in patients with follicular lymphoma significantly increases event-free survival and response duration compared with the standard weekly x 4 schedule*. Blood, 2004. 103(12): p. 4416-23.
117. Gordan, L.N., et al., *Phase II trial of individualized rituximab dosing for patients with CD20-positive lymphoproliferative disorders*. J Clin Oncol, 2005. 23(6): p. 1096-102.
118. Pfreundschuh, M., et al., *CHOP-like chemotherapy plus rituximab versus CHOP-like chemotherapy alone in young patients with good-prognosis diffuse large-B-cell lymphoma: a randomised controlled trial by the*

MabThera International Trial (MInT) Group. Lancet Oncol, 2006. 7(5): p. 379-91.

119. Habermann, T.M., et al., *Rituximab-CHOP versus CHOP alone or with maintenance rituximab in older patients with diffuse large B-cell lymphoma. J Clin Oncol, 2006. 24(19): p. 3121-7.*
120. Sehn, L.H., et al., *Introduction of Combined CHOP Plus Rituximab Therapy Dramatically Improved Outcome of Diffuse Large B-Cell Lymphoma in British Columbia. J Clin Oncol, 2005. 23(22): p. 5027-5033.*
121. Feugier, P., et al., *Long-Term Results of the R-CHOP Study in the Treatment of Elderly Patients With Diffuse Large B-Cell Lymphoma: A Study by the Groupe d'Etude des Lymphomes de l'Adulte. J Clin Oncol, 2005. 23(18): p. 4117-4126.*
122. Hagenbeek, A., et al., *First clinical use of ofatumumab, a novel fully human anti-CD20 monoclonal antibody in relapsed or refractory follicular lymphoma: results of a phase 1/2 trial. Blood, 2008. 111(12): p. 5486-5495.*
123. Press, O.W., et al., *Phase II Trial of CHOP Chemotherapy Followed by Tositumomab/Iodine I-131 Tositumomab for Previously Untreated Follicular Non-Hodgkin's Lymphoma: Five-Year Follow-Up of Southwest Oncology Group Protocol S9911. J Clin Oncol, 2006. 24(25): p. 4143-4149.*
124. Hekman, A., et al., *Initial experience with treatment of human B cell lymphoma with anti-CD19 monoclonal antibody. Cancer Immunol Immunother, 1991. 32(6): p. 364-72.*
125. Zalevsky, J., et al., *The impact of Fc engineering on an anti-CD19 antibody: increased Fc{gamma} receptor affinity enhances B-cell clearing in nonhuman primates. Blood, 2009. 113(16): p. 3735-3743.*
126. Czuczman, M.S., et al., *Phase I/II study of galiximab, an anti-CD80 antibody, for relapsed or refractory follicular lymphoma. J Clin Oncol, 2005. 23(19): p. 4390-8.*
127. Leonard, J.P., et al., *Phase I/II trial of epratuzumab (humanized anti-CD22 antibody) in indolent non-Hodgkin's lymphoma. J Clin Oncol, 2003. 21(16): p. 3051-9.*
128. Leonard, J.P., et al., *Epratuzumab, a humanized anti-CD22 antibody, in aggressive non-Hodgkin's lymphoma: phase I/II clinical trial results. Clin Cancer Res, 2004. 10(16): p. 5327-34.*

129. Hurwitz, H., et al., *Bevacizumab plus irinotecan, fluorouracil, and leucovorin for metastatic colorectal cancer*. N Engl J Med, 2004. 350(23): p. 2335-42.
130. Salven, P., et al., *Simultaneous elevation in the serum concentrations of the angiogenic growth factors VEGF and bFGF is an independent predictor of poor prognosis in non-Hodgkin lymphoma: a single-institution study of 200 patients*. Blood, 2000. 96(12): p. 3712-8.
131. Stopeck, A.T., et al., *A phase II trial of single agent bevacizumab in patients with relapsed, aggressive non-Hodgkin lymphoma: Southwest oncology group study S0108*. Leukemia and Lymphoma, 2009. 50(5): p. 728 - 735.
132. Ganjoo, K.N., et al., *Rituximab, Bevacizumab and CHOP (RA-CHOP) in untreated diffuse large B-cell lymphoma: Safety, biomarker and pharmacokinetic analysis*. Leukemia and Lymphoma, 2006. 47(6): p. 998 - 1005.
133. Oltersdorf, T., et al., *An inhibitor of Bcl-2 family proteins induces regression of solid tumours*. Nature, 2005. 435(7042): p. 677-681.
134. Tse, C., et al., *ABT-263: A Potent and Orally Bioavailable Bcl-2 Family Inhibitor*. Cancer Res, 2008. 68(9): p. 3421-3428.
135. Trudel, S., et al., *Preclinical studies of the pan-Bcl inhibitor obatoclax (GX015-070) in multiple myeloma*. Blood, 2007. 109(12): p. 5430-8.
136. Konopleva, M., et al., *Mechanisms of antileukemic activity of the novel Bcl-2 homology domain-3 mimetic GX15-070 (obatoclax)*. Cancer Res, 2008. 68(9): p. 3413-20.
137. Myung, J., K.B. Kim, and C.M. Crews, *The ubiquitin-proteasome pathway and proteasome inhibitors*. Med Res Rev, 2001. 21(4): p. 245-73.
138. Pham, L.V., et al., *Inhibition of constitutive NF-kappa B activation in mantle cell lymphoma B cells leads to induction of cell cycle arrest and apoptosis*. J Immunol, 2003. 171(1): p. 88-95.
139. Strauss, S.J., et al., *Bortezomib Therapy in Patients With Relapsed or Refractory Lymphoma: Potential Correlation of In Vitro Sensitivity and Tumor Necrosis Factor Alpha Response With Clinical Activity*. J Clin Oncol, 2006. 24(13): p. 2105-2112.
140. Orlowski, R.Z., et al., *Phase I trial of the proteasome inhibitor bortezomib and pegylated liposomal doxorubicin in patients with advanced hematologic malignancies*. Blood, 2005. 105(8): p. 3058-3065.

141. Leleu, X., et al., *Targeting NF- κ B in Waldenstrom macroglobulinemia*. Blood, 2008. 111(10): p. 5068-5077.
142. Pei, X.-Y., Y. Dai, and S. Grant, *Synergistic Induction of Oxidative Injury and Apoptosis in Human Multiple Myeloma Cells by the Proteasome Inhibitor Bortezomib and Histone Deacetylase Inhibitors*. Clin Cancer Res, 2004. 10(11): p. 3839-3852.
143. Yu, C., et al., *The proteasome inhibitor bortezomib interacts synergistically with histone deacetylase inhibitors to induce apoptosis in Bcr/Abl+ cells sensitive and resistant to STI571*. Blood, 2003. 102(10): p. 3765-74.
144. Duan, J., et al., *Nuclear factor-kappaB p65 small interfering RNA or proteasome inhibitor bortezomib sensitizes head and neck squamous cell carcinomas to classic histone deacetylase inhibitors and novel histone deacetylase inhibitor PXD101*. Mol Cancer Ther, 2007. 6(1): p. 37-50.
145. Emanuele, S., et al., *SAHA induces apoptosis in hepatoma cells and synergistically interacts with the proteasome inhibitor Bortezomib*. Apoptosis, 2007. 12(7): p. 1327-38.
146. Chen, L.F. and W.C. Greene, *Regulation of distinct biological activities of the NF-kappaB transcription factor complex by acetylation*. J Mol Med, 2003. 81(9): p. 549-57.
147. Graham, B. and S.B. Gibson, *The two faces of NFkappaB in cell survival responses*. Cell Cycle, 2005. 4(10): p. 1342-5.
148. Felsenfeld, G. and M. Groudine, *Controlling the double helix*. Nature, 2003. 421(6921): p. 448-53.
149. Sandman, K., S.L. Pereira, and J.N. Reeve, *Diversity of prokaryotic chromosomal proteins and the origin of the nucleosome*. Cell Mol Life Sci, 1998. 54(12): p. 1350-64.
150. Luger, K., et al., *Crystal structure of the nucleosome core particle at 2.8 A resolution*. Nature, 1997. 389(6648): p. 251-60.
151. Allfrey, V.G., V.C. Littau, and A.E. Mirsky, *On the role of of histones in regulation ribonucleic acid synthesis in the cell nucleus*. Proc Natl Acad Sci U S A, 1963. 49: p. 414-21.
152. Goll, M.G. and T.H. Bestor, *Histone modification and replacement in chromatin activation*. Genes Dev, 2002. 16(14): p. 1739-42.

153. Strahl, B.D. and C.D. Allis, *The language of covalent histone modifications*. Nature, 2000. 403(6765): p. 41-5.
154. Marks, P., et al., *Histone deacetylases and cancer: causes and therapies*. Nat Rev Cancer, 2001. 1(3): p. 194-202.
155. Dou, Y., et al., *Phosphorylation and an ATP-dependent process increase the dynamic exchange of H1 in chromatin*. J. Cell Biol., 2002. 158(7): p. 1161-1170.
156. Lachner, M., et al., *Methylation of histone H3 lysine 9 creates a binding site for HP1 proteins*. Nature, 2001. 410(6824): p. 116-120.
157. Grunstein, M., *Histone acetylation in chromatin structure and transcription*. Nature, 1997. 389(6649): p. 349-52.
158. Brownell, J.E., et al., *Tetrahymena histone acetyltransferase A: a homolog to yeast Gcn5p linking histone acetylation to gene activation*. Cell, 1996. 84(6): p. 843-51.
159. Taunton, J., C.A. Hassig, and S.L. Schreiber, *A mammalian histone deacetylase related to the yeast transcriptional regulator Rpd3p*. Science, 1996. 272(5260): p. 408-11.
160. Kouzarides, T., *Acetylation: a regulatory modification to rival phosphorylation?* Embo J, 2000. 19(6): p. 1176-9.
161. Sterner, R., G. Vidali, and V.G. Allfrey, *Studies of acetylation and deacetylation in high mobility group proteins. Identification of the sites of acetylation in HMG-1*. J Biol Chem, 1979. 254(22): p. 11577-83.
162. Luo, J., et al., *Acetylation of p53 augments its site-specific DNA binding both in vitro and in vivo*. Proc Natl Acad Sci U S A, 2004. 101(8): p. 2259-64.
163. Bereshchenko, O.R., W. Gu, and R. Dalla-Favera, *Acetylation inactivates the transcriptional repressor BCL6*. Nat Genet, 2002. 32(4): p. 606-13.
164. Bali, P., et al., *Inhibition of histone deacetylase 6 acetylates and disrupts the chaperone function of heat shock protein 90: a novel basis for antileukemia activity of histone deacetylase inhibitors*. J Biol Chem, 2005. 280(29): p. 26729-34.
165. L'Hernault, S.W. and J.L. Rosenbaum, *Chlamydomonas alpha-tubulin is posttranslationally modified by acetylation on the epsilon-amino group of a lysine*. Biochemistry, 1985. 24(2): p. 473-8.

166. Bannister, A.J., et al., *Acetylation of importin-alpha nuclear import factors by CBP/p300*. *Curr Biol*, 2000. 10(8): p. 467-70.
167. Gross, D.S. and W.T. Garrard, *Nuclease hypersensitive sites in chromatin*. *Annu Rev Biochem*, 1988. 57: p. 159-97.
168. Lee, D.Y., et al., *A positive role for histone acetylation in transcription factor access to nucleosomal DNA*. *Cell*, 1993. 72(1): p. 73-84.
169. McGhee, J.D. and G. Felsenfeld, *Nucleosome structure*. *Annu Rev Biochem*, 1980. 49: p. 1115-56.
170. Norton, V.G., et al., *Nucleosome linking number change controlled by acetylation of histones H3 and H4*. *J Biol Chem*, 1990. 265(32): p. 19848-52.
171. Lavu, S., et al., *Sirtuins [mdash] novel therapeutic targets to treat age-associated diseases*. *Nat Rev Drug Discov*, 2008. 7(10): p. 841-853.
172. Furukawa, Y., et al., *Isolation and mapping of a human gene (RPD3L1) that is homologous to RPD3, a transcription factor in Saccharomyces cerevisiae*. *Cytogenet Cell Genet*, 1996. 73(1-2): p. 130-3.
173. Kijima, M., et al., *Trapoxin, an antitumor cyclic tetrapeptide, is an irreversible inhibitor of mammalian histone deacetylase*. *J Biol Chem*, 1993. 268(30): p. 22429-35.
174. Yoshida, M., S. Horinouchi, and T. Beppu, *Trichostatin A and trapoxin: novel chemical probes for the role of histone acetylation in chromatin structure and function*. *Bioessays*, 1995. 17(5): p. 423-30.
175. Grozinger, C.M. and S.L. Schreiber, *Deacetylase enzymes: biological functions and the use of small-molecule inhibitors*. *Chem Biol*, 2002. 9(1): p. 3-16.
176. Gregoret, I.V., Y.M. Lee, and H.V. Goodson, *Molecular evolution of the histone deacetylase family: functional implications of phylogenetic analysis*. *J Mol Biol*, 2004. 338(1): p. 17-31.
177. Gray, S.G. and T.J. Ekstrom, *The human histone deacetylase family*. *Exp Cell Res*, 2001. 262(2): p. 75-83.
178. Ashburner, B.P., S.D. Westerheide, and A.S. Baldwin, Jr., *The p65 (RelA) subunit of NF-kappaB interacts with the histone deacetylase (HDAC) corepressors HDAC1 and HDAC2 to negatively regulate gene expression*. *Mol Cell Biol*, 2001. 21(20): p. 7065-77.

179. Li, J., et al., *Specific targeting and constitutive association of histone deacetylase complexes during transcriptional repression*. Genes Dev, 2002. 16(6): p. 687-92.
180. Yang, X.J. and E. Seto, *Collaborative spirit of histone deacetylases in regulating chromatin structure and gene expression*. Curr Opin Genet Dev, 2003. 13(2): p. 143-53.
181. Lagger, G., et al., *Essential function of histone deacetylase 1 in proliferation control and CDK inhibitor repression*. EMBO J, 2002. 21(11): p. 2672-81.
182. Chen, L., et al., *Duration of nuclear NF-kappaB action regulated by reversible acetylation*. Science, 2001. 293(5535): p. 1653-7.
183. Verdin, E., F. Dequiedt, and H.G. Kasler, *Class II histone deacetylases: versatile regulators*. Trends Genet, 2003. 19(5): p. 286-93.
184. Zhang, C.L., et al., *Class II histone deacetylases act as signal-responsive repressors of cardiac hypertrophy*. Cell, 2002. 110(4): p. 479-88.
185. Hubbert, C., et al., *HDAC6 is a microtubule-associated deacetylase*. Nature, 2002. 417(6887): p. 455-8.
186. Gao, L., et al., *Cloning and functional characterization of HDAC11, a novel member of the human histone deacetylase family*. J Biol Chem, 2002. 277(28): p. 25748-55.
187. Glozak, M.A. and E. Seto, *Histone deacetylases and cancer*. Oncogene, 2007. 26(37): p. 5420-32.
188. Fraga, M.F., et al., *Loss of acetylation at Lys16 and trimethylation at Lys20 of histone H4 is a common hallmark of human cancer*. Nat Genet, 2005. 37(4): p. 391-400.
189. Zhu, P., et al., *Induction of HDAC2 expression upon loss of APC in colorectal tumorigenesis*. Cancer Cell, 2004. 5(5): p. 455-63.
190. Jaehwi, S., et al., *Increased expression of histone deacetylase 2 is found in human gastric cancer*. Apmis, 2005. 113(4): p. 264-268.
191. Huang, B.H., et al., *Inhibition of histone deacetylase 2 increases apoptosis and p21Cip1/WAF1 expression, independent of histone deacetylase 1*. Cell Death Differ, 2005. 12(4): p. 395-404.

192. Witt, O., et al., *HDAC family: What are the cancer relevant targets?* Cancer Letters, 2009. 277(1): p. 8-21.
193. Zhang, Z., et al., *HDAC6 expression is correlated with better survival in breast cancer.* Clin Cancer Res, 2004. 10(20): p. 6962-8.
194. Kim, M.S., et al., *Histone deacetylases induce angiogenesis by negative regulation of tumor suppressor genes.* Nat Med, 2001. 7(4): p. 437-443.
195. Lin, R.J., et al., *Transcriptional regulation in acute promyelocytic leukemia.* Oncogene, 2001. 20(49): p. 7204-15.
196. Wang, J., et al., *ETO, fusion partner in t(8;21) acute myeloid leukemia, represses transcription by interaction with the human N-CoR/mSin3/HDAC1 complex.* Proc Natl Acad Sci U S A, 1998. 95(18): p. 10860-5.
197. Sykes, S.M., et al., *Acetylation of the p53 DNA-Binding Domain Regulates Apoptosis Induction.* Molecular Cell, 2006. 24(6): p. 841-851.
198. Riggs, M.G., et al., *n-Butyrate causes histone modification in HeLa and Friend erythroleukaemia cells.* Nature, 1977. 268(5619): p. 462-4.
199. Cousens, L.S., D. Gallwitz, and B.M. Alberts, *Different accessibilities in chromatin to histone acetylase.* J Biol Chem, 1979. 254(5): p. 1716-23.
200. Yoshida, M., et al., *Potent and specific inhibition of mammalian histone deacetylase both in vivo and in vitro by trichostatin A.* J Biol Chem, 1990. 265(28): p. 17174-9.
201. Furumai, R., et al., *FK228 (depsipeptide) as a natural prodrug that inhibits class I histone deacetylases.* Cancer Res, 2002. 62(17): p. 4916-21.
202. Tsuji, N., et al., *A new antifungal antibiotic, trichostatin.* J Antibiot (Tokyo), 1976. 29(1): p. 1-6.
203. Yoshida, M., S. Nomura, and T. Beppu, *Effects of trichostatins on differentiation of murine erythroleukemia cells.* Cancer Res, 1987. 47(14): p. 3688-91.
204. Finnin, M.S., et al., *Structures of a histone deacetylase homologue bound to the TSA and SAHA inhibitors.* Nature, 1999. 401(6749): p. 188-93.
205. Kelly, W.K., et al., *Phase I study of an oral histone deacetylase inhibitor, suberoylanilide hydroxamic acid, in patients with advanced cancer.* J Clin Oncol, 2005. 23(17): p. 3923-31.

206. Piekarz, R.L., et al., *Phase II Multi-Institutional Trial of the Histone Deacetylase Inhibitor Romidepsin As Monotherapy for Patients With Cutaneous T-Cell Lymphoma*. J Clin Oncol, 2009. 27(32): p. 5410-5417.
207. Kortenhorst, M.S.Q., et al., *A Multiple-Loop, Double-Cube Microarray Design Applied to Prostate Cancer Cell Lines with Variable Sensitivity to Histone Deacetylase Inhibitors*. Clin Cancer Res, 2008. 14(21): p. 6886-6894.
208. Van Lint, C., S. Emiliani, and E. Verdin, *The expression of a small fraction of cellular genes is changed in response to histone hyperacetylation*. Gene Expr, 1996. 5(4-5): p. 245-53.
209. Mariadason, J.M., G.A. Corner, and L.H. Augenlicht, *Genetic Reprogramming in Pathways of Colonic Cell Maturation Induced by Short Chain Fatty Acids: Comparison with Trichostatin A, Sulindac, and Curcumin and Implications for Chemoprevention of Colon Cancer*. Cancer Res, 2000. 60(16): p. 4561-4572.
210. Glaser, K.B., et al., *Gene expression profiling of multiple histone deacetylase (HDAC) inhibitors: defining a common gene set produced by HDAC inhibition in T24 and MDA carcinoma cell lines*. Mol Cancer Ther, 2003. 2(2): p. 151-63.
211. Peart, M.J., et al., *Identification and functional significance of genes regulated by structurally different histone deacetylase inhibitors*. Proc Natl Acad Sci U S A, 2005. 102(10): p. 3697-702.
212. Marks, P.A., V.M. Richon, and R.A. Rifkind, *Histone deacetylase inhibitors: inducers of differentiation or apoptosis of transformed cells*. J Natl Cancer Inst, 2000. 92(15): p. 1210-6.
213. Munster, P.N., et al., *The Histone Deacetylase Inhibitor Suberoylanilide Hydroxamic Acid Induces Differentiation of Human Breast Cancer Cells*. Cancer Res, 2001. 61(23): p. 8492-8497.
214. Vrana, J.A., et al., *Induction of apoptosis in U937 human leukemia cells by suberoylanilide hydroxamic acid (SAHA) proceeds through pathways that are regulated by Bcl-2/Bcl-XL, c-Jun, and p21CIP1, but independent of p53*. Oncogene, 1999. 18(50): p. 7016-25.
215. Ellis, L., et al., *The histone deacetylase inhibitors LAQ824 and LBH589 do not require death receptor signaling or a functional apoptosome to mediate tumor cell death or therapeutic efficacy*. Blood, 2009: p. blood-2008-10-182758.

216. Guo, F., et al., *Cotreatment with histone deacetylase inhibitor LAQ824 enhances Apo-2L/tumor necrosis factor-related apoptosis inducing ligand-induced death inducing signaling complex activity and apoptosis of human acute leukemia cells*. *Cancer Res*, 2004. 64(7): p. 2580-9.
217. Mitsiades, N., et al., *Molecular sequelae of histone deacetylase inhibition in human malignant B cells*. *Blood*, 2003. 101(10): p. 4055-4062.
218. Piekarz, R.L., et al., *Inhibitor of histone deacetylation, depsipeptide (FR901228), in the treatment of peripheral and cutaneous T-cell lymphoma: a case report*. *Blood*, 2001. 98(9): p. 2865-2868.
219. Garcia-Manero, G. and J.P. Issa, *Histone deacetylase inhibitors: a review of their clinical status as antineoplastic agents*. *Cancer Invest*, 2005. 23(7): p. 635-42.
220. O'Connor, O.A., et al., *Clinical experience with intravenous and oral formulations of the novel histone deacetylase inhibitor suberoylanilide hydroxamic acid in patients with advanced hematologic malignancies*. *J Clin Oncol*, 2006. 24(1): p. 166-73.
221. Kelly, W.K., et al., *Phase I clinical trial of histone deacetylase inhibitor: suberoylanilide hydroxamic acid administered intravenously*. *Clin Cancer Res*, 2003. 9(10 Pt 1): p. 3578-88.
222. E. Olsen, Y.H.K., T. Kuzel, T. R. Pacheco, F. Foss, S. Parker, J. G. Wang, S. R. Frankel, J. Lis, M. Duvic. *Vorinostat (suberoylanilide hydroxamic acid, SAHA) is clinically active in advanced cutaneous T-cell lymphoma (CTCL): Results of a phase IIb trial*. in *2006 ASCO Annual Meeting Proceedings Part I*. 2006. Atlanta: Journal of Clinical Oncology.
223. Duvic, M., et al., *Phase 2 trial of oral vorinostat (suberoylanilide hydroxamic acid, SAHA) for refractory cutaneous T-cell lymphoma (CTCL)*. *Blood*, 2007. 109(1): p. 31-9.
224. Siu, L.L., et al., *Phase I Study of MGCD0103 Given As a Three-Times-Per-Week Oral Dose in Patients With Advanced Solid Tumors*. *J Clin Oncol*, 2008. 26(12): p. 1940-1947.
225. Garcia-Manero, G., et al., *Phase 1 study of the oral isotype specific histone deacetylase inhibitor MGCD0103 in leukemia*. *Blood*, 2008. 112(4): p. 981-989.
226. Nolan, L., et al., *Will histone deacetylase inhibitors require combination with other agents to fulfil their therapeutic potential?* *Br J Cancer*, 2008. 99(5): p. 689-94.

227. Valentini, A., et al., *Valproic acid induces apoptosis, p16INK4A upregulation and sensitization to chemotherapy in human melanoma cells.* Cancer Biol Ther, 2007. 6(2): p. 185-91.
228. Marchion, D.C., et al., *Valproic Acid Alters Chromatin Structure by Regulation of Chromatin Modulation Proteins.* Cancer Res, 2005. 65(9): p. 3815-3822.
229. Marchion, D.C., et al., *In vivo synergy between topoisomerase II and histone deacetylase inhibitors: predictive correlates.* Mol Cancer Ther, 2005. 4(12): p. 1993-2000.
230. Munster, P., et al., *Phase I trial of histone deacetylase inhibition by valproic acid followed by the topoisomerase II inhibitor epirubicin in advanced solid tumors: a clinical and translational study.* J Clin Oncol, 2007. 25(15): p. 1979-85.
231. www.clinicaltrials.gov. ClinicalTrials.gov. [cited; Available from: <http://clinicaltrials.gov>.
232. Johnson, C.A., et al., *Deacetylase activity associates with topoisomerase II and is necessary for etoposide-induced apoptosis.* J Biol Chem, 2001. 276(7): p. 4539-42.
233. Tsai, S.C., et al., *Histone deacetylase interacts directly with DNA topoisomerase II.* Nat Genet, 2000. 26(3): p. 349-53.
234. Marchion, D.C., et al., *Sequence-specific potentiation of topoisomerase II inhibitors by the histone deacetylase inhibitor suberoylanilide hydroxamic acid.* J Cell Biochem, 2004. 92(2): p. 223-37.
235. Bevins, R.L. and S.G. Zimmer, *It's About Time: Scheduling Alters Effect of Histone Deacetylase Inhibitors on Camptothecin-Treated Cells.* 2005. p. 6957-6966.
236. Rikiishi, H., et al., *Chemosensitization of oral squamous cell carcinoma cells to cisplatin by histone deacetylase inhibitor, suberoylanilide hydroxamic acid.* Int J Oncol, 2007. 30(5): p. 1181-8.
237. Sato, T., et al., *Sequence-dependent interaction between cisplatin and histone deacetylase inhibitors in human oral squamous cell carcinoma cells.* Int J Oncol, 2006. 28(5): p. 1233-41.
238. Bali, P., et al., *Activity of suberoylanilide hydroxamic Acid against human breast cancer cells with amplification of her-2.* Clinical Cancer Research, 2005. 11(17): p. 6382-9.

239. Dowdy, S.C., et al., *Histone deacetylase inhibitors and paclitaxel cause synergistic effects on apoptosis and microtubule stabilization in papillary serous endometrial cancer cells*. Mol Cancer Ther, 2006. 5(11): p. 2767-76.
240. Crabb, S.J. and S.K. Chia, *HER2 directed therapies*. Advances in Breast Cancer, 2007. 4: p. 40-47.
241. Chinnaiyan, P., et al., *Enhancing the antitumor activity of ErbB blockade with histone deacetylase (HDAC) inhibition*. International journal of cancer, 2006. 118(4): p. 1041-50.
242. Fuino, L., et al., *Histone deacetylase inhibitor LAQ824 down-regulates Her-2 and sensitizes human breast cancer cells to trastuzumab, taxotere, gemcitabine, and epothilone B*. Molecular Cancer Therapeutics, 2003. 2(10): p. 971-84.
243. Scott, G.K., et al., *Transcriptional repression of ErbB2 by histone deacetylase inhibitors detected by a genomically integrated ErbB2 promoter-reporting cell screen*. Molecular cancer therapeutics, 2002. 1(6): p. 385-92.
244. Edwards, A., et al., *Effect of the histone deacetylase inhibitor LBH589 against epidermal growth factor receptor dependent human lung cancer cells*. Mol Cancer Ther, 2007. 6(9): p. 2515-2524.
245. Witta, S.E., et al., *Restoring E-Cadherin Expression Increases Sensitivity to Epidermal Growth Factor Receptor Inhibitors in Lung Cancer Cell Lines*. Cancer Res, 2006. 66(2): p. 944-950.
246. Smith, A., *Protein misfolding*. Nature, 2003. 426(6968): p. 883-883.
247. Altucci, L., et al., *Acute myeloid leukemia: therapeutic impact of epigenetic drugs*. Int J Biochem Cell Biol, 2005. 37(9): p. 1752-62.
248. Bug, G., et al., *Clinical trial of valproic acid and all-trans retinoic acid in patients with poor-risk acute myeloid leukemia*. Cancer, 2005. 104(12): p. 2717-25.
249. Kuendgen, A., et al., *The histone deacetylase (HDAC) inhibitor valproic acid as monotherapy or in combination with all-trans retinoic acid in patients with acute myeloid leukemia*. Cancer, 2006. 106(1): p. 112-119.
250. Hodges-Gallagher, L., et al., *Inhibition of histone deacetylase enhances the anti-proliferative action of antiestrogens on breast cancer cells and blocks tamoxifen-induced proliferation of uterine cells*. Breast Cancer Res Treat, 2007. 105(3): p. 297-309.

251. Jang, E.R., et al., *The histone deacetylase inhibitor trichostatin A sensitizes estrogen receptor alpha-negative breast cancer cells to tamoxifen*. *Oncogene*, 2004. 23(9): p. 1724-36.
252. Zhou, Q., P. Atadja, and N.E. Davidson, *Histone deacetylase inhibitor LBH589 reactivates silenced estrogen receptor alpha (ER) gene expression without loss of DNA hypermethylation*. *Cancer Biol Ther*, 2007. 6(1): p. 64-9.
253. Fiskus, W., et al., *Cotreatment with Vorinostat (Suberoylanilide Hydroxamic Acid) Enhances Activity of Dasatinib (BMS-354825) against Imatinib Mesylate-Sensitive or Imatinib Mesylate-Resistant Chronic Myelogenous Leukemia Cells*. *Clin Cancer Res*, 2006. 12(19): p. 5869-5878.
254. Yu, C., et al., *Histone Deacetylase Inhibitors Promote STI571-mediated Apoptosis in STI571-sensitive and -resistant Bcr/Abl+ Human Myeloid Leukemia Cells*. *Cancer Res*, 2003. 63(9): p. 2118-2126.
255. Dasmahapatra, G., et al., *Synergistic interactions between vorinostat and sorafenib in chronic myelogenous leukemia cells involve Mcl-1 and p21CIP1 down-regulation*. *Clin Cancer Res*, 2007. 13(14): p. 4280-90.
256. Garcia-Manero, G., et al., *DNA methylation of multiple promoter-associated CpG islands in adult acute lymphocytic leukemia*. *Clin Cancer Res*, 2002. 8(7): p. 2217-24.
257. Yang, H., et al., *Antileukemia activity of the combination of 5-aza-2'-deoxycytidine with valproic acid*. *Leuk Res*, 2005. 29(7): p. 739-48.
258. Garcia-Manero, G., et al., *Phase 1/2 study of the combination of 5-aza-2'-deoxycytidine with valproic acid in patients with leukemia*. *Blood*, 2006. 108(10): p. 3271-9.
259. Gore, S.D., et al., *Combined DNA methyltransferase and histone deacetylase inhibition in the treatment of myeloid neoplasms*. *Cancer Res*, 2006. 66(12): p. 6361-9.
260. Chou, T.-C. and P. Talalay, *Quantitative analysis of dose-effect relationships: the combined effects of multiple drugs or enzyme inhibitors*. *Advances in Enzyme Regulation*, 1984. 22: p. 27-55.
261. Coiffier, B., *Rituximab therapy in malignant lymphoma*. *Oncogene*, 2007. 26(25): p. 3603-13.

262. Butler, L.M., et al., *Suberoylanilide hydroxamic acid, an inhibitor of histone deacetylase, suppresses the growth of prostate cancer cells in vitro and in vivo*. Cancer Res, 2000. 60(18): p. 5165-70.
263. Crabb, S.J., et al., *Characterisation of the in vitro activity of the depsipeptide histone deacetylase inhibitor spiruchostatin A*. Biochem Pharmacol, 2008. 76(4): p. 463-75.
264. Fantin, V.R., et al., *Constitutive activation of signal transducers and activators of transcription predicts vorinostat resistance in cutaneous T-cell lymphoma*. Cancer Res, 2008. 68(10): p. 3785-94.
265. Teeling, J.L., et al., *Characterization of new human CD20 monoclonal antibodies with potent cytolytic activity against non-Hodgkin lymphomas*. Blood, 2004. 104(6): p. 1793-1800.
266. Cardarelli, P.M., et al., *Binding to CD20 by anti-B1 antibody or F(ab')(2) is sufficient for induction of apoptosis in B-cell lines*. Cancer Immunol Immunother, 2002. 51(1): p. 15-24.
267. Pedersen, I.M., et al., *The chimeric anti-CD20 antibody rituximab induces apoptosis in B-cell chronic lymphocytic leukemia cells through a p38 mitogen activated protein-kinase-dependent mechanism*. Blood, 2002. 99(4): p. 1314-9.
268. Demidem, A., et al., *Chimeric anti-CD20 (IDEC-C2B8) monoclonal antibody sensitizes a B cell lymphoma cell line to cell killing by cytotoxic drugs*. Cancer Biother Radiopharm, 1997. 12(3): p. 177-86.
269. Vega, M.I., et al., *Rituximab-Induced Inhibition of YY1 and Bcl-xL Expression in Ramos Non-Hodgkin's Lymphoma Cell Line via Inhibition of NF- κ B Activity: Role of YY1 and Bcl-xL in Fas Resistance and Chemoresistance, Respectively*. J Immunol, 2005. 175(4): p. 2174-2183.
270. Alas, S. and B. Bonavida, *Rituximab Inactivates Signal Transducer and Activation of Transcription 3 (STAT3) Activity in B-Non-Hodgkin's Lymphoma through Inhibition of the Interleukin 10 Autocrine/Paracrine Loop and Results in Down-Regulation of Bcl-2 and Sensitization to Cytotoxic Drugs*. Cancer Res, 2001. 61(13): p. 5137-5144.
271. Henderson, C., et al., *Role of caspases, Bid, and p53 in the apoptotic response triggered by histone deacetylase inhibitors trichostatin-A (TSA) and suberoylanilide hydroxamic acid (SAHA)*. J Biol Chem, 2003. 278(14): p. 12579-89.
272. Ruefli, A.A., et al., *The histone deacetylase inhibitor and chemotherapeutic agent suberoylanilide hydroxamic acid (SAHA) induces a cell-death*

pathway characterized by cleavage of Bid and production of reactive oxygen species. Proc Natl Acad Sci U S A, 2001. 98(19): p. 10833-8.

273. Pei, X.Y., Y. Dai, and S. Grant, *Synergistic induction of oxidative injury and apoptosis in human multiple myeloma cells by the proteasome inhibitor bortezomib and histone deacetylase inhibitors. Clin Cancer Res, 2004. 10(11): p. 3839-52.*
274. Zhao, W.L., et al., *Combined effects of histone deacetylase inhibitor and rituximab on non-Hodgkin's B-lymphoma cells apoptosis. Exp Hematol, 2007.*
275. Ghetie, M.-A., et al., *Rituximab but not Other anti-CD20 Antibodies Reverses Multidrug Resistance in 2 B lymphoma Cell Lines, Blocks the Activity of P-glycoprotein (P-gp), and Induces P-gp to Translocate out of Lipid Rafts. Journal of Immunotherapy, 2006. 29(5): p. 536-544 10.1097/01.cji.0000211307.05869.6c.*
276. Kinoshita, T., et al., *CD20-negative relapse in B-cell lymphoma after treatment with Rituximab. J Clin Oncol, 1998. 16(12): p. 3916a-.*
277. Katja, S., et al., *CLONAL SELECTION OF CD20-NEGATIVE NON-HODGKIN'S LYMPHOMA CELLS AFTER TREATMENT WITH ANTI-CD20 ANTIBODY RITUXIMAB. Br J Haematol, 1999. 106(2): p. 571-572.*
278. Jazirehi, A.R., M.I. Vega, and B. Bonavida, *Development of rituximab-resistant lymphoma clones with altered cell signaling and cross-resistance to chemotherapy. Cancer Res, 2007. 67(3): p. 1270-81.*
279. Czuczman, M.S., et al., *Acquirement of Rituximab Resistance in Lymphoma Cell Lines Is Associated with Both Global CD20 Gene and Protein Down-Regulation Regulated at the Pretranscriptional and Posttranscriptional Levels. Clin Cancer Res, 2008. 14(5): p. 1561-1570.*
280. Tomita, A., et al., *Epigenetic regulation of CD20 protein expression in a novel B-cell lymphoma cell line, RRBL1, established from a patient treated repeatedly with rituximab-containing chemotherapy. Int J Hematol, 2007. 86(1): p. 49-57.*
281. Daniels, I., et al., *Caspase-independent killing of Burkitt lymphoma cell lines by rituximab. Apoptosis, 2006. 11(6): p. 1013-23.*
282. Hofmeister, J.K., D. Cooney, and K.M. Coggeshall, *Clustered CD20 induced apoptosis: src-family kinase, the proximal regulator of tyrosine phosphorylation, calcium influx, and caspase 3-dependent apoptosis. Blood Cells Mol Dis, 2000. 26(2): p. 133-43.*

283. Nakagawa, T. and J. Yuan, *Cross-talk between Two Cysteine Protease Families: Activation of Caspase-12 by Calpain in Apoptosis*. J. Cell Biol., 2000. 150(4): p. 887-894.
284. Cittera, E., et al., *Rituximab induces different but overlapping sets of genes in human B-lymphoma cell lines*. Cancer Immunol Immunother, 2005. 54(3): p. 273-86.
285. Dennis, G., Jr., et al., *DAVID: Database for Annotation, Visualization, and Integrated Discovery*. Genome Biol, 2003. 4(5): p. P3.
286. Ashburner, M., et al., *Gene ontology: tool for the unification of biology*. The Gene Ontology Consortium. Nat Genet, 2000. 25(1): p. 25-9.
287. Mootha, V.K., et al., *PGC-1alpha-responsive genes involved in oxidative phosphorylation are coordinately downregulated in human diabetes*. Nat Genet, 2003. 34(3): p. 267-73.
288. Smyth, G.K., *Linear Models and Empirical Bayes Methods for Assessing Differential Expression in Microarray Experiments* Statistical Applications in Genetics and Molecular Biology: , (2004) 3 (1): p. Article 3
289. Grumont, R.J., I.J. Rourke, and S. Gerondakis, *Rel-dependent induction of A1 transcription is required to protect B cells from antigen receptor ligation-induced apoptosis*. Genes Dev, 1999. 13(4): p. 400-11.
290. Margitta M. Worm, A.T.R.S.G., *CD40 ligation and IL-4 use different mechanisms of transcriptional activation of the human lymphotoxin α promoter in B cells*. European Journal of Immunology, 1998. 28(3): p. 901-906.
291. Sanchez-Mateos, P., et al., *Expression of a gp33/27,000 MW activation inducer molecule (AIM) on human lymphoid tissues. Induction of cell proliferation on thymocytes and B lymphocytes by anti-AIM antibodies*. Immunology, 1989. 68(1): p. 72-9.
292. Hamann, J., H. Fiebig, and M. Strauss, *Expression cloning of the early activation antigen CD69, a type II integral membrane protein with a C-type lectin domain*. J Immunol, 1993. 150(11): p. 4920-7.
293. Lopez-Cabrera, M., et al., *Transcriptional regulation of the gene encoding the human C-type lectin leukocyte receptor AIM/CD69 and functional characterization of its tumor necrosis factor-alpha-responsive elements*. J Biol Chem, 1995. 270(37): p. 21545-51.

294. Jazirehi, A.R., et al., *Inhibition of the Raf-MEK1/2-ERK1/2 Signaling Pathway, Bcl-xL Down-Regulation, and Chemosensitization of Non-Hodgkin's Lymphoma B Cells by Rituximab*. Cancer Res, 2004. 64(19): p. 7117-7126.
295. Leoni, F., et al., *The antitumor histone deacetylase inhibitor suberoylanilide hydroxamic acid exhibits antiinflammatory properties via suppression of cytokines*. Proc Natl Acad Sci U S A, 2002. 99(5): p. 2995-3000.
296. Sailhamer, E.A., et al., *Acetylation: a novel method for modulation of the immune response following trauma/hemorrhage and inflammatory second hit in animals and humans*. Surgery, 2008. 144(2): p. 204-216.
297. Cheung, W.L., S.D. Briggs, and C.D. Allis, *Acetylation and chromosomal functions*. Curr Opin Cell Biol, 2000. 12(3): p. 326-33.
298. Allfrey, V.G., R. Faulkner, and A.E. Mirsky, *Acetylation and Methylation of Histones and Their Possible Role in the Regulation of Rna Synthesis*. Proc Natl Acad Sci U S A, 1964. 51: p. 786-94.
299. Place, R.F., E.J. Noonan, and C. Giardina, *HDAC inhibition prevents NF-kappa B activation by suppressing proteasome activity: down-regulation of proteasome subunit expression stabilizes I kappa B alpha*. Biochem Pharmacol, 2005. 70(3): p. 394-406.
300. Vanden Berghe, W., et al., *p38 and extracellular signal-regulated kinase mitogen-activated protein kinase pathways are required for nuclear factor-kappaB p65 transactivation mediated by tumor necrosis factor*. J Biol Chem, 1998. 273(6): p. 3285-90.
301. Habens, F., et al., *Distinct promoters mediate constitutive and inducible Bcl-XL expression in malignant lymphocytes*. Oncogene, 2007. 26(13): p. 1910-9.
302. Ishii, M., et al., *Epigenetic regulation of the alternatively activated macrophage phenotype*. Blood, 2009. 114(15): p. 3244-3254.